

IASI-NG Science Plan

Prepared by the IASI Sounding Science Working Group

Editors: Fiona Smith and Cyril Crevoisier

v 1.0, December 2018

Contents

| | | |
|----------|--|-----------|
| I | The IASI-NG mission and instrument | 9 |
| 1 | IASI-NG mission rationale and objectives | 10 |
| 1.1 | The EPS-SG Programme | 10 |
| 1.2 | IASI-NG Scientific Objectives | 11 |
| 2 | IASI-NG instrument design | 14 |
| 2.1 | Instrument Overview | 14 |
| 2.2 | Interferometer overview | 18 |
| 2.3 | Detection chain | 20 |
| 2.3.1 | Overview | 20 |
| 2.3.2 | B1 Chain | 22 |
| 2.3.3 | B2 to B4 Chain | 22 |
| 2.4 | Instrument volume and mass budgets | 22 |
| 2.5 | Main instrument characteristics and comparison with IASI | 23 |
| 3 | Processing from interferogram to Level 1c | 25 |
| 3.1 | Space Segment | 25 |
| 3.1.1 | Objectives and design drivers | 25 |
| 3.1.2 | Sounder interferogram data processing | 26 |
| 3.1.2.1 | Processing presentation and logic | 26 |
| 3.1.2.2 | Processing overview | 27 |
| 3.1.3 | Image data processing | 29 |
| 3.1.4 | Sampling and metrology data processing | 30 |
| 3.1.4.1 | Governing principles | 30 |
| 3.2 | Ground segment | 30 |
| 3.2.1 | Objectives and design drivers | 30 |
| 3.2.2 | Science data processing | 30 |
| 3.2.2.1 | Decompression | 31 |
| 3.2.2.2 | Fast Fourier Transform | 31 |
| 3.2.2.3 | NZPD detection | 31 |
| 3.2.2.4 | Spectral calibration | 32 |
| 3.2.2.5 | Radiometric calibration | 32 |
| 3.2.2.6 | Band merging | 32 |
| 3.2.2.7 | Compression | 33 |
| 3.2.3 | ISRF Estimation Model | 33 |
| 3.2.3.1 | ISRF Model | 34 |
| 3.2.3.2 | Absolute Spectral Shift Estimation | 37 |
| 3.2.4 | Image data processing | 37 |
| 4 | Construction of L1c data files and their dissemination | 39 |
| 4.1 | Scene processing | 39 |
| 4.1.1 | Quality Control Flags | 39 |
| 4.1.2 | Sub-pixel heterogeneity | 39 |
| 4.1.3 | Cloud/Aerosol Detection | 40 |
| 4.1.4 | Land/Sea/Ice mask | 40 |
| 4.2 | Dissemination of L1c data files | 40 |

| | | |
|--|--|---------------|
| 4.2.1 | Data representation and compression | 41 |
| 4.2.1.1 | BUFR encoding and dissemination | 41 |
| 4.2.1.2 | Principal Component compression | 42 |
| 4.2.2 | Considerations for direct broadcast | 43 |
| 4.2.3 | Provision of adequate meta-data including noise specifications | 43 |
| 4.3 | Reprocessing: storage of metadata | 43 |
| 4.4 | Remapping | 43 |
| 4.5 | Information channels | 44 |
| II Science Plan | | 45 |
| 5 Radiative Transfer and Spectroscopy | | 46 |
| 5.1 | Radiative transfer modelling for IASI-NG | 46 |
| 5.1.1 | Line-by-line models | 46 |
| 5.1.2 | Pseudo line-by-line models | 51 |
| 5.1.3 | Narrow-band fast RT models on fixed pressure levels or on levels of fixed absorber amount | 52 |
| 5.1.4 | Library look-up based fast RT models | 53 |
| 5.1.5 | Neural network based fast RT models | 53 |
| 5.1.6 | Fast RT Models based on optimal sampling of absorption coefficients . . . | 53 |
| 5.1.7 | Principal Component Based Radiative Transfer Models | 53 |
| 5.2 | Scattering models | 54 |
| 5.3 | Surface models | 55 |
| 5.3.1 | Surface radiation models | 55 |
| 5.3.2 | Surface emissivity models | 56 |
| 5.4 | Models for the microphysical and optical properties of scattering particles | 57 |
| 5.4.1 | Ice clouds | 57 |
| 5.4.2 | Aerosols | 58 |
| 5.5 | Input data to radiative transfer models | 59 |
| 5.5.1 | Spectroscopic data | 59 |
| 5.5.1.1 | Spectroscopic parameters | 59 |
| 5.5.1.2 | Spectroscopic databases | 60 |
| 5.5.1.3 | The GEISA database | 61 |
| 5.5.1.4 | The HITRAN database | 63 |
| 5.5.2 | Optical properties of Cloud and aerosols | 64 |
| 5.5.3 | Surface emissivity data | 65 |
| 5.5.4 | Datasets of atmospheric profiles | 66 |
| 5.6 | Radiative transfer model validation | 68 |
| 6 Level 2 Products: Retrieval of Geophysical Parameters | | 71 |
| 6.1 | Retrieval Theory | 71 |
| 6.1.1 | Physical retrieval schemes | 71 |
| 6.1.1.1 | Variational Analysis | 71 |
| 6.1.1.2 | Optimal Estimation and Twomey-Tikhonov approaches | 73 |
| 6.1.1.3 | Generalized noise covariance matrix | 74 |
| 6.1.1.4 | Direct Inversion | 74 |
| 6.1.2 | Parametric approaches | 75 |
| 6.1.2.1 | Regression and Look-up Tables | 75 |
| 6.1.2.2 | Neural Networks | 76 |
| 6.2 | Input data | 76 |

| | | |
|----------|--|------------|
| 6.2.1 | Unprocessed L1c radiance data | 76 |
| 6.2.1.1 | Reducing the vector length via channel selection | 77 |
| 6.2.1.2 | Reducing the vector length via microwindows | 77 |
| 6.2.2 | Transformed datasets | 78 |
| 6.2.2.1 | Principal component scores | 78 |
| 6.2.3 | Interferogram transforms | 81 |
| 6.2.4 | Reconstructed Radiances | 83 |
| 6.2.5 | Superchannels | 84 |
| 6.3 | Specific considerations for retrieval schemes | 84 |
| 6.3.1 | Clouds and aerosols | 84 |
| 6.3.1.1 | Cloud and aerosol detection | 84 |
| 6.3.1.2 | Cloud clearing | 85 |
| 6.3.2 | Computation and correction of radiative biases | 85 |
| 6.3.3 | A priori error characteristics | 86 |
| 6.3.4 | Observation error characteristics | 86 |
| 6.4 | Retrieval of atmospheric and surface properties | 87 |
| 6.4.1 | Thermodynamic Variables | 87 |
| 6.4.1.1 | Temperature and water vapour profiles | 87 |
| 6.4.1.2 | Surface properties | 88 |
| 6.4.2 | Clouds and Aerosols | 88 |
| 6.4.2.1 | Cloud properties | 88 |
| 6.4.2.2 | Aerosols | 89 |
| 6.4.3 | Atmospheric composition | 91 |
| 6.4.3.1 | Ozone (O ₃) | 93 |
| 6.4.3.2 | Carbon Monoxide (CO) | 95 |
| 6.4.3.3 | Methane (CH ₄) | 96 |
| 6.4.3.4 | Methanol (CH ₃ OH) and other Volatile Organic Compounds | 97 |
| 6.4.3.5 | Nitric Acid (HNO ₃) | 97 |
| 6.4.3.6 | Sulphur Dioxide (SO ₂) | 97 |
| 6.4.3.7 | Ammonia (NH ₃) | 98 |
| 6.5 | Synergistic retrievals and applications | 98 |
| 6.5.1 | Temperature and water vapour profiles | 98 |
| 6.5.2 | Volcanic eruptions | 98 |
| 6.5.3 | Wildfires | 99 |
| 6.5.4 | Sandstorms | 99 |
| 6.5.5 | Extreme urban air pollution | 99 |
| 6.5.6 | Climate | 100 |
| 7 | Assimilation of IASI Level 1 and 2 data | 101 |
| 7.1 | Input data | 101 |
| 7.2 | Dimensionality reduction | 102 |
| 7.2.1 | Spectral compression | 102 |
| 7.2.1.1 | Raw radiances | 102 |
| 7.2.1.2 | PC scores | 102 |
| 7.2.1.3 | Reconstructed radiances | 103 |
| 7.2.1.4 | L2 retrievals | 104 |
| 7.2.2 | Observation selection and thinning | 105 |
| 7.3 | Forward model operator | 106 |
| 7.4 | Observation errors | 106 |
| 7.5 | Bias correction | 108 |

| | | |
|----------|---|------------|
| 7.6 | Background errors | 109 |
| 8 | Applications of IASI-NG data and products | 110 |
| 8.1 | Numerical Weather Prediction | 110 |
| 8.1.1 | Main Current Areas of Research | 110 |
| 8.1.2 | Expected performance of IASI-NG in NWP | 110 |
| 8.1.3 | Contamination by unmodelled species. | 113 |
| 8.1.4 | The assimilation system | 113 |
| 8.1.5 | Clouds | 114 |
| 8.1.5.1 | Cloudy PC scores | 115 |
| 8.1.6 | Additional considerations | 115 |
| 8.2 | Detecting climate change and variability | 116 |
| 8.2.1 | Context | 116 |
| 8.2.2 | Establishing long time-series | 117 |
| 8.2.3 | Long-term monitoring of essential climate variables | 118 |
| 8.2.3.1 | Temperature profiles | 118 |
| 8.2.3.2 | Water vapour profiles | 119 |
| 8.2.3.3 | Ozone | 120 |
| 8.2.3.4 | UTLS | 120 |
| 8.2.3.5 | Clouds | 121 |
| 8.2.3.6 | Aerosols | 122 |
| 8.2.3.7 | Greenhouse gases: CO ₂ , CH ₄ , N ₂ O | 123 |
| 8.2.3.8 | Surface | 124 |
| 8.2.3.9 | Earth Radiation budget | 126 |
| 8.2.3.10 | Synergistic use of IASI-NG | 127 |
| 8.3 | Air Quality Events and Environmental Monitoring | 128 |
| 8.3.1 | Volcanic eruptions | 129 |
| 8.3.2 | Wildfires | 133 |
| 8.3.3 | Sandstorms | 135 |
| 8.3.4 | Extreme urban air pollution | 135 |
| 8.3.5 | Industrial/nuclear accidents | 138 |
| 8.4 | Process Studies | 138 |
| 8.4.1 | Atmospheric Processes | 138 |
| 8.4.2 | Processes at the land surface-atmosphere interface | 139 |
| 8.4.2.1 | Soil moisture daily cycle and its impact over surface emissivity | 139 |
| 8.4.3 | Identifying climate processes and trends coupling observations and models | 140 |
| 8.5 | Assessing the impact of IASI-NG | 141 |
| 8.5.1 | Assessment of impact in NWP | 141 |
| 9 | Calibration and Validation | 143 |
| 9.1 | User contributions to calibration and validation activities | 144 |
| 9.2 | An airborne demonstrator for IASI-NG | 145 |
| 9.3 | Synergistic Cal/Val activities | 146 |
| 9.3.1 | Some examples of post-2022 campaigns already planned | 146 |
| 9.3.1.1 | The MAGIC initiative - multi-instrument campaigns with ground-based and airborne measurements | 146 |
| 9.3.1.2 | The Stratéole 2 campaign | 147 |
| 9.3.1.3 | CNES annual balloon campaign | 148 |
| 9.3.2 | Validation using NWP model data | 149 |
| 9.3.2.1 | Level 1 | 149 |

| | | |
|-----------|---|------------|
| 9.3.3 | Validation of Level 2 Products | 150 |
| 9.4 | The challenge | 150 |
| 10 | Priorities for Research | 153 |
| 10.1 | Data processing | 153 |
| 10.2 | Development of radiative transfer capabilities | 153 |
| 10.2.1 | Spectroscopic data | 153 |
| 10.2.2 | Radiative Transfer Modelling | 154 |
| 10.2.3 | Radiative transfer in scattering atmospheres | 154 |
| 10.2.4 | Surface modelling | 155 |
| 10.2.5 | Datasets for RT development and validation | 155 |
| 10.3 | Development of Retrieval Algorithms | 156 |
| 10.4 | Data assimilation and Numerical Weather Prediction | 157 |
| 10.5 | Climate Applications | 157 |
| 10.6 | Calibration and Validation | 157 |
| A | IASI-NG specification from the EPS-SG end-user requirements document | 159 |
| A.1 | Data Acquisition Requirements | 159 |
| A.2 | Quality Criteria | 159 |
| A.3 | Spectral Requirements | 159 |
| A.4 | IAS Level 1 Radiometric Requirements | 160 |
| A.5 | IAS Level 1 Geometric Requirements | 161 |
| B | Current Members of the ISSWG | 164 |
| C | Other contributing authors | 165 |

Background to the IASI-NG science plan

The Infrared Atmospheric Sounding Interferometer-New Generation (IASI-NG) instrument fulfils the infrared sounding requirement on the EUMETSAT Polar System Second Generation (EPS-SG) satellites to be launched by EUMETSAT/ESA after 2020.

The purpose of this science plan is to ensure the full exploitation of IASI-NG data, so that the mission requirements set by users can be met. The plan thus explores the current requirements and techniques available to process hyperspectral data, and identifies the current limitations in the exploitation of IASI, such that research can be prioritised to ensure that we have enhanced capabilities by the time of launch.

NWP, atmospheric composition and climate

At the present time, there are few centres that operate across the boundaries of NWP, atmospheric composition and climate. However, it is envisaged that as time progresses, more centres will begin to perform simultaneous NWP and chemical composition forecasts, and will assimilate IASI-NG for both purposes. Equally, reanalysis projects, which are becoming more common, form a bridge between NWP and Climate models. Thus, traditionally independent modelling and assimilation communities are becoming more connected over time. The requirements of data assimilation systems are the same, regardless of the targeted user base, being largely related to the form of the data (radiances or retrieved products) and the assimilation system itself (e.g. 4D-Var; Kalman filter or ensemble based methods) rather than the end application.

The requirements of the three traditionally separate communities are of course similar, but there are different priorities depending on the application. For example, all applications require bias-free data, but correcting for biases that exist in the measurements or forward model will require different approaches depending on the processing scheme and a priori information available.

The structure of this document

The gradual shift towards more combined approaches to use of the data, and the fact that some variables, like surface emissivity, are both products in their own right and required inputs for applications make it hard to structure this document. Effort has been made to separate out what is common to any application, and what is specific, but there will naturally be some duplication.

Part I describes the mission and instrument, and the processing chain from the raw measurements to the Level 1c (L1c) data files that are expected to be the format of choice for most users. The addition of auxiliary data, such as cloud flags and surface type masks, is expected for L1c and some ideas are put forward and techniques explored. The topic of data compression is also discussed here.

Part II describes how the L1c data will be used in its applications. In common to all applications of IASI-NG data is the requirement to be able to forward model measurements using radiative transfer models and spectroscopic databases. This is a critical area where further research is necessary, and is covered in chapter 5. This section then goes on to explore how geophysical parameters may be retrieved from the observations in chapter 6. Chapter 7 discusses the

requirements for assimilation of data whether as radiances or other formats. The specific requirements for NWP, climate monitoring and air quality event monitoring are discussed in the three following chapters. A fundamental requirement for any use of IASI-NG observations is that the instrument is well characterised. Chapter 9 outlines the main challenges in the Calibration and Validation of IASI-NG L1 data and L2 products in order to specify where research should be prioritised. IASI-NG will be a demanding instrument to validate: it promises very low radiometric noise with high spectral resolution and is thus a more advanced instrument than many similar instruments that would be used in Cal/Val campaigns of hyperspectral sounders at the present time. The user requirements for the L2 products are also challenging to validate. A priority for research is to identify new technologies or ways of planning field campaigns that address the deficiencies in the suite of measurements available to us at the present time.

Part I

The IASI-NG mission and instrument

Chapter 1

IASI-NG mission rationale and objectives

1.1 The EPS-SG Programme

The current EUMETSAT Polar System (EPS) will require a follow-on programme in the time frame following 2020, the so-called EPS Second Generation (EPS-SG), to be in place by then to continue operational meteorological measurements from polar orbiting satellites in the mid-morning orbit.

It has been agreed between EUMETSAT and NOAA to establish the Joint Polar System in order to provide long-term continuity of observations from polar orbit supporting operational meteorology, oceanography, atmospheric chemistry, and climate monitoring including additional environmental services to support meteorology, hydrology, and land surface processes. The Metop Second Generation (Metop-SG) satellites for the EPS-SG will be developed in cooperation between EUMETSAT and the European Space Agency (ESA). EUMETSAT will be responsible for the development and operation of the related EPS-SG ground segment to control and monitor the satellite and its data and to process data up to level 1. The operational processing of level 1 data to higher levels, i.e. the generation of geophysical products will be done either at the EPS-SG ground segment or in the network of Satellite Application Facilities (SAF Network).

The mission of the EPS-SG System is to provide global observations from which information on variables of the atmosphere and the ocean and land surfaces can be derived, using satellite based sensors from the Low-Earth Orbit (LEO). To fulfil its mission it is required to deploy sustained capabilities to acquire, process, and distribute to down-stream application users and second tier processing centres environmental data on a broad spectral range (from UV to MW), covering extensive areas (global and regional), and within a variety of different time scales to continue and enhance the services offered by the EPS.

The EPS-SG encompasses the following observation missions:

- The Infra-red Atmospheric Sounding mission (IAS), covering a wide swath of hyper-spectral infra-red soundings in four spectral bands, covering the spectral domain from 3.62 to 15.5 μm at a spatial sampling of about 25 km;
- The Microwave Sounding Mission (MWS), allowing for all-weather soundings over a wide swath in the spectral region between 23 and 229 GHz, at a spatial sampling of about 30 km;
- The Scatterometry Mission (SCA), providing back-scattered signals in the 5.3 GHz band at a spatial resolution of 25 km;
- The Visible/Infra-red Imaging mission (VII), providing cross-purpose, moderate-resolution optical imaging in ≥ 20 spectral channels ranging from 0.443 to 13.345 μm with a spatial sampling of 500 m (250 m in two channels);
- The Microwave Imaging Mission (MWI), providing precipitation and cloud imaging in the spectral range from 18.7 to 183 GHz at a spatial sampling of about 8 km (highest frequency) to 12 km (lowest frequency);
- The Ice Cloud Imaging Mission (ICI), providing ice-cloud and water-vapour imaging in

the spectral range from 183 to 664 GHz at a spatial sampling of <15 km;

- The Radio Occultation Mission (RO), providing high vertical resolution, all-weather soundings by tracking GPS (Global Positioning System) and Galileo satellites;
- The Nadir-viewing Ultraviolet, Visible, Near-infra-red, Short-wave-infra-red sounding mission (UVNS), providing hyper-spectral sounding with a spectral resolution of 0.05 to 1 nm within the spectral range from 0.27 to 2.4 μm at a spatial sampling of 7 km;
- The Multi-viewing Multi-channel Multi-polarisation Imaging mission (3MI), providing moderate resolution aerosol imaging in the spectral region ranging from ultra-violet to short-wave infra-red (0.342 to 2.13 μm), at a spatial sampling of 4 km.

The space segment of the EPS-SG system will consist of a dual satellite configuration with three sounding and optical imaging satellites (embarking IAS, MWS, VII, UVNS, 3MI, and RO) and three microwave satellites (embarking SCA, MWI, ICI, and RO) to span an operational life time of the programme over 21 years. The launch of the first Metop-SG satellite is foreseen in 2021.

1.2 IASI-NG Scientific Objectives

The objectives for the EPS-SG infra-red atmospheric sounding mission (IAS), to be implemented by the IASI-NG system, are established by the EPS-SG mission needs and requirements and laid down in the EPS-SG End User Requirements Document (EURD). The text of each of requirements, which are identified by blue numbering, is taken from the EURD.

The main IAS mission rationale is the measurement of temperature and moisture profiles in clear or partly cloudy scenes at high accuracy (about 1 K and 5 %, respectively) at a vertical resolution in the lower troposphere of about 1 km. The requirements are established on the basis of user requirements, but also taking into account the heritage from similar missions such as IASI.

The primary objective of the IAS mission is to support Numerical Weather Prediction at regional and global scales, through the provision of infra-red radiance spectra measurements with information on:

- Atmospheric temperature profiles at high vertical resolution in clear and partly cloudy air;
- Atmospheric water-vapour profiles at high vertical resolution in clear and partly cloudy air;
- Surface temperature over sea, ice, and land surfaces;
- Cloud variables;
- A number of atmospheric trace gases.

Infra-red soundings with high vertical, horizontal, vertical/spectral resolution greatly enhance the National Meteorological Services' (NMS) ability to initialise global and regional NWP models with realistic information on temperature and moisture.

The frequent availability of detailed temperature and moisture soundings would also contribute to fulfil other key requirements common to Nowcasting and Very Short-Range Forecast (VSRF) at regional scales:

- Monitoring of atmospheric instability, for early warning of convective intensity;
- Cloud microphysical structure.

The level of fulfilment of these objectives will depend strongly on the space-time resolution of the IAS mission, and is particularly critical at high latitudes where information from geostationary

spacecraft is scarce or even unavailable.

The secondary objectives of the IAS mission is to support air quality monitoring at global and regional scales by observation of pollutants in the free troposphere, and the assessment of composition-climate interaction by the observation of greenhouse gases.

The IAS mission provides also support to climate monitoring due to the importance of spectrally resolved infra-red observations in the field of inter-sensor calibration and spectral corrections of irradiances, as performed by using IASI.

The main users of the IAS mission will be the WMO real time users, i.e. NWP centres of National Meteorological Services and ECMWF. Operational nowcasting services of National Meteorological Services may also be users of the IAS mission. The IAS mission is also relevant to non real-time users, such as for climate monitoring and atmospheric chemistry.

The IAS mission will primarily provide infra-red radiance spectra with information on the following variables (in descending order of priority):

1. Temperature profile
2. Water vapour profile
3. Sea surface temperature
4. Land surface temperature
5. Cloud cover
6. Cloud top height
7. Cloud top temperature
8. Outgoing spectral radiance at the top of the atmosphere
9. Surface emissivity in window channels
10. O₃ concentration in deep atmospheric layers
11. CO concentration in deep atmospheric layers
12. Volcanic SO₂ plume concentration
13. CH₄ concentration in the free atmosphere
14. NH₃ concentration in the free atmosphere
15. HNO₃ concentration in the free atmosphere
16. CO₂ concentration in the upper troposphere
17. N₂O concentration in the free troposphere

Further variables to which IAS contributes information:

18. Volcanic ash
19. Downwelling longwave spectral irradiance at the surface
20. PAN

The spectral soundings are transmitted to the ground as spectral samples and are calibrated (radiometrically and spectrally) and geo-located by ground processing, before dissemination to the end users as level 1 datasets.

Requirements for the mission are given at the user product level 1C in appendix A. L1c corresponds to geo-located atmospheric spectra, spectrally and radiometrically calibrated, after equalisation of the instrument spectral response function and numerical apodisation with a truncated Gaussian function with a full-width half maximum of 0.25 cm^{-1} .

The instrument requirements are specified at different levels of performance. Threshold (T) is the performance level below which the observation becomes ineffective and is of no use for

the targeted application. Breakthrough (B) level represents the level beyond which a significant improvement in the target application is achieved. Objective (O) is the performance level beyond which the observation gives no significant improvement for the targeted application. Requirements which do not explicitly state a performance level are to be considered as Threshold requirements.

Chapter 2

IASI-NG instrument design

The IASI-NG mission aims to provide continuity of the IASI service but with a challenging performance improvement with respect to IASI. Table 2.1 gives the main instrument characteristics, in comparison with IASI. The requirements are for spectral resolution and signal-to-noise ratio to be improved by a factor of two compared with IASI. One way to fulfill the requirements is to increase the range of the interferometer Optical Path Difference (OPD) relative to IASI to obtain the desired spectral resolution and spectral sampling, and to increase the pupil size and/or the time observing the signal to reduce the radiometric noise. Increasing pupil size is difficult because it increases the mass and volume of the instrument. Increasing the time of observation is possible by increasing the instantaneous field of view (FOV) of the instrument, but the size of each footprint within the FOV must be no bigger than that of IASI. However, it is well known that increasing OPD range and increasing FOV in a classical Michelson interferometer leads to an increase in the so called self-apodisation function of the instrument, which will lead unavoidably to a reduction in the spectral resolution. A classical Michelson interferometer requires a compromise between FOV size, spectral resolution and signal-to-noise ratio.

The only way to fulfil the requirements is to find a way to compensate the self-apodisation function that arises from the increase in the FOV size. The IASI-NG instrument is based on a classical Michelson interferometer, but to counteract the self-apodisation adds a Mertz compensator, where a plate of variable thickness is introduced in a pupil plane allowing compensation of the optical path difference between the on-axis and the off-axis rays for each OPD value. This technique allows a field-widened interferometer. One of the novel features of the instrument is in the implementation of the OPD and compensation mechanisms with a unique actuator (driven by a single motor). This will be described in section 2.2. The compensation of the field allows a field of $100 \times 100 \text{ km}^2$ to be used, and the installation of a four by four array of detectors in the detection chain. This will be described in more detail in section 2.3.

2.1 Instrument Overview

The overall layout of the instrument is shown in figure 2.2. The instrument is composed of various sub-systems, for which a summary of the instrument functions and operations is presented in this section.

The beam coming from the observed point on the Earth's surface enters the instrument via a reflection off a pointing mirror. A two-axis scan mechanism provides the desired target direction and compensates for satellite velocity during the interferogram acquisition. The required swath (around 2000 km) is covered during a regular cycle which is repeated along the orbit.

In addition to the nominal Earth target acquisition, the scan mechanism allows five extra pointing directions:

- one internal black-body and two deep space views for radiometric calibration.
- a Fabry-Perot filter for spectral calibration. The spectral calibration is performed periodically by looking at cold space through this filter, which provides a reference spectrum comb that is used to ensure good knowledge of the ISRF centroid shift in flight.

| Characteristic | IASI-NG | IASI |
|-------------------------------|--|---|
| Spectral Coverage | continuous from 645 to 2760 cm^{-1} | continuous from 645 to 2760 cm^{-1} |
| Spectral Sampling | 0.125 cm^{-1} 16921 channels | 0.25 cm^{-1} 8461 channels |
| Absolute spectral calibration | 0.5 ppm | 1 ppm |
| Radiometric Calibration | Absolute 0.25 K Inter-channel 0.1 K Inter-pixel 0.1 K Over the orbit 0.1 K End of Life 0.1 K | 0.5 K |
| Radiometric Noise | See figure 2.1 | See figure 2.1 |
| Sounding Point Density | 25 km \times 25 km | 25 km \times 25 km |
| On-ground Pixel Surface | Equivalent to circle of $d = 12$ km at nadir | Equivalent to circle of $d = 12$ km at nadir |
| Imager | Integrated and based on mi- crobolometers | Integrated and based on mi- crobolometers |
| Data Rate | 6 Mbit/sec | 1.5 Mbit/sec |
| Availability | >98 % over lifetime | >97.5 % over lifetime |
| Reliability | >0.84 over lifetime | >0.8 over lifetime |
| Lifetime | 7.5 years | 5 years |

Table 2.1: IASI-NG instrument performance in comparison with requirements

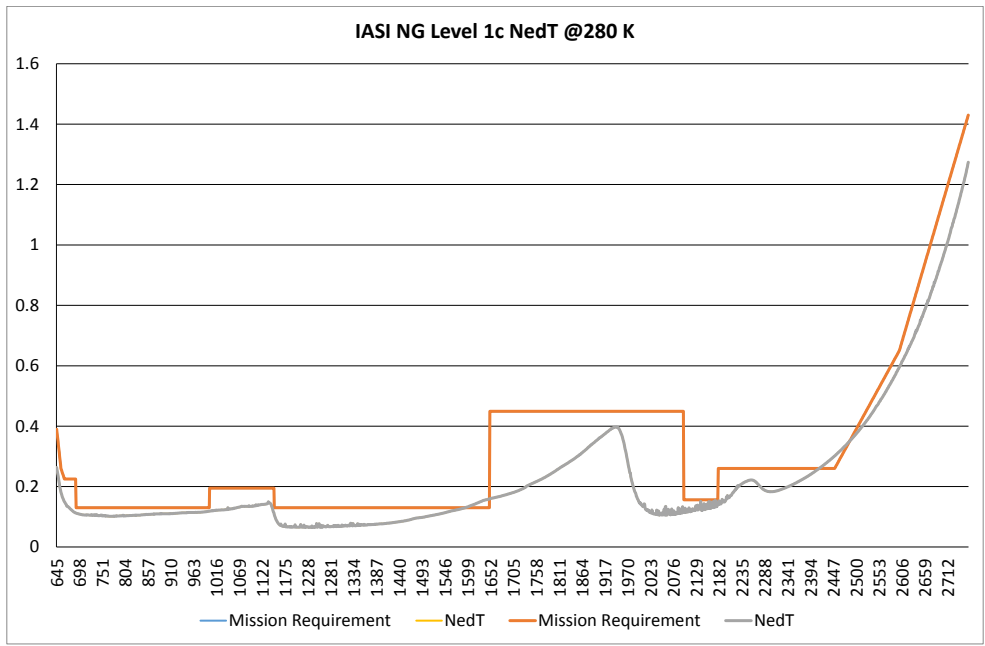


Figure 2.1: IASI-NG performance as at December 2018, plotted together with the user requirements as stated in the EURD

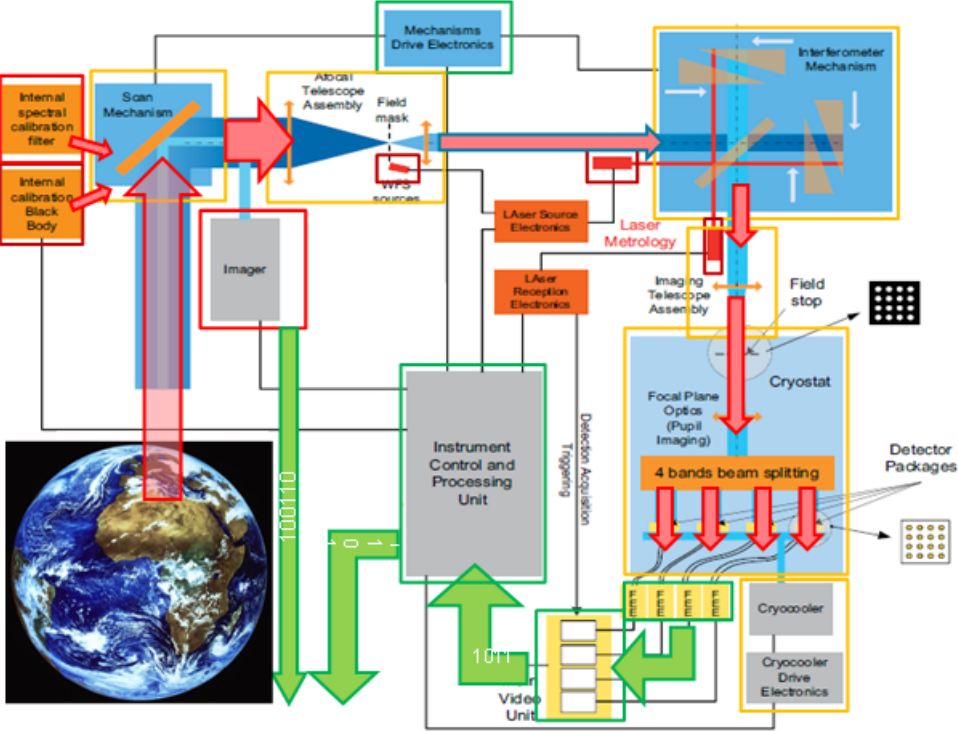


Figure 2.2: IASI-NG instrument: overview of layout

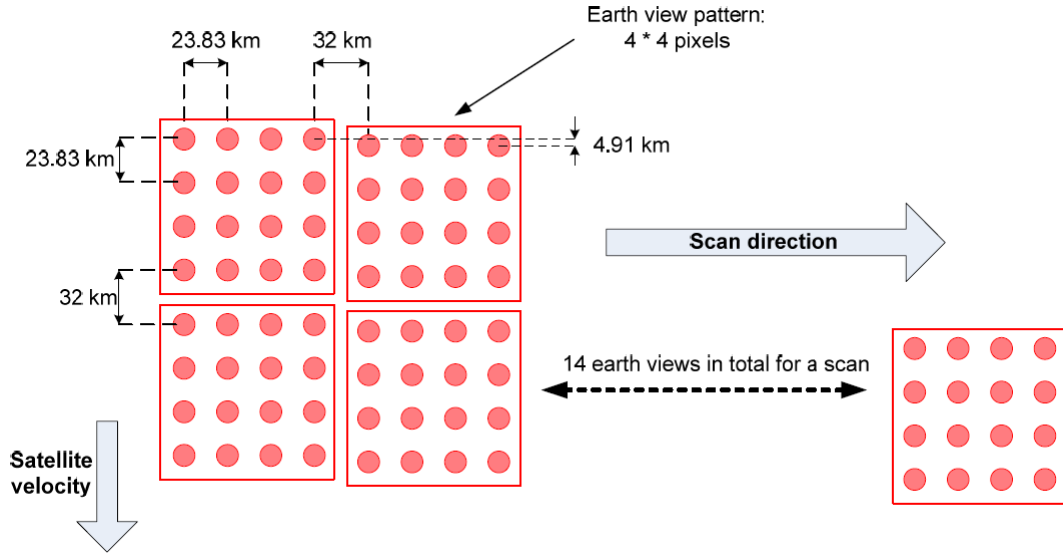


Figure 2.3: Instrument FOV footprint on ground and spatial sampling

- an interferometer wavefront calibration, referred to as the Wave Front monitoring System (WFS). This is also used to ensure good knowledge of the ISRF centroid shift in flight.

A typical observation sequence begins by pointing the scan mirror successively towards the 14 Earth views to cover the required swath (figure 2.3). It is then switched towards two successive radiometric calibration positions, one aiming at a reference blackbody and one aiming at cold space. This cycle is repeated automatically and the instrument performs continuous data acquisition throughout the mission lifetime. The other three calibration views will be used periodically to provide extra data to monitor the long term behaviour of the instrument and, if required, to make adjustments to on-board and/or ground processing parameters to ensure the good quality of the delivered data (i.e. the spectra).

The diameter of the entrance pupil of the instrument is around 90 mm but this is reduced to a diameter of 40 mm inside the interferometer (a magnification ratio of 2.25) by the entrance telescope (Afocal Telescope Assembly) in order to reduce the size of the interferometer (and thus the overall size of the instrument). The resulting field angle increase is acceptable because of the Mertz compensation, which allows wide field angles without compromising spectral resolution.

The optical path difference resulting from the motion of the interferometer mechanism is monitored by the Laser Metrology sub-system. A frequency-stabilised laser source sends several beams into the interferometer that undergo interference in the interferometer in the same way as the science beams and specific detectors receive the resulting metrology interference signals. The Laser Reception Electronics sub-system acquires and processes these data. A computed OPD is used to synchronise the science detector acquisitions so that interferogram data are acquired at constant OPD intervals. The laser signals are also used to derive the tilt of the differential wavefront, which is used in the ground segment for correction of the instrument spectral response function (ISRF).

The outgoing beam of the interferometer is then focused by the Imaging Telescope Assembly onto a field stop consisting of a four by four pattern of holes that define the sounder pixels' size and relative positions. The field stop is located at the cryostat input port. The cryostat also includes the focal plane cold optics and the detectors. The focal plane optics transmit the signal to four by four arrays of detectors in a pupil imaging mode. The cold optics also include

| Band Limits | | |
|-------------|-------------------------|----------------------------|
| Band | Wavelength | Wavenumber |
| B1 | 8.70–15.5 μm | 645–1150 cm^{-1} |
| B2 | 5.13–8.70 μm | 1150–1950 cm^{-1} |
| B3 | 4.35–5.13 μm | 1950–2300 cm^{-1} |
| B4 | 3.62–4.35 μm | 2300–2760 cm^{-1} |

Table 2.2: IASI-NG Band definitions

three spectral beam splitters that separate the beam into the four spectral bands of IASI-NG, as detailed in table 2.2. Compared to IASI, a fourth band is needed to fulfil the radiometric noise requirement between 2200 and 2760 cm^{-1} .

The cryostat cools the detectors to the operating temperature of 75 K using an active cryo-coolers. This sub-system has redundancy to avoid a single-point failure. The signals from the detectors are then read and formatted by an analogue Front End Electronics (FEE) sub-system, before being digitised in the Main Video Unit (MVU) and sent to the Instrument Control and Processing Unit (ICPU).

The on-board data processing is performed by the IPCU. Most of the processing is actually performed by the ground segment for better flexibility and optimal accuracy. The on-board processing is mostly for compression, and is described in section 3.1. The ICPU also contains the control electronics of the instrument. It handles power unit distribution, schedules command and control messages between the instrument and the satellite and manages the sequencing of activities between all the sub-systems.

The IASI-NG processing chain also needs to perform the geolocation of the sounding points. This is done via co-registration of the IASI-NG sounding pixels with already geolocated MetImage images. The co-registration is carried out using a dedicated integrated infrared imager (IMA) inside the IASI-NG instrument, for which co-registration with the sounding pixels is known precisely. This imager uses an uncooled microbolometer in the 10.5–12.5 μm band.

2.2 Interferometer overview

As already mentioned, the IASI-NG Mertz interferometer is a type of Michelson interferometer modified to introduce compensation for the field self-apodisation. The principle of the compensation technique is to introduce a thick plate in one arm of the interferometer to limit the variation of the OPD in the field, which is the aspect we would like to suppress. Figure 2.4 demonstrates the main differences between the structure of the classical Michelson interferometer and the Mertz compensated interferometer.

It is straightforward to demonstrate the relationship between the OPD, the mirror displacement, D , the plate thickness, e , and the optical index, n , of the plate. On-axis this relation is:

$$\text{OPD} = 2(D + e(n - 1)) \quad (2.1)$$

For the Mertz instrument, compensation is achieved when D , e and n vary simultaneously according to the relation:

$$D = \frac{e(n - 1)}{n} \quad (2.2)$$

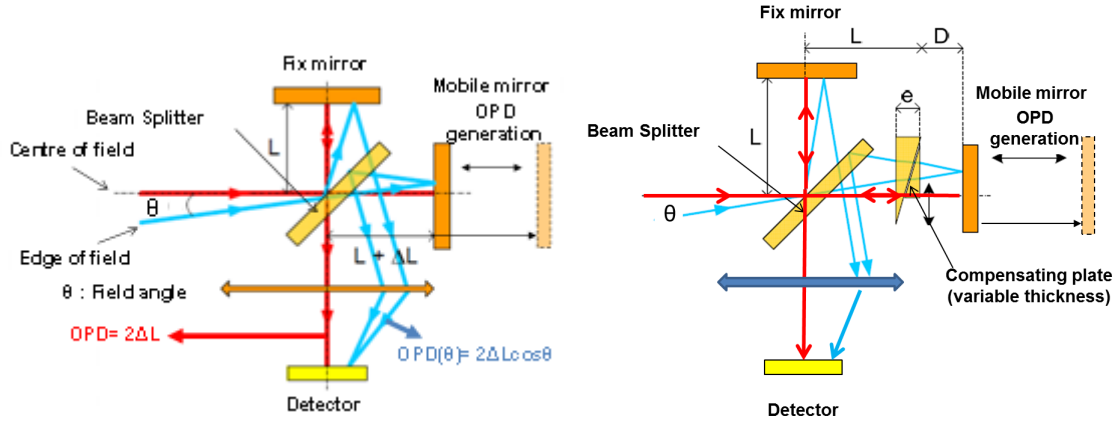


Figure 2.4: Michelson Interferometer principle (a) classical (b) with Mertz compensator

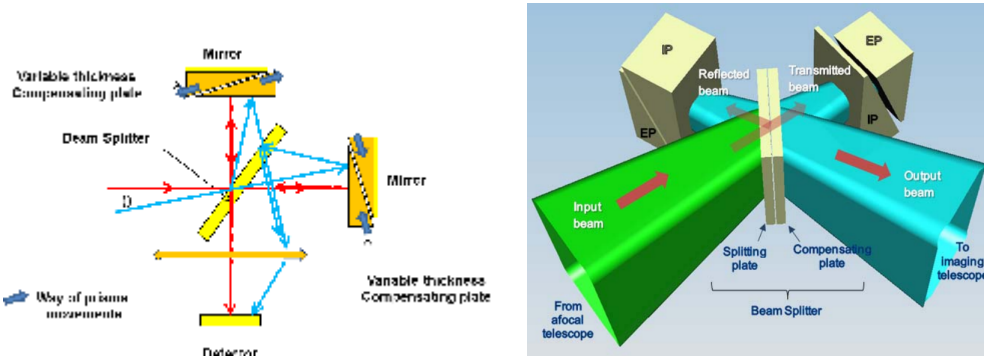


Figure 2.5: Dual swing mechanism: (a) principle (b) scheme of implementation

For a classical Michelson instrument, at $OPD = 0$ the interferometer has no field effect and it can be shown that this is also the case for the Mertz instrument, i.e. $D = 0$ if $e = 0$.

The technical challenge is to be able to continuously adapt the plate thickness, e , to the varying mirror displacement, D : in other words, there is a need to synchronize the mechanism for the mirror displacement with the mechanism that adapts the plate thickness to that displacement. In the proposed concept, the compensation and displacement mirror scan are performed simultaneously, using a novel principle called the Dual Swing Mechanism (DSM; figure 2.5).

This interferometer principle is based on the translation of two pairs of optical prisms in opposite directions (hence the term dual swing). Each arm of the interferometer contains an internal prism (IP) and an external prism (EP) that are mounted head to toe and, in combination, IP+EP could be thought of as a parallel face blade. A reflective coating will be deposited on the outside face of the EP, so the outside face of EP could be thought of as a plane mirror for the interferometer.

The OPD is obtained by moving the EP (with the mirror on the outside face) along the plane of its hypotenuse (the face in contact with the IP). To ensure the Mertz compensation conditions are met (equation 2.2), the movement must be such that the image of each outside mirror is always at the same position at the exit of the interferometer. To achieve this condition, as the distance between the EP mirror and the beam splitter increases, the plate thickness has to increase also. Conversely, when the distance between the EP mirror and the beam splitter decreases, so must the the plate thickness decrease.

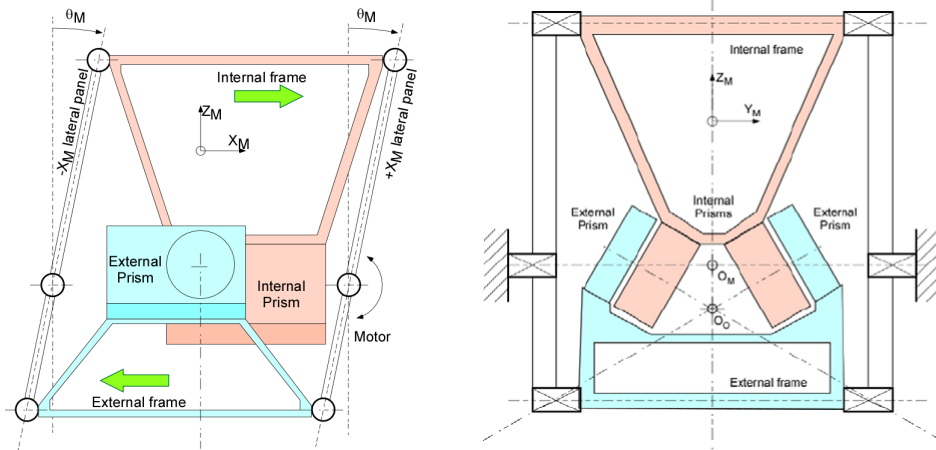


Figure 2.6: Dual swing mechanism mechanical description

To implement the mechanical displacement, the two IPs are mounted on the same supporting frame head to toe (first swing) and the two EPs are mounted on another frame head to toe (second swing). The frames move in opposite directions, and translation between the prisms is provided by a deformable parallelogram principle: composed of four articulated levers, the deformation of the parallelogram provides a differential translation between two of its levers, with the frames supporting the optical parts as shown on figure 2.6. The resulting frame motions translate the prisms in a direction transverse to the optical beam, generating the variation of both mirror and plate thickness simultaneously. The accuracy of the compensation, i.e. the synchronization of the mirror displacement and the plate thickness variation, is obtained by purely mechanical means. The circular motion of the lateral panels also generates a pure translation (transverse motion) of the prisms, which has no effect on the optical performance because the variation is identical on both interferometer arms.

The proposed design is thus a plane mirror interferometer, so the DSM has to ensure that the dual swing motion of the prisms has minimum parasitic tilt, together with a sufficiently high kinematic stability along the stroke.

In order to demonstrate the principle of the compensated interferometer and to check the feasibility and performance of the design, a mock-up of the DSM has been studied (figure 2.7). First interferograms of a monochromatic source have been obtained. Some mechanical and thermal validation has also allowed the verification of the stability of the concept under appropriate environmental conditions.

2.3 Detection chain

2.3.1 Overview

The detection chain is composed of Detector Packages (DP), analogue Front End Electronics and the Main Video Unit. As already mentioned, the observable spectrum has been divided into 4 bands and there will be a four by four array of detectors in each band. In order to minimise mission unavailability in the case of failure of equipment in the chain, the detection architecture is organized to lose non-adjacent pixels, and no more than 25 % of the useful pixels. In other words, the chain is divided into 4 groups of 2×2 pixels in each band, each group being independent of the others and composed of non-adjacent pixels. This is shown in figure 2.8.

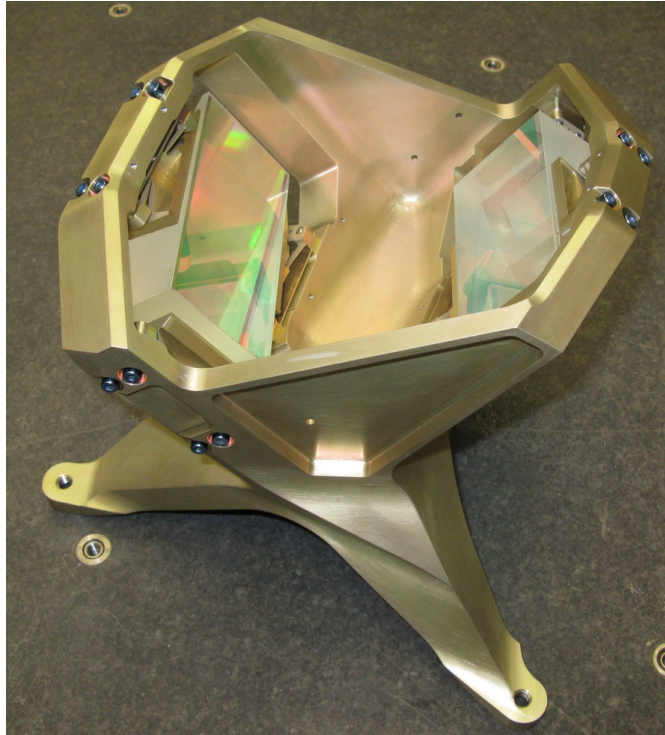


Figure 2.7: Mock-up of the internal prism frame

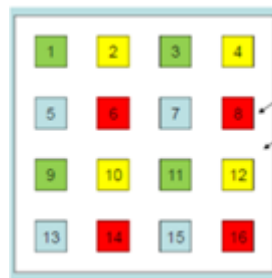


Figure 2.8: Distribution of the 4×4 soundings pixels in 4 groups (shown by different colours) of 2×2 non-adjacent pixels.

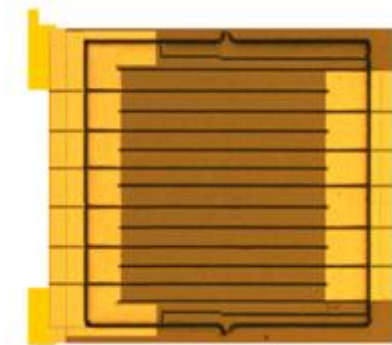


Figure 2.9: Mock-up of individual B1 PC Detector Monolith/element (Courtesy of Selex ES)

2.3.2 B1 Chain

Band 1 measurements will be made with an array of 4×4 PC MCT¹ detectors (Baker et al., 1996). To improve the signal to noise ratio, each monolith detector will be “multi-striped” (as shown in figure 2.9) to increase impedance and thereby reduce the need for a very low noise floor in the downstream electronics. The use of this kind of detector is made possible by pupil imaging: rather than an image of the earth being projected onto the detector, an image of the instrument pupil is projected, which results in a simpler optical architecture. The use of PC detectors for Band 1 also allows sufficient signal to noise ratio with a reasonable degree of cooling. Several prototypes have already been fabricated and tested: they show preliminary performance in line with requirements.

2.3.3 B2 to B4 Chain

Bands 2 to 4 will use MOVPE PV² detectors, made also with the MCT material (Hipwood et al., 2012). The detector circuit will be connected to an electronic circuit containing a Transimpedance Amplifier (TIA), allowing a drastic increase of the the signal-to-noise ratio at the output of the cryostat. The requirements of the detection circuit are in line with state of the art performance for detectors at these wavelengths.

2.4 Instrument volume and mass budgets

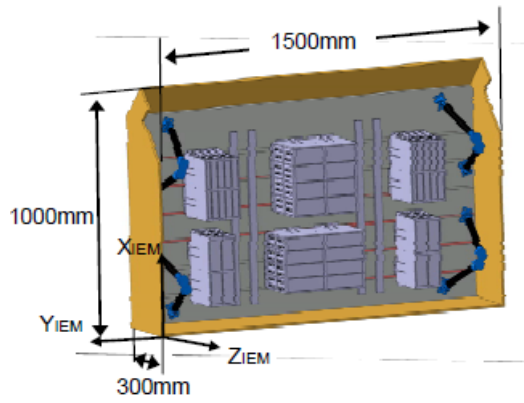
The IASI-NG instrument will be composed of two modules:

- an Electronics Module (called I-EM). This includes most of the electronics, except for the FEE, which is kept close to the cryostat, the Imager Video Electronics, which is located in the vicinity of the imager optics, and the LASE (Laser Source Electronics), which is located inside the I-OH to avoid having optical fibres between the two modules.
- an Optical Head (called I-OH). This mainly includes the opto-mechanical parts of the instrument, for both the sounder and the imager

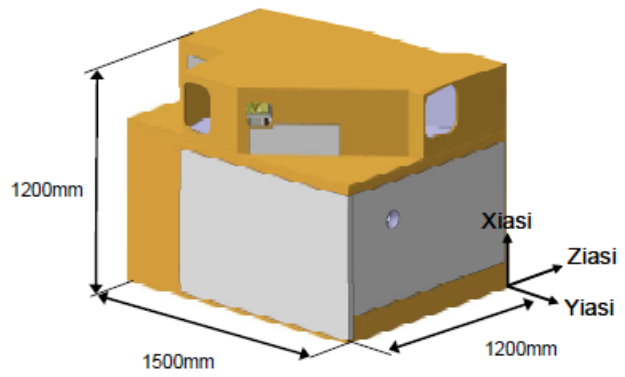
The volume of the two modules is shown graphically in figure 2.10. The mass allocation for the overall instrument is 360 kg and the power budget is about 500 W.

¹Photoconductive Mercury Cadmium Telluride

²MetalOrganic Vapour Phase Epitaxy PhotoVoltaic



(a) I-EM



(b) I-OH

Figure 2.10: Instrument Volume

2.5 Main instrument characteristics and comparison with IASI

Table 3 summarises the main characteristics of the instrument.

| Characteristic | IASI-NG | IASI |
|--------------------------|--|---|
| Instrument Type | Cross-Track Scanner | Cross-Track Scanner |
| Interferometer Principle | Bilateral Michelson interferometer with a Mertz compensator | Bilateral Michelson interferometer |
| Swath | 99.4° | 99.4° |
| Instrument Field Of View | 4 × 4 pixels in a box of 100 km ² × 100 km ² Inter-pixel distance 23.83 km Inter-scan distance 32 km | 2 × 2 pixels in a box of 50 km ² × 50 km ² Inter-pixel distance 18 km Inter-scan distance 23 km |
| Pupil size | 90 mm | 90 mm |
| Cycle Scan | 19 views: 14 Earth views + 2 Calibrations + 3 transitions - duration ≈ 15.6 s | 37 views: 30 Earth views + 4 Calibrations + 3 transitions - duration ≈ 8 s |
| Spectral sampling | Constant OPD sampling | Constant OPD sampling |
| Radiometric Calibration | 1 BB and 1 CS on each line | 1 BB and 1 CS on each line |
| Spectral Calibration | Fabry-Perot and associated model of the instrument | Model of the instrument |
| Optics | Input telescope and imagery telescope: three mirror anastigmat optical design | |
| Detector Package | 4 Bands PC multi-striped Mono-elements in B1 PV Mono-elements in B2 to B4 Cryogenic Amplifier | 3 Bands PC Mono-elements in B1 PV Mono-elements in B2 and B3 Cryogenic Amplifier |
| Cryocooling | Active redundant Cryocooler. Focal plane at 75 K | |
| On board metrologies | Five lasers : OPD & tilt measurement Wave Front Sensor | One laser: OPD measurement |
| Imager | Integrated and based on microbolometers | Integrated and based on microbolometers |
| Data transmitted | Un-calibrated complex spectra | Calibrated spectra |

Table 2.3: Characteristics of the main instrument components of IASI-NG compared with IASI

Chapter 3

Processing from interferogram to Level 1c

The IASI-NG instrument measures interferograms, rather than directly recording spectra as is done by a spectrometer such as AIRS. An interferogram can be mathematically defined as the Fourier transform of a spectrum. In general, users work in spectral space. For IASI, the spectra are available at various levels of processing: L1a are radiometrically calibrated and geolocated; L1b are resampled onto a regular spectral grid; L1c radiances (the product in most common usage) are apodised. (L1d radiances are further processed and are a compressed representation using a truncated principal component approach.) For IASI-NG, the processing chain is different, and there will be no L1a or L1b products. This chapter describes the processing chain that takes the raw interferogram measured by IASI-NG to the L1c radiance spectrum. The following chapter will describe the construction and dissemination of the L1c data files, including any compression required, and additional information about the scene that is added to help users, such as cloud analysis from associated imagery.

Level 1c spectra will have the following properties:

- They are fully calibrated spectrally and radiometrically
- All channels have a single Instrument Spectral Response Function (ISRF) for every spectrum
- Sounding pixels are geo-located

The processing chain from interferogram to Level 1c spectra is divided between the space and ground segments, and will be described in this chapter.

3.1 Space Segment

3.1.1 Objectives and design drivers

Unlike for IASI, the majority of the processing of IASI-NG spectra will be performed on the ground. The objective of the on-board processing is thus to perform a near-lossless compression of the useful spectral information contained in the interferograms. The raw data rate of 200 Mb/s is roughly divided into 175 Mb/s for raw interferograms (science and calibration) and 25 Mb/s for other data (mainly metrology and images). The data is compressed on-board to 6 Mb/s.

Near-lossless compression of the spectral information shall be understood to mean:

- For all relevant spectral channels of IASI-NG (i.e in the “useful band” defined by the mission specifications), the on-board processing shall not introduce significant uncorrectable bias with respect to absolute spectral and radiometric performance, or loss of information with respect to instrument noise.
- There will be no cross-correlation introduced between spectral channels.

The main design drivers are:

- the MetOp-SG telemetry data rate allocated to IASI-NG science data is 6 Mb/s (on average)

- the need to master all instrumental/acquisition artifacts that potentially introduce aliasing and radiometric errors in the useful band (e.g. sampling, non-linearity of detection chains, spikes, NZPD knowledge). These artifacts will be explained further in this chapter.
- the OPD sampling regularity and a knowledge of potential irregularities for on-ground correction
- provision of metrology data in order to be able to accurately model the ISRF
- computing time: note that for each position of the scan mirror, 64 interferograms (16 pixels \times 4 spectral bands) are acquired simultaneously in 820 ms and have to be processed.

3.1.2 Sounder interferogram data processing

3.1.2.1 Processing presentation and logic

The input data of the on-board processing are sampled interferograms. This is independent of the concepts chosen to:

- collect the light (front optics)
- create an interference pattern (interferometer optics and mechanisms)
- detect it (back optics, cold box, type of imagery, detector and detection chain)
- sample the continuous interferogram (sampling method and Analogue to Digital Converter or ADC)

In the sampled interferogram, the information content is consistent with the Shannon criteria. Therefore, all the relevant spectral information is accessible within the range $[0, 2\nu_s]$, where ν_s is the wavenumber associated to the sampling frequency ($2\nu_s$ is approximately 7820 cm^{-1}).

The logic of the design is:

- to preserve the information content by keeping the Fourier transform reversible at least in the useful spectral band.
- to be compliant with computation time and telemetry data rate.

Following this logic, the processing must thus remove any effects prior to FFT that would otherwise cause spectral patterns in the useful band. One example of such a phenomenon is the spike in the interferogram that occurs when a proton hits a detector. Spikes must be detected prior to the FFT computation. These result from very high energy particles that disrupt the measuring of the interferogram, but only on some samples, which corrupts the spectrum. Non-linearities that are introduced by the detection chain also require correction. The radiometric calibration scheme is based on the assumption of a linear response between two different scene temperatures. Not correcting for the non-linearity can introduce significant radiometric errors in spectra.

The ZPD (“Zero Path Difference”) is the position of the central fringe of the interferogram. The NZPD is the index of the sample detected as the ZPD within the sampled interferogram. The interferogram is re-centered with respect to the NZPD prior to FFT in order to limit asymmetry, which would cause a spectral shift for the ISRF centroid. In IASI-NG, the data rate allocated is 4 times greater than for IASI. So, in addition to the increasing the number of channels by a factor of 2, it is possible to transmit a complex spectrum defined by its real and imaginary parts within the telemetry requirements. The main advantage over the IASI processing chain is that the FFT becomes reversible on the ground. Therefore, a fully accurate radiometric complex calibration does not need to be carried out on-board, as is the case for IASI. As a consequence, the accuracy requirement for the detection of the NZPD is not as stringent as for IASI. A rough NZPD is sufficient to ensure that the transmitted interferograms are compliant with the

spectral resolution required. The complex radiometric calibration is performed on the ground, as described in section 3.2.

After non-linearity correction, spike detection and interferogram re-centering using a rough NZPD, the FFT is calculated. The spectrum is then truncated from $[0, 2\nu_s]$ to $[\nu_{min}, \nu_{max}]$, where ν_{min} and ν_{max} are respectively the minimum and maximum wavenumber of each spectral band, including a buffer at each end to perform corrections related to any irregularity of sampling. This frequency truncation is the main way in which compression is applied to the interferogram, and is called the “FFT truncation compression”. It decreases the interferogram data rate by 25. The assumption behind the FFT formulation is that the OPD is regularly sampled. Any deviation from this regularity needs to be quantified, measured, and eventually corrected by a proper resampling. Usually resampling cannot be done on-board because of computation time. This means that any source of OPD sampling irregularity has to be analyzed case-by-case in order to determine what can or cannot be corrected on the ground after frequency truncation. If the irregularity cannot be corrected on the ground, the design of the instrument or the detection chain has to be constrained so that a correction will not be required. For instance, this is the case for the moving mirror velocity, and the sampling wavelength. During the interferogram acquisition, their stability has to be achieved through instrument design.

A further decrease in the data rate is still required, so in addition to the “FFT truncation compression”, a more “conventional compression” is also done on-board. This compression is done for each spectral band. It is a near-lossless compression based on usual methods: quantization, and lossless spatial and spectral correlation. They are optimized to take into account the level of noise (for the quantization) and the specific spectral correlation between channels and spatial correlation between pixels. The “conventional compression” leads to an additional compression factor of about 2–3 with a slight degradation of the noise limited to 1%. This degradation is only introduced by the quantization; the other compression steps don’t cause any degradation of product quality (lossless).

3.1.2.2 Processing overview

An overview of IASI-NG on-board interferogram processing is shown graphically in figure 3.1.

To achieve a low output data rate, a series of on-board algorithms is applied to each interferogram (IFG):

Non-linearity correction (NLC)

The detection chain non linearity is corrected first. Corrected IFGs are obtained by reading the appropriate value in Look Up Tables (LUTs) (64 LUTs of 4000 points in total) using the measured intensity. This step also takes into account offset and gain corrections. When necessary, NLC can be fine-tuned by updating the LUTs after on-ground post-processing of verification raw interferograms.

Spike detection (SPK)

In order to detect spikes, each IFG is convolved with a weighting function of less than 13 points wide that defines a high pass filter. Spikes are detected by comparing the result to a specific threshold. When a spike is detected, the IFG is flagged as contaminated. IFGs are otherwise unaffected by this operation.

Proposed baseline

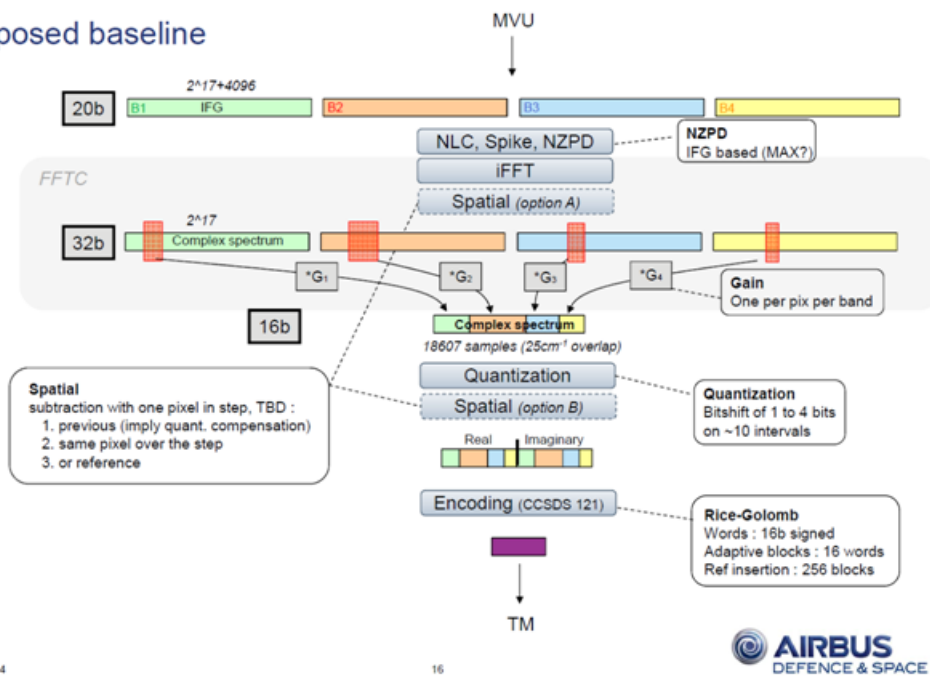


Figure 3.1: Onboard interferogram processing

Rough NZPD detection

In order to center the interferogram and thus avoid degradation of the spectral resolution and to optimize the conventional compression rate, a rough estimate of the NZPD (referred to as NZPD_1) is made on-board. This task is performed only on one IFG for each pixel, i.e. on only one of the four bands, which can be selected post-launch.

Three algorithms are specified, and can be selected post-launch:

1. The sample that minimizes the distance between the interferogram and its reflection can be found (requiring around 1000 points to be examined).
2. The maximum of the interferogram can be selected.
3. A fixed value can be used.

An accurate NZPD is determined on-ground prior to performing the radiometric calibration, with a much more complex scheme (the Connes algorithm).

Re-centering

The acquired IFGs are re-centered using the computed NZPD_1 index.

Inverse Fourier transform (iFFT)

For each band, a complex spectrum is obtained by computing a discrete inverse Fourier transform over the re-centered IFG.

Spectral information extraction

In each band, the spectrum in the wavenumber range of interest is extracted.

Quantization

Quantization is the process of rounding values to some unit of precision. A device or algorithmic function that performs this function is called a quantizer. The round-off error introduced by the rounding is referred to as quantization error. The error signal is modeled as an additional random signal called quantization noise because of its stochastic behaviour. Quantization also forms the core of essentially all lossy compression algorithms. The encoding step is adapted with respect to the noise level in the useful band in order to not introduce any additional noise greater than 0.5%. The resultant dynamic range of the quantized signal is lower than the initial 16b.

JPEG-LS 2D de-correlation and Rice encoding

This algorithm takes advantage of both spectral and spatial correlation of the output data to achieve an initial compression prior to Rice encoding, which compresses the spectra further before being sent to the ground in order to reduce the overall data rate.

3.1.3 Image data processing

Images are not processed on-board other than to perform the summation of 14 elementary images during the acquisition time in order to meet the signal-to-noise requirement.

Raw images and corresponding calibration data are transmitted to the ground for further radiometric calibration.

3.1.4 Sampling and metrology data processing

3.1.4.1 Governing principles

The objectives assigned to metrology data are:

- To provide the reference OPD sampling to the detection chain. This reference is used on-board to trigger interferogram acquisition.
- To provide all required inputs to the ISRF model for an accurate simulation of the spectral response function as part of the on-ground processing.

Note that with respect to IASI, the IASI-NG metrology data are greatly enhanced because they provide inputs to the ISRF model, not just the reference sampling of the interferograms.

The laser metrology electronics (LARE) unit performs measurements via five laser detection chains. One in the centre of the field and the pupil is used to provide the sampling OPD for science interferograms, while four others are provided to the ground segment for input to the ISRF model computation (the main contribution is to provide near real time wavefront tilt values and some long term tuning). The OPD sampling allows interpolation of the exact IFG acquisition time. This enables IFG sampling at constant OPD intervals by the sounder detection chain.

The LARE processing unit actually handles interferograms coming from each of the five metrology chains and generates an Optical Path Difference (OPD) estimation for each. These OPDs are transmitted to the ground at a lower frequency in order to limit the data rate.

3.2 Ground segment

3.2.1 Objectives and design drivers

The objectives assigned to the ground processing are:

- To provide fully calibrated atmospheric spectra (spectrally and radiometrically) that are geo-located.
- To perform the ISRF removal (de-convolution). The variable ISRF with respect to channel, pixel and time is replaced by a single and standard spectral response function. This makes the spectra easier to simulate using radiative transfer models. This process is designed to limit additional inter-channel signals and noise cross-correlation.
- To manage the processing in near real time (noting that there are more than 1 million spectra acquired per day!)
- To provide additional geophysical characteristics of the scene (at pixel and sub-pixel scale) in order to help the exploitation of IASI-NG spectra. This additional information may be extracted from other available products or computed by the IASI-NG L1 processing chain itself.

The main design drivers are:

- Reliability and accuracy of the ISRF Estimation Model
- Radiometric, spectral and geo-location performance at the system level
- Computing time

3.2.2 Science data processing

A schematic overview of the science data processing is presented in figure 3.2.

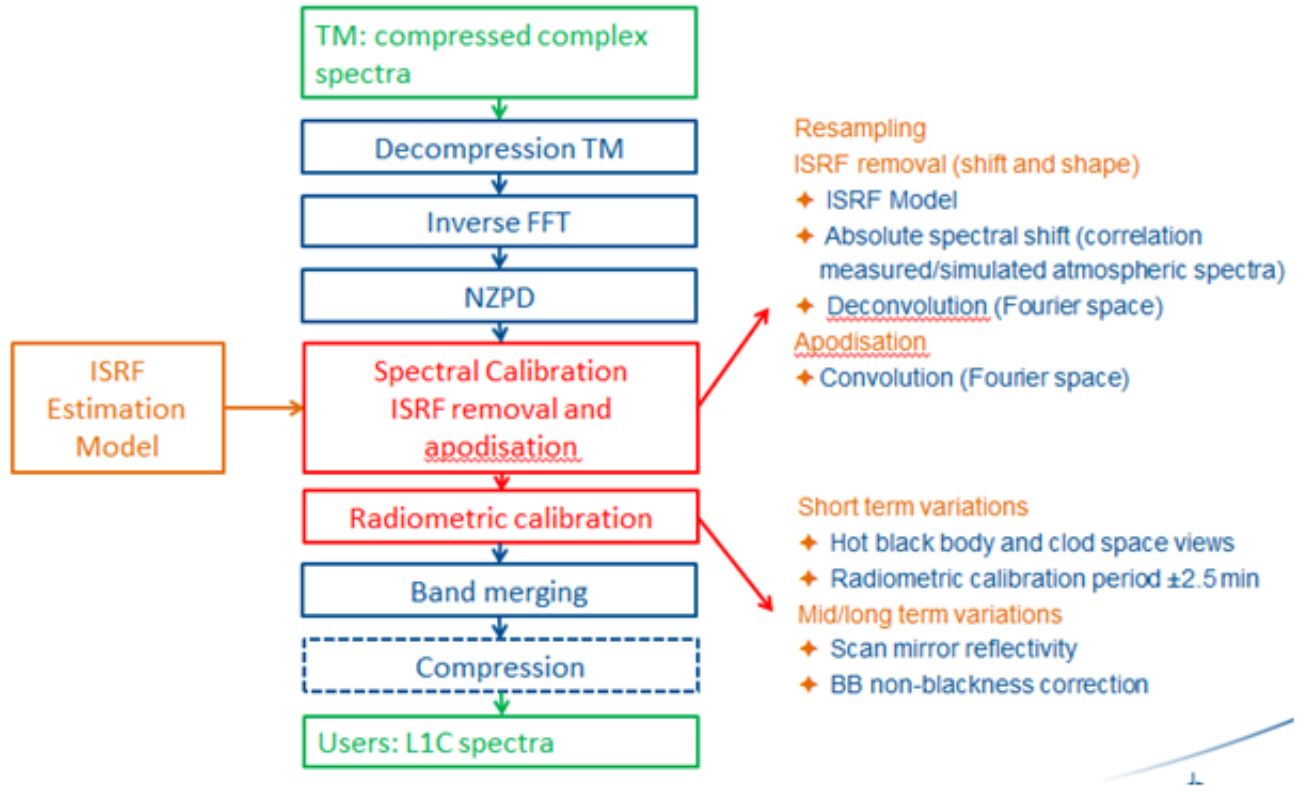


Figure 3.2: Flow diagram of the science data processing steps

3.2.2.1 Decompression

After having been received on the ground, complex spectra are decompressed using the inverse function of the conventional compression algorithms applied on-board.

3.2.2.2 Fast Fourier Transform

The data are returned to interferogram space by applying the FFT (i.e. the inverse of the iFFT that was done by the on-board processing module) in order to prepare for the ISRF removal. This is done in interferogram space.

3.2.2.3 NZPD detection

In order to perform a centered inverse iFFT, the sample corresponding to ZPD (i.e. the NZPD) is determined accurately. This task is performed only on one IFG for each pixel, i.e. on only one of the four bands. There are two possible algorithms:

IASI algorithm This determines a preliminary NZPD by finding the sample that maximizes the distance to the average of the sub-sampled IFG (around 1000 points are required). A more precise estimation is then performed by working in the spectral domain and incorporating information from the black body and cold space calibration target spectra.

Connes algorithm This involves selecting the sample corresponding to NZPD after a linear fit of the phase function.

3.2.2.4 Spectral calibration

ISRF removal

The nominal ISRF, which is variable with respect to channel, pixel and time is replaced by a sinc function. This deconvolution is done in the interferogram space. The Self Apodisation Function (SAF) is the equivalent of the ISRF in interferogram space. The SAF correction process removes the complex modulation efficiency degradation of the interferometer resulting from the optics wave front error, by means of a set of tilt correction coefficients that are a function of the wave front error tilt measured by the on-board laser metrology. The metrology information is sent by the spacecraft through the auxiliary data stream. The SAFs are determined by means of an interferometer simulator, representative of the interferometer design and optics characteristics as determined on the ground during the instrument integration phase, and complemented during in-orbit operation by the data measured by the on-board Wave Front monitoring System (WFS) combined with the absolute spectral shift estimation from atmospheric spectra.

Apodisation

The next step is to perform a classical apodisation by multiplication of the interferogram with the apodisation function, which is the Fourier Transform of the desired ISRF at user level. In fact, ILS removal and apodisation are done simultaneously. In the case of an instrument with non-negligible self-apodisation, the multiplying function should be such that its product with the self apodisation function is equal to the FT of the desired ISRF at L1c. In the case of IASI-NG an additional complication arises because the self-apodisation is wavenumber dependent.

Resampling

The objective here is to resample the interferogram on the grid defined by the end-users i.e. corresponding to a sampling of 0.125 cm^{-1} .

3.2.2.5 Radiometric calibration

Radiometric short term calibration

IASI-NG calibration is based on linear interpolation in the complex plane of the FT of the interferograms. The two linear laws (one per corner cube motion direction) are determined for all 64 chains (4 bands and 16 pixels) through measurements of interferograms associated with two well defined reference targets: one gives the origin by looking to cold space; the other gives a point corresponding to the other end of the dynamic range by looking at an on-board blackbody. This calibration is done at full spectral resolution. The calibration coefficients are contaminated by measurement noise on the target views which is filtered by a polynomial interpolation using ± 5 to 10 consecutive views.

Radiometric long term calibration

This will deal with parameters that vary slowly over a long time-period, such as the variation of scan mirror reflectivity with scan angle and the effect of non-unity emissivity of the black body. To correct the latter, the environment equivalent temperature has to be known.

3.2.2.6 Band merging

There are overlap areas between spectral bands due to instrument transmission. In these areas there are two independent determinations of the spectrum. These two determinations are com-

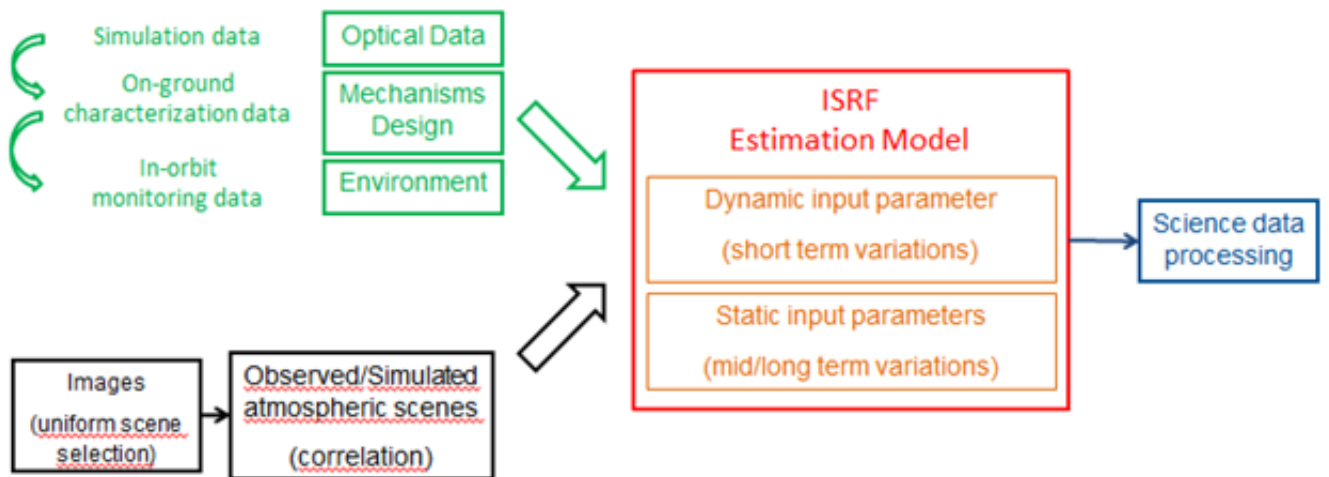


Figure 3.3: Schematic of the ISRF Estimation Model

binned linearly with weights that are inversely proportional to the square of their expected noise level.

3.2.2.7 Compression

L1c spectra will be compressed using classical quantization and lossless compression. This step is optional in the IASI-NG ground segment: instead it could be done in EPS-SG ground segment before dissemination of data to users.

3.2.3 ISRF Estimation Model

The ISRF-EM is the key element that ensures spectral quality, and is shown schematically in figure 3.3.

It relies on the following components:

The ISRF model

This is the best knowledge of the Instrument Spectral Response Functions (ISRFs) that we have. Its input parameters are characterized by both on-ground characterization and in-flight measurements (using Metrology, the Fabry-Perot source, and the WFS).

Absolute spectral shift estimation

This is estimated on selected spectral bands by determining the correlation between a collection of measured spectra and their corresponding simulated spectra, using NWP analysis and a radiative transfer model.

Monitoring

There are several components that are actively monitored:

- The relative spectral shift calibration law is monitored in-flight using the Fabry-Perot view. This allows adjustments to certain input parameters of ISRF Model (in particular, the prism refractive index) when required.

- Metrology information: this mainly provides the monitoring of the OPD law, the WFE tilt (the first order term of the WFE), and the impact of deviations from nominal geometry on the sounder pixel OPD. Information on higher order WFE terms could also be estimated. This information also allows adjustments to input parameters of ISRF Model as and when required. Note that short term tilt variations are measured and corrected in near real time by the ISRF-EM.
- The residual wave front error (of order 2 or higher) is monitored using the WFS device. This is also an input to the ISRF Model, and monitoring allows adjustments as and when required.
- The absolute spectral calibration over the spectrum is monitored using correlation methods.

3.2.3.1 ISRF Model

There are two basic objectives to the ISRF Model:

- To provide an interferometer characterization tool to determine the parameters of the SAF correction process that is used by the ground processing to convert the interferogram into the radiance spectrum. In this context the ISRF Model, as currently defined, is intended to evolve into an operational model used for the in-orbit operation of the instrument.
- To provide an interferometer simulation tool, allowing end-to-end spectral performance assessment. By incorporating manufacturing errors, potential instabilities at different periods of the instrument life, and environmental perturbations into the interferometer model, it can be used to assess the actual achievable spectral performance of the instrument.

These two objectives can be met using the same model of the interferometer, run in different conditions. The input data used in the model will evolve during the course of the instrument development. In the current phase, the model is based on the nominal interferometer design, combined with simulated perturbations and defects. Then, these inputs will be replaced by as-built interferometer characteristics, using measured performance of the optical and mechanical components. Finally, instrument in-orbit monitoring data (such as the on-board wave front monitoring sensor) can be used as input data to the model to refine the SAF model.

Metrology data

The output of a Fourier transform interferometer is an interferogram giving the detector signals as a function of the optical path difference of the interferometer. As described above, this interferogram is discretely sampled for various OPD values. The spectrum of the observed object is obtained by a Fourier transform of this interferogram. This requires accurate knowledge of the OPD variation between the acquired interferogram samples. Therefore accurate laser metrology is implemented to estimate the optical path variations in real time. This accurate estimation is also used to trigger the focal plane science data detector arrays' acquisition at equal OPD intervals, thus avoiding large resampling of the interferogram. In the Mertz interferometer concept, the modulation of the interferogram is dependent on the tilt of the moving prisms during OPD scan. In order to correct this effect it is necessary to measure the tilt in addition to the OPD. This task is also performed by the laser metrology.

The laser metrology thus provides in the first instance a trigger to the detection at equal OPD intervals, being used for the computation of the spectral data together with the metrology for the sounder pixels (e.g. position in the field, differential WFE, optical indices, etc.). It also provides the wave front tilt values that are used for computation of the radiometric data, together with the the wave front error and in-field apodisation metrology.

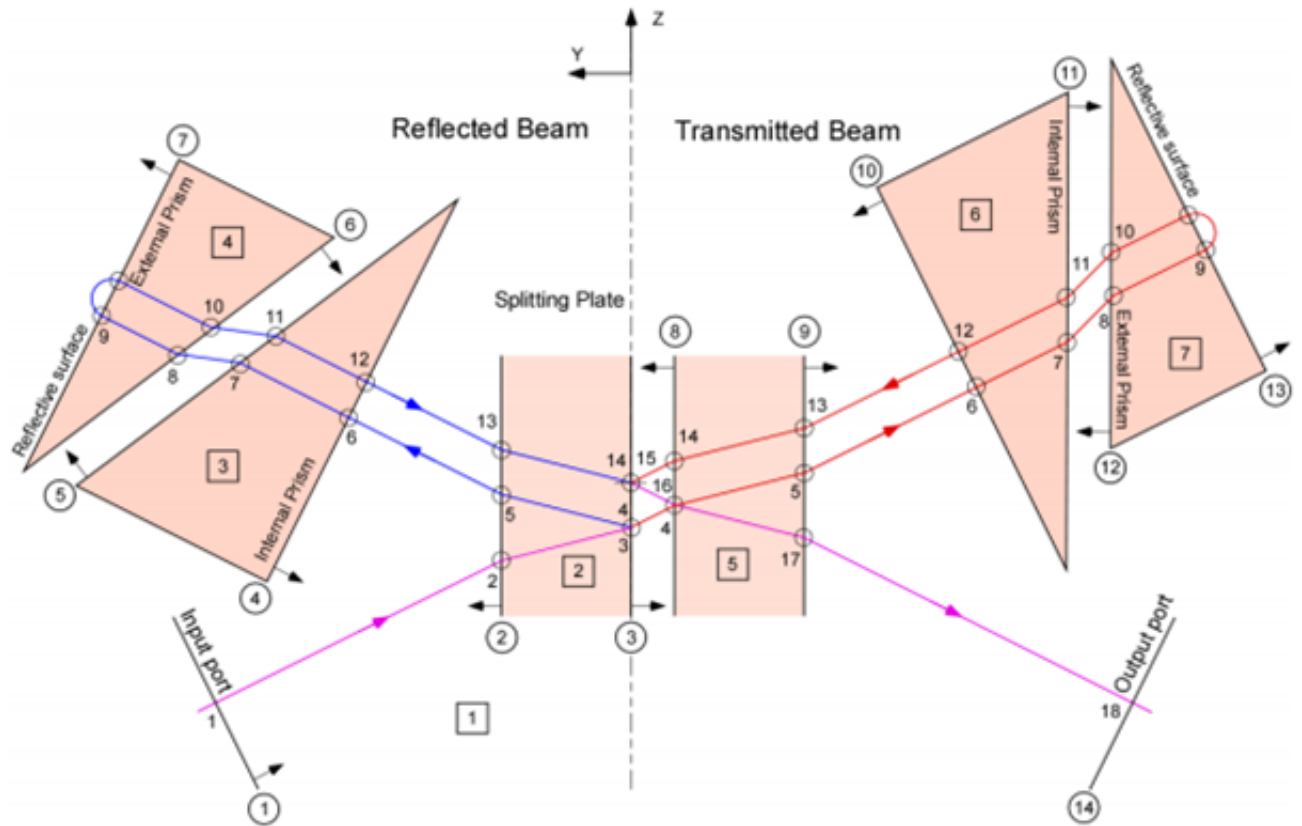


Figure 3.4: Interferometer Optical Path Model

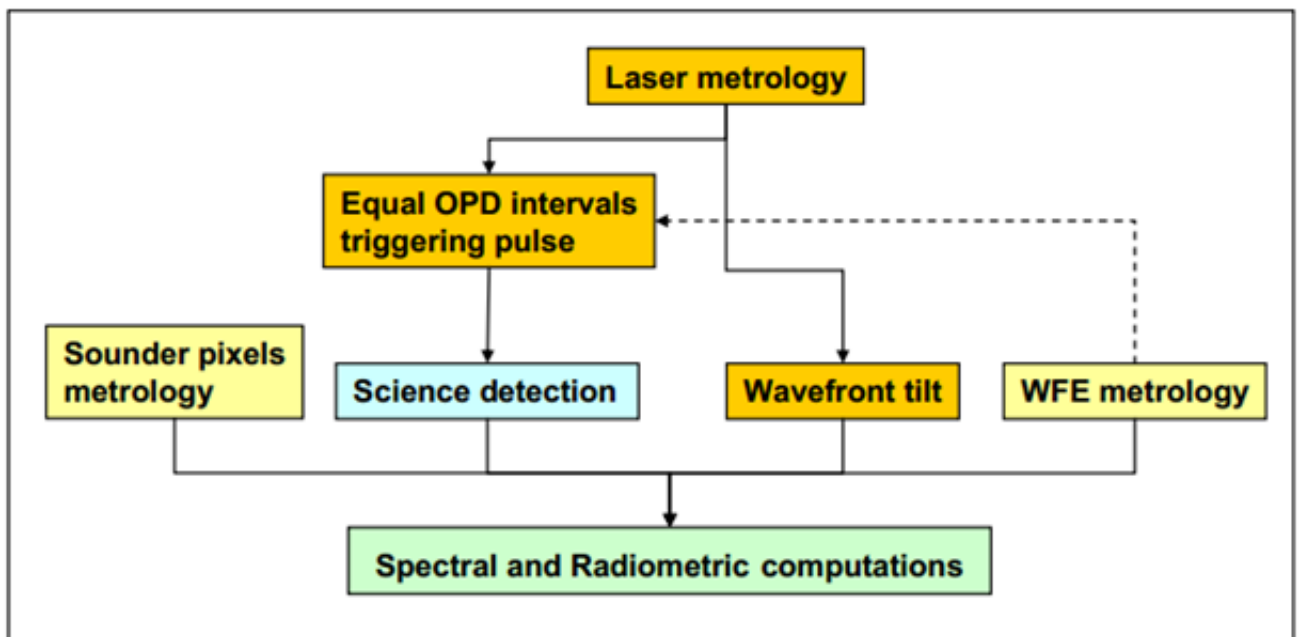


Figure 3.5: Schematic of the ISRF_EM

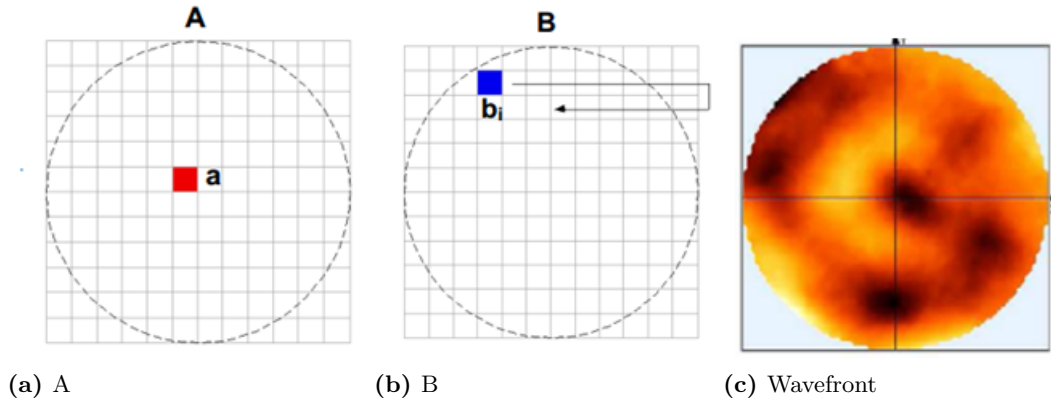


Figure 3.6: Example of the sounder-pixel B wave front over the full pupil

The proposed 1.55 μm IASI-NG reference laser is similar to the one developed in the framework of the IASI program. It is based on a 1.55 μm DFB (distributed feedback) laser source providing a narrow line width and high reliability. It is controlled by an acetylene cell to ensure the stability of the laser wavelength.

Wave Front Sensor data

The WFS data provides better knowledge of the WFE surface and therefore better correction of the self-apodisation. The operating principle consists of pointing the instrument field of view towards a laser source to illuminate two macro-pixels. The two selected sounder pixels (A and B) of the detector of spectral Band 4 are acquired at sub-pixel level. Sounder pixel A is used as reference. The two sub-pixel signals are sent to the ground and processed using the nominal metrology chain. This gives the local OPD of the two sub-pixels, which enables the determination of the phase between the reference sub-pixel and the WFS sub-pixel. Combining the phase obtained for each sub-pixel provides the sounder-pixel B wave front over the full pupil as a function of the OPD, as shown in figure 3.6.

Fabry-Perot data

The principle of the on-board spectral calibration is to place in front of the instrument a black body seen through a Fabry-Perot interferometer (FPI). The FPI filters the black body radiation and provides a comb of spectral lines that are regularly spaced in wavenumber. The principle is shown in figure 3.7.

The determination of one of the spectral line peaks by means of the atmospheric spectral calibration enables the peak spectral position of all the other lines to be determined, and consequently provides spectral calibration over the entire IASI-NG useful spectral band.

Spectral calibration based on direct deep-space view is the preferred solution for two reasons. Firstly, the additional hardware is limited to the Fabry-Perot interferometer: there is no need for an additional on-board source, and secondly, the system is purely passive. There is no hot source with heating power, thermal control and associated electronics, and therefore there is no need to provide redundancy.

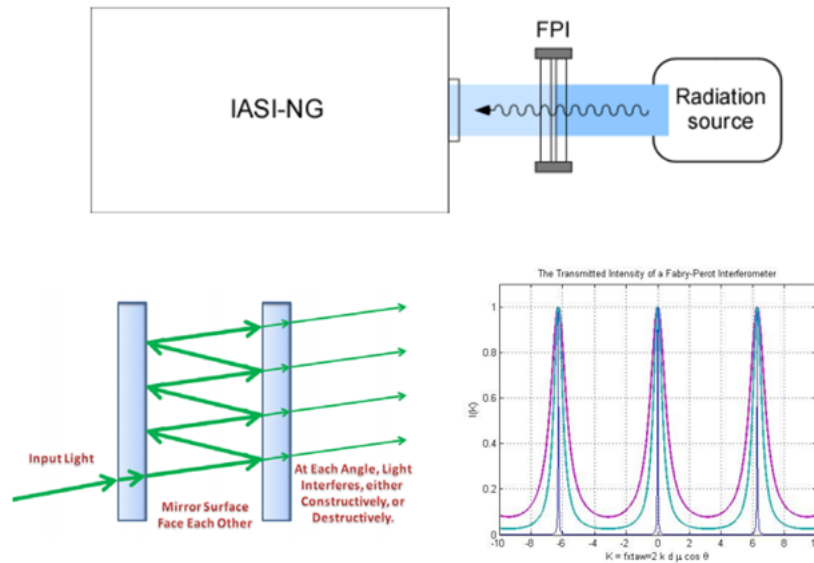


Figure 3.7: The Fabry-Perot interferometer.

3.2.3.2 Absolute Spectral Shift Estimation

Absolute Spectral Calibration can be measured through the recognition and accurate location of well-defined patterns in the atmospheric spectrum.

Three methods can be used, that are all based on searching for the maximum correlation between the measured spectrum and a simulated spectrum based on line by line computations:

- Direct correlation of spectrum
- Correlation of the spectral derivative
- Correlation in Fourier transform space (IASI method). In this case, the search for the maximum correlation is equivalent to the computation of the phase difference at the fundamental frequency of the studied pattern, between the transform of the reference spectra and the transform of the measured one.

The resulting accuracy is limited by the noise level on the measured spectrum and by the differences between the atmospheric state used to compute the synthetic spectrum and the true atmospheric state at the location of the measurement. The first effect is reduced by averaging determinations over a period of the order of 10 minutes; the second is minimized by selection of rather insensitive line patterns and by using the best possible description of the atmospheric state (source as yet undecided) for the synthetic spectrum computations.

3.2.4 Image data processing

The image data processing of IASI-NG images is very similar to that of IASI.

Radiometric calibration

IASI-NG images are first radiometrically calibrated using hot black body and cold space images. This process is in common usage and will not be detailed further here.

MetImage co-registration

There are several steps to the co-registration with MetImage:

- First, resample the MetImage image to the IASI-NG imager raster assuming a nominal geometry for both instruments.
- Compute the correlation surface for different displacements of the IASI-NG imager for selected spatial windows in the MetImage image.
- Find the offsets corresponding to the maximum correlation.

The co-registration offsets are thus determined for the IASI-NG imager raster. The offsets will then be used to convert the IASI-NG sounder Instrument Point Spread Functions (IPSFs) to the MetImage raster as described in the next paragraph.

Integrated imager vs sounder registration

There are several steps to co-register the sounder to the integrated imager.

- Generate, for the sounder pixels, a measurement consistent with the spectral response function of the imager.
- Compute equivalent imager measurements by integration over the image, weighting the image pixels by the IPSF centered at different positions and in a square domain corresponding to possible offsets.
- Over a number of scan lines (chosen to present high radiometric contrast) compute correlations at all offsets between the two synthetic measurements.
- Locate the position of maximum correlation and refine the offset values by fitting a second degree surface to the vicinity of the maximum.

This operation characterises instrument misalignments caused by launch stresses and aging. The process will be carried out during Cal/Val and monitored periodically, with adjustments made as required.

Geometric and time annotations

The computation of geometric annotations is straightforward given the METOP-SG orbit and attitude data.

Chapter 4

Construction of L1c data files and their dissemination

This chapter describes the required contents of the L1c data files, in terms of additional meta data provided with the spectra, and the expected process of dissemination to the users. At the present time, it is too early to define the L1c explicitly, and certainly we do not yet know what bandwidth restrictions will be at the time of launch, or whether more flexible arrangements for data dissemination will exist (for example enabling users to generate a tailor-made “L1c” file on a EUMETSAT facility before dissemination). We therefore focus on user expectation, such that areas requiring additional resourcing can be identified at the earliest opportunity.

4.1 Scene processing

This section discusses scene processing applied to the IASI-NG data to aid users in data selection. For IASI, useful information regarding sub-pixel heterogeneity, including the presence of cloud, is available from the collocated AVHRR imager. For IASI-NG, we expect similar information to be provided from MetImage.

Scene processing for IASI-NG should ensure provision of:

- Quality Control Flags
- Sub-pixel heterogeneity information
- Cloud/aerosol detection
- Land/Sea/Ice mask

4.1.1 Quality Control Flags

It is expected that flagging for IASI-NG should be similar to that of IASI, with an overall indicator of quality by Band, and additional flags that describe the reason for the scene to be rejected. In the case that data are disseminated via a compressed method, an indicator of the quality of the reconstructed spectrum relative to the original spectrum should also be provided.

4.1.2 Sub-pixel heterogeneity

Information on scene heterogeneity should build on the IASI heritage. The L1c data should contain the results of an unsupervised radiance classification of MetImage scenes within the field of view, providing the mean and standard deviation of each MetImage channel within the field of view in each cluster. Requirements for the radiance classification include:

- The channels used to classify the scenes should be consistent between day and night scenes, and avoid the use of channels that may not be available in the case of limited data dumps.
- The mean and standard deviation should additionally be provided for channels that were not used for the radiance classification.
- Up to seven classes should be provided.
- If bandwidth is sufficient, and processing time is negligible, a map of which cluster each MetImage pixel falls into should also be provided.

For IASI, the radiance scene classification is performed for all four pixels within the same FOV simultaneously. For IASI-NG, applying to all pixels simultaneously would mean 16 rather than 4, and a 50 km area rather than 25 km. This would increase the heterogeneity of the full scene considerably. Further research should be undertaken to determine whether this is acceptable, or whether each 12 km pixel should be processed independently.

In the absence of MetImage, a measure of sub-pixel heterogeneity could be established using the IASI-NG imager, but because this imager is not multi-channel the level of sophistication of the measure will be much less.

4.1.3 Cloud/Aerosol Detection

The IASI L1c BUFR product used by NWP centres contains a single cloud variable based on analysis of the AVHRR pixels located within each IASI pixel. The cloud variable reports the percentage of AVHRR pixels within the IASI footprint that are declared cloud-free. This information is very useful if the user is searching for scenes which can be declared unaffected by cloud with a high certainty, but is of limited use for applications that aim to use information from above the cloud top, such as NWP. The AVHRR cloud flag is based on three tests combined into a single cloud flag. For IASI-NG, the equivalent cloud detection will be based on MetImage, but a more sophisticated algorithm will be used, combining information from a series of seven tests into one cloud flag. ISSWG has endorsed the provision of enhanced information compared with the product provided for IASI. The information to be incorporated into the IASI-NG product from MetImage is described in the MetImage ATBD.

At the present time, it is believed that aerosol detection from MetImage is likely to be unreliable; however, more research into a reliable aerosol detection algorithm based on MetImage data for quick quality flagging of IASI-NG data, similar to the anticipated cloud flagging, would be welcomed by the community.

In terms of cloud or aerosol information derived from IASI-NG itself, it is anticipated that users will each want to develop their own cloud detection methods, and that there would be little appetite for an IASI-NG cloud flag based on the spectra. The information regarding the heterogeneity of the cloud detected within each pixel, and of the scene itself, is much more likely to be of use to L1c users.

4.1.4 Land/Sea/Ice mask

It is anticipated that the fraction of MetImage pixels falling into each surface type category will be provided as part of the IASI-NG meta-data, according to algorithms applied early in the MetImage processing chain.

4.2 Dissemination of L1c data files

Although bandwidth available for dissemination of L1c data files is at present unknown, it is expected that for many users some form of data compression will be applied to the main data feed. At the present time it is expected that Principal Component (PC) compression is the most likely form of data compression where information from across the full spectrum is required. Nevertheless, for some users the application of a smoothing algorithm is unappealing and they are likely to want to receive unprocessed spectral information. For applications focused on particular spectral lines, for example chemistry applications, it may be sufficient to disseminate portions of the spectrum.

At recent meetings, EUMETSAT have mentioned various approaches that may be possible to provide users with a more tailored data flow. Such suggestions have included:

- A high-reliability compressed data stream, coupled with a non-guaranteed full-resolution spectrum data stream available on a best-endeavours basis.
- Investigation of different types of processing facility, including use of the GEANT network (<http://www.geant.org>).
- Provision of computing facilities to users that enable each centre to create its own dataset prior to dissemination.

Although it is not anticipated that the last of these would be available on the timescale of the EPS-SG satellite launch, IASI-NG users welcome such investigations by EUMETSAT and encourage their continuation.

The IASI dissemination to non-EUMETCast near-real-time users via the GTS employs a selection of 500 sparse channels. Further insight should be sought from the GTS community as to whether they would prefer sparse channels for IASI-NG or a compressed data set such as PC scores.

4.2.1 Data representation and compression

For IASI, in the level 1 processor, the level 1b and level 1c radiances are initially computed as floating point numbers (resulting from Fourier Transform operations) and then converted to integer representation. Following this, “scaled radiances” are stored in 16-bit words at both level 1b and level 1c. The scaling factors are simple powers of 10, and up to ten different scaling factors are possible, depending on wavenumber. The same scheme is used in the BUFR data that are distributed to NWP centres.

Choice of scaling factor is important. If the dynamic range of the scaled radiance values is too small, information is lost (i.e. quantisation noise approaches or exceeds instrument noise). But if the dynamic range is too high then the ability to compress the data is degraded (Atkinson, 2013a; 2013b). The ideal is to keep quantisation noise about a factor 10 below instrument noise, bearing in mind that the RMS quantisation noise is equal to the digitisation step divided by $\sqrt{12}$. This suggests that it would be beneficial to have more control over the scaling factors than is the practice for IASI, e.g. one value per spectral point.

Another important consideration is that for apodised radiances the instrument noise is not a simple function of wavenumber, it is a covariance. Some users may wish to convert apodised 1c radiances back to self-apodised, or even unapodised form. It is important that digitisation process does not degrade the ability to transform apodised radiances back to self-apodised form.

It is recommended that the scheme to be used for IASI-NG is examined critically in this regard: (i) look for any evidence of the spectra being damaged by the digitisation process, and (ii) confirm that the expected compression is achieved. Note that BUFR-encoding is an effective way of producing compressed datasets.

4.2.1.1 BUFR encoding and dissemination

NWP centres currently receive BUFR-encoded IASI radiance data and it is assumed that NWP centres will also require IASI-NG data in BUFR.

For IASI level 1c, there are several different BUFR sequences in circulation:

3-40-001: superseded in 2010. 8700 channels (unused channels set to zero)

3-40-007: in use from 2010. 8700 channels. Includes additional quality information

3-40-008: Used by DBNet (e.g. EARS-IASI) and in the global distribution of Principal Component scores. Includes channel subset and/or PC scores. The number of channels/PCs is set by delayed replication.

3-61-207: Used internally by NOAA. Similar to 3-40-001 but the number of channels is set by delayed replication.

As well as different BUFR sequences, there are datasets with different channel selections:

- Full set of channels
- The EUMETSAT recommended selection of 500 channels (was originally 314, later increased to 366)
- A NOAA selection of 616 channels (only limited overlap with the EUMETSAT set).

As a result of these multiple formats, we have the unfortunate situation that NOAA cannot use the standard DBNet IASI product, and the DBNet system cannot use data tailored for NOAA. (Note that it is not possible to use the full-channel product for DBNet because of limited dissemination bandwidths in some parts of the world). One solution would be to disseminate PC scores and then each centre can generate their own reconstructed radiances, but such a solution is not currently seen as acceptable.

This highlights the fact that for IASI-NG a more coordinated approach is needed, with sample BUFR data being made available well before the launch of the first IASI-NG. Furthermore we note the recommendation of the WMO (2015):

Any products exchanged inter-regionally shall be at channel subset of level 1 radiances, optionally supplemented with Principal Component (PC) Scores that allow a reconstruction of the full spectra with minimal loss of information. The definition of the set of selected channels for each of the hyperspectral sounders as well as the selection of the appropriate PC score representation is performed by the agencies, in consultation with users, according to the following table ... [see table in the document]

In other words, responsibility for the IASI-NG channel selection, for datasets subject to international distribution, lies with EUMETSAT. Agencies should be encouraged to adopt the EUMETSAT recommendation.

Detailed design of the BUFR sequence is beyond the scope of this document. However, it does need careful design in order to ensure effective use of scaled radiances, scaling factors, etc. ISSWG request that proposals for the BUFR sequence for Level 1c and 1d products are assessed by the group and other key users early in the definition of the product, such that feedback can be made in a timely manner.

4.2.1.2 Principal Component compression

Despite many attempts by the ISSWG to stimulate research into lossless compression, there have been very few promising lines of investigation for IASI. It is therefore expected that PC compression remains the most likely algorithm to be applied to IASI-NG data.

EUMETSAT have outlined a proposal for the construction and update of an eigenvector basis for PC-compression of IASI-NG data. Unlike for IASI, the proposal for IASI-NG is to continually update the covariance matrix from which the eigenvector basis is determined. Periodic updates are proposed.

Careful thought needs to be given to the frequency of update of the eigenvector basis, because it is likely that items such as assumed noise covariance matrices, and possibly even channel

selections, may need updating following a change of eigenvector basis. It is vital that users are informed well in advance of each update. ISSWG requests a proposal for how such updates will be notified and performed.

4.2.2 Considerations for direct broadcast

It is important that differences between direct readout data (including that disseminated by retransmission services such as EARS-IASI) and the global data stream are kept to a minimum. WMO (2015) recommends that “brightness temperature products derived from both paths agree within tolerances that are not greater than few tenths (goal is 10 %) of the respective performance requirements for bias error at a reference brightness temperature.” For IASI-NG, as described in chapter 3, more processing will be done on the ground than onboard the satellite. Thus more software will be required at direct readout centres, compared with IASI, in order to ensure that the data are fully calibrated. In practice, it is not envisaged that this will be a problem, because provision of direct broadcast processing software (level 0 to level 1) is a formal requirement for all the EPS-SG sounder instruments.

Note also that, as with IASI, the software and supporting data updates are likely to be have different origins, e.g. CNES for level 0 to level 1c processing and EUMETSAT/NWP SAF for data formatting (e.g. BUFR encoding and/or generation of Principal Component scores). ISSWG requests a proposal for how these updates will be managed.

4.2.3 Provision of adequate meta-data including noise specifications

EUMETSAT must make available to users the latest estimates of instrument noise. ISSWG request a proposal for how this information is to be made available to users.

4.3 Reprocessing: storage of metadata

It is expected that periodic changes to calibration parameters and software improvements will improve the quality of the IASI-NG data. Reprocessing of archived L1c data will be required to provide the best quality data for climate studies. There is wide agreement that all original Level 0 data (i.e. the data received on the ground directly from the satellite) should be archived, along with any calibration datasets and other metadata, to allow full reprocessing at any time in the future.

4.4 Remapping

There will be a need to remap IASI-NG data onto the grid of other instruments (or vice versa) for many applications, for example combined microwave/infrared retrieval schemes. For anticipated applications, the main instruments for which such remapping will be required are MWS, MetImage, and Sentinel 5. It is anticipated that there will be no provision of remapped data by EUMETSAT, and that this processing will be done by the user, with packages such as AAPP. Note that MetImage is used in the geolocation of IASI-NG and for scene characterisation of L1c data and thus collocation of the footprints is already done for this purpose. Summary data derived from MetImage will be made available as part of the IASI-NG L1c product, as described in section 4.1.

4.5 Information channels

Users need to be kept informed of changes to the data, enhanced features, and problems with the instruments. The EUMETSAT User Notification Service has been used to keep users informed with instrument problems, planned satellite manoeuvres and new data product launches. However, users are often concerned that the level of information available from the UNS is insufficient. Many users rely on additional information provided by contacts at CNES and EUMETSAT. ISSWG requests that EUMETSAT consider how to keep users informed about instrument health, and help them prepare for changes to datasets that they use.

In addition, the availability of reference information is of paramount importance. The reference information for IASI is scattered, and in some cases it has been declared to be confidential and removed from public access. It is important that all required reference materials for IASI-NG are made fully available and are easy for users to locate. Details of all processing algorithms applied to the data for inclusion in Level 1 data products must be documented centrally and the documentation needs to be maintained in the public domain and held in English. ISSWG undertakes to collate such documents as we feel are required by users; these documents can be held for ISSWG purposes on the ISSWG members website. In due course, all reference documents must be available to all users, and ISSWG request that EUMETSAT make it a priority to ensure that such documents are indeed made available.

Part II

Science Plan

Chapter 5

Radiative Transfer and Spectroscopy

5.1 Radiative transfer modelling for IASI-NG

The exploitation of IASI-NG satellite radiance data requires the use of an accurate radiative transfer (RT) model to simulate radiances from an input state vector that consists of atmospheric and surface parameters. There are two main types of radiative transfer models for IASI-NG. The first type comprises the computationally expensive line-by-line (LBL) models which use first principles of physics to accurately simulate atmospheric transmittances and radiance spectra at a spectral resolution much higher than the instrument resolution. LBL models can be coupled to full scattering codes to simulate the radiative effects of atmospheric scattering due to particles like aerosols, water droplets and ice crystals. Alongside full LBL models, pseudo LBL models have been developed that are more computationally efficient but less accurate than full LBL models. The second type comprises fast RT models, which are generally based on LBL models. Fast RT models use computationally efficient parameterisations that allow them to simulate radiances at a fraction of the cost required by a LBL model. Fast RT model models can reproduce LBL radiances to an accuracy typically below the instrument noise and their computational efficiency fulfils the NWP requirement of near-real time monitoring and assimilation of satellite radiance data. In general, fast RT models can be used for any application where the computational cost of a LBL model would be prohibitively expensive. Many fast RT models have the capability of simulating radiances in a scattering atmosphere and most of them cover a wide region of the electromagnetic spectrum from the microwave to the infrared. The latter capability is of fundamental importance for NWP applications where the same fast model should ideally be used for all operational sounders (e.g IASI-NG, MTG-IRS, MWS, MetImage). In addition, current NWP assimilation techniques require that operational fast models are also capable of performing the fast computation of the gradient (Jacobian) of the radiances with respect to the state vector variables (e.g. temperature, constituent profiles and surface parameters). A list of the current state-of-the-art radiative transfer models and their details are given in table 5.1 and table 5.2.

5.1.1 Line-by-line models

For IASI-NG, LBL models can be used for any application that requires the accurate calculation of atmospheric radiances and transmittance at high spectral resolution. Because LBL models are too computationally expensive, their use is limited to not-real time applications. LBL models are typically used to generate the large databases of atmospheric radiances and transmittances required for the training and the validation of the parameterised schemes used in fast RT models.

The list of available LBL models include, among others, GENLN2 (Edwards, 1992), KOPRA (Stiller, 2001), LBLRTM (Clough et al., 2005), RFM (Dudhia, 1997), STRANSAC (Scott, 1974). LBL algorithms divide the atmosphere into a number of layers which should be chosen thin enough to be considered homogeneous. Once the absorber amount of each radiative molecule present in the layer has been specified, representative values for temperature and pressure in the layer are used to compute the absorption coefficient for each point of a chosen spectral

| Name | Last Version | Spectroscopy | WV cont. | Line Mixing | Variable gases | Jacobians | Freely Available |
|-------------------|--------------|-----------------|-------------|-----------------------------------|--|-----------|------------------|
| LBL | | | | | | | |
| LBLRTM | 12.2 | HITRAN08 | MTCCKD2.5.2 | CO ₂ , CH ₄ | All from spectroscopy | Yes | Yes |
| KOPRA | | Own model | Own model | CO ₂ | All from spectroscopy | Yes | Yes |
| RFM | 4.34 | HITRAN12, GEISA | | CO ₂ , CH ₄ | All from spectroscopy | Yes | Yes |
| Pseudo-LBL | | | | | | | |
| 4A/OP | 2012 | GEISA2011 | MTCCKD | CO ₂ | All from spectroscopy | Yes | Yes |
| FORLI | | HITRAN | | | All from spectroscopy | Yes | No |
| kCARTA | 1.16 | | | | All from spectroscopy | Yes | Yes |
| σ -IASI | | | | | All from spectroscopy | Yes | No |
| Fast | | | | | | | |
| RTTOV | 11.2 | LBLRTM12.2 | MTCCKD2.5.2 | CO ₂ , CH ₄ | H ₂ O, O ₃ , CO, N ₂ O, CH ₄ , CO ₂ | Yes | Yes |
| CRIM | 2.2.3 | LBLRTM | | | | Yes | Yes |
| OSS | | LBLRTM | | | | Yes | No |
| HT-FRTC | | | | | All from spectroscopy | Yes | No |
| PCRTM | | | | | | Yes | No |
| PC-RTTOV | RTTOV11.2 | LBLRTM12.2 | MTCCKD2.5.2 | CO ₂ , CH ₄ | H ₂ O, O ₃ , CO, N ₂ O, CH ₄ , CO ₂ | Yes | Yes |

Table 5.1: Details of the current state-of-the-art radiative transfer models

| Name | Scattering | NLTE | Solar | Range | Website | Reference | Comments |
|------------------------|------------|------|-------|-----------|---|-------------------------------|-----------------------------|
| LBL | | | | | | | |
| LBLRTM | No | Yes | | MW-IR-VIS | http://rtweb.aer.com/lblrtm.html | Clough et al. (2005) | |
| KOPRA | No | Yes | | IR | https://www.imk-asf.kit.edu/english/312.php | Stiller (2001) | |
| RFM | No | Yes | | MW-IR | http://www.atm.ox.ac.uk/RFM/ | Dudhia (1997) | |
| Pseudo-LBL | | | | | | | |
| 4A/OP | Yes | No | | IR-VIS | http://4aop.noveltis.com/ | Scott and Chedin (1981) | |
| FORLI | No | No | | IR | | Hurtmans et al. (2012) | |
| KCARTA | No | Yes | | IR | http://asl.umbc.edu/pub/packages/kcarta.html | DeSouza-Machado et al. (1998) | |
| σ -IASI Fast | Yes | | | IR | | Amato et al. (2002) | |
| RTTOV | Yes | Yes | Yes | MW-IR-VIS | https://nmpsaf.eu/deliverables/rtm/index.html | Matricardi et al. (2004) | Coupled with surface models |
| CRTM | Yes | Yes | | MW-IR | http://ftp.emc.ncep.noaa.gov/jcsda/CRTM | Han et al. (2006) | Coupled with surface models |
| OSS | Yes | | | IR | http://rtweb.aer.com/oss_frame.html | Moncet et al. (2008) | |
| HT-FRTC | Yes | | | MW-IR-VIS | | Havemann et al. (2014) | |
| PCRTM | | | | | | Lin et al. (2006) | |
| PC-RTTOV | Yes | Yes | Yes | IR | https://nmpsaf.eu/deliverables/rtm/index.html | Matricardi (2010) | Coupled with surface models |

Table 5.2: Further details of the current state-of-the-art radiative transfer models

grid whose spacing should be of the order of $2 \times 10^{-2} \text{ cm}^{-1}$ for a gas at atmospheric pressure down to $2 \times 10^{-4} \text{ cm}^{-1}$ for absorption in the middle atmosphere. Using the length of the path across the layer, the absorption coefficient is converted into the corresponding optical depth and by combining the contribution of all radiating species the corresponding profile of atmospheric transmittances can be easily obtained from Lambert's law.

The computation of the absorption coefficient requires the knowledge of the molecular parameters (e.g. line position, strength, half width) of the absorption/emission lines associated with all known discrete molecular transitions of each atmospheric molecule. The accuracy of molecular parameters is of crucial importance for high resolution sounders like IASI-NG. Infrared line parameters can be obtained from the HITRAN (Rothman et al., 2013) and GEISA (Jacquinet-Husson, N. and others, 2011) databases (see section 5.5.1). Both databases are regularly updated and they not only contain parameters for lines that have been measured in the laboratory but also calculated values for lines that have not been measured yet. For heavy molecules line data are typically not available. To model the absorption of these molecules, LBL models use cross section data which for accurate calculations should be temperature and pressure dependent.

In conjunction with the line parameters, the computation of the absorption coefficient also requires the specification of the line shape which should describe the effects of pressure and Doppler line broadening. The molecular line shape commonly used in LBL models is a Voigt profile, i.e. a convolution of Lorentzian (pressure-broadened) and Gaussian (Doppler-broadened) contributions. The simplified assumptions on which the Voigt profile is based (e.g. the collisional parameters are independent from the velocity of the absorber) can negatively affect the accuracy of the simulated spectra. There is thus the need for a better representation of the line shape than the Voigt profile. Proposed replacements to the Voigt profile (Ngo et al., 2014, e.g.) will require different broadening coefficients for all the molecules and consequently the need for significant updates to LBL models. Recently it has been recommended by IUPAC that the partially Correlated quadratic-Speed-Dependent Hard-Collision Profile (pCqSD-HCP), or more simply the Hartmann-Tran profile (HTP), should be adopted as the appropriate model for high-resolution spectroscopy ((Tennyson et al., 2014)). High resolution sounders like IASI-NG allow the use of channels placed between spectral lines. These channels have weighting functions that are sharper than the weighting functions that characterise the channels placed on top of the spectral lines and consequently particular attention must be paid to the spectral line shape of species like water vapour and carbon dioxide for which optical depths in the atmosphere can reach very large values.

The effect of line-mixing (i.e. the change in line shape due to the redistribution of radiation in over-lapping spectral lines) in the carbon dioxide Q-branch lines (Rodrigues et al., 1998; Strow and Reuter, 1988) is now routinely incorporated in LBL algorithms and in the recent past progress has been made in the development of improved carbon dioxide line shapes by taking into account the effect of line-mixing in carbon dioxide P/R-branches (Niro et al., 2005, e.g.). It should be noted that because of the symmetry of the states involved in the molecular transitions, P/R-branch line mixing in the CO_2 ν_3 region between 2200 and 2300 cm^{-1} is expected to be twice as strong as in the ν_2 region between 700 and 750 cm^{-1} . Line-mixing effects can also alter the spectral shape of the ν_3 (3000 cm^{-1}) and ν_4 (1300 cm^{-1}) absorption bands of methane (Tran et al., 2006) and there is evidence of line mixing for a very limited number of transitions in the P and R branches of the water vapour ν_2 band centred at 1594 cm^{-1} (Brown et al., 2004). State-of-the-art LBL models (e.g LBLRTM) already incorporate all above effects. Although line mixing effects have also been studied for N_2O infrared spectra (e.g. Rachet et al., 1996), N_2O line mixing has not yet been introduced in LBL models. For all cases discussed above, line-mixing coefficients are generally computed using first order perturbation theory which is considered adequate for most applications.

The difficulty of achieving good measurements of water vapour amounts in the atmosphere and in the laboratory is still hindering progress in the development of improved water vapour line shapes further from line centres where a slowly varying (with wavelength) continuum absorption is observed. For instance, long paths with relatively cool temperatures (e.g. around 260 K) are common in the atmosphere but are difficult to simulate in the laboratory as comparable column amounts of WV have to be produced in a smaller volume with practical limitations due to liquid water condensation. Consequently, the nature of water vapour continuum absorption and its effect on atmospheric radiance is still an outstanding and unresolved issue (e.g. Ma et al., 2008). A unifying theory of the water continuum is still lacking, with competing formulations based on the far wings of allowed transitions of the water monomer (Ma et al., 2008) and on the existence of bound water complexes known as dimers (Ptashnik et al., 2011). A revived interest in dimers has seen some recent papers (Vaida et al., 2001) suggesting an important role for dimers in contributing to atmospheric absorption optical depths. Although in principle the adoption of a physically based approach to the treatment of the water continuum absorption should be sought, it is not yet clear whether the science is mature enough. Thus, because of the uncertainty of the cause of the continuum, semi-empirical parameterisations of water vapour continuum have been developed based on laboratory and aircraft measurements. These parameterisations of the continuum have evolved from the Clough-Kneizys-Davies (CKD) model (Clough et al., 1989) to the Mlawer-Tobin_CKD (MT_CKD) (Clough et al., 2005) model, the latter being used in the vast majority of LBL models. The MT_CKD model is based on the assumption that the continuum absorption in water vapour bands is dominated by the collision-induced absorption resulting from the generation of a short lived complex of water vapour and colliding molecules. The MT_CKD model has been used successfully for many years in atmospheric radiative transfer codes, and is capable of reproducing many of the observed water vapour features in the mid-infrared spectral region. Radiative closure studies such as those by Turner (2004) and Delamere et al. (2010) have constrained the MT_CKD continuum model to improve the parameterization in some spectral intervals, leading to a demonstrable improvement in the ability to simulate the terrestrial infrared spectrum. Some issues, however, still remain. For example, the temperature dependence of the continuum has been found not to be well captured when compared with recent laboratory data (Baranov et al., 2008; Paynter et al., 2009). MT_CKD also appears to underestimate the strength of the continuum in some high transmittance atmospheric windows by as much as an order of magnitude (Paynter et al., 2009). It should be stressed that when implementing the MT_CKD continuum in a LBL model, care should be taken to ensure that the line absorption (especially cut-off) is combined with the continuum component in a consistent manner.

The development of models of the water vapour continuum such as MT_CKD have relied on high accuracy measurements of the thermal infrared radiance spectra along with well characterised measurements of the thermodynamic state of the atmosphere. A recent study by Newman et al. (2012b) reported on data gathered by field campaigns involving the UK Facility for Airborne Atmospheric Measurements research aircraft which collected a comprehensive dataset, comprising remotely sensed infrared radiance observations collocated with accurate measurements of the temperature and humidity structure of the atmosphere. These field measurements were used to validate the strength of the infrared water vapour continuum in comparison with the latest laboratory measurements. The recent substantial changes to self-continuum coefficients in the widely used MT_CKD model between 2400 and 3200 cm^{-1} were shown to be appropriate and in agreement with field measurements. Results for the foreign continuum in the 1300–2000 cm^{-1} region suggested a weak temperature dependence that is not currently included in atmospheric models. A one-dimensional variational retrieval experiment was performed that showed a small positive benefit from using new laboratory-derived continuum coefficients for humidity retrievals.

The MT_CKD model also accounts for the continuum contribution due to carbon dioxide, oxygen and nitrogen. The collision-induced bands of oxygen at 1600 cm^{-1} and nitrogen at 2350 cm^{-1} are included as broad-band continuum contributions to the absorption using the models by Tibault et al. (1997) and Lafferty et al. (1996) respectively. For CO_2 , like for water vapour, the continuum is used to include the contribution to the absorption due to far wings. It should be noted, however, that, due to the presence of line-mixing effects, the parameterization used for the CO_2 continuum absorption is different from that used for water vapour.

LBL models compute the absorption due to minor isotopologues of a molecule using the fractional abundances of the minor isotopologues relative to the abundance of the major isotopologue of that molecule. These fractional abundances are consistent with those used in the molecular databases. In practice, the actual isotopic ratios may differ from the default values used in the LBL calculations. This can potentially affect the accuracy of the simulations in spectral regions where isotopologues have substantial absorption features. It is then important that isotopic ratios are correctly specified. Moreover, isotopic ratios can exhibit significant variations in space (horizontally and vertically) and time. This is certainly the case for water vapour and it could eventually mean that in order to model vertically-varying water vapour isotopic ratios, water vapour isotopologues should be treated as separate molecules in the LBL computations. An effort in that direction has already been undertaken within the framework of the GEISA database which will soon include HDO as a separate molecular specie.

The improved IASI-NG noise figure in the short wave should facilitate the exploitation of the excellent temperature sounding channels present in that region of the spectrum. A possible obstacle is represented by the presence of non-local thermodynamic equilibrium (non-LTE) and solar effects which, if not accounted for, could result in errors in excess of 20 K. Most LBL models can accurately simulate non-LTE effects as long as different vibrational temperature profiles for different vibrational states and different isotopes can be externally specified. Progress has also been made towards the treatment of non-LTE effects using parameterised schemes (Chen et al., 2013). Regarding the simulation of solar effects, a crucial element is the specification of the surface spectral bi-directional reflectance of solar radiation.

5.1.2 Pseudo line-by-line models

Alongside LBL models, pseudo LBL models have been developed where monochromatic absorption coefficients are computed using a database of look-up tables created using a full LBL model. Because the monochromatic absorption coefficient varies slowly with temperature and is directly proportional to the absorber amount, the monochromatic absorption coefficients stored in the look-up table can be interpolated in temperature and modified for changes in absorber amount to give the most appropriate absorption coefficients for a given profile. Typically, pseudo LBL models have the same capabilities of LBL models and their accuracy is comparable to that of the underlying LBL model. Under general conditions (e.g. non scattering atmosphere in LTE) they can perform calculations up to two orders of magnitude faster than LBL models. Available pseudo LBL models include 4A/OP 2012 (Scott and Chedin, 1981), FORLI (Hurtmans et al., 2012), kCARTA (DeSouza-Machado et al., 1998) and σ -IASI (Amato et al., 2002). It should be noted that despite their speed advantage over LBL models, many pseudo LBL models are not yet considered fast enough to be used in near-real time applications. FORLI, which is not just an RT model, but includes retrieval codes also, is used in near-real time.

5.1.3 Narrow-band fast RT models on fixed pressure levels or on levels of fixed absorber amount

There are several types of fast RT models, in use or under development, that are relevant to IASI-NG applications. One type comprises fast RT models that use regression coefficients derived from accurate LBL computations to compute atmospheric optical depths as a linear combination of profile dependent predictors that are functions of temperature, absorber amount, pressure and viewing angle. The regression coefficients are computed using a training set of typically less than 100 diverse atmospheric profiles chosen to represent the range of variations in temperature and absorber amount found in the atmosphere. The optical depths can be computed at fixed pressure levels as in the RTTOV (Matricardi et al., 2004) and SARTA (Strow et al., 2003) models or at levels of fixed absorber amount as in the OPTRAN model (McMillin et al., 1995). These models use the polychromatic form of the radiative transfer equation (i.e. they use channel averaged transmittances in the radiative transfer equation based on the assumption that this is equivalent to the convolution of the monochromatic radiances). The polychromatic approximation is more than adequate for IASI-NG because the width of the channels is narrow enough that the convolution of the Planck function can be replaced with its value at the central wave number of the channel with no practical loss of accuracy. The CRTM model (Weng et al., 2005) offers the possibility of using either the fixed pressure level or the fixed absorber amount approach.

The RTTOV model is used in a number of operational NWP centres and satellite agencies and consequently it can be anticipated that it will be extensively used for IASI-NG applications. The most recent version of RTTOV (RTTOV-11, Saunders et al., 2013) is based on LBL computations performed using version 12.2 of the LBLRTM model which incorporates version 2.5.2 of the MT_CKD continuum model. The database of molecular parameters is largely drawn from HITRAN_2008 (Rothman et al., 2009) with customised updates. Radiative molecules included in the RTTOV underlying LBL computations include H₂O, CO₂, O₃, N₂O, CO, CH₄, O₂, NO, SO₂, NO₂, HNO₃, OCS, N₂, CCl₄, CFC-11, CFC-12 and CFC-14. It should be noted that at present RTTOV only allows the variation of the concentrations of H₂O, O₃, CO₂, N₂O, CO and CH₄. Although in principle the number of variable gas species could be increased based on specific applications, this will require an appropriate set of training profiles for each single species and the computation of dedicated regression coefficients.

RTTOV has the capability to include the effects of solar radiation (Matricardi, 2003) and non-LTE. The latter is parameterised using the scheme adopted in the CRTM model (Chen et al., 2013). In addition, RTTOV can also perform computationally efficient radiative transfer computations in a scattering atmosphere (Matricardi, 2005) using a parameterisation of multiple scattering based on the approach by (Chou et al., 1999). RTTOV includes optical properties of aerosols, water droplets and ice crystals. Optical properties of aerosols and water droplets are derived from the Lorenz-Mie theory using the microphysical properties available from the OPAC database (Hess et al., 1998). Optical properties of ice crystals are calculated using the Geometric Optics and T-matrix methods and are parameterised as a function of ice water content, temperature and effective size of the ice particle and are available for two different ice crystal shapes: hexagonal and aggregates. The most recent version of RTTOV, RTTOV-11, includes two additional aerosol types (Asian dust and new volcanic ash) and a new parameterisation of bulk ice crystal optical properties (Vidot et al., 2015) derived from the database assembled by (Baran et al., 2014).

5.1.4 Library look-up based fast RT models

These fast RT models are based on the library look-up approach (e.g. 3R; Rapid Radiance Recognition Chedin et al., 1985). They make use of an extensive library of profiles and associated radiances created from a collocation dataset. The fast model matches the input profile with one or a group of profiles in the library and then computes a radiance spectrum using the spectra associated to the matched profiles.

5.1.5 Neural network based fast RT models

Neural network based schemes have been developed for radiative transfer modelling applications (e.g. Chevallier et al., 2000) and their computational efficiency could mean that their use could be in principle extended to the simulation of IASI-NG spectra. An artificial neural network realizes a nonlinear application from an input space (e.g. atmospheric parameters) to an output space (e.g. atmospheric radiances). The development of a neural network based fast RT model requires the selection of learning datasets of atmospheric situations for all the variables that are included in the radiative computations. The accuracy of the scheme hinges on the statistical characteristics of these datasets. Several thousand atmospheric profiles are typically required for this purpose. The training of a neural network based fast model involves the accurate simulation of the radiances associated to each atmospheric situation. This task should be carried out using an accurate LBL model. Although the learning process is very time consuming, it should be noted that it has to be done only once unless the training has to be repeated due to a change in the vertical discretisation of the atmosphere. Ideally, the development a neural network based fast RT model should include the capability of performing radiative transfer computations in an atmosphere with scattering, solar and non-LTE effects.

5.1.6 Fast RT Models based on optimal sampling of absorption coefficients

The Optimal Spectral Sampling method (Moncet et al., 2008) approximates spectrally integrated (i.e. polychromatic) radiances (or transmittances) with a weighted average of monochromatic radiances (or transmittances) calculated at a selected number of spectral points. The OSS approach is an extension of the k-distribution technique to vertically inhomogeneous atmospheres. OSS is a fast method that allows to perform accurate radiative transfer computations for a wide range of applications. The training of OSS involves LBL computations carried out for a range of representative atmospheric situations. The OSS method can be easily extended to scattering atmospheres and can be in principle applied to any linear transformation of the spectral space (e.g. principal components). Having mentioned the k-distribution technique, it should be noted that this approach has recently been exploited by Doppler et al. (2014) in the MOMO model which can simulate the whole infrared spectrum. Whilst these models are computationally efficient and accurate, it is yet to be proven that they have an obvious advantage (in terms of speed and accuracy) over narrow-band fast RT models like RTTOV.

5.1.7 Principal Component Based Radiative Transfer Models

IASI-NG will have twice as many channels as IASI. Because the computational time required by conventional fast RT models like RTTOV is proportional to the number of simulated channels, there is the need for a more computationally efficient simulation of hyperspectral sounder radiances. This can be achieved by fast radiative transfer models based on principal components (PC) because they only require the simulation of the leading (typically less than 300) PC of the spectrum. A number of PC based radiative transfer models have been developed, namely the PC Radiative Transfer Model (PCRTM; Liu et al., 2006), the Havemann-Taylor Fast Radiative Transfer Code (HT-FRTC; Havemann, 2006; Havemann et al., 2014) and PC-RTTOV

(Matricardi, 2010). The HT-FRTC is the most general of these models because it covers the complete electromagnetic spectrum from the microwave through to the ultraviolet and allows the variation of profiles of temperature, water vapour and all the trace gas species available in the HITRAN compilation. PCRTM, PC-RTTOV and HT-FRTC are capable of performing RT simulations over many different surface types and in a scattering atmosphere that can include liquid clouds, ice clouds and aerosols.

The training of PC based fast RT models requires the computation of a large database of LBL spectra for a diverse set of atmospheric and surface situations. The training spectra are assembled in a large matrix from which the PCs of the radiance spectra are computed by applying singular value decomposition to the radiance matrix. Whilst the principal components are fixed, their scores (weights) vary from profile to profile and they can be predicted using a linear regression scheme where they are expressed as a linear combination of profile-dependent predictors. In PCRTM and HT-FRTC the predictors are monochromatic radiances at selected frequencies whereas PC-RTTOV uses polychromatic (channel) radiances calculated by RTTOV. The linear relationship between radiance predictors and principal component scores is established by a regression on the training data set. It should be noted that while monochromatic radiances are comparatively straight-forward to calculate, even if many trace gases are involved, the calculation of polychromatic radiances requires a more complicated and time-consuming transmittance prediction system. Havemann et al. (2014) have recently demonstrated that in the context of HT-FRTC it is possible to generate sensor-independent principal components at full line-by-line resolution allowing flexible changes regarding the specification of the instrument response function. PC based fast RT models have been employed in the retrieval of atmospheric and surface information (e.g. HT-FRTC ; Thelen et al., 2009). In the context of operational NWP data assimilation, PC-RTTOV has been successfully used at ECMWF for the testing of the direct 4D-Var assimilation of principal components derived from IASI fully clear spectra (Matricardi and McNally, 2014).

5.2 Scattering models

In addition to the clear air radiative transfer solvers, it is necessary to have scattering models for aerosols and clouds. The radiative transfer equation (RTE) in absence of scattering is readily solved by recursive evaluation of the radiance using calculated layer emissions and absorptions along the satellite viewing angle. For solving the RTE with scattering, other directions have to be taken into account too. Several algorithms are based on a Gaussian quadrature of the RTE into a number of upward and downward angles or streams.

The most widely known and used algorithms are the discrete ordinates method and the adding-doubling (AD) method which have implemented in the DISORT (Stamnes et al., 1988) and the PolRadtran (Evans and Stephens, 1991) model respectively. Examples of radiative transfer solvers with scattering that have been coupled to line-by-line models for the simulation of high resolution spectra include 4A/DISORT (e.g. Peyridieu et al., 2013), LBLRTM/AD (Moncet and Clough, 1997), AZIMUTH/LIDORT (Spurr, 2008; Vandenbussche et al., 2013) and Atmosphit/AD (Clarisse et al., 2010). It is also worth mentioning the libRadtran (Mayer and Kylling, 2005) collection of C and Fortran functions and programs for the calculation of solar and thermal radiation in the Earth's atmosphere. It allows the use of 10 different solvers, several of which are able to account for scattering, e.g. DISORT, PolRadtran and MYSTIC, a Monte Carlo solver.

For operational NWP data assimilation or retrieval applications, radiative transfer solvers with full scattering are usually too slow and have to be replaced with fast approximate methods

or parameterizations. A typical example of approximate methods is represented by two stream models. This category includes the RTSPEC (Deeter and Evans, 1998) and kTWostream models which have both been coupled to the kCARTA (DeSouza-Machado et al., 2006) pseudo LBL model. An interesting development for hyperspectral applications is represented by the fast scattering model FIRTM-AD (Zhang et al., 2007) which is based on the AD approach. It uses a pre-computed look-up table of bidirectional reflection and transmission functions and emissivities of ice clouds to significantly improve the computational efficiency of the RTE solver with a marginal degradation of the accuracy of the simulations. An example of parameterized approach to the problem of atmospheric scattering is represented by the scaling approximation which is currently being used in RTTOV (Matricardi, 2005) and AIRSRTA/SCARTA (DeSouza-Machado et al., 2010). In the scaling approximation (Chou et al., 1999), scattering is parameterized by an appropriate scaling of the clear sky layer emission and absorption. The scaling approximation has the advantage that it allows the use of clear sky RT solvers thus retaining the same computational efficiency. Although the accuracy of the scaling approximation is adequate for most applications, especially in the long wave, it should be stressed, however, that the simulation of scattering in presence of short wave solar radiation can be affected by very large errors.

5.3 Surface models

The representation of top of atmosphere radiance by infrared radiative transfer models typically includes three important contributions from the surface boundary; direct emission, surface reflection from the downwelling atmosphere, and surface reflection from solar radiation. A useful summary of the terminology used in the definitions of surface radiation can be found in (Norman et al., 1995). Various approximations to reality have been made over the years to account for the surface contribution to top of atmosphere radiance. In particular, it is assumed that infrared sensors are only sensitive to the “skin” layer depth comparable to the wavelength of the channel.

As infrared sensors have evolved from broadband 8-12 micron and 3.5-4 micron channels, to narrow bands with half a dozen surface sensing channels, to hyperspectral sensors with thousands of micro-windows that can sense between atmospheric absorption lines, the complexity of surface models have also evolved to explain the observations (Matricardi and Saunders, 1999). While the hyperspectral infrared observations provide sharper weighting functions in the mid-troposphere, it is the surface sensitive channels that contain the information about the lowest layer of the atmosphere. Error in the estimation of boundary layer temperature and dewpoint temperature is thus strongly correlated with error in the estimation of the surface emission or reflection. Roughly speaking, a 2% error in the knowledge of the land surface emissivity near 10 μm leads to an error in the derived surface temperature of about 1 K (Tobin et al., 2006). Improving the modelling of surface radiation in radiative transfer models then becomes a necessary requirement for improving the remote sensing of the atmosphere in the lowest 1 to 3 kilometres from space using passive retrieval methods. Unfortunately the Earth’s surface has a wide variety of surface types that need to be accounted for in global remote sensing from satellites. At the same time, for any given location on the Earth we now have at least a decade of quality observations that characterize the seasonal variations of surface properties and which can form the basis for a priori climatological information used as input to a surface radiation model designed to accommodate that information.

5.3.1 Surface radiation models

Surface radiation models can be separated into three classes, each of which require somewhat different implementation in radiative transfer models. The most rigorous approach is to incor-

porate a directional emission and bi-directional reflectance which are a function of sensor view zenith and azimuth angles, solar zenith and azimuth angles, and in-homogenous atmospheric conditions (e.g. clouds). However, only within the recent past have instrumentation been developed to provide reference standards for bi-direction reflectance measurements in the laboratory (Hanssen and Kaplan, 1999). This class of models has so far been implemented only on small scales, such as the modelling of a vegetation canopy on scales of 500 meters or less (Roman et al., 2011). While this can be done fairly rigorously, it has not been possible so far to scale these experiments up to the 10.000 m scales relevant for infrared satellite observations. The two practical classes of surface radiation models for satellite observations are specular and lambertian (diffuse) surfaces. The specular approximation assumes that the sensor views emission at the view angle of the sensor but the reflected energy only comes from a narrow cone at the specular angle (negative of the sensor zenith angle). Water is highly specular when there are no waves, hence sun glint is always a large contribution in satellite observation over the ocean at near-infrared wavelengths but only for certain viewing geometries. Sun glint is also observed over land in the near-infrared but only over highly reflective surfaces (e.g. deserts). Wind driven ocean waves causes non-specular effects, however these can be incorporated into the ocean emissivity model (e.g. Masuda et al., 1988; Nalli et al., 2008; Wu and Smith, 1997) and the specular assumption is assumed to continue to hold. For land and rough ice surfaces, a lambertian assumption is often used. In this approximation, the surface emission is at the sensor view angle but the reflected radiance comes from the integral of all downwelling radiance in the hemisphere above the point of interest and is weighted by the hemispheric reflectance. Clough et al. (1992) provides details on the efficient RT calculation of the hemispheric downwelling flux at the surface. For any real surface, some linear weighting between specular and lambertian (diffuse) properties should be probably be used, although the weighting factor between specular and diffuse contributions may need to be determined empirically.

5.3.2 Surface emissivity models

Emissivity is defined to be the ratio of a radiance measurement of a surface at a given wavelength to the radiance that would be produced by a blackbody, i.e. Planck radiance, at the surface temperature. The use of surface emissivity models for the characterization of satellite radiances raises the immediate question of whether either surface emissivity or surface temperature can have physical meaning for heterogeneous scenes. An analysis of this issue for high altitude aircraft and satellite observations leads to the conclusion that satellite surface emissivity can usefully be modelled as the linear combination of individual surface types, e.g. bare soil and vegetation, but the derived surface temperature from remote sensing is a non-physical effective temperature which only serves the purpose of satisfying the radiative transfer equation (Knuteson et al., 2004). In the limit where only a single surface type is present then the radiative surface temperature does represent the true surface temperature. With this important caveat in mind, current radiative transfer models implement one or both of the surface radiation models described in the previous section; specular and/or diffuse, using surface emissivity from some a priori database. Surface temperature in remote sensing applications is often a retrieved variable chosen to minimize the difference between observations and calculations for a subset of surface sensitive spectral channels specific to that sensor.

Until fairly recently a constant surface emissivity was used for most Earth infrared radiative transfer calculations (e.g. 0.98) without any spectral, spatial or temporal dependence and even without including the reflected energy from the atmospheric downwelling infrared and the sun. The advent of hyperspectral observations from the NASA AIRS and EUMETSAT IASI sensors has prompted fairly rapid progress in the improvement of radiative transfer models treatment of surface properties. For non-frozen ocean surfaces, the Masuda model as modified by Wu and

Smith provide a convenient parameterization of ocean emissivity as a function of wavenumber, wind speed, and salinity suitable for use in specular radiation models (Masuda et al., 1988; Wu and Smith, 1997). Subsequent work using satellite and aircraft observations has been performed that yield further small refinements (Nalli et al., 2008; Newman et al., 2005; Smith et al., 1996). For land surfaces a collection of laboratory measurements of terrestrial materials was begun by Salisbury and extended by others (Salisbury et al., 1994). In particular, the NASA MODIS and ASTER science teams have developed online collections of emissivity measurements of terrestrial surfaces at high spectral resolution that have proven quite valuable in characterizing the range of spectral information content (Baldrige et al., 2009). In particular, Seemann et al. (2008) used these laboratory data for guidance in the creation of a low spectral resolution and high spatial resolution atlas for sounding applications from narrow band sensors, in particular MODIS. Smith Sr. et al. (2005) and Zhou et al. (2011) have taken the further step to apply a principal component analysis to the laboratory emissivity data to extract the principle component spectra which explain the variance in the dataset. Borbas et al. (2007) used this PCA approach to create a high spectral resolution and high spatial resolution atlas which fits 5 km resolution MODIS multi-channel emissivity to the six leading principle components of high spectral resolution laboratory emissivity spectra. This can open up the opportunity to assimilate IASI surface sensitive channels over land into NWP models although much work is needed in this area to fully exploit the information contained in the infrared high spectral resolution observations. The examples given here are not intended to be comprehensive of all the recent activities in surface emissivity modelling, however they do represent a successful path forward which can be improved upon as longer measurement records with better accuracy become available. It is worth noting that in the same way that radiative transfer modelling of the gaseous absorption is limited by the accuracy and availability of laboratory measurements, the radiative transfer modelling of the surface is limited by the accuracy and the availability of laboratory measurements of terrestrial surface types. In particular, there is a real need for low-altitude aircraft observations from high performance hyperspectral sensors to characterize the most representative surface types across all continents (Sobrino et al., 2008; Thelen et al., 2009). Moreover, emissivity spectra (or equivalent principal component eigenvalues) derived from IASI data itself could in principle be folded back into the a priori information to keep the emissivity atlas up to date on weekly time scales (Zhou et al., 2011).

5.4 Models for the microphysical and optical properties of scattering particles

5.4.1 Ice clouds

The radiative transfer modelling in a scattering atmosphere is limited by the accuracy of the scattering properties of atmospheric ice. Across the IASI wavenumber range, the methods that can be used to compute the scattering properties of atmospheric ice are exclusively electromagnetic-based. This is because ice can be very absorbing at wavenumbers in the infrared, and as a consequence of the longer wavelengths in the infrared, the size parameters are generally too small for approximations such as geometric optics.

Electromagnetic methods that have or are finding wide use are based on T-matrix but applied to non-axisymmetric particles by Havemann and Baran (2001), Kahnert et al. (2001), and Kahnert (2013). More recently, the invariant imbedding T-matrix method has been “re-discovered” by Bi et al. (2013), and this extension of T-matrix can be applied to any particle shape, which could also be inhomogeneous and be of any size (limited only by available computational resources). The numerical accuracy of the T-matrix method has been tested against the Finite-Difference-

Time-Domain method by Baran et al. (2001) who found for the case of a single randomly oriented finite hexagonal ice column the T-matrix and FDTD solutions were generally within 1% of each other. The pros and cons of current electromagnetic methods have already been discussed throughout the review article by Kahnert (2010), with regard to efficiency, memory requirements and particle complexity (i.e., shape, homogeneous or inhomogeneous). A review of the application of electromagnetic and asymptotic methods and variants of those, to scattering by atmospheric ice, can be found in Baran (2012).

In atmospheric science, there is a method that has received very little attention, which is the boundary element method (BEM++) which has been developed by the group of Betcke at UCL. The application of BEM++ to far-field scattering by atmospheric ice has been achieved by Groth et al. (2015). The method, in principle, can be applied to any complex particle shape at any frequency and at any size, as long as the particle is an isotropic dielectric, homogeneous and has a Lipschitz-continuous boundary (Grisvard, 1992, Section 1.2). At the moment, if inhomogeneous particles need to be considered, then a suitable effective medium theorem needs to be applied to adjust the dielectric properties of the particle through its complex refractive index. The size of the particle also limits BEM++ to small to moderate size parameters on commonly available Linux machines with about 12 Gbyte of RAM. Currently, the computational loading of BEM++ goes as $5.5X^{2.71}$ (Groth et al., 2015), where X is the size parameter of the particle (i.e. the ratio of the circumference to the incident wavelength of an equivalent area or volume sphere, $2\pi r/\lambda$). The only limitation of BEM++, at the moment, is the computational resources available to the user. Within the framework of BEM++ the macroscopic Maxwell equations are re-written in the form of boundary integral equations on the surface of the particle. Thus, the immediate advantage of BEM is that it reduces the 3D unbounded problem to a 2D bounded problem. This reduction in dimension saves considerable computational time, but the method still requires substantial amounts of computer memory. The details of the application of BEM++ to atmospheric ice particles of varying complexity can be found in Groth et al. (2015). The accuracy of BEM++ has been tested against the standard T-matrix method of Havemann and Baran (2001) by Groth et al. (2015) and that they found that BEM++ and T-matrix solutions found for the total optical properties differed by about only 1%. Moreover, they also found that the scattering phase matrix solutions obtained from BEM++, and T-matrix were virtually indistinguishable. Of course, the examples presented in Groth et al. (2015) are for a single orientation only but scattering solutions for 3D random orientations can also be found, this will, however, considerably increase the computational time of BEM++.

The most applied electromagnetic method to inhomogeneous particles is the discrete dipole approximation (DDA), and a description of this method can be found in Zubko et al. (2008), and the publicly available DDA code is described by Yurkin and Hoekstra (2011). The other most notable electromagnetic method is of course the finite-difference time-domain method (FDTD) used by Sun et al. (1999) and developed as well as used by Yang et al. (2000). There have also been attempts of combining the desirable properties of DDA with T-matrix by Mackowski (2002), who has developed the discrete dipole method of moments (DDMM) approach, which shows promise for computing the single-scattering properties of ice crystals for size parameters of about 40.

5.4.2 Aerosols

In the infrared, the optical properties of many aerosol particles can be calculated accurately using the Lorentz-Mie theory for spherical shaped particles (Van de Hulst, 1981). However, some aerosol particles, especially mineral particles, can have highly irregular shapes. For these particles the spherical assumption can be a major source of error either in the computation of

the total radiation budget or in the retrieval of optical properties especially if the particle size is large compared to the wavelength of the radiation. For instance, in the short wave region of the infrared spectrum the spherical assumption can be a significant source of error in the computation of the phase function.

In principle, all the electromagnetic methods mentioned in section 5.4.1 could also be applied to irregular shaped aerosols, at least for a range of particle sizes. In addition to electromagnetic methods, some advanced physical optics methods are also available. These include those developed by Bi and Yang (2013). A combination methods has been used by Meng et al. (2010) and Bi et al. (2009) to compute single-scattering properties of triaxial ellipsoidal mineral dust aerosols whereas Legrand et al. (2014) and Koepke et al. (2015) have applied the T-matrix method and geometric optics calculations (Yang et al., 2007) to derive optical properties of spheroids of mineral dust.

5.5 Input data to radiative transfer models

5.5.1 Spectroscopic data

IASI-NG has been designed to improve upon satellite sounders of the current and previous generation and will allow unparalleled improvements in the retrieval of temperature and atmospheric constituent profiles both in terms of accuracy and vertical resolution. The quality of the products retrieved from IASI-NG spectra will hinge on the accuracy of the forward calculations carried out in the algorithms used in retrieval or inversion process. Thus, alongside state-of-the-art models of the line shape (see section 5.1.1 for e.g. line mixing effects, continuum effects and the Voigt profile) the full exploitation of IASI-NG data will require an accurate specification of the spectroscopic parameters used as input to LBL models because they play a major role in determining the accuracy of the forward model simulations of IASI-NG observations.

In the spectral region covered by IASI-NG, H₂O and CO₂ are among the most important molecular species. The accurate knowledge of their spectral signature is crucial for the retrieval of high quality atmospheric temperature and humidity information. For instance, a good knowledge of water vapour spectroscopy (and water vapour continuum) is of paramount importance for the optimal assimilation of hyperspectral satellite data in NWP. Water vapour sounding channels are increasingly used in NWP global assimilation schemes and errors in radiative transfer model computations will degrade the ability to retrieve humidity accurately. In addition, water vapour channels with high-peaking Jacobians, or weighting functions, are of interest in acting as anchoring channels for upper troposphere/lower stratosphere humidity, where the current generation of NWP models shows relatively large humidity biases (Hilton et al., 2012b). There is thus a pressing need to improve and consolidate the databases of spectroscopic parameters (and of course the LBL models that use them). In that respect, a fundamental role is played by the laboratory studies (experimental and theoretical) which provide the spectroscopic data and by the activities aimed at the validation of the spectroscopic parameters. The latter should be ideally carried out for a range of conditions (i.e. temperature, pressure, absorber amount) as wide as possible in relation to the viewing geometry of IASI-NG.

5.5.1.1 Spectroscopic parameters

The spectroscopic parameters used as input to LBL models can be categorised as:

- Line parameters for the molecules that have an IR spectrum where the absorption can be described fully or partially (i.e. there is a continuum component) in terms of line absorption (e.g. H₂O, CO₂, O₃, CH₄, N₂O, CO, etc.).

- Cross-section parameters to model the absorption by heavy molecules (e.g. CFCs, etc.).

The line parameters can be divided in two classes: firstly, “general” parameters (i.e. line position, line intensity, line width and temperature dependence) for which uncertainties can have significant effects on the forward calculations irrespective of the spectral resolution; secondly, “minor” parameters (pressure shift for example) for which the effect of uncertainties on forward calculations tends to increase with the spectral resolution (as it is the case for IASI-NG). The first class of parameters are usually obtained through experimental studies of gases either in pure form or component in a gas mixture (usually including O₂, N₂ or synthetic air) using very high resolution (typically 0.002 cm⁻¹) laboratory instruments and absorption cells where the path length, temperature and pressure conditions can be controlled. At high resolution, however, a purely empirical approach is rendered impractical by the sheer number of lines to be considered. Consequently, a theoretical analysis and modelling of the experimentally acquired spectra must be carried out using vibration-rotation Hamiltonian and dipole moment operators, firstly to check the consistency of the assignments/measurements, secondly to interpolate and to extrapolate the model parameters to lines which have not been observed (i.e. they are too weak) or unusable (i.e. they are blended) under the experimental conditions. In this context, Tashkun et al. (2003; 1998) have used the method of effective operators to fit the parameters of effective Hamiltonian and dipole moment operators to all CO₂ line data (line positions and line intensities) available in the literature. They have thus obtained more accurate models of Hamiltonian and dipole moment operators that have then been used to generate new line parameters for the four most abundant isotopic species of carbon dioxide. The new intensities and positions are available through the Carbon Dioxide Spectroscopic Databank (CDSDB). Likewise, to cover the whole spectral range of H₂O in the infrared, the recent compilation by Coudert et al. (2008) of H₂O line positions and intensities for the range 10 to 2500 cm⁻¹ includes parameters measured in the laboratory (for wave numbers less than 1750 cm⁻¹) and calculated values for lines that have not been observed.

5.5.1.2 Spectroscopic databases

The present status of the atmospheric databases is the result of numerous studies performed during the last 20 years in several dedicated spectroscopic laboratories all over the world; the sensitivity of IASI-NG to many molecules places an increased demand on high quality measurements of parameters for strong absorbers and new measurements for many weak species such as organic compounds. International cooperation has contributed to the establishment of a number of spectroscopic databases for atmospheric applications. These include:

- GEISA under the responsibility of N. Jacquinet-Husson and R. Armante from LMD, Palaiseau, France. The last update was release at the end of 2015.
- HITRAN under the responsibility of Phillips Laboratory, Cambridge, USA (Rothman et al., 2013).
- MIPAS specifically dedicated to satellite experiments in the Earth’s atmosphere
- BEAMCAT, for millimeter and sub-millimeter wave propagation in the Earth’s atmosphere
- JPL Catalog of microwave to sub-millimeter transitions. It mostly contains rotational transitions of a few hundred molecules which can be potentially observed in the Earth’s atmosphere or in the atmosphere of other planets. It also features molecules present in the Inter Stellar Medium (ISM) or in Circum Stellar Envelopes (CSE) of late type stars. It comprises a small, but increasing, number of entries for infrared transitions.
- CDMS Catalog. Like the JPL catalogue, it mostly contains rotational transitions of molecules important for the ISM or CSEs. Some of the molecules are of course also relevant for application in Earth’s atmosphere or in the atmosphere of other planets and a number

of entries are for infrared transitions of such molecules.

- The VAMDC consortium (<http://www.vamdc.eu>). <http://www.vamdc.org/activities/outreach/> aims at being an interoperable e-infrastructure that provides the international research community with access to a broad range of atomic and molecular data.

Of all the databases listed above, GEISA and HITRAN are of primary importance for IASI-NG and will be discussed in some detail in the next two sections.

5.5.1.3 The GEISA database

The GEISA database is maintained and developed by the ARA/ABC(t) group at LMD (<http://ara.abct.lmd.polytechnique.fr>). In its present form, GEISA is a computer accessible database system that contains the spectroscopic data needed by RT models to simulate terrestrial and planetary atmospheric observations. It comprises three independent sub-databases dedicated respectively to:

- line parameters
- infrared and ultraviolet absorption cross-sections
- aerosols and cloud refractive indices

The ISSWG working group has indicated GEISA as the reference database for IASI and IASI-NG applications. GEISA is used in the 4A (Scott, 1974; Scott and Chedin, 1981), 4A/LMD and 4A/OP radiative transfer models for the validation of the level-1 IASI data. The latest version of the GEISA database (hereafter referred to as GEISA-15) is planned to be released in 2015. The planned content and evolution of the three sub-databases featured in GEISA-15 is summarized below.

GEISA-2015 line parameters

The GEISA-15 sub-database of line parameters archives data for 52 molecular species (113 isotopologues) at the reference temperature of 296 K. This corresponds to a total of 4 800 000 entries in the spectral range from 10×10^{-6} to $35\,877.031\text{ cm}^{-1}$ (1010–0.28 μm). Two new molecular species have been added/updated since the GEISA-09 (Jacquinet-Husson, N. and others, 2011) edition:

- H₂O and HDO are now considered as two independent molecules
- SO₃ is a newly added molecular species

Compared to the previous release of GEISA, the spectroscopic line parameters of 28 molecules, i.e. N₂O, CO, NO, NO₂, PH₃, OH, HF, HCl, HBr, HI, ClO, OCS, GeH₄, C₃H₈, HC₃N, HOCl, N₂, H₂O₂, HCOOH, COF₂, SF₆, C₃H₄, HO₂, ClONO₂, CH₃OH, C₆H₆, C₂HD, CF₄, CH₃CN, have not changed. The planetary atmospheres heritage of GEISA is represented by the presence of molecules such as GeH₄, C₃H₈, C₂N₂, C₃H₄, HNC, C₆H₆, and C₂HD. These species are specific to GEISA. On the other hand, species such as HOBr, O, H₂ and CS are specific to HITRAN. It should also be noted that in HITRAN, HDO, CH₃D and C₂HD are considered as isotopologues of water, methane and acetylene respectively, whereas they are treated as independent molecules in GEISA. Another difference between GEISA and HITRAN is represented by the different format used to represent the molecular data. However, the GEISA package offers the capability to convert the format of one database into the format of the other database using a dedicated software program. In GEISA-15, updated molecular parameters are available for the following species: H₂O, CO₂, O₃, CH₄, O₂, SO₂, NH₃, HNO₃, H₂CO, C₂H₆, CH₃D, C₂H₂, C₂H₄, HCN, C₂N₂, C₄H₂, CH₃Cl, H₂S, CH₃Br, HNC. The most significant updates regard H₂O and CO₂

(e.g. Gamache, 2014; Gamache and A.L.Laraia, 2009; Gamache and Lamouroux, 2013) for the following parameters:

- Air-broadening pressure half-widths
- Temperature dependence coefficients of the air broadening half-widths
- Self-broadening pressure half-width
- Air pressure shifts of the line transitions.

Following the heritage of IASI, a separate database is available dedicated solely to IASI-NG. The rationale being that this would allow the streamline collection of newly available spectroscopic data which could be then made available in a timely fashion for research applications. This database is restricted to the spectral range 599–3001 cm^{-1} and features 11 of the 52 molecular species catalogued in the main GEISA-15 database. These eleven species are H_2O , HDO, CO_2 , CH_4 , O_2 , NH_3 , HNO_3 , H_2CO , $12\text{C}_2\text{H}_2$, C_2H_4 , HCN. In the IASI-NG database, an estimation of the error is given for each parameter. In addition, the Einstein A-coefficients have also been included.

GEISA-15 infrared absorption cross-sections

The volume of the archive of molecular cross-section data has risen significantly (more than 50%) following the introduction of new molecular species based on two sources:

- University of Oslo (Hodnebrog et al., 2013): this compilation features compounds that participate in the climate warming, e.g. halocarbons (CFC), bromocarbons, bromofluorocarbons, bromochlorofluorocarbons, halogenated alcohols, halogenated and fluorinated ethers (HFE), perfluorinated compounds (PFC).
- York University (Harrison and Bernath, 2012): this compilation features species (i.e. C_2H_6 , C_3H_8 , CH_3CN , $\text{C}_3\text{H}_6\text{O}$) that were already present in the previous GEISA catalogue but also includes a new specie, i.e. CH_3OH , whose spectral signature has been clearly identified in IASI spectra measured during biomass burning.

GEISA-15 aerosols and cloud refractive indices

Compared to previous GEISA catalogues, the GEISA-15 database features important updates which are summarized below. Data for the 40 species labeled in blue have been collected at NCAR by Massie and Hervig (2013). These species include acids, organic acids, dusts, ashes, water and ice particles. Data for the 20 species labeled in red have instead been obtained from the ARIA archive developed at Oxford University ([urlhttp://www.atm.ox.ac.uk/project/RI/index.html](http://www.atm.ox.ac.uk/project/RI/index.html)). Species catalogued in this archive include minerals, dust, soot and water particles.

Minerals: Clay, Illite, Kaolin, Montmorillonite, Anhydrite, Dolomite, Hematite, Illite, Kaolinite, Montmorillonite, Olivine, Olivine Fayalite, Quartz, Wustite.

Organic Acids: Ammonium sulphate $(\text{NH}_4)_2\text{SO}_4$, Benzoic acid $\text{C}_7\text{H}_6\text{O}_2$, Glutaric acid $\text{C}_3\text{H}_6(\text{COOH})_2$, Hydroxymalonic acid $\text{C}_3\text{H}_4\text{O}_5$, Malonic acid $\text{CH}_2(\text{COOH})_2$, Oxalic acid $\text{H}_2\text{C}_2\text{O}_4$, Phthalic acid $\text{C}_6\text{H}_4(\text{CO}_2\text{H})_2$, Pinonic acid $\text{C}_{10}\text{H}_{16}\text{O}_3$, Pyruvic acid $\text{CH}_3\text{COCO}_2\text{H}$, Succinic acid $\text{C}_4\text{H}_6\text{O}_4$

Acids: H_2SO_4 , HNO_3 , $\text{H}_2\text{SO}_4 + \text{HNO}_3$, Nitric acid dihydrate (NAD)

Water, ice and sea salt: Supercooled Water, Ice, Ice, Water, Ice, Water

Dusts and sands: Saharan dust, Andesite, Basalt, Granite, Limonite, Obsidian, Pumice, Sand.

Ashes, soots and burning aerosols: Flame soot, Volcanic ash, Biomass aerosols, Pyrolytic graphite, Propane, Organic-Based nonvolatile aerosols, Diesel, Volcanic Ash.

Carbonaceous: Brown carbon spheres, Amorphous carbon, Different HULIS

Others: Martian Dust, Organic haze

5.5.1.4 The HITRAN database

The HITRAN database is developed at the Atomic and Molecular Physics Division, Harvard-Smithsonian Center for Astrophysics, USA. In parallel to HITRAN, a version for high-temperature spectroscopic absorption parameters (HITEMP) is also developed. Similarly to GEISA, it comprises sub-databases dedicated to:

- line parameters
- infrared absorption cross-sections
- aerosol refractive indices

HITRAN2012 line parameters

The latest release of the HITRAN database, HITRAN2012 (Rothman et al., 2013) contains 7400 447 spectral lines for 47 different molecules, incorporating 120 isotopologues. The complete list of molecules includes H₂O, CO₂, O₃, N₂O, CO, CH₄, O₂, NO, SO₂, NO₂, NH₃, HNO₃, OH, HF, HCl, HBr, HI, ClO, OCS, H₂CO, HOCl, N₂, HCN, CH₃Cl, H₂O₂, C₂H₂, C₂H₆, PH₃, COF₂, SF₆, H₂S, HCOOH, HO₂, O, CLONO₂, NO⁺, HOBr, C₂H₄, CH₃OH, CH₃Br, CH₃CN, CF₄, C₄H₂, HC₃N, H₂, CS, SO₃. Several new molecules (i.e. C₄H₂, HC₃N, H₂, CS, SO₃ and isotopologues) have been added to the compilation although it should be noted that they are intended for applications beyond those associated with the terrestrial atmosphere. This new edition of HITRAN has incorporated improved line position, intensity, and line-shape parameters for many of the previously existing molecules and isotopologues. The database has been expanded to include more vibration-rotation bands, weaker transitions, and refined line-shape parameters and formalisms. The compilation also includes for the first time sets of collision-induced absorption data.

HITRAN2012 infrared absorption cross-sections

Infrared absorption cross-sections are available for molecules for which line-by-line data are not available or incomplete. This is generally the case for large polyatomic molecules for which the generation of line data is very difficult due to the lack of detail concerning e.g. hot band or the characterization of other specific phenomena. For some of the molecules, there are ample temperature-pressure sets in the given spectral range to provide an ability to perform quasi-quantitative atmospheric simulations. Rothman et al. (2013) point out that the sets of absorption cross sections in HITRAN are far from complete and may not include some additional useful sets. It should be noted, however, that HITRAN2012 features significant additions to the infrared cross-section data. More specifically, data are now available for a number of important organic molecules, i.e. CClF₂CF₂CHClF (HCFC-225cb), CH₂F₂ (HFC-32), CHF₂CF₃ (HFC-125), CHF₂CHF₂ (HFC-134), CFH₂CF₃ (HFC-134a), CF₃CH₃ (HFC-143a), CH₃CHF₂ (HFC-152a), SF₅CF₃ (Trifluoromethyl sulphur pentafluoride), CH₃C(O)OONO₂ (PAN), CH₃CN (methyl cyanide). Successive generations of HITRAN are likely to include new cross-section measurements such as those for CFC-12 (Harrison, 2015).

HITRAN2012 aerosol and cloud refractive indices

HITRAN2012 contains refractive indices in the visible, infrared, and millimetre spectral ranges of many of the materials which comprise the compositions of aerosols and clouds. Many indices are based upon field measurements of aerosols in their natural setting in addition to laboratory measurements. It is useful to include field measurements because the composition of aerosols

is chemically very diverse and evolves daily. Additions to HITRAN mainly concern absorptive aerosol species. New HITRAN refractive indices include secondary organic acid, carbonaceous indices, mineralogical indices, Saharan dust (as a function of hematite content), brown carbon, volcanic ash indices, and vegetation-fire indices. Organic acids, which scatter primarily and are precursors to secondary organic aerosols, are also available.

5.5.2 Optical properties of Cloud and aerosols

Because most water cloud types have an emissivity close to one, the only information currently used for the assimilation of overcast IR radiances in NWP (McNally, 2009; Pavelin et al., 2008) and for atmospheric composition retrievals in low cloud contamination (Clerbaux et al., 2009) is the cloud top pressure and temperature and the effective emissivity of the cloud (i.e. the emissivity times the effective cloud fraction). Although the cloud top information and the effective emissivity can be retrieved using different techniques, e.g. CO₂-slicing method, clustering, 1D-VAR, minimum residual (see Lavanant et al., 2011, for a comparison of the various techniques), recent studies (Martinet et al., 2013b; Okamoto, 2013) have shown that the use of vertical profiles of water content and cloud fraction can potentially improve NWP forecasts. For this reason, the full exploitation of cloud affected IASI-NG radiances will require RT scattering computations where the input optical properties (e.g. extinction coefficient, single scattering albedo and phase function) of scattering particles are accurately known. These optical properties depend on the shape, size distribution and the refractive indices of the scattering particles. For practical use in RT scattering codes, optical properties are typically parameterised as a function ice/liquid water content, temperature and effective particle size.

In the context of IR RT cloudy computations, a crucial role is played by ice clouds because the optical properties of ice particles are difficult to characterise and errors in the computation of these optical properties can significantly alter the radiation at the top of the atmosphere. For instance, the assumption of a simple spherical shape for ice particles can lead to significant errors and consequently more realistic shapes have to be considered. State-of-the-art methods for the computation of optical properties of non-spherical particles have been discussed in section 5.4.1. Here we want to note that publicly available electromagnetic codes that are sufficiently general are not immediately on hand to use by atmospheric scientists wishing to exploit instruments like IASI-NG. The ones that are publicly available are listed on the website <http://www.scattport.org/>, and these can be downloaded by users wishing to obtain their own electromagnetic solutions using their particular ice crystal models (i.e. particle shape). If users do not wish to obtain their own electromagnetic solutions, then there are already available databases of ice single-scattering optical properties that can be downloaded from the website http://www.ssec.wisc.edu/ice_models/ compiled by Baum et al. (2014) and from Baran et al. (2014), where the latter databases can be obtained on request to the first author. These databases cover the complete wavenumber range of IASI-NG as well as the solar and far-infrared spectrum. It is worth noting that the database by Baran et al. (2014) has already been implemented in RTTOV-11. For water clouds, realistic and accurate optical properties can be calculated using the Lorentz-Mie theory (Van de Hulst, 1981) for spherical particles. Alternatively, optical properties for several types of water clouds are available in the Optical Properties of Aerosols and Clouds (OPAC) database (Hess et al., 1998).

Background concentrations of aerosols have in general a small impact on radiances measured by IR nadir sounders. However, in many instances (e.g. dust storms, volcanic eruptions) aerosol concentrations can greatly exceed the background values. In that case, the impact on IASI-NG spectra can be very significant above all in the short wave region of the spectrum. Similarly to clouds, the absorption and scattering properties of aerosols depends on the shape,

size distribution and the refractive indices of the aerosol particles. Likewise, inputs to RT codes will generally include the single scattering properties and the phase function of the aerosol particles. Aerosol optical properties can be computed using the electromagnetic and the advanced physical optics methods discussed in section 5.4.1 and section 5.4.2. This will require the refractive index of aerosol particles. Refractive indices are obtained via laboratory measurements. A comprehensive compilation of refractive indices can be found in the HITRAN and GEISA molecular databases or in specialised databases such as the ARIA database (<http://www.atm.ox.ac.uk/project/RI/index.html>). RT model developers or users who do not wish to obtain their own electromagnetic solutions can resort to the use of optical properties available from existing databases. For instance, the OPAC database comprises optical properties for various aerosols types (e.g. maritime, urban, desert and volcanic ash) under the assumption that aerosol particles are spherical whereas the databases assembled by Meng et al. (2010) and Bi et al. (2009) comprise optical properties of triaxial ellipsoidal mineral dust aerosols. More recently, Legrand et al. (2014) and Koepke et al. (2015) have assembled databases of optical properties of spheroids of mineral dust.

5.5.3 Surface emissivity data

For the regions of the IR spectrum where the atmosphere is relatively transparent, RT simulations of IASI-NG spectra need the definition of the surface properties. At IR wavelengths the surface skin temperature and the emissivity of the surface, which is a function of surface type, viewing angle and wavelength, are the primary variables affecting the up-welling radiance. For the sea surface the skin temperature is normally within a few tenths of a degree of the bulk sea surface temperature (SST) and the emissivity is close to unity which allows the SST to be a good approximation for the radiative skin temperature. Datasets exist (see section 5.3.2) that give the small departure of the sea surface emissivity from unity as a function of viewing angle and wind speed over a range of wavelength.

Over land, however, the definition of both the land skin temperature and the land surface emissivity is difficult to specify and is a subject of active research. Land surfaces can be subdivided into specific surface types with defined emissivities (e.g. desert, agricultural, forest, snow, etc). L and surface skin temperatures are computed by NWP models although they can have large differences (5 K) when compared with measured radiative skin temperatures. Over sea-ice the emissivity is close to unity but the ice radiative temperature can be difficult to estimate as over land. The surface elevation is also an important parameter as the intervening atmospheric absorption will be reduced as the path length is reduced.

The global database of infrared (IR) land surface emissivity included in RTTOV (Seemann et al., 2008) was developed to support more accurate retrievals of atmospheric properties such as temperature and moisture profiles from multispectral satellite radiance measurements. Emissivity is derived using input from the Moderate Resolution Imaging Spectroradiometer (MODIS) operational land surface emissivity product (MOD11). The baseline fit method, based on a conceptual model developed from laboratory measurements of surface emissivity, is applied to fill in the spectral gaps between the six emissivity wavelengths available in MOD11. Emissivity in the database presented here is available globally at 10 wavelengths (3.6 μm , 4.3 μm , 5.0 μm , 5.8 μm , 7.6 μm , 8.3 μm , 9.3 μm , 10.8 μm , 12.1 μm and 14.3 μm) with 0.05° spatial resolution. The wavelengths in the database were chosen as hinge points to capture as much of the shape of the higher-resolution emissivity spectra as possible between 3.6 and 14.3 μm . Other land surface emissivity databases are available.

5.5.4 Datasets of atmospheric profiles

Atmospheric RT studies and the training of fast RT models in preparation for IASI-NG require datasets of realistic profiles of atmospheric temperature, gaseous constituents, cloud water/ice and aerosols. These variables should be given on a defined set of pressure levels from about 0.005 to 1050hPa with levels spaced at least every 30hPa in the troposphere. Constituent profiles may also be required with pressure and temperature specified on constant absorber amount levels, in order to ensure there is enough information on the absorber in the layers in which most of the absorption is occurring. These levels will vary from gas to gas, e.g. with more levels for ozone in the stratosphere and more levels for water vapour in the lower troposphere.

Atmospheric gases range from those that are constant or predictable in time to those that are variable and unpredictable. At one end of the range are well-mixed gases, with known height profiles and constant or slowly varying concentrations. For these gases one profile is sufficient. Carbon dioxide and oxygen are examples of this class. In the case of carbon dioxide, the concentration is gradually increasing with time and so a profile valid for the period that IASI-NG is expected to be in orbit is required. At the other end of the range is water vapour, which varies enormously in time and space along with ozone. Other minor constituents have hugely varying temporal variability, depending on their stability in the atmosphere. For some purposes (e.g. temperature retrieval) they may be treated as quasi-fixed, i.e. for these gases, profiles for different latitude bands and seasons may be sufficient to capture the variability. For other purposes, namely constituent retrieval, they must of course be treated as variable gases. For IASI-NG simulations, a minimum requirement is for a dataset with profiles of temperature and H₂O, O₃, CO₂, N₂O, CO and CH₄ concentrations. Profiles of the chlorofluorocarbons (CFCs) are also required as these exotic gases can have significant effects in some spectral bands. In some cases it may be useful to estimate concentrations for the period after the launch of Metop-SG by extrapolating using climate trends.

Model atmospheres are often used as a source of profiles to create a few transmittance or radiance spectra representative of a typical air mass. Commonly used model profiles are the US AFGL profiles for mean tropical, mid-latitude and polar atmospheres and the US standard atmosphere as a global mean profile (Rothman et al., 1983). There also exist new updates to these atmospheres such as The Reference Atmospheres for MIPAS: Standard Atmospheres (RAMstan) database. Originally designed for the stratosphere, this has become a set of climatological profiles on a 1 km vertical grid covering 0 to 120 km. The two components of the RAMstan database are: i) version 3.1 of the Standard Atmospheres, and ii) version 5 of the IG2 (Initial Guess 2) database consisting of the averaged profiles with the standard atmospheres. The profiles in these databases are of pressure, height, temperature, water vapour and all other atmospheric constituents relevant for IASI-NG. The model profiles are from the surface to 100 km and so encompass the full range of heights of interest for IASI-NG transmittance modelling. There are two major limitations of model atmospheres. Firstly they do not encompass the full range of extremes encountered in the real atmosphere in terms of temperature and constituent concentration. Secondly the profiles are much smoother than in the real atmosphere with no sharp structures present.

For these reasons it is often desirable to use a selection of atmospheric profiles measured in situ or obtained from remote sensing techniques subjected to careful quality control. These datasets exist for temperature, water vapour and ozone profiles and many minor constituents. Radiosondes are often used as the primary source of data for temperature and water vapour profiles, though they have their own errors and certain types of sonde can exhibit large biases, particularly in water vapour measurements. The lack of reliable water vapour profiles frustrates attempts to accurately validate RT models and also L2 products. The GRUAN working group

has formulated a list of corrections for the VAISALA RS-92 measurements that correct for systematic errors due to solar radiation, calibration and sensor time-lag factors. The uncertainties in the correction mainly arise from incomplete knowledge of surface albedo, sensor calibration, ventilation and errors in the fitting parameters. Those are combined into a total uncertainty that is provided along with the radiosonde measurements enabling the computation of error estimates during atmospheric RT studies. In the stratosphere and mesosphere, rocketsondes have traditionally provided information. GNSS-RO data are now widely available also, and are able to provide temperature retrievals in the upper atmosphere. A good stratospheric WV profile dataset will be required to exploit the regions of the IR spectra with strong WV absorption lines. In addition, a dataset of HDO profiles is also needed to study the effect of HDO depletion (i.e. relative to what is assumed for instance in HITRAN) on IASI-NG spectra.

Ozonesondes can provide important data for ozone profiles in the upper troposphere and lower stratosphere although a ground-based network of total column ozone measurements gives more information on the total column variability in space and time. There are several satellite sensors which can provide total column ozone amounts globally (e.g. the Total Ozone Mapping Spectrometer (TOMS), GOME) or stratospheric profiles (SAGE, the Solar Backscatter Ultraviolet radiometer (SBUV)). Estimates of the remaining atmospheric constituents of interest are even harder to come by, and in general validation is based on comparison with measurements from dedicated campaigns or instruments including IASI, along with those on focused chemistry research missions, such as TES, MOPPITT or SCHIAMACHY.

Various collections of diverse atmospheric profiles derived from in situ measurements are available for general use. For instance, the NOAA dataset of temperature and water vapour radiosonde profiles comprises 8000 diverse profiles. This dataset exists in two versions featuring different numbers of vertical levels. Alongside the NOAA dataset, the CIMSS dataset of 383 diverse profiles is dedicated solely to ozone data. The TIGR v3 dataset (Chedin et al., 1985) assembled by LMD comprises 2311 temperature, water vapour and ozone profiles on 40 vertical levels from 0.05 to 1013hPa. A recent addition to the family of LMD datasets is the Analysed Radio Soundings Archive (ARSA) database of atmospheric profiles. ARSA (<http://ara.abct.lmd.polytechnique.fr/index.php?page=arsa>) is an archive of global radiosonde measurements of temperature, water vapour and ozone profiles supplemented with ECMWF ERA-interim data (Dee et al., 2011) for the extrapolation of the profiles into the upper levels of the atmosphere.

In recent years, NWP forecasting systems have been increasingly used to produce datasets of atmospheric profiles of temperature, constituents and surface parameters. In particular, ECMWF has released several of such datasets reflecting the evolution of the forecasting/assimilation system and of the techniques used to sample the data. These datasets have been extensively used for the training of the RTTOV fast model (e.g. Matricardi, 2008) and have proven to be extremely valuable for PC based fast models whose training requires large datasets encompassing the full range of realistic atmospheric and surface situations (Matricardi, 2010). The most recent datasets released by ECMWF are those assembled by Eresmaa et al. (2012) and by Eresmaa and McNally (2014). The Eresmaa et al. (2012) database was originally produced for the Monitoring Atmospheric Composition and Climate (MACC) project. The database comprises 40 000 vertical profiles on 60 model levels and it is divided in ten subsets, each representing the spatio-temporal variability of one sampling variable in the global NWP modelling system. The ten sampled variables include temperature and specific humidity, mixing ratios of ozone, carbon dioxide and methane and mixing ratios of sulphate, organic matter, black carbon, sea salt, and desert dust aerosols. Resolution upgrades and improvements in the representation of physical processes in the ECMWF forecasting system have led to the release of the Eresmaa and McNally (2014) database which comprises 25 000 atmospheric profiles on 137 model levels. The database

is divided in five subsets representing temperature, specific humidity, ozone mixing ratio, cloud condensates, and precipitation. Note that both datasets described above also include surface parameters.

A comprehensive list of the currently available datasets is tabulated in table 5.3. From table 5.3, it can be noted that many profiles are specified on 40 vertical levels. Given the spectral resolution of IASI-NG, consideration should be given as to whether the vertical discretisation of these profiles is too coarse; coarse enough, for instance, for the assumptions regarding the average temperature of the absorbing gas in the layer (i.e. assumptions regarding the vertical variation of absorbers (and temperature) within the layer) to give rise to significant differences in the layer average temperature and ultimately, the simulated radiances. In addition it is worth noting that a coarse vertical grid could represent an additional source of error due to the interpolation of initial profile data into RT model levels. For instance, fast RT models like RTTOV typically use 100 vertical levels for the simulation of hyperspectral sounding radiances.

5.6 Radiative transfer model validation

In order to estimate the accuracy of the RTMs they have to be validated. Two approaches are possible: comparison with other models and comparisons with real measurements.

There are two types of model comparisons. Firstly comparing similar models (e.g. all LBL models) to check the basic spectroscopic data and coding of the model results in realistic transmittances. Such comparisons have been carried out in the past and have been useful to identify problems with the models or their implementation on various computers. The differences should only be due to differences in input data and model formulation. The second class of comparison is to compare fast model results with those from a LBL model to assess the accuracy of the fast model. This comparison should be carried out on a set of profiles independent of those used in the training dataset.

Comparisons of model predictions with reliable radiance measurements can be used to assess the accuracy of the models. However care must be taken to ensure not only that the radiance measurements are accurate but also that the characteristics of the atmospheric path through which the radiance is emitted are fully known, otherwise differences may be due to an inaccurate description of the atmospheric path. There are several possible configurations for atmospheric measurements by an interferometer similar to IASI-NG. An upwards-looking ground-based system can view the down-welling atmospheric emission from the zenith or slant paths. If the measurements are made coincident with good quality profile measurements these data can be valuable for validation of the models. Cold space provides a known background radiance. Downward- and upward-looking measurements from an aircraft-borne or balloon-borne interferometer can validate the models for a wider range of different path conditions. In particular a nadir-looking interferometer under a stratospheric aircraft or balloon could encompass a range of optical thickness (variable during ascent up to float) which could provide stringent tests of the LBL forward models. Finally, satellite radiance measurements with similar characteristics to IASI-NG may also be available shortly to validate the models. The latter have the advantage of making measurements over a wide range of different atmospheric conditions. Comparisons can be made globally by collocation with profiles from NWP analyses. However these are likely to be most accurate in the vicinity of reliable radiosonde stations.

One way to assess fast RTM error characteristics in advance of IASI-NG is to look at the biases of the models with other satellite IR radiometers already flying (e.g. IASI, AIRS, CrIS, AVHRR, SEVIRI). Collocation datasets which compare modelled and measured radiances over the globe can be useful to characterise the biases and determine how they vary with mean layer temperat-

| Dataset | Profiles | Levels | Minimum Pressure (hPa) | Variables | Data source |
|---|-------------|--------|------------------------|--|-------------------|
| TIGR v3 | 2311 | 40 | 0.05 | P, T, q, O ₃ (climatology) | Radiosonde |
| ARSA | Jan 1979 on | 43 | 0.0025 | P, T, q, O ₃ (partly climatology) | Radiosonde/Model |
| ECMWF 50L | 13 766 | 50 | 0.1 | P, T, q, O ₃ (climatology) | Model |
| ECMWF 60L | 13 495 | 60 | 0.1 | P, T, q, O ₃ , cloud, surface | Model |
| NOAA-88/89 | 8000 | 66/101 | 0.005/0.1 | P, T, q | Rocket/radiosonde |
| SeeBor V4.0 | 15 705 | 101 | 0.005 | P, T, q, O ₃ | Mixed |
| UMBC | 49 | 101 | 0.005 | P, T, q, O ₃ , CO, CH ₄ , N ₂ O | Radiosonde |
| Garand | 42 | 43 | 0.1 | P, T, q, O ₃ , CO ₂ , CO, CH ₄ , N ₂ O | Radiosonde/SAGE |
| CIMSS Ozone | 380 | 40 | | O ₃ | Ozonesonde |
| ECMWF trace gas | 43 | 90 | 0.005 | P,T,q, O ₃ , CO ₂ , CO, CH ₄ , N ₂ O | Mixed |
| ECMWF trace gas | 83 | 101 | 0.005 | P,T,q, O ₃ , CO ₂ , CO, CH ₄ , N ₂ O | Mixed |
| MOZART trace gas | 98 304 | 67 | 0.005 | O ₃ , CO, CH ₄ , N ₂ O | Model |
| COSPAR | 396 | 71 | 2.54×10^{-5} | T, wind | Mixed |
| ECMWF aerosol and trace gas concentration | 40 000 | 60 | 0.1 | P, T, q, O ₃ , CO ₂ , CH ₄ , Aerosol mixing ratios of sulphate, organic matter, black carbon, sea salt, desert dust | Model |
| ECMWF 91L | 25 000 | 91 | 0.1 | P, T, q, O ₃ , cloud, surface | Model |
| ECMWF 137L | 25 000 | 137 | 0.1 | P, T, q, O ₃ , cloud, surface | Model |

Table 5.3: List of current publicly available atmospheric profile datasets

ure, scan angle, total column, WV, etc. These biases have to be removed before assimilation into NWP models. Difficulties arise when trying to assign the biases to the instrument calibration or pre-processing or to the RTM and the studies described in the previous paragraphs need to be carried out to give an absolute error estimate for the RTMs.

These activities are strongly related to instrument CAL/VAL activities and understanding the sources of bias between observations and their forward-modelled counterparts (as well as the standard deviation) will help to ensure that the IASI-NG user requirements can be met. As an example, during the commissioning phase of the IASI instrument, the spectral calibration demonstrated that good knowledge/precision of the pressure shift spectroscopic parameter was necessary for the CO₂ lines studied during CAL/VAL activities.

Chapter 6

Level 2 Products: Retrieval of Geophysical Parameters

6.1 Retrieval Theory

Retrieval theory addresses the problem of deriving the thermodynamical state of the atmosphere, or more in general a given set of geophysical parameters, at a given time t , given a set of independent observations of the spectral radiance, $R(\sigma)$, (σ is the wave number in units of cm^{-1}). If the spectral radiance is observed at different wave numbers, $\sigma_i, i = 1, \dots, M$ then the radiance vector, \mathbf{R} is defined according to

$$\mathbf{R} = (R(\sigma_1), \dots, R(\sigma_M))^T \quad (6.1)$$

where the superscript T means transpose. Physical approaches are common, particularly where the retrieval state vector consists of temperature and water vapour profiles, in which case the basic physical radiative transfer equation is directly used to seek for a suitable estimation. These are discussed in section 6.1.1. Retrieval schemes can also be based on parametric approaches where we assume a given functional relationship between data and parameters (e.g. linear regression) and an optimal solution is obtained through Least Squares or Neural Network methods. Parametric approaches are discussed in section 6.1.2. The choice of method for retrieval of geophysical parameters needs to be chosen dependent on the quality and type of available a priori data and meta data, and timeliness requirements.

It is worth noting that the retrieval state vector, whilst normally consisting of layer-average quantities of geophysical variables (from many layers in a full profile retrieval to total column retrieval of some atmospheric constituents), it may be desirable to perform the retrieval in a transformed space, such as principal components of the atmospheric profile, or in a reduced normalised space such as that proposed by Migliorini (2012).

6.1.1 Physical retrieval schemes

The science underlying many retrieval schemes is very similar to that of data assimilation (DA) (e.g. Daley, 1991; Kalnay, 2003; Wikle and Berliner, 2007). DA is discussed in chapter 7, but the basic equations are presented here as they form the basis of many of the methods that are reviewed briefly here, and have been used extensively for many IASI applications (e.g. Hilton et al., 2012a). In particular, the methods that consider the a-priori covariance as a static application data, that is Rodgers' Optimal Estimation (Rodgers, 2000), 1D to 3D variational analysis (Courtier, 1997; Talagrand, 1997), and the Maximum Likelihood Estimation approach, are formally equivalent (Wikle and Berliner, 2007).

6.1.1.1 Variational Analysis

Under the assumption of multivariate normality our retrieval problem can be seen as one of variational analysis in which a suitable estimation of the state vector is obtained by minimizing

the form:

$$\min_{\mathbf{v}} \frac{1}{2} \left[(\mathbf{R} - F(\mathbf{v}))^T \mathbf{S}_\epsilon^{-1} (\mathbf{R} - F(\mathbf{v})) + (\mathbf{v} - \mathbf{v}_a)^T \mathbf{S}_a^{-1} (\mathbf{v} - \mathbf{v}_a) \right] \quad (6.2)$$

where:

F is the forward model function

\mathbf{v} is the atmospheric state vector, of size N

\mathbf{v}_a is the atmospheric background state (or a priori) vector, of size N

\mathbf{S}_ϵ is the observational covariance matrix, of size $M \times M$

\mathbf{S}_a is the background covariance matrix, of size $N \times N$

Of course the factor 1/2 is not essential for the minimization, it is just a reminder of the Gaussian assumptions about the probability density functions of observations and parameters.

For practical purposes, equation 6.2 has to be linearized in the forward model, so that its minimum can be sought through, for example, a Gauss-Newton iterative sequence. Linearization is obtained through Taylor series expansion of $F(\mathbf{v})$ around a first guess state vector, \mathbf{v}_0 :

$$\mathbf{R} = \mathbf{R}_0 + \frac{\delta F(\mathbf{v})}{\delta \mathbf{v}} \Big|_{\mathbf{v}=\mathbf{v}_0} (\mathbf{v} - \mathbf{v}_0) + \text{higher order terms} \quad (6.3)$$

where $\mathbf{R}_0 = F(\mathbf{v}_0)$. The introduction of the Jacobian,

$$K = \frac{\delta F(\mathbf{v})}{\delta \mathbf{v}} \Big|_{\mathbf{v}=\mathbf{v}_0} \quad (6.4)$$

allows us to replace equation 6.2 with the quadratic form

$$\min_{\mathbf{x}} \left[(\mathbf{y} - \mathbf{K}\mathbf{x})^T \mathbf{S}_\epsilon^{-1} (\mathbf{y} - \mathbf{K}\mathbf{x}) + (\mathbf{x} - \mathbf{x}_a)^T \mathbf{S}_a^{-1} (\mathbf{x} - \mathbf{x}_a) \right] \quad (6.5)$$

where:

$$\mathbf{y} = \mathbf{R} - \mathbf{R}_0$$

$$\mathbf{x} = \mathbf{v} - \mathbf{v}_0$$

$$\mathbf{x}_a = \mathbf{v}_a - \mathbf{v}_0$$

It should be stressed that, formally, the state vector, \mathbf{v} can be thought of as a 3-D geophysical field, and not necessarily of a vector in one dimension (altitude coordinate). The formal solution of equation 6.2 is well established and can be found in many textbooks (e.g. Rodgers, 2000; Tarantola, 1987). The estimation, $\hat{\mathbf{x}}$ of \mathbf{x} and its covariance matrix, $\hat{\mathbf{S}}$ are given by:

$$\begin{aligned} \hat{\mathbf{x}} &= \mathbf{x}_a + (\mathbf{K}^T \mathbf{S}_\epsilon^{-1} \mathbf{K} + \mathbf{S}_a^{-1})^{-1} \mathbf{K}^T \mathbf{S}_\epsilon^{-1} (\mathbf{y} - \mathbf{K}\mathbf{x}_a) \\ \hat{\mathbf{S}} &= (\mathbf{K}^T \mathbf{S}_\epsilon^{-1} \mathbf{K} + \mathbf{S}_a^{-1})^{-1} \end{aligned} \quad (6.6)$$

A useful matrix to define is the averaging kernel, which describes how information from the observation is filtered through the above equations and mapped into retrieval space. It is defined as:

$$\mathbf{A} = (\mathbf{K}^T \mathbf{S}_\epsilon^{-1} \mathbf{K} + \mathbf{S}_a^{-1})^{-1} \mathbf{K}^T \mathbf{S}_\epsilon^{-1} \mathbf{K} \quad (6.7)$$

or

$$\mathbf{A} = \mathbf{I} - \hat{\mathbf{S}} \mathbf{S}_a^{-1} \quad (6.8)$$

The averaging kernel describes the sensitivity of the retrieval to the true state, as seen by the current observing system. For a profile retrieval, row j of the averaging kernel, $\mathbf{A}(j, *)$ describes the proportion of information on retrieval level j that comes from each element of the true state profile (the remainder comes from the a priori). A perfect observing system would directly observe each element of the retrieval vector, and the averaging kernel would tend towards the identity matrix. For satellite radiance observations, the measurement in a given channel is sensitive to a wide layer of the atmosphere, meaning that \mathbf{K} is highly non-diagonal. Furthermore, the error in the a priori profile is often highly correlated between levels, so \mathbf{S}_ϵ is also highly non-diagonal. The consequence of this is that the information from the true atmospheric state is smoothed in the vertical by the retrieval system, and the averaging kernel describes this smoothing function. The averaging kernel is required for assimilation of retrieved products, as it forms part of the observation operator. It is also required for Cal/Val activities, where profiles of different vertical resolutions are to be compared (Rodgers and Connor, 2003).

The trace of the averaging kernel ($\text{Tr } \mathbf{A}$) gives the quantity known as Degrees of Freedom for Signal (DFS), which describes the number of independent pieces of information provided to the retrieval by the observation. This is a useful concept that can be used when setting up a retrieval scheme to determine the vertical resolution of products, as demonstrated in table 6.2. It is also used to help select subsets of channels for assimilation (see section 6.2.1.1, section 6.2.1.2).

The retrieval scheme outlined above is generally known as 1D-Var when it is used in an iterative set-up to find the retrieval by the minimisation of the cost function. Other approaches to finding the best fit between the a priori and the observation are possible, some of which are outlined here with their strengths and weaknesses.

6.1.1.2 Optimal Estimation and Twomey-Tikhonov approaches

The various retrieval schemes used for IASI mostly differ from each other in the way \mathbf{x}_a and \mathbf{S}_a in equation 6.6 are prescribed. In the context of optimal estimation, \mathbf{x}_a is normally the forecast at a given time t and \mathbf{S}_a is the forecast error covariance matrix. Then, the estimation, $\hat{\mathbf{x}}$ is referred to as the analysis. On the other hand, in the context of inversion using a climatological a priori, \mathbf{x}_a and \mathbf{S}_a are the mean and covariance of a suitable ensemble of states, e.g., local radiosonde observations, Numerical Weather Prediction centres' analyses and so on. Optimal estimation schemes have been used by various centres with IASI observations to retrieve atmospheric state vectors consisting of elements such as temperature (T), H_2O (Q) and O_3 mixing ratio profiles and surface temperature (T_s) and emissivity (ϵ) (see Hilton et al., 2012a, for example). Optimal estimation is also a mainstay of most offline algorithms for IASI atmospheric chemistry processing and increasingly these are being implemented for operational processing. Examples include Hurtmans et al. (2012), Schneider and Hase (2011), Illingworth et al. (2011), Dufour et al. (2012) and Siddans et al. (2016).

If \mathbf{S}_a^{-1} in equation 6.6 is identified with a mathematical kernel of the type $\gamma\mathbf{H}$, where \mathbf{H} , can be chosen to minimize, for example, the mean squared difference between \mathbf{x}_a and \mathbf{x} (in which case $\mathbf{H} = \mathbf{I}$), or the mean squared first/second difference for a smooth solution, we have what is normally referred to as the Twomey-Tikhonov approach (e.g. Colton and Kress, 1991). This approach has been largely used for AIRS (see Susskind et al., 2003, for example). In the case of the Twomey-Tikhonov approach the solution given by equation 6.6 has to be modified in such a way that $\mathbf{v}_a = \mathbf{v}_0$. In addition, the *a posteriori* covariance matrix, $\hat{\mathbf{S}}$, is derived according to the non-statistical role of the first guess, \mathbf{v}_0 . Now we have

$$\begin{aligned}\hat{\mathbf{x}} &= (\mathbf{K}^T \mathbf{S}_\epsilon^{-1} \mathbf{K} + \gamma \mathbf{H})^{-1} \mathbf{K}^T \mathbf{S}_\epsilon^{-1} \mathbf{y} \\ \hat{\mathbf{S}} &= (\mathbf{K}^T \mathbf{S}_\epsilon^{-1} \mathbf{K} + \gamma \mathbf{H})^{-1} \mathbf{K}^T \mathbf{S}_\epsilon^{-1} \mathbf{K} (\mathbf{K}^T \mathbf{S}_\epsilon^{-1} \mathbf{K} + \gamma \mathbf{H})^{-1}\end{aligned}\tag{6.9}$$

One possible problem with retrievals that use a climatological covariance is that \mathbf{S}_a may provide too loose a constraint, in which case the solution can tend towards the unconstrained least square solution and show jackknifing. Conversely if the constraint is too tight, the solution will just follow \mathbf{x}_a and get no contribution from the observation. For these cases, the introduction of a global inflation parameter, γ which properly scales \mathbf{S}_a^{-1} can help to get a regularized solution. In this approach \mathbf{S}_a^{-1} in equation 6.6 is substituted with $\gamma\mathbf{S}_a^{-1}$ and as shown by Masiello et al. (2012) the scheme is equivalent to regularization. In addition, the approach performs much better if we previously rotate \mathbf{S}_a and \mathbf{S}_ϵ in order to work with diagonal covariance matrices (e.g. Carissimo et al., 2005). For this case the *a posteriori* covariance matrix appearing in the second line of equation 6.6 has to be changed as well. The formal solution reads (see, for example, Masiello et al., 2012)

$$\begin{aligned}\hat{\mathbf{x}} &= \mathbf{x}_a + (\mathbf{K}^T\mathbf{S}_\epsilon^{-1}\mathbf{K} + \gamma\mathbf{S}_a^{-1})^{-1}\mathbf{K}^T\mathbf{S}_\epsilon^{-1}(\mathbf{y} - \mathbf{K}\mathbf{x}_a) \\ \hat{\mathbf{S}} &= (\mathbf{K}^T\mathbf{S}_\epsilon^{-1}\mathbf{K} + \gamma^2\mathbf{S}_a^{-1})^{-1}(\mathbf{K}^T\mathbf{S}_\epsilon^{-1}\mathbf{K} + \gamma\mathbf{S}_a^{-1})(\mathbf{K}^T\mathbf{S}_\epsilon^{-1}\mathbf{K} + \gamma^2\mathbf{S}_a^{-1})^{-1}\end{aligned}\quad (6.10)$$

6.1.1.3 Generalized noise covariance matrix

Rodgers (2000) and Clarmann et al. (2001) have shown that in a linear optimal estimation, retrieving interfering uncertain parameters (other species, spectroscopic parameters, atmospheric parameters) is completely equivalent to retrieving just the species of interest, but incorporating those other uncertainties in a generalized noise covariance matrix. Walker et al. (2011) have shown that this can be exploited in a very powerful way for qualitative retrievals (i.e. those that result in a kind of “index” rather than a physical quantity) of sporadic atmospheric constituents (rare trace gases and aerosols) such as NH_3 and SO_2 or aerosols (Clarisse et al., 2013). The general noise covariance matrix in this case can straightforwardly be built from spectra uncontaminated by the species of interest, and in this way includes knowledge of uncertain parameters. The main advantage is that the spectral background and uncertainties are better characterized than any traditional forward model can do. The resulting detection index can be converted to columns via look-up-tables (Van Damme et al., 2014). Alternatively, one can make use of partial knowledge of the interfering parameters (e.g. from IASI L2 information) to construct a partially generalized noise covariance matrix which can be used in an optimal estimation setting. This technique has been successfully applied for the retrieval of SO_2 (Carboni et al., 2012). The connection between the generalized noise covariance matrix technique, principle components analysis, and other detection techniques is discussed in detail in Clarisse et al. (2013).

6.1.1.4 Direct Inversion

In any inverse problem, it is theoretically possible to perform a direct inversion of the radiative transfer equation,

$$\mathbf{R} = F(\mathbf{v}) \quad (6.11)$$

if the problem is sufficiently well determined.

To invert equation 6.11 to generate an estimate of the atmospheric state would require that the Jacobians were delta functions and the error terms fully diagonal. This approach is therefore completely unrealistic for most applications of IASI-NG data. However, for a few channels where the sensitivity is restricted to surface properties, given adequate knowledge of skin temperature, it is possible to calculate surface emissivity by direct inversion of the radiative transfer equation (for example Capelle et al., 2012; Péquignot et al., 2008). Alternatively, if emissivity is well-known, skin temperature can be estimated directly from the radiances. One application of this is the derivation of sea-surface temperature estimates from window channels where surface emissivity is close to 1.

6.1.2 Parametric approaches

With physical approaches described in section 6.1.1, it is assumed that the relation between data and parameters is expressed by a suitable forward model, which is based on the basic physical principles of radiative transfer, as shown in equation 6.11. In general, the inverse of equation 6.11 is not analytical and the vector \mathbf{v} cannot be obtained simply by

$$\mathbf{v} = F^{-1}(\mathbf{R}) \quad (6.12)$$

Rather than performing radiative transfer calculations and determining weights between the observation and a priori for each observation in turn (whether by direct calculation or iteration), an alternative approach is to parameterise the relationship between the radiance and the atmospheric state. F^{-1} can be approximated with, for example, a linear form or a polynomial function,

$$\mathbf{v} = P(\mathbf{R}) \quad (6.13)$$

The retrieval problem is then moved to that of obtaining the polynomial coefficients of P (or regression parameters) which better approximate equation 6.12. A training phase is typically required to set up these relationships. Once the parameters are obtained, for a given observation vector \mathbf{R} , the state vector \mathbf{v} is obtained by a straightforward use of equation 6.13.

The advantage of this approach is that the regression relationship is defined empirically during the learning phase, rather than via an abstracted process of estimating and regularising error covariance matrix estimates. A common misconception is that the errors and averaging kernels of the retrieved product is not able to be expressed explicitly, but this is not the case. EUMETSAT are encouraged to explore the advantages and disadvantages of parametric approaches, and to find new approaches to validation of products that demonstrate the ways in which products derived from machine learning approaches differ from those derived from physical retrieval techniques.

6.1.2.1 Regression and Look-up Tables

The regression coefficients can be obtained on the basis of a suitable training data set which is made up of a set of pairs (\mathbf{v}, \mathbf{R}) . The choice of the training data set is an important step in regression analysis. Due to its importance, this data set is also called gold standard, for which the state vector corresponding to each real observation \mathbf{R} is assumed to be exactly known. In practice in many applications this is not possible. As a consequence the sample is not fully representative of the full population and the statistical properties estimated from the data set are not robust. When a “gold standard” is not available or not fully representative, it is usual to choose a training data set starting from a representative set of state vectors which are paired to observations by using a forward model, that is $(\mathbf{v}, \mathbf{R}) = (\mathbf{v}, F(\mathbf{v}))$. In this case, this data set is called “silver” standard. One of the most popular silver standard used for IASI relies on the so-called Chevalier database (F., 2001), a diverse profile set derived from the ECMWF model, which has been used, for example, in the simultaneous retrieval of T_s, T, Q and O_3 by Grieco et al. (2010).

Today silver standard sets for IASI can be very highly specialized and tuned for applications such as the retrieval of atmospheric species and trace gases (see, for example, Hilton et al., 2012a) and publications available at the IASI web site http://iasi.cnes.fr/en/IASI/A_publications.htm).

Look-up tables (LUT) are arrays that replace runtime computation of $\mathbf{R} = F(\mathbf{v})$ with simpler array indexing operations, and have been also used for IASI retrievals. The savings in terms

of processing time can be significant, since retrieving a value from memory is often faster than undergoing an expensive computation of $F(\mathbf{v})$. The approach has been largely used for the retrieval of aerosol properties, which normally involves heavy computation based on Mie scattering theory.

6.1.2.2 Neural Networks

Since Hornik et al. (1989) proved that multilayer perceptron (MLP) or feedforward networks are universal approximators, the interest in neural networks (NNs) has rapidly grown. Today, NNs have widespread applications in many areas of remote sensing and are frequently applied to many classes of strongly nonlinear or highly noisy problem typologies.

Alternative inversion approaches such as NNs have been tested since the early stage of IASI development (e.g. Clerbaux et al., 1999; Luchetta et al., 2003). Applications to IASI can be found within the references of Hilton et al. (2012a) and on the website http://iasi.cnes.fr/en/IASI/A_publications.htm One of the main problems with using hyperspectral sensors such as IASI and IASI-NG is the huge amount of spectral radiance data points these instruments produce. Variational and other iterative methods require costly forward model calculations at each iteration, and work best when an accurate first guess is available. Another advantage of the NN approach is that the error covariances of the training data do not need to be provided explicitly, and thus non-linear relations can be represented within the NN (in a variational scheme, the background and observation errors are provided as a covariance matrix, which may be a simplification of the true form of the error relationships).

6.2 Input data

The data may be provided to the retrieval scheme in various forms, the simplest of which is a radiance vector. Data may be further processed or filtered, and such processing may alter the error characteristics of the data. This section discusses the implications of the way input data are processed prior to ingest into the retrieval or assimilation scheme.

6.2.1 Unprocessed L1c radiance data

The L1c IASI-NG data consist of calibrated, geolocated apodised radiance spectra, as described in chapter 3. In principle, the use of L1c radiances does not require any change or transform of the instrument observational covariance matrix, which means that there is no loss of information content.

In addition to the spectral radiance domain, the Brightness Temperature (BT) data space has been also largely used for the retrieval of atmospheric profiling. The reason is that the BT data points are much more linearly related to the parameter space (temperature and moisture). BTs are normally preferred to spectral radiances when we deal with regression or neural networks. The use of BT in physical retrieval schemes is not universal because for optimal use the observational covariance matrix has to be transformed to the BT space and the transform depends on the brightness temperature value itself. Conversely, for the case of the physical radiance space, the observational covariance matrix can be assumed independent of the spectral radiance. Thus, for physical inversion and assimilation the use of spectral radiances should be recommended.

For IASI, the number of spectral ordinates for each single spectrum is $M_{IASI} = 8461$. This figure will double for IASI-NG because of the improved spectral sampling (0.25 cm^{-1} for IASI and 0.125 cm^{-1} for IASI-NG). The high dimensionality of the IASI data space has meant that for many applications much of the spectrum is discarded prior to use, making it is difficult to extract

the full information content from each observation. As an example, of the 8461 IASI channels received at the European Centre for Medium Range Weather Forecasts (ECMWF) only 366 are routinely monitored and even fewer (168) are actively assimilated (Collard and McNally, 2009). Nowadays full IASI spectra (covering 645–2760 cm^{-1}) can be processed easily off-line for science applications (e.g. Masiello et al., 2012). However, despite the improvement in telecommunication and computing hardware and software technology, it is likely that operational applications such as NWP will still be unable to process the full spectrum for each observation in near-real-time on the timescales on which IASI-NG data will be ready for dissemination to end users.

6.2.1.1 Reducing the vector length via channel selection

The most common approach to reduce dimensionality of the retrieval or assimilation problem is to select only those channels that provide the majority of the information pertaining to the state vector. The number of channels may be more or less depending on the application; for temperature and water vapour there are many channels from which to choose and selection algorithms are required. For species with only a few absorption lines within the spectral range of IASI-NG it may be possible to choose channels based on spectroscopic knowledge.

The use of an algorithmic approach to channel selection is based on the choice of suitable selection criteria which can be optimized for the particular end-use. For example, the method of (Collard, 2007), which uses degrees of freedom for signal (DFS) optimized with respect to the retrieval information content for temperature and water vapour as a measure of the information content of the selected channels, is used by many NWP centres. Further work is ongoing to improve upon this basic method and to tailor it further to the application (e.g. Eresmaa et al., 2014; Migliorini et al., 2014; Smith, 2015; Ventress and Dudhia, 2013).

The use of a suitable set of sparse channels does not require further modification of the observational covariance matrix.

6.2.1.2 Reducing the vector length via microwindows

A microwindow is a small set of contiguous channels over a very limited spectral interval. Its purpose is to isolate the absorption features of a given molecule within the small spectral interval for use in a physical retrieval scheme. By selecting spectrally contiguous channels, the radiative transfer computations are reduced because only a few spectral lines need to be considered.

Techniques for optimal selection of a microwindow have been developed for MIPAS and for other chemistry mission instruments (e.g. Dudhia et al., 2002). The general principle is related to the sequential channel selection methods used for sparse channel selection, but once a selection of candidate channels has been chosen using a figure of merit, each is used to “grow” a microwindow by adding adjacent channels until subsequent channels fail to add any more information. Candidate microwindows can then be compared for their information content.

The use of microwindows is not expected to be of use for temperature and humidity sounding with IASI-NG, because the relevant information is contained in the many absorption lines of CO_2 and H_2O respectively that are spread throughout the spectrum.

It is possible that dissemination of channels in a microwindow could be a solution for low bandwidth data dissemination (see section 4.2).

6.2.2 Transformed datasets

6.2.2.1 Principal component scores

Applications such as NWP require access to information that is distributed across the spectrum in CO₂ and H₂O absorption lines. Quite apart from the prohibitive computational cost of accessing the information on these species from across the whole spectrum, it is understood that the independent information on the atmosphere contained in an IASI (or IASI-NG) spectrum is significantly less than the total number of channels (e.g. Huang et al., 1992). There is thus a need to find a more efficient way of communicating the measured information to the analysis system than simply increasing the number of channels. Similarly, satellite agencies are seeking a more efficient means of near-real time data dissemination for instruments such as IASI - as the traditional practice of transmitting full spectral data at full spatial resolution is likely to become prohibitively expensive in the future (as instruments are flown on multiple polar and geostationary platforms).

Principal Component Analysis (PCA) is a classical statistical method for the efficient encapsulation of information from voluminous data (Jolliffe, 2002). As such, it has been proposed as a solution to the above problems although - while noting that the two issues are quite similar- the requirements are quite separate. There are strong indications that data providers will evolve to the dissemination of Principal Component (PC) scores to improve efficiency. It is thus timely and opportune to investigate the feasibility of directly assimilating PC scores into NWP models.

PCA is a method that allows the reduction of the dimensionality of a data set by exploiting the interrelation between all the variables contained in the data set. The reduction of the dimension of the dataset is obtained by replacing the original set of correlated variables with a smaller number of uncorrelated variables called principal components. Because the new derived variables retain most of the information contained in the original data set, PCA theory provides a tunable mechanism to efficiently represent the information in the dataset.

The mathematical basis for PC compression

Within the context of satellite data assimilation, a training data set consisting of a sample of l spectra of n radiances is first arranged into an l by n data matrix \mathbf{R} . These training data can then be represented by the vector population $\mathbf{r} = (r_1, r_2, \dots, r_n)^T$ (where T denotes the transpose). If \mathbf{C} is the n by n covariance matrix of the data matrix \mathbf{R} , and \mathbf{A} is the n by n matrix formed by the eigenvectors of the covariance matrix arranged as row vectors in descending order according to the magnitude of their eigenvalues, the PCs, \mathbf{p} , of the vector population can be written as:

$$\mathbf{p} = \mathbf{A}\mathbf{r} \tag{6.14}$$

The eigenvectors represent the directions of maximum variance in the data; consequently, each PC gives the linear combination of the variables that provides the maximum variation. The PCs are orthogonal, hence uncorrelated (although this does not imply that they are statistically independent), and the values associated with each spectrum are known as PC scores. If λ_i is the eigenvalue associated with the i th eigenvector, then the value of $\lambda_i / \sum_{i=1}^n \lambda_i^2$ gives the proportion of variation explained by the i th PC. Because the matrix \mathbf{A} is orthogonal, its inverse is equal to its transpose and we can write:

$$\mathbf{r} = \mathbf{A}^T \mathbf{p} \tag{6.15}$$

Equations equation 6.14 and equation 6.15 can be written in discrete notation form as:

$$p_{i,j} = \sum_{k=1}^n A_{i,k} r_{k,j} \quad (6.16)$$

$$r_{i,j} = \sum_{k=1}^n A_{k,i} p_{k,j} \quad (6.17)$$

where $i = 1, n$ represents the i th channel and $j = 1, l$ is the j th spectrum. A number of PCs, m , fewer than n can often represent most of the variation in the data. The dimension of the data set can then be reduced by replacing the n original variables with the first m PCs. In many applications, the choice of the number of dimensions is based on the total variation accounted for by the leading PCs and it will in general depend on specific aspects of the original dataset.

For any new observed radiance spectrum, \mathbf{r}^{obs} , the equivalent PC scores can be computed by projecting the radiances upon the full set of eigenvectors derived from the covariance matrix of the training dataset. As discussed above, less than n eigenvectors are typically required to reproduce most of the information in the observed spectra. Therefore, the vector of m truncated observed PC scores, \mathbf{p}^{obs} , can be computed as:

$$p_i^{obs} = \sum_{k=1}^n A_{i,k} r_k^{obs} \quad (6.18)$$

where $i = 1, m$. The truncated PC scores may be regarded as an efficient encapsulation of the original observation that may be used for storage, transmission or indeed assimilation.

It should be noted that in addition to reducing the dimension of the observed information, the value of m can also be tuned to achieve filtering of the observations, using PCA to separate variations of the atmospheric signal from variations of the random instrument noise. It is argued that the atmospheric signal is more highly correlated across the spectrum and as such is represented by the high rank eigenvectors (i.e. those with larger eigenvalues). Conversely, the random instrument noise is spectrally uncorrelated and is thus represented by low rank eigenvectors. In principle, an attempt to exploit this separation (in ranked eigenvector space) can be made by retaining only eigenvectors related to atmospheric signal and discard those eigenvectors describing instrument noise. Atkinson et al. (2010) show how this technique can be exploited to improve the signal in the case of detection of various atmospheric trace gases.

Of course great care must be taken if truncating the PC scores for this specific purpose. Small scale and small amplitude atmospheric features can be important sources of rapid forecast error growth in NWP. However, such features may not be strongly correlated across the measured spectrum and could potentially be confused with noise (and removed if the truncation is too severe). Optimal noise filtering can be achieved by noise normalising the spectra. For interferometer instruments whose radiances have been apodised, it is important that spectra are normalised using the full instrument error covariance matrix. This will ensure that the noise signal is evenly distributed among all eigenvectors (see Antonelli et al., 2004, for details).

PC compression forms the baseline for MTG-IRS radiance dissemination. However, the truncated representation of high spectral resolution infrared observations is not a lossless compression, which could be of some concern for certain applications where the signal is small. Further research is also needed in the use of PC-compressed data in cloudy regions: the PC scores themselves will contain information on the cloud. It is possible that in spectra reconstructed from the PC scores, radiative signals from low cloud could be mapped into higher peaking channels. More research to determine whether this is a non-negligible effect is required.

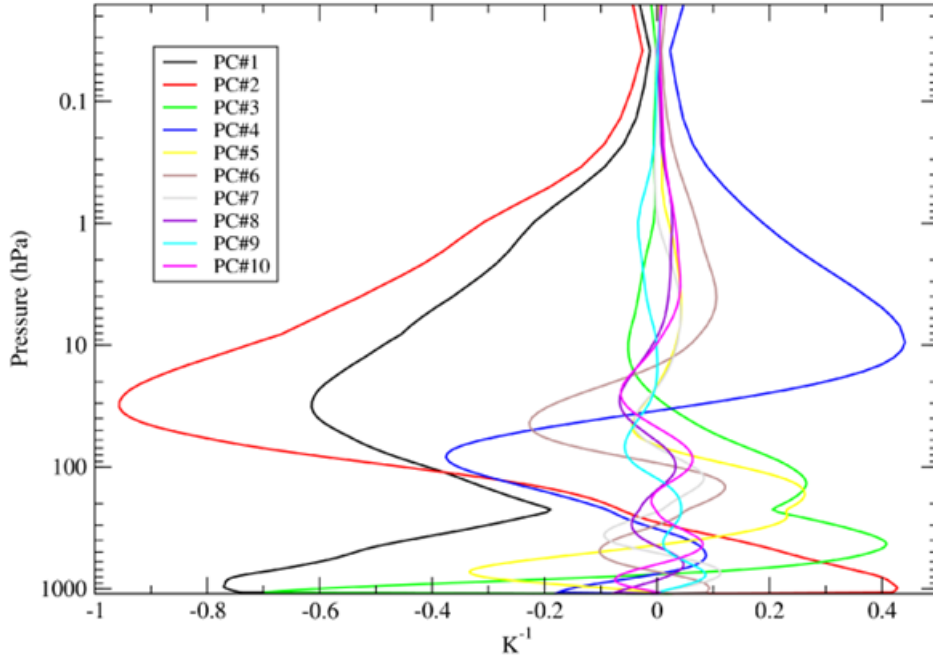


Figure 6.1: The temperature Jacobian for the first 10 PCs for the US Standard Atmosphere.

Interpretation of PC scores

When compared to spectral radiances, the physical interpretation of PC score observations is less intuitive. This is illustrated in figure 6.1, which shows the temperature Jacobians for the US Standard Atmosphere for the first ten PC scores of a portion of the IASI spectrum that comprises 165 long-wave channels whose primary sensitivity is to temperature and the surface, although they also convey some humidity information. Radiance temperature Jacobians are broad, but relatively localized in a given part of the atmosphere (e.g. surface or stratosphere) whereas the PC score Jacobians are not localized and can have multiple maxima throughout the entire atmosphere (e.g. at the surface and in the stratosphere).

Near-surface layers give a contribution to the signal that is significantly larger for the first three PCs. While sensitivity to the stratosphere is apparent to a variable extent in a number of PCs, PC#2 has the largest contribution from that region. It should be noted that the highest ranking PCs also have a significant sensitivity to changes in the surface skin temperature (see table 6.1).

This is particularly true for PC#1 whose behaviour is closely related to that of a window channel radiance and has the strongest response to the presence of cloud. However, in this case if the warm surface is obscured by a cold cloud, we expect a warming of the observed PC#1 score (opposite to the response of an infrared window channel that would cool). Cloud signals appear as an asymmetry (i.e. a warm tail) in the histogram of the observed minus computed PC#1 score departures. Although not shown here, the ten PCs in figure 6.1 are also sensitive to humidity. It should be stressed that the behaviour and the nature of the PCs is affected by the choice of the channel set used for the PC generation. By choosing a different channel set for the PC

| PC number | Jacobian (K ⁻¹) |
|-----------|-----------------------------|
| 1 | -9.181 |
| 2 | 5.459 |
| 3 | -11.783 |
| 4 | -2.428 |
| 5 | 4.281 |
| 6 | -0.896 |
| 7 | -0.797 |
| 8 | 0.487 |
| 9 | -1.357 |
| 10 | 0.565 |

Table 6.1: The skin temperature Jacobian for the first 10 PCs for the U.S. Standard Atmosphere.

generation, Jacobians may become more or less localized, signals from different spectral regions may become more or less separable and an intuitive effect like that of PC#1 behaving like a radiance window channel may be lost.

6.2.3 Interferogram transforms

In addition to the PC transform, a further obvious unitary transform is the well-known Fourier transform, which has been so far used in many applications for data compression and reduction. For IASI and IASI-NG the Fourier transform has a special meaning, since both instruments are Fourier transform spectrometers, and as such measure the Fourier transform of the spectrum, which is usually referred to as the interferogram.

In Fourier spectroscopy the spectrum, $r(\sigma)$ (with σ the wavenumber) and the interferogram, $c(\chi)$ (with χ the optical path difference) constitute a Fourier pair defined by the following equations (see e.g. Bell, 1972),

$$r(\sigma) = \int_{-\infty}^{+\infty} c(\chi) \exp(-2\pi i \sigma \chi) d\chi \quad (6.19)$$

$$c(\chi) = \int_{-\infty}^{+\infty} r(\sigma) \exp(2\pi i \sigma \chi) d\sigma \quad (6.20)$$

with i the imaginary unit.

The spectrum and the interferogram are in practice band-limited functions, therefore taking into account that the interferogram is sampled up to a given maximum optical path difference, χ_{max} , we modify equation 6.19 by introducing the data-sampling window, $W(\chi)$

$$r(\sigma) = \int_{-\infty}^{+\infty} W(\chi) c(\chi) \exp(-2\pi i \sigma \chi) d\chi \quad (6.21)$$

with

$$W(\chi) = \begin{cases} 1 & \text{for } |\chi| \leq \chi_{max} \\ 0 & \text{otherwise} \end{cases} \quad (6.22)$$

where $|\cdot|$ means absolute value, χ_{max} is the maximum optical path difference.

The maximum optical path difference, χ_{max} also determines the sampling rate, $\Delta\sigma$ within the spectral domain. According to the Nyquist rule, the relation is

$$\Delta\sigma = \frac{1}{2\chi_{max}}, \quad \Delta\chi = \frac{1}{2(\sigma_2 - \sigma_1)} \quad (6.23)$$

where $\sigma_2 - \sigma_1$ is the spectral band-width. For IASI (IASI-NG) we have $\sigma_1 = 645 \text{ cm}^{-1}$, $\sigma_2 = 2760 \text{ cm}^{-1}$, hence $\chi_{max} = 2$ ($\chi_{max} = 4$) cm and $\Delta\sigma = 0.25$ ($\Delta\sigma = 0.125$) cm^{-1} .

The fact that the spectrum may be apodized (see e.g. Amato et al., 1998) is of no concern here. For IASI and/or IASI-NG we just consider the interferogram obtained from the calibrated, apodized spectrum, which, as said, is a band nd limited function over the range $645\text{--}2760 \text{ cm}^{-1}$.

According to the Shannon-Whittaker sampling theorem (Bell, 1972), in case we want to re-sample the spectrum at sampling rate lower than the original, we just have to introduce in equation 6.21 a data-sampling window with its new cutting point at $\chi_\tau < \chi_{max}$. The number, M_τ of independent data points which are left after applying this truncation is:

$$\frac{M_\tau}{M_{IASI}} = \frac{\chi_\tau}{\chi_{max}} \quad (6.24)$$

whereas the new sampling rate in the spectral domain involves again the Nyquist rule:

$$\begin{cases} \Delta\sigma_\tau = & (2\chi_\tau)^{-1} \\ \frac{M_\tau}{M_{IASI}} = & \frac{\Delta\sigma}{\Delta\sigma_\tau} \end{cases} \quad (6.25)$$

The *partial interferogram* can be easily introduced using the concept of a data-sampling window applied to the complete interferogram extending from $\chi = 0$ to $\chi = \chi_{max}$.

The data-sampling window considers both a lower and upper truncation point (Kyle, 1977):

$$\tilde{W}(\chi) = \begin{cases} 1 & \text{for } \chi_{\tau_l} \leq |\chi| \leq \chi_{\tau_u} \\ 0 & \text{otherwise} \end{cases} \quad (6.26)$$

An appropriate definition of the lower end-points χ_{τ_l} can remove from the spectrum all those broad features, which are represented by interferometric radiances below χ_{τ_l} . In fact we have:

$$\tilde{W}(\chi) = W(\chi)_{\tau_u} - W(\chi)_{\tau_l} \quad (6.27)$$

where W is the box-car window as defined in equation 6.22 and where the under scripts τ_l and τ_u identify the window function with end-points, χ_{τ_l} and χ_{τ_u} , respectively.

It is worth noting that both truncated interferogram and partially scanned interferogram samples are characterized by an observational covariance matrix which is diagonal.

An example of how we can use the concept of partial interferogram is provided in figure 6.2 where we consider the partial interferogram corresponding to truncation points $\chi_{\tau_l} = 0.65$ cm and $\chi_{\tau_u} = 0.68$ cm. The contrast shown in figure with an interferogram corresponding to a CO_2 load equal to zero helps to understand how much this short segment is dominated by CO_2 emission. The emission for the whole spectrum finds a strong positive interference or correlation in a very short segment of the interferogram. This interference is caused by the regular spacing of CO_2 lines. In the wave number domain this regular spacing has a period of about

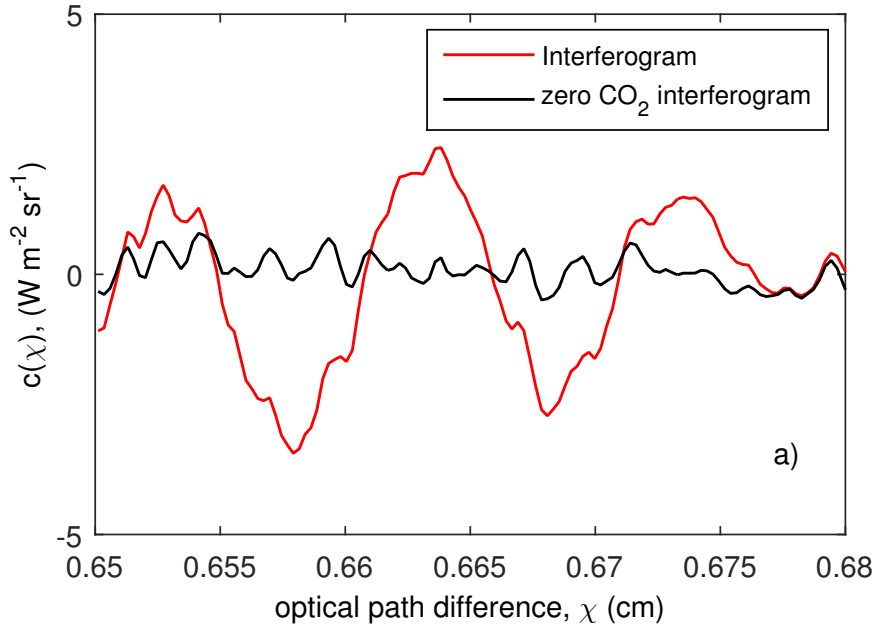


Figure 6.2: Example of partial interferogram in the range $[\chi = 0.65, \chi = 0.68]$ cm for a case of CO_2 load equal to 0 and 385 ppmv, respectively.

1.6 cm^{-1} and modern satellite infrared sensors have been designed with a spectral resolution better than 0.8 cm^{-1} in order to resolve the periodic structure, which is much more marked in the ν_2 CO_2 band. Figure 6.2 shows that the interferogram interval $[0.65, 0.68] \text{ cm}$ contains much of the information about CO_2 lines.

Exploiting the concept of the truncated interferogram, Grieco et al. (2010) has shown how to perform a dimensionality reduction of IASI data, which preserves the IASI spectral coverage. Once compared to the usual way of reducing the IASI data by simply considering a selection of IASI sparse channels, the truncated transform methodology has shown a better performance mostly for the retrieval of water vapour (Grieco et al., 2011).

The concept of the partial interferogram has proven to be really effective to retrieve columnar abundance of atmospheric minor and trace species (CO_2 , CO , CH_4 , N_2O) with unprecedented accuracy (Grieco et al., 2013; 2015).

6.2.4 Reconstructed Radiances

The backward transform of the truncated expansions that have been described in the previous in the two previous section yields a set of reconstructed radiances. It is believed that reconstructed radiances can provide some of the benefits of the truncated dataset, but should have a lesser impact on current data assimilation software because their form is equivalent to that of spectral radiances. (Collard et al., 2010). The Jacobian and adjoint matrix would be similar to those produced with raw radiances. In addition, the cloud scene analysis which is preliminary to most data assimilation systems would be not modified with respect to that currently performed with original spectral radiances.

The property of reconstructed radiances in terms of independence can be tricky as discussed by Masiello et al. (2012), which also addresses the issue of how to produce linearly independent

reconstructed radiances. The observational error covariance matrix has to be modified by the same transforms and normally it is not diagonal.

With reconstructed radiances we can reduce the dimensionality of the data space by a factor of around 100, which does not occur at the expense of the instrument spectral coverage. Dimensionality reduction occurs through the selection of channels, as for the L1c spectrum. In this case the selection should take account of the modified error covariance matrix. The subject of reconstructed radiances and their use in data assimilation is a subject of active research (Smith, 2015), which hopefully will lead to definite results by the time IASI-NG is put in orbit.

6.2.5 Superchannels

The concept of superchannels is similar to that of reconstructed radiances, in that channels are grouped together by the use of a function that depends upon their sensitivity. It relies on a suitable transform of the raw radiances which is not necessarily unitary. As an example, in the early stage of AIRS mission, superchannels were proposed based on the spectral average of groups of contiguous channels, or channels mostly linearly correlated with geophysical parameters. These methods do not save the instrument spectral coverage, do modify the observational covariance matrix and can even reduce the spectral resolution of the instrument. The use of unitary transforms via PC scores or Fourier coefficients is preferred over such ad hoc, somewhat heuristic, transforms.

The superchannel approach is not documented for use in any retrieval schemes at the present time, although it was one approach examined for IASI (P. Schlüssel, pers. comm.). However, a multi-channel averaging approach can be useful to compare the performance of instruments with different spectral characteristics, and indeed are used for instrument intercomparisons performed by the IASI Technical Expertise Centre (Jouglet et al., 2013).

6.3 Specific considerations for retrieval schemes

6.3.1 Clouds and aerosols

By the time of launch of IASI-NG, it is anticipated that some applications, such as NWP, will use an all-sky approach to assimilation and the screening of cloud will therefore not be necessary for many users. However, some applications will always require cloud-free data and even for NWP some form of cloud characterisation is likely to form an important part of the data processing chain. In offline retrieval schemes, there are already treatments of cloud in some schemes, for example via effective fraction and height of a blackbody cloud.

6.3.1.1 Cloud and aerosol detection

The quality of the cloud detection mask is of paramount importance for the retrieval of surface and atmospheric parameters. For cloud detection it is of great benefit to exploit synergy with imagers to qualify the scene. Following from IASI, where a cloud fraction in the IASI field-of-view is defined using AVHRR, MetImage data will be used to assist with determination of cloud fraction in IASI-NG. Data from collocated MetImage pixels will be provided as part of the IASI-NG L1c as described in section 4.1 and further research should be undertaken into the development of cloud characterisation schemes that make use of this information. The MAIA scheme developed at Météo-France by Lydie Lavanant could form a good starting point.

A stand alone IASI-NG cloud detection and scene analysis is also desirable for real time usage of the data and in case of failure of MetImage. Eventually the IASI-NG stand alone scene analysis

should be tuned and calibrated with a dedicated validation campaign during commissioning of the instrument.

Fewer applications contain dedicated aerosol detection algorithms, but the effect of aerosol on IASI observations has been demonstrated and so affected observations should be identified and potentially screened out. Aerosol products are now important for air quality applications, as described in section 8.3. Radiative transfer models are increasingly able to simulate the radiative effects of different types of particulate and so it is becoming both important and possible to develop aerosol detection algorithms. This research should be prioritised.

6.3.1.2 Cloud clearing

An alternative approach to cloud screening is to use the information from adjacent observations (or combined with sub-pixel information from an imager) to construct a clear-sky radiance from a group of partially cloudy pixels. This approach was investigated before the launch of IASI, but then rejected for Level 2 processing. However, the approach remains in use at NOAA, with NCEP investigating the assimilation of cloud-cleared radiances and obtaining positive impact in the NWP model.

Cloud-cleared radiances may have complex error characteristics and will always be a blend of information from adjacent observations. However, it may be worthwhile to revisit their use prior to the launch of IASI-NG given the increasing sophistication of error handling within retrieval and assimilation systems.

6.3.2 Computation and correction of radiative biases

Biases between the observation and a forward-modelled atmospheric profile may result from the instrument, the forward model and from the atmospheric profile itself. Such biases will propagate through to the retrieval or analysis, and it is an underlying assumption of any scheme based on the optimal estimation/data assimilation equations that there is no bias between the observation and the prior information. Any remaining bias will therefore result in a retrieval that does not provide the best representation of the true atmospheric state. In general, for any kind of retrieval or assimilation scheme, it is desirable to eliminate biases from the observation that originate in the instrument and forward model, but to avoid correcting biases in the a priori.

The problem with bias correction is the lack of information about the source of bias. Observations can be compared with their forward modelled counterparts, but it is not possible from these comparisons to form a definitive estimate of how much of the resulting bias is from the observation and forward model, and how much is from the estimate of the atmospheric state. Radiances can also be compared against other observations from different instruments, and some understanding may be reached, but this sort of detailed study is often only possible in the context of climate monitoring and is not really suitable for development of a near-real-time bias correction scheme.

For NWP, bias correction has a long heritage, and various atmospheric predictors (such as layer thickness terms) and scan-dependent terms are in use around the world. The most common way bias correction is implemented in variational analysis schemes is to add the bias predictors to the control variable and thus nudge the bias correction for the next assimilation cycle. This is known as VarBC. Bias correction in an assimilation context is described in section 7.5.

For standalone retrieval schemes, particularly those with climatological a priori, although it is possible to retrieve bias corrections as part of the estimated vector, the problem is significantly underdetermined. Rodgers (2000) proposes Kalman filtering as a solution to this, allowing the

bias parameters to change a tiny bit during a series of retrievals, similar to the VarBC approach. There are many practical steps to implementing such a scheme for example the selection of error covariances for the bias parameters. Research is ongoing at Reading University into the development of such a scheme for broadband radiometers, that may be applicable to hyperspectral instruments as well (C. Merchant, pers. comm.). One idea also worth exploring is that it may be possible to use the physics of the measurement method and the IR spectrum to impose some restrictions on the relative biases across the spectrum.

Although it is desirable to not remove model biases from the observations for assimilation, for climate applications, it is critical that model biases are not attributed to observations, and furthermore it is important to be able to partition biases between the instrument itself and the forward model. These different sources of bias may have different spatio-temporal scales, but any such analysis is complex and prone to error in the absence of bias-free reference observations.

Given the importance of bias within assimilation and retrieval systems, and the anticipated low noise of IASI-NG, the development and enhancement of bias correction schemes should be considered a priority.

6.3.3 A priori error characteristics

Physical retrieval schemes always start with some prior estimate of the atmospheric state, as described in section 6.1.1, often referred to as the background. This estimate can be derived from a climatology or from a recent forecast of the atmospheric state. Hilton et al. (2009a) show that the use of a bland climatological background state often results in a retrieval without the sharp features visible in the observation. Short-range NWP forecasts are usually the best source of background data where they are available. There is a continuing challenge to understand variability of the atmosphere in order to better estimate appropriate statistics for atmospheric chemistry products.

Techniques exist, within the context of an assimilation system, to estimate background errors for temperature and humidity at least, (e.g. Andersson et al., 2000; Hollingsworth and Lönnerberg, 1986), and in the case where NWP profiles are used as a priori, may be provided by the originating centre. Regardless of the source of the a priori information, its error characteristics must be well defined because they have a fundamental relationship to the error properties of the retrieval. This is of particular importance for the assimilation of L2 products (see chapter 7). Migliorini (2012) shows that it is important that the errors ascribed to the background error term do not underweight the observation in the retrieval scheme if the maximum information is to be extracted from the profile by the assimilation system. Note that the opposite is true of the background error term in the assimilation system itself: Eyre and Hilton (2013) demonstrate that damage can be done to the assimilation system if the background error term is overestimated relative to the true errors.

6.3.4 Observation error characteristics

In the context of a retrieval scheme, the observation error term will usually combine several sources of error that are ascribed to the observation rather than the a priori or background. The most important sources of error to be accounted for are instrument noise (transformed by any post-processing of the observation such as PC compression) and forward model errors. It is important that correlations between the channels are specified, as well as the error variance.

It is expected that the instrument noise variance will be well-understood from careful analysis of calibration data by CNES. The correlation terms introduced by apodisation will also be well-

understood because this is a straightforward mathematical function. Scene heterogeneity may affect the error variance and introduce error correlations that are not present in homogeneous calibration scenes. It is important that the errors are as well characterised for homogeneous scenes as possible.

Radiative transfer errors are often harder to estimate directly. Most forward model errors manifest as a bias, but what remains after bias correction is usually treated as a random component of the observation error covariance matrix. The RT error term should include:

- errors that result from insufficient knowledge of spectroscopy,
- errors in the line-by-line modelling,
- errors introduced by fast models resulting from parameterisation of the line-by-line model output (where a fast RT model is used).

The last of these is the easiest to estimate but requires careful comparisons over an extensive database of atmospheric scenes (e.g. Matricardi, 2007). Intercomparisons of line-by-line models can provide insight into the likely magnitude of spectroscopic errors for certain parts of the spectrum.

It is worth noting that some sources of observation error (notably certain contributions to the instrument noise) are properly random errors (i.e. if one were to be able to measure exactly the same scene twice, there would be a small random difference in the measurement), whilst other sources are pseudo-random, in that they depend upon the atmospheric state. Both types of error are combined into the same error covariance matrix in practical application.

Since IASI-NG is expected to have very low instrument noise, it is likely that radiative transfer errors will dominate, especially for the water vapour absorption band. Because of the fact that radiative transfer modelling is a fundamental part of the extraction of information from IASI-NG observations for any physical retrieval scheme, understanding forward model errors should be considered a priority.

Some of the same techniques that are used to estimate background errors for NWP, notably Hollingsworth and Lönnberg (1986) can be used to estimate the observation error term, and may be applied to a retrieval scheme outside of NWP (such an analysis has been performed for the EUMETSAT IASI L2 retrieval scheme as reported in Smith, 2015). The technique of Desroziers et al. (2005) is another alternative that is used in NWP; this could potentially be adapted to work for a standalone retrieval scheme. Such techniques are only estimates and have drawbacks in their practical application, but may provide useful information that, when used in conjunction with other sources of information on the various error terms, can be used to generate covariance matrices for use in retrieval schemes or for assimilation. These techniques are discussed further in section 7.4.

6.4 Retrieval of atmospheric and surface properties

6.4.1 Thermodynamic Variables

6.4.1.1 Temperature and water vapour profiles

Post-launch validation of retrievals of temperature and water vapour profiles derived from IASI has confirmed an accuracy of less than 1 K for temperature between 800hPa and the tropopause and better than 10% for relative humidity in the 800-300 hPa altitude range (Kwon et al., 2012; Pougatchev et al., 2009). However, as for any existing thermal infrared sounder, IASI still suffers from a limited sensitivity to the lower part of the troposphere near the surface, and to the

tropopause region. Accordingly, the estimated accuracy reaches 2–3 K at the surface and around 2 K at the tropopause for temperature, and is higher than 10 % near the surface for H₂O where it is the most abundant. Improving the retrievals near the surface is thus a clear priority and one of the main objectives of the IASI-NG mission. It is worth noting that, beyond the impact on operational meteorology, any improvement in the characterization of the thermodynamic profiles will positively impact the retrievals of other atmospheric variables which usually require a good knowledge of the thermodynamic state of the atmosphere.

6.4.1.2 Surface properties

Surface emissivity is a key parameter to improve temperature and moisture profiling of the lower atmosphere over land, and especially over desert sand. So far surface emissivity retrieval has been based on sequential strategy (for example the AIRS algorithm of Susskind et al., 2003; 2011) or systems assisted by suitable emissivity atlases (e.g. Capelle et al., 2012; Zhou et al., 2011; Zhou et al., 2008)). Among emissivity atlases, those based on satellite data (e.g. MODIS, SEVIRI) have been really successful in providing the initialization for the simultaneous retrieval of surface and atmospheric parameters (Masiello and Serio, 2013; Masiello et al., 2014). To date the most widely used emissivity atlas is that developed by University of Wisconsin (Seemann et al., 2008, see also <http://cimss.ssec.wisc.edu/iremisp/>).

A true simultaneous retrieval methodology for surface and atmospheric parameters has been limited up to now to the realm of research issues (Masiello and Serio, 2013; Masiello et al., 2014). The dimensionality of the emissivity spectrum is the same as that of IASI and IASI-NG spectra. Thus an effective retrieval methodology has to find an effective representation of the emissivity spectrum with a number of degrees of freedom less than the number of IASI-NG spectral ordinates or channels. Both truncated EOF and Fourier transforms seem to be adequate for the retrieval problem, although more research is needed to draw firm conclusions.

To date satellite surface parameters are still questionable as far as their quality and accuracy is concerned, the effective separation of the surface temperature from emissivity is still an open issue, as well as the influence of the atmospheric state over the final surface products and vice versa. For this reason, a retrieval method capable of simultaneously estimating land surface and atmospheric parameters is highly desirable and IASI-NG should provide enhanced data to address this issue. Research in this area should be prioritised.

6.4.2 Clouds and Aerosols

6.4.2.1 Cloud properties

In addition to the usual cloud parameters (e.g. cloud type, cloud top pressure and temperature, cloud fraction, cloud liquid water and ice content), specific points that should be addressed with dedicated studies based on a realistic concept of IASI-NG instrument (both ISRF and noise model) include:

- which kind of microphysical optical parameters and compositions we can retrieve: equivalent shape and effective radius, optical depth, ice/water, phase.
- the need to deal with single layer and multilayer clouds
- the need to identify data sets of cloud profiles (cloud fraction, cloud liquid water and ice water content) to have a better insight on what we can retrieve; again it is important to define a suitable training data set
- what information we can retrieve about ice cirrus clouds: what we have done with IASI and what we will be able to do with IASI-NG.

Retrieval of cloud properties is a less mature area of research than the retrieval of thermodynamic quantities or chemical species. More work in this area is urgently needed.

6.4.2.2 Aerosols

The quality of aerosol retrievals depends critically on several parameters affecting the baseline, namely surface temperature and emissivity and cloud coverage. While simultaneous retrieval of these parameters by one instrument is an unsolved problem, one can make use of external measurement data or use climatological databases (in case of surface emissivity). In addition to these difficulties, and in contrast to trace gases, there is the problem of variable aerosol optical properties stemming from variabilities in composition (refractive indices) and size distributions. Retrieval techniques should be sought which minimize their dependency on these. Similarly to cloud parameters, there is also the need to define a comprehensive data set of profiles for training and validation.

Aerosols affect the environment and climate in a number of ways. Several dedicated aerosol sounders are currently in operation, using the UV/VIS spectral range to retrieve the aerosol optical depth at 550 nm. Infrared sounders can provide complementary and independent information and offer

- the possibility of night-time measurements
- good sensitivity over bright surfaces
- good sensitivity of coarse mode aerosols.

In addition, high spectral resolution infrared sounders allow retrieving two important climate parameters namely altitude and aerosol composition.

Detection and differentiation

The IASI and IASI-NG spectral range has three atmospheric windows around 4, 5 and 8–12 μm , suitable for the retrieval of aerosol properties. Apart from water droplets and ice crystals in clouds, at least five distinct aerosol types have been observed with IASI, these are: windblown dust, biomass burning aerosols, sulfate aerosols, volcanic ash and ammonium sulphates. The most pronounced aerosol signatures are illustrated on observed IASI spectra in figure 6.3.

Mineral aerosols has been the main focus for IASI (see next section). Work on the other aerosol types has until now been mainly qualitative, dealing with aerosol detection and type differentiation. A detailed overview of aerosol detection methods is given in Clarisse et al. (2013), where also a unified method is presented for distinguishing aerosol types from each other. The outlined method is particularly promising for the minerals and the sulfates. Type differentiation in the infrared exploits directly the spectral dependency of the refractive index, and complements techniques in the UV/VIS which rely on size parameters, the single scattering albedo and polarization. The potential of high resolution infrared sounders for this purpose has now been demonstrated, and with its improved instrumental properties, it can be hoped that the IASI-NG measurements will be exploited fully for this purpose.

Mineral aerosols

Owing to a strong Si–O resonance band centered in the atmospheric window at 8–12 μm , thermal infrared sounders are well suited to measure mineral aerosols. Building on the heritage of algorithms developed for AIRS, several groups have now developed algorithms for the retrieval of windblown dust aerosols (Clarisse et al., 2010; Klüser et al., 2011; Peyridieu et al., 2013; Vandenbussche et al., 2013). In addition to optical depth, high resolution infrared observations

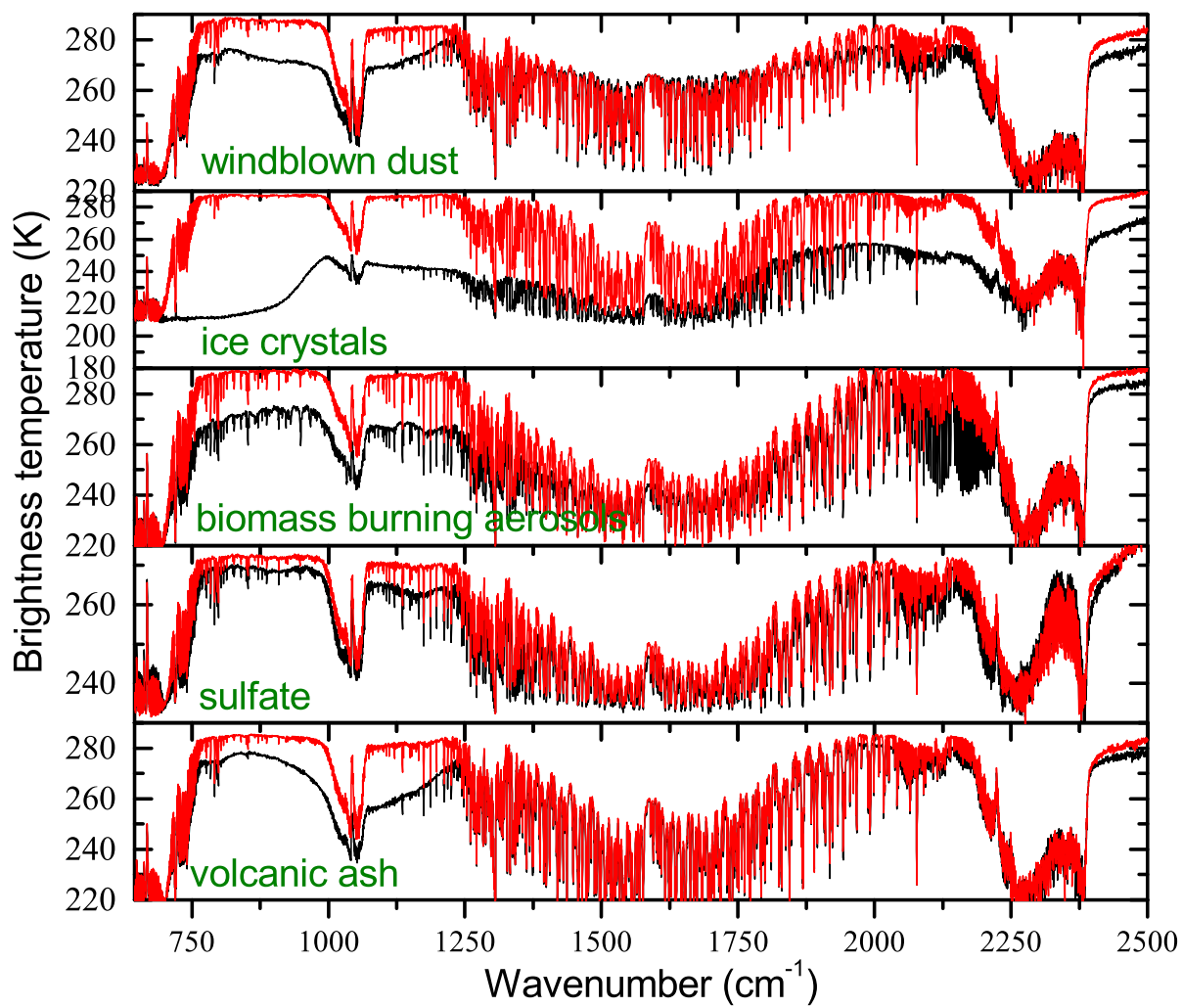


Figure 6.3: Examples of how different type of aerosols can impact IASI spectra (black). The spectra in red are uncontaminated spectra observed outside the respective aerosol plumes.

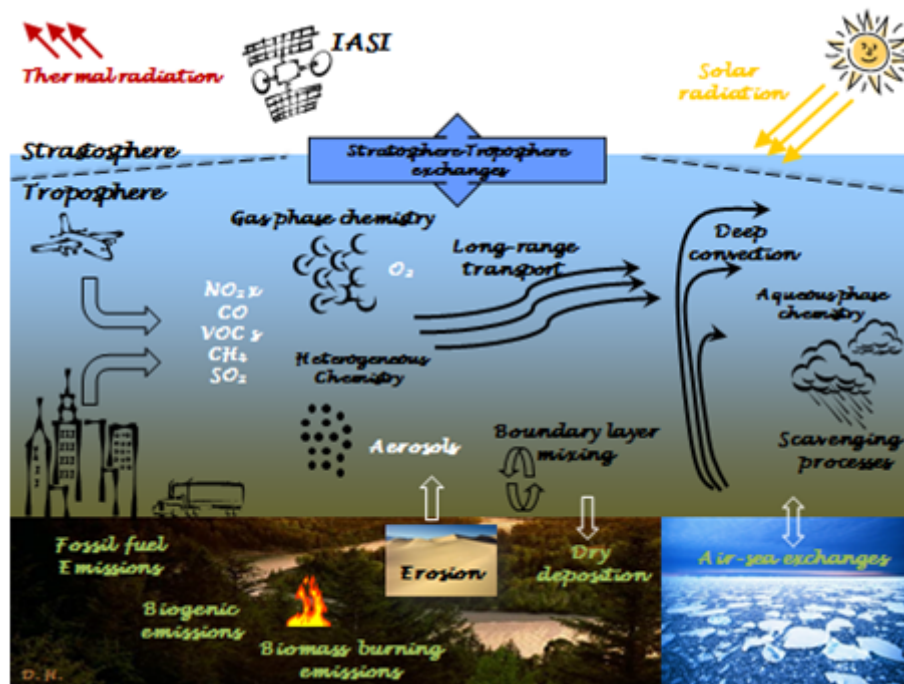


Figure 6.4: Tropospheric chemistry: natural and man-made emissions along with chemical reactions and transport occurring in the atmosphere. Courtesy D. Hauglustaine (LSCE).

also allow retrievals of altitude and effective radius (DeSouza-Machado et al., 2010; Peyridieu et al., 2010; Pierangelo et al., 2005). For the moment, studies have been focused mainly on Saharan dust retrievals over ocean, but global products are in development. As part of ESA's Aerosol-CCI project for instance, four IASI dust products are being intercompared and prepared for a global reprocessing of the entire IASI dataset.

The algorithms developed for windblown sand can easily be applied to volcanic ash, which has a similar spectral signature as sand. Example studies with IASI include Newman et al. (2012a) and Klüser et al. (2013). Volcanic ash observations have an important operational application related to aviation safety as detailed in section 8.3.

6.4.3 Atmospheric composition

The atmospheric composition varies with natural emissions (land, ocean, fires) and other emission sources associated with anthropogenic activities (car traffic, industry, biomass burning). Gases and particulates are generated and destroyed through physico-chemical transformations cycles (figure 6.4).

As for IASI, IASI-NG will be able to measure a series of infrared absorbing compounds (see figure 6.5), provided two conditions are met:

- Each molecule has infrared absorption bands falling into the spectral range recorded by the instrument.
- The gas persists in the atmosphere long enough in order to accumulate (lifetimes = days or longer).

The accuracy required for a product to be useful is linked to its lifetime in the atmosphere. For long-lived species that affect our climate, such as CO_2 , N_2O , CFCs, HCFCs, HFCs and CH_4 , the level of accuracy required is around 0.5–2%, in order to capture seasonal, inter-annual

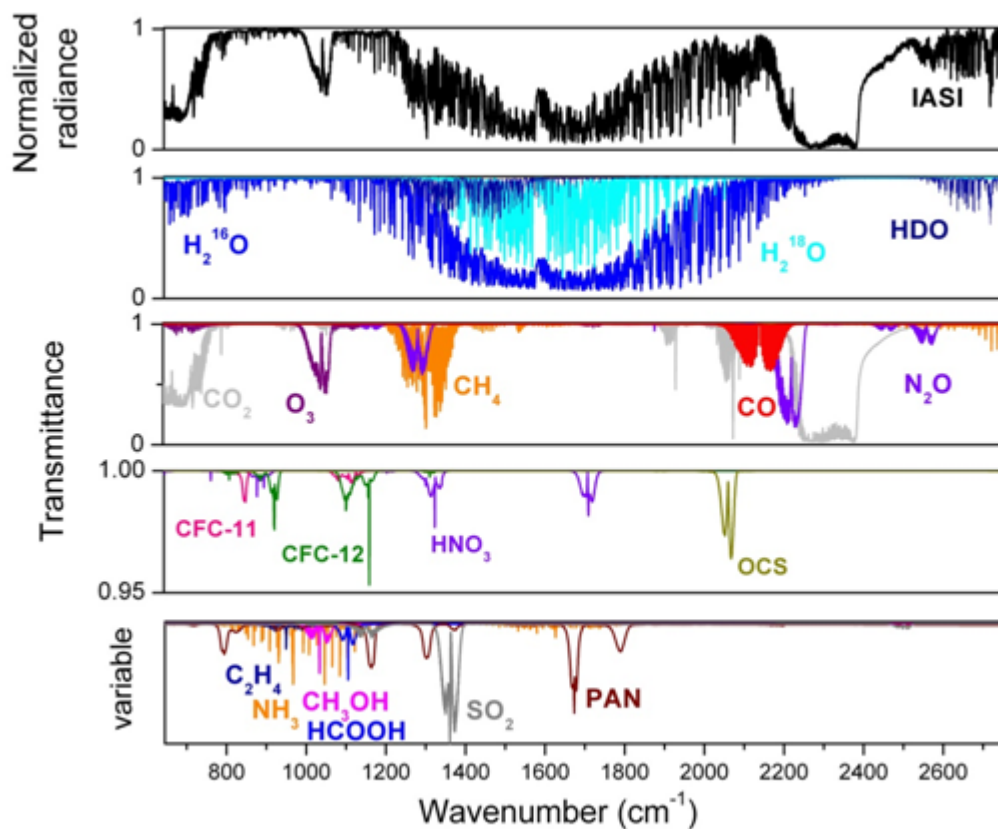


Figure 6.5: Top panel: Radiance atmospheric spectrum (in normalised units) recorded by IASI/MetOp, over West of Australia, on December 20, 2006. Middle panels: Radiative transfer transmittance simulations to identify the main absorbing gases (middle panels) and the weaker absorbers (lower panel, with a variable scale). All the species indicated on the plot have been detected by IASI, although not all in this particular observation, as some are only detectable when special events occur, such as fires or volcanic eruptions.

| Chemistry Product | IASI | | IASI-NG | | Impact of IASI-NG |
|-------------------------------|---------------------------|-----------------------------|---------------------------|----------------------------------|--|
| | Vertical Resolution (DFS) | Accuracy | Vertical Resolution (DFS) | Accuracy | |
| O ₃ | 3–4 | PBL: 60 % Tropo: 11 % | 4–5 | PBL: 40 % Tropo: 8 % | Improved coverage of the PBL |
| CO | 1–2 | PBL: 16 % Tropo: 8 % | 2–3 | PBL: 10 % Tropo: 6 % | Improved coverage of the PBL |
| HNO ₃ | 1 or less | | 2 | | Tropospheric and stratospheric discrimination |
| NH ₃ | Total column | Varies between 25 and 100 % | Total Column | Factor of 2 improvement expected | More sensitivity at the surface |
| Formic acid, methanol | Detection only | N/A | Measured | | Signal now > instrument noise |
| C ₂ H ₄ | Detection only | N/A | Measured | | Signal now > instrument noise |
| SO ₂ | Measured if >2 DU | | Measured if >1 DU | | Plume altitude discrimination. More sensitivity at the surface |

Table 6.2: Estimated accuracy (in %) and vertical resolution (quantified using Degrees of Freedom for Signal; DFS) for retrievals of certain chemical species for IASI and IASI-NG. The final column highlights the expected improvements for IASI-NG.

and spatial variability which are of a similar order. For reactive gases, such as O₃, CO, HNO₃, etc., the accuracy of the retrieval does not need to be so high for the product to be of use. Retrievals of around 5–20 % accuracy are still very useful as the spatial and temporal variability are still not well known and are not well represented in the models. For some highly reactive species with large variabilities, products with accuracies of only 25–50 % can even be useful. For example, for NH₃, modellers still rely on a constant emission profile for all regions in Europe, but data from IASI have shown that there is large regional variability, which had previously not been characterized.

The list of species measured or detected by the IASI mission is provided in tables 6.2 and 6.3, together with an estimation of the improvement brought by the increased radiometric and spectral performances of IASI-NG. Each species is discussed in more detail below.

6.4.3.1 Ozone (O₃)

Ozone is one of the key trace gases in the troposphere and stratosphere, playing significant roles in atmospheric radiative forcing, atmospheric chemistry and air quality. Stratospheric O₃ is sensitive to changes in (photo-)chemical and dynamical processes and, as a result, presents large variations on seasonal and annual time scales. Previous analysis of total column O₃ observations indicated a downward trend in stratospheric ozone over the period from the 1980s to the late 1990s, relative to the pre-1980 values, mainly attributed to the growth of the reactive bromine and chlorine species coming from anthropogenic emissions. As a response to the 1987 Montreal Protocol and its amendments, with a reduction of the ozone-depleting substances, a recovery of stratospheric ozone concentrations to the pre-1980 values is expected.

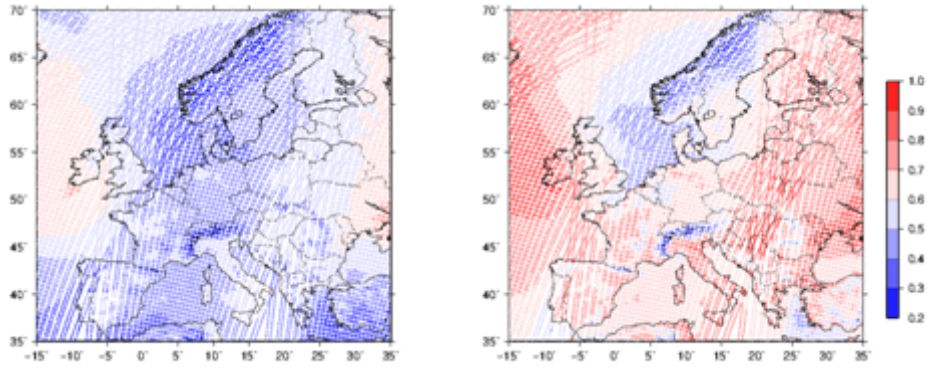
| Climate Product | IASI | | IASI-NG | | Impact of IASI-NG |
|---------------------------|---------------------------|--------------|---------------------------|--------------|---|
| | Vertical Resolution (DFS) | Accuracy | Vertical Resolution (DFS) | Accuracy | |
| H₂O | 5–6 | ~13 % | 6–7 | ~10 % | Factor of 1.5 improvement in accuracy |
| T | 6 | ~0.6 K | 12 | ~0.45 % | Factor of 2 improvement in accuracy |
| CO₂ | 1 or less | ~1 % | 1–2 | <1 % | Sensitivity in the mid-troposphere |
| CH₄ | 1 or less | ~3 % | 1–2 | | Less interference with H ₂ O |
| N₂O | Detection only | N/A | Measured | | |
| Aerosols | | | | | IASI sensitive to dust, IASI-NG sensitive to other types e.g. biomass burning |
| Surface Emissivity | | 0.04 at 4 μm | | 0.02 at 4 μm | |

Table 6.3: Estimated accuracy (in %) and vertical resolution (using Degrees of Freedom for Signal; DFS) for retrievals of climate variables for IASI and IASI-NG. The final column highlights the expected improvements for IASI-NG.

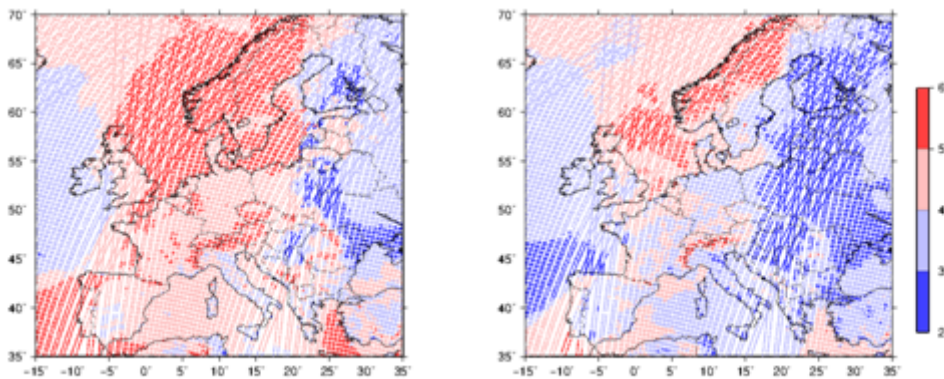
In the troposphere, ozone controls the oxidizing capacity of the atmosphere, as the primary precursor of the OH^- radical oxidant, and is of main importance for many studies. Principally produced by photochemical oxidation of CO and CH_4 in presence of nitrogen oxide radicals, tropospheric ozone is very sensitive to photochemical and chemical processes as well as to dry deposition and transport from the stratosphere via stratosphere-troposphere exchange. Quantification of individual contributions of chemical and dynamical processes to trends, and even of the trend values themselves, from observations is challenging due to influence of large seasonal, year-to-year variations, geographical location, altitude (troposphere) and to other effects.

Sensitivity studies have shown that improving spectral resolution and radiometric noise improves the vertical sensitivity, and that most of the improvement in terms of accuracy for O_3 retrievals will be in the 0–6 km layer. In the lower atmosphere, between the surface and 2 km, there is only a slight improvement and the information content will still be weak as the full discrimination of single lines is not possible. On average, the DFS for IASI is around 4 pieces of independent information and it increases to 5 IASI-NG. Improvement in terms of errors and vertical information are summarized in tables 6.2 and 6.3.

For air quality purposes, there is a need to discriminate tropospheric ozone from stratospheric ozone, which is a complicated task using nadir thermal infrared sounder as there is a major absorption contribution due to high levels of stratospheric ozone encountered along the optical path. For most atmospheric situations, with a noticeable exception for high thermal contrast cases (Clerbaux et al., 2009), tropospheric columns are associated with DFS lower than one, which means that part of the information in the retrieved tropospheric product comes from the a priori information. Studies were performed to investigate how increasing the spectral resolution and reducing the radiometric noise helps to improve this situation. Figure 6.6 provides the DFS (top) associated with the 0–6 km columns for a polluted case over Europe, as well as the maximum altitude (bottom) for the corresponding averaging kernel. It can be seen that in the



(a) Information Content (DFS)



(b) Altitude of Maximum Sensitivity

Figure 6.6: DFS ((a)) and altitude of the maximum sensitivity ((b), in km) associated with the 0-6 km ozone retrieved on 20th August 2009, for IASI (left) and for IASI-NG (right). This simulation was performed using a regional model that described an increase of ozone observed in Europe at that time. (Crevoisier et al., 2014)

0–6 km region, the DFS exceeds 1 for the simulation, with associated maximum sensitivities lower in the atmosphere (2 to 4 km instead of 5 km or higher).

Future work that exploits the separated use of the tropospheric and stratospheric O_3 columns should benefit from the new information provided by IASI-NG.

6.4.3.2 Carbon Monoxide (CO)

Carbon monoxide plays a central role in tropospheric chemistry owing to its reaction with the hydroxyl radical. In the background atmosphere a combination of carbon monoxide and methane are the main loss routes for OH^- . The main sources of carbon monoxide are from the oxidation of methane or other non-methane hydrocarbons (NMHC) with 40–60 % of surface CO levels over the continents, slightly less over the oceans, and 30–60 % of CO levels in the free troposphere, estimated to come from NMHC oxidation. The other major source of about equal magnitude is the incomplete combustion of either fossil fuels or biomass.

Owing to the nature of CO as a marker of anthropogenic pollution and biomass burning, it has been used in a number of studies to assess the importance of transport pathways. Satellite CO data has found great utility in the investigation of the magnitude and impact of the hemispheric transport of air pollution. For example, satellite CO data in combination with in situ aircraft data

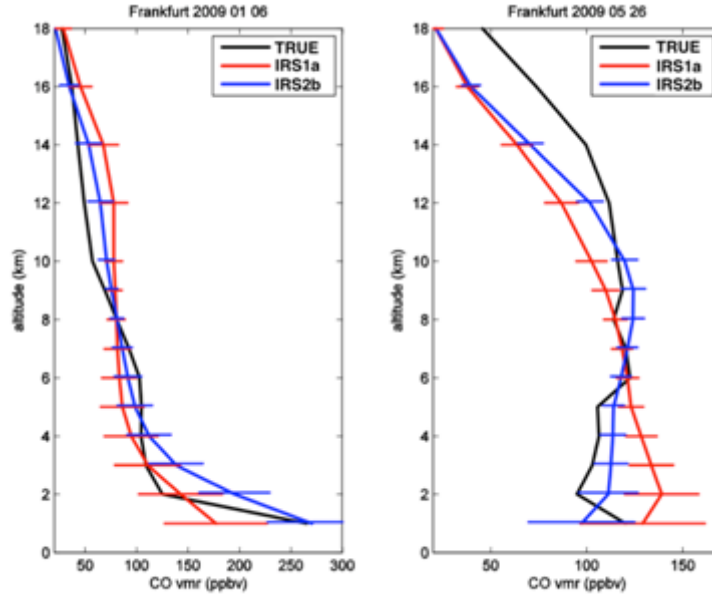


Figure 6.7: Impact of spectral resolution and radiometric noise on the CO retrieved profiles for IASI and IASI-NG, compared with CO aircraft observation (in black). The left plot corresponds to observation taken at the Frankfurt airport on January 6 2009 and the right to May 26 2009 (Crevoisier et al., 2014).

and models have been used to characterize the Asian chemical outflow and relate it quantitatively to its sources as well as determining its chemical evolution during transport. Global estimates for the total anthropogenic (fossil fuel + biofuel + biomass burning) surface sources of CO have been derived using inverse modelling of the satellite observations.

Simulations have quantified the expected improvement in the error for different CO atmospheric layers (total column, 6–12 km, 0–6 km and 0–2 km). The improvement in terms of vertical information is listed in tables 6.2 and 6.3. As expected, both the improved spectral resolution and the better signal to noise lead to better resolved profiles: DFS improves from 1.8 IASI to 2–3 for IASI-NG. In terms of the errors, we see a major impact in the the 0–6 km column: the reduction of the error is significant when improving the spectral resolution and signal/noise by a factor of 2. It should be noticed that the sounding of the boundary layer in particular is improved. However, the error still remains more than 4 times higher than the error on the total column. As seen in figure 6.7 which compares simulations where aircraft data are available, there is significant impact near the surface, in particular for the polluted winter case (left).

Better accuracy, in particular near the surface, should be of great benefit to inverse modeling and source estimation.

6.4.3.3 Methane (CH₄)

Methane is the second most important anthropogenic greenhouse gas. It also has an indirect effect on climate through chemical feedbacks. More than 50 % of present-day global methane emissions are anthropogenic, the largest contributors being fossil fuel production, ruminants, rice cultivation, and waste handling. The natural source strength of CH₄, mainly constituted by wetlands, is particularly uncertain, because these emissions vary considerably in time and space and available ground-based measurements are sparse, albeit precise, and of limited representativeness at larger scales. Crevoisier et al. (2013) presents monthly average CH₄ retrievals for the period 2007-2011. The largest seasonal variations are caused by rice emissions in Asia,

which are very intense during a relatively short time period. Strong deviations between observed and modelled CH_4 abundances are found in tropical regions. Better knowledge of the methane distribution and emissions is indispensable for a correct assessment of its impact on global change.

IASI-NG is expected to allow better retrievals of methane, because the finer spectral resolution will allow better distinction between absorption in methane lines relative to water vapour lines. The vertical resolution of the retrievals is expected to improve by at least a factor of two.

6.4.3.4 Methanol (CH_3OH) and other Volatile Organic Compounds

Methanol is the most abundant oxygenated hydrocarbon gas in the atmosphere and is therefore a major contributor to non-methane volatile organic compounds (NMVOC). The primary source of atmospheric methanol is plant growth and decay, the second largest source is atmospheric production with minor sources from biomass burning and anthropogenic emissions. There is considerable uncertainty in the atmospheric methanol budget. In the remote troposphere, methanol concentrations are 0.1–1 ppb while the concentrations in the continental boundary layer are an order of magnitude larger. With an improved accuracy, IASI-NG will be able to better constrain emission sources, even at regional scales.

6.4.3.5 Nitric Acid (HNO_3)

Nitric acid is the main form of oxidized nitrogen and is one of the main species involved in the chemistry of stratospheric polar ozone. Its principal sources are NO_x which are directly emitted in the troposphere as a result of fuel combustion and biomass burning. On the other hand, the primary source of NO_x in the stratosphere is nitrous oxide (N_2O), also emitted at the surface (by agricultural activities), but quickly transported into the stratosphere. The presence of HNO_3 in the stratosphere allows the formation of polar stratospheric clouds which, through heterogeneous reactions at their surface transforming chlorine species into active radicals, enhance ozone destruction during the polar winter.

The sensitivity of IASI to the HNO_3 vertical profile is located in the lower stratosphere, between 15 and 25 km altitude, which is also where the maximum concentrations are found. But the instrument only allows one level of information to be distinguished. The DFS values are around 1 for all latitudes at all periods. Thus only a total column (or a partial one, getting rid of regions of the atmosphere with a low sensitivity, such as low troposphere and high stratosphere) can be considered in the analyses. The improvement of IASI-NG in the vertical resolution should allow the discrimination of one tropospheric and one stratospheric column. Even though it seems that most of HNO_3 is located in the stratosphere, it might be that the location of the maximum concentration is influenced by the location of the maximum sensitivity. Hence it should be of great interest to have an independent piece of information in the troposphere to validate/invalidate the conclusions based on our current product.

6.4.3.6 Sulphur Dioxide (SO_2)

Sulphur compounds in the atmosphere have both natural and anthropogenic sources. In modern times, the atmospheric sulphur budget is dominated by anthropogenic emissions, particularly from fossil fuel burning. It is estimated that 75 % of the total sulphur emission budget is from anthropogenic sources, with 90 % of it occurring in the Northern Hemisphere. The natural sources include volcanoes, plants, soil and biogenic activity in the oceans (Fioletov et al., 2013). The oxidation of sulphur compounds in the atmosphere has implications in a number of different atmospheric problems such as acidification, climate balance and the formation of a sulphate

layer in the stratosphere. By far the largest sulphur component emitted into the atmosphere is SO₂. Coal and oil combustion contribute up to 80% of the global budget while volcanoes contribute around 10%.

Satellite measurements of tropospheric SO₂ (and ash) have seen extensive application to identification and quantification of volcanic emissions. IASI-NG should allow better estimates of plume altitude. Owing to the sensitivity of SO₂ measurements from space there has been less published on the anthropogenic sources. Here, again, IASI-NG should be of benefit, because the instrument should have more sensitivity near the surface.

6.4.3.7 Ammonia (NH₃)

Excess ammonia in the atmosphere is responsible for severe impacts on air quality and ecosystems. It also affects the Earth radiative budget through the formation of secondary aerosols by reacting with acid species. It is commonly acknowledged that major uncertainties in the nitrogen cycle are associated with reduced nitrogen and in particular NH₃ (Erisman et al., 2007; Fowler et al., 2013).

At global scale, NH₃ emissions are largely dominated by agricultural sources (livestock and fertilizers), followed by biomass burning and oceans (Sutton et al., 2013). Its lifetime in the atmosphere is relatively short (from a few hours to days) due to its high reactivity and deposition rates (wet and dry).

The expected sensitivity gain retrieving NH₃ from IASI-NG spectra is ranging from a factor of 3 to 5, in comparison with current method developed for IASI spectra (Crevoisier et al., 2014).

6.5 Synergistic retrievals and applications

For certain types of retrieval, the best use of IASI-NG may be to combine its measurements with those of other instruments that sense in different viewing geometries or at different wavelengths to produce a combined product. Although this results in a product that is dependent on the correct functioning of both (or all) of the instruments that are to be combined, the benefits in such products may be great.

There are also synergistic applications of IASI-NG, where retrievals from different sensors can be combined to provide improved information to end users.

6.5.1 Temperature and water vapour profiles

There are advantages in combining information from microwave instruments with that from IASI-NG. Microwave instruments are able to provide information about the thermodynamic profile in the presence of cloud. Strong sensitivity to optically thick cloud is a fundamental limitation of IR data, and a combined MWS/IASI-NG retrieval scheme will incorporate the high-vertical resolution of IASI-NG with the information from below the cloud top that the microwave provides. In addition, it is possible to achieve benefits in some schemes from joint retrieval of effective emissivity and effective cloud. Combined infrared+microwave retrievals have heritage in ATOVS products and in the first stage of the IASI Level 2 temperature and humidity product generation. Such products are likely to be continued.

6.5.2 Volcanic eruptions

There would be added-value of combining measurements from IASI-NG and other sounders.

- IASI-NG will operate on EPS-SG in parallel with the Sentinel 5 UV-VIS-NIR and the 3-MI sounder, which will provide complementary measurements (in terms of detection capabilities, vertical sensitivity) of SO₂ and aerosols. The synergies between these sounders for providing the most accurate information on the plume composition and altitude should be explored but is expected to be highly beneficial.
- The combination of the different UV-vis and IR sounders in polar orbits, with complementary overpass times, should be exploited (as initially done in the SACS system) to increase temporal sampling and allow for a rapid response system in case of volcanic eruption.
- Similarly, applications that can combine information from IASI-NG and planned missions on geostationary orbits (especially IRS and Sentinel 4 on the MTG-S) should be very beneficial. Although geostationary satellites do not provide the global coverage and may have reduced monitoring performances (e.g. MTG IRS will not cover the SO₂ ν_3 band), the geostationary sounders have the capability to track the volcanic plumes at high frequency, which would provide strong constraints on the trajectory models.

6.5.3 Wildfires

The IASI-NG will be complemented by measurements of Sentinel-5, of CO from the SWIR, and of other fire-emitted species in the UV-visible (NO₂, H₂CO, C₂H₂O₂), which together will improve the characterization of fire plumes in terms of composition.

For near-real time applications, combining information from IASI with information derived from the MTG-S sounders, and in particular the IRS, should be exploited.

6.5.4 Sandstorms

There will be several instruments operating in parallel to IASI-NG that will have good monitoring capabilities on sand/dust storms, including multispectral imagers. On geostationary orbit (e.g. MTG), the latter will provide crucial spatial and temporal sampling of the event. IASI-NG, on the other hand, would offer enhanced sensitivity to large particles, and more accurate determination of column abundance and altitude. The tandem operation of EPS-SG with the UV-Vis-NIR Sentinel 5, which would have sensitivity to smaller particles, will be an asset.

6.5.5 Extreme urban air pollution

There is a high potential for synergistic applications using satellite sounders on different platforms for monitoring air quality. The combination of IASI-NG with Sentinel 5 on EPS-SG will in particular be important:

- Sentinel 5 will complete the picture of air pollution provided by IASI-NG by adding measurements of NO₂ and H₂CO from the UV-visible spectral ranges, putting observational constraints on models for predicting O₃ photochemical production and particulate matter formation.
- The measurements of O₃ in the low troposphere will be improved during the daytime by combining the measurements of IASI-NG in the TIR with those of Sentinel-5 in the UV-visible; there are schemes that are already in place for IASI and GOME-2. Likewise, the determination of the CO profile and near-surface pollution will be significantly improved by combining the measurements of IASI-NG with those of Sentinel 5 in the SWIR (2-0 band of CO). Aerosol products may also benefit from combining measurements from different sensors.

An important limitation with IASI-NG, alone or in combination with Sentinel 5, will be the temporal sampling, which, with one to two overpasses, will not allow monitoring of the development

of pollution episodes with a strong diurnal cycle. Combining IASI-NG retrievals with those from US sounders within the joint polar satellite system might increase the sampling to some extent. The principal source of complementary information might, however, be with MTG-S, which will be less sensitive but will have better spatial resolution and high temporal sampling.

6.5.6 Climate

From a methodological point of view, further exploration of the synergistic use between various instruments, either from current missions (A-Train) or planned missions (Sentinel, EPS-SG, EarthCare), is needed by coupling active (radar, and lidar) and passive (visible, near and short-wave infrared, thermal infrared, multi-angles) techniques. For instance, coupling measurements of GHGs in the short-wave infrared, sensitive to the full atmospheric column, and in the thermal infrared, sensitive to the mid-troposphere, can help isolate the greenhouse gas evolution near the ground where emissions happen. This is particularly true for methane but there is potential also for synergy with carbon dioxide data. Another example comes the characterization of aerosols: combination of observations in the visible and in the TIR can help distinguish fine and coarse modes of aerosols.

Chapter 7

Assimilation of IASI Level 1 and 2 data

This chapter discusses the assimilation of IASI-NG data into forecasting models. These may be numerical weather prediction models, or chemical forecasting and dispersion models. IASI data form a critical component of the global observing system for NWP, and following this heritage, the assimilation of IASI-NG data is expected to provide significant forecast impact in the coming decades.

A readable introduction to advanced data assimilation techniques including 4D-Var and the Extended Kalman Filter is provided in Daley (1991) and Kalnay (2003). The mathematics of data assimilation follows Bayesian theory and the equations are similar to those presented in section 6.1.1, except that the calculations are carried out for the whole globe simultaneously and generally taking account of the model trajectory across a time window. The a priori information comes directly from the forecasting model and the background error covariance is generally determined from the system itself and is a constraint on the way observation data can be used. For users of IASI-NG data, the critical metadata required by the assimilation system for each observation are:

- Observation error covariance information
- An accurate forward model and its Jacobian. In the context of assimilation of Level 2 products the forward operator is the averaging kernel. See equations 6.4 and 6.7.
- Any information required for forward modelling that is not available from the assimilating model, such as skin temperature and surface emissivity

At the present time, almost all NWP centres assimilate Level 1c IASI radiances, and are restricted in their use of the spectrum because of the computational cost of forward modelling; thus they use a sparse selection of around 200 channels chosen to give the most information content possible in as few channels as possible (Collard, 2007). For IASI-NG, the development of techniques to present the data to the assimilation system in a way that compresses the full spectrum into a manageable number of quantities becomes critical.

In contrast, models such as CAMS (Copernicus Atmosphere Monitoring Service) that assimilate chemical information from IASI generally make use of Level 2 products. In this case, the provision of adequate meta data is critical. In the medium term, studies will investigate the use of radiances for information on chemical retrievals also, as this will make a single stage data assimilation for weather and chemistry prediction more feasible.

7.1 Input data

It is envisaged that there are six main methods (described above in section 6.1) for presenting IASI-NG data to the assimilation system that may be of interest for the assimilation into a model with an NWP forecast component. Raw radiances, principal components and reconstructed radiances already have operational heritage or are areas of active research; L2 retrievals of thermodynamic variables have recently received renewed attention; interferograms and superchannels are possible avenues for investigation but at lower priority than the other approaches.

The technique of micro-window selection that may be used in retrieval of trace species is unlikely to be of use for NWP applications where the main components of interest are temperature and water vapour, for which there is sensitivity across the spectral range of IASI-NG. However, this may be of relevance to assimilation within chemical models if radiance products are assimilated rather than L2 retrievals. Alternatively, individual channels centred on absorption lines for chemical components may be considered.

Other techniques may become apparent over the next few years.

Specific aspects of the assimilation system related to each method will be discussed further in the following sections as appropriate.

7.2 Dimensionality reduction

Most assimilation applications require data selection or thinning for reasons of computational cost and because of finite spatial resolution of models. The dimensionality of the spectrum also needs to be reduced because the atmospheric information content is much less than the number of channels in the full spectrum, leading to potential mathematical instabilities in the system.

7.2.1 Spectral compression

Some of the methods of presenting IASI NG to the assimilation system, such as transformation to a truncated PC score set, inherently reduce the number of quantities assimilated. Interferograms may also be truncated at a specific point to reduce the equivalent spectral resolution to a chosen degree.

Specific considerations are detailed for the assimilation of raw radiances (section 7.2.1.1), PC scores (section 7.2.1.2), reconstructed radiances (section 7.2.1.3) and Level 2 products (section 7.2.1.4).

7.2.1.1 Raw radiances

In this case, for reasons of computational cost, it is unlikely that the full spectrum would be used. In chemical models, channels will be chosen based on sensitivity to specific species based on the location of absorption lines within the thermal infrared. For use in NWP, a channel selection taking channels from throughout the spectrum will be required. Given that the cost of selecting channels is very high, such a selection will need to be made in advance, and should therefore take into account the range of likely conditions in which the data will be assimilated. Channel selections can be further tuned during assimilation. For example, to remove channels contaminated by cloud that cannot be accurately forward modelled, methods such as Pavelin et al. (2008) or McNally and Watts (2003) can be employed.

Many NWP centres use the channel selection of Collard (2007) as a starting point, but this is an area of active research. Recent contributions include those of Martinet et al. (2013b), Eresmaa et al. (2014), Ventress and Dudhia (2013), No et al. (2014) and Migliorini et al. (2014). The development of advanced channel selection methods is identified as a priority.

7.2.1.2 PC scores

The number of PC scores assimilated is chosen to maximise the information content while minimising processing time. PCs may be constructed from the full spectrum, or from a subset of channels. The assimilation of PC scores is attractive not only for reasons of computational

advantage during assimilation, but because the dissemination of L1c data in the form of PC scores is a possibility for certain classes of user, depending on the available bandwidth at the time of launch. In this case, the direct assimilation of the disseminated PC scores would minimise pre-processing tasks required by users.

At the present time, research into the use of IASI PC scores in an operational context does not make use of the IASI L1c PC score dataset, but instead uses a dedicated set of PCs derived from a subset of channels. The direct 4D-Var assimilation of PC scores derived from IASI fully clear spectra is currently being developed and tested at ECMWF (Matricardi and McNally, 2014). The observed IASI spectra are first screened for the presence of clouds and contaminated spectra are discarded. This must be done before assimilation as the PC training has been performed with only completely clear data and none of the eigenvectors correspond to cloud signals. The clear spectra are then projected on to the fixed basis of synthetic eigenvectors used for the training of the PC based observation operator PC-RTTOV (Matricardi, 2010) to produce a vector of observed PC scores. Each vector of observed PC scores has length n , but crucially only the first m of these, when ranked in order of eigenvalue, are assimilated (where $m < n$). In truncating the vector of observed PC scores the assimilation is made highly efficient, while preferentially retaining highest rank PC scores (1, 2, 3, ... m) that convey most information about the atmospheric state. The m observed PC scores are then provided as input to the 4D-Var.

It should be noted that although the use of EUMETSAT L1C PC score data has not been tested, it should be possible to replace the observed PC scores within this same framework with the PC score data generated operationally by EUMETSAT. This would require a re-projection from the EUMETSAT truncated real data eigenvector basis to the synthetic PC-RTTOV eigenvector basis, but otherwise no major obstacles are foreseen.

The primary objective of developing a PC score assimilation system is to improve computational efficiency. Performance tests indicate that the use of PC scores in the 4D-Var minimization requires 25 % less computer resources (elapsed CPU time) compared to a system that assimilates the full number of equivalent radiances. This figure represents a significant saving inside the time critical processing path for NWP centres, but could potentially be improved even further by better tuning the computational efficiency of the PC based fast model simulations.

Recent work (Matricardi and McNally, 2014) in the development of the ECMWF PC based 4D-Var assimilation system has focussed on maximising the spectral information of IASI in clear sky, assimilating 50 PCs generated from selected radiances in the IASI long-wave temperature band augmented with channels from the water vapour and ozone spectral bands (a total of 305 channels). The current status is that the PC assimilation system (in clear sky only) performs as well as - and in some respects slightly better than - the current ECMWF operational IASI radiance assimilation that also uses radiances peaking above clouds and overcast scenes. These results demonstrate the viability of an alternative route to radiance assimilation for the exploitation of data from high spectral resolution infrared sounders in NWP. However, it is important to highlight that the use of PC data is currently restricted to fully clear spectra. This aspect will be discussed further in section 8.1.5.

7.2.1.3 Reconstructed radiances

Instead of assimilating PC scores directly, a radiance spectrum may instead be reconstituted and assimilated as though they were raw radiances, according to equation 6.15. The advantage of assimilating reconstructed radiances is that it should be possible to make use of the noise-reduced properties of principal component scores, but with the data in a physically-interpretable radiance form that allows for more intuitive interpretation and easier removal of cloud-affected

data. There are two important differences from the assimilation of raw radiances.

Firstly, for correct use of reconstructed radiances, the observation error term is required to take account of the inter-channel correlations. In other words, a full matrix must be used rather than just a diagonal term. This aspect will be discussed in more detail in section 7.4.

Secondly, the channel selection step is critical. The PC truncation step restricts the number of orthogonal elements to the number of retained PCs. Upon reconstruction, there should be no more reconstructed radiances than PC scores assimilated, i.e. a maximum of m reconstructed channels can be used. Any further channels reconstructed would contain no new information, and would be linear combinations of the previous channels. Quite apart from the lack of new information, the use of too many reconstructed channels is prohibited by the fact that the observation error covariance matrix would be non-positive definite if linearly dependent channels are used. In fact, for an NWP application, even m channels may be too many. For example, where radiances are reconstructed from PC scores designed for data dissemination, the PC basis is constructed carefully to include information from all absorbing species across the spectrum, many of which are contaminants to an NWP system.

Because of the need to retain a positive definite and well-conditioned observation error covariance matrix, a general channel selection method such as those listed above for raw radiances is insufficient. Channel selection for reconstructed radiances is an area of active research, with new methods proposed by Smith (2015) and Hultberg and August (2013).

Research here should be prioritised because the use of PC compression for data dissemination would, in many cases, require the assimilation of reconstructed radiances.

It should be noted that although current research is focussed on radiances reconstructed from PC-compressed data, it is also possible to reconstruct from truncated interferograms.

7.2.1.4 L2 retrievals

Thermodynamic variables

Until the late 1990s, it was common to assimilate profiles of temperature and humidity retrieved from satellite observations, i.e. L2 products, into NWP models. Assimilation of L2 retrievals has been almost universally rejected for NWP applications since then, in favour of direct assimilation of radiances, because of complex error properties and biases in the retrievals. Inconsistencies between the data to be assimilated and the forecast geophysical state that violate the standard Bayesian assumptions used in data assimilation have restricted the utility of retrievals in modern, highly accurate, weather forecasting models. However, retrieving an atmospheric profile is, theoretically, one of the most efficient forms of dimensionality reduction.

Over the last few years, several studies (e.g. Rodgers, 2000) have proposed ways to transform the vector of the radiances measured by a satellite instrument in such a way as to determine a reduced set of transformed measurements that can be optimally assimilated. Recent research by Migliorini (2012) shows that under certain circumstances the assimilation of retrievals is actually equivalent to the assimilation of radiances. An initial retrieval of all relevant components of the geophysical state (i.e. temperature and water vapour profiles and surface parameters, as well as cloud fields if present) is made using prior information that matches as closely as possible that used for subsequent assimilation. Via calculation of the DFS of the satellite measurements used in the retrieval, it is possible to project the set of noise-normalized measurements (previously linearized about the retrieval and appropriately shifted) along the “most informative” directions to generate transformed retrievals.

Migliorini (2012) shows that these transformed retrievals can then be assimilated in an optimal way. Many fewer transformed components have notable DFS than the number of available radiances (typically less than twenty, compared with thousands of infrared channels), so that the number of observational components to be assimilated is significantly reduced. An observation operator, however, needs to be assigned to each observation and the number of its components can be fairly large when the assimilating model has a large number of levels on which the relevant components of the state are defined. This has implications for the utility of the method if retrievals are performed before data dissemination; however, possible ways to improve the data volume issue include the transmission of observation operators over a smaller number of levels defined in such a way to minimize the vertical representation error.

Since the restrictions imposed on the equivalence relate to the consistency of the a priori assumptions in the retrieval relative to the assimilating system, it is more likely that the retrievals will need to be performed in the context of the assimilation system rather than by EUMETSAT or other data providers. Thus, the assimilation of transformed retrievals produced by data providers is not considered a priority for the community at the present time. However, the approach is being investigated further at the Met Office in a theoretical framework, because of the possibility of removing the radiative transfer step from the forward operator during assimilation.

Atmospheric composition

As stated above, at the present time assimilation of L2 atmospheric composition products is limited to a very few centres, and notably the MACC project (precursor of the Copernicus Atmosphere Monitoring Service, or CAMS) at ECMWF. Currently, information presented to the assimilation system is still in the form of L2 products in order to avoid aliasing information between thermodynamic variables (that are served by radiance assimilation) and chemical species. However, in the future it is likely that the CAMS will investigate the direct use of radiances also.

In the case of assimilation of L2 products, it is critical that averaging kernels are provided with each observation so that the correct forward operator can be constructed. A good understanding of the biases of the products and of their random error characteristics is also vital, and these metadata should, where possible, be provided with the observations.

7.2.2 Observation selection and thinning

The method of data selection in the horizontal domain, or thinning, may be tailored to suit the application. Depending on the horizontal resolution of the model relative to the size of the footprint, it may be better to create super-observations (combining several observations together) or to thin the data using time windows of the assimilation system and effective grid size.

Thinning is generally of two varieties: blind thinning (where no information is available to make a choice of observation within a specified area) and informed thinning (where many sources of information may be drawn upon to choose an observation). In general, it is preferred to use as much information as possible to choose the observation that will be of most use to the system: although some centres may prefer to perform blind thinning at the outset, informed thinning will usually be applied at a later stage. The information used to choose the observation may include:

- Information on sub-pixel heterogeneity
- Information on contaminants or things that can't be modelled well such as cloud
- The presence or absence of other observations in the same area at the same time

- Data quality flags
- Information content

Research into the best way to thin the data based on sub-pixel information should be prioritised; at the present time centres tend to favour either the straightforward selection of a fixed field of view, or the selection of the warmest or most homogeneous field of view. Enhanced sub-pixel information from IASI-NG may allow new and more advantageous methods of thinning to be used earlier in the processing chain.

In the case of assimilation of retrieved products, any correlation between observations (for example relating to correlations in the a priori for the retrieval) should be taken into account. Depending on the a priori for the retrieval, correlation between the assimilation a priori and the retrieved products may exist.

7.3 Forward model operator

Except in the case of assimilation of retrieved products at the same horizontal and vertical resolution as the model and located on model grid-points, which is a practical impossibility for any kind of product derived from radiance data, a forward model operator will be required to assimilate the observations. The purpose of the forward model is to convert from model space to observation space and back, to enable the generation of an increment to the background state at the observation location. In the case of the direct assimilation of radiances, or transformed observations such as PC scores or reconstructed radiances, an important component of the forward model operator is typically a fast radiative transfer model, such as RTTOV. However, for assimilation in high-resolution models where there are many model grid points within one pixel, the forward model operator should include spatial processing to maximise representativeness. It may also be necessary to take account of a slant path across model grid boxes.

Interpolation/averaging and indeed forward modelling generally may depend on the resolution of the assimilating model. Research in this area should be prioritised, with particular focus on the assimilation of data into convective-scale models where the model grid is considerably smaller than the FOV of IASI-NG.

Research into improved use of cloudy and aerosol-affected pixels should also be prioritised, including research into potential forward operators (e.g. splitting of qttotal-type control variables).

For assimilation of straightforward L2 products, the correct forward model operator is usually the averaging kernel, and this should be provided with every observation. Other types of transformed retrievals may have different forward model operators, but wherever the operator depends upon the observation or a varying a priori state vector, the operator should be provided with the observation by the data provider.

7.4 Observation errors

The specification of an adequate observation error covariance matrix, usually referred to as \mathbf{R} in data assimilation, is key to maximising the impact of the observations. Even in the case of raw radiance assimilation, estimation of the error covariance matrix is extremely difficult. The components of such a matrix usually include: instrument noise, forward model error, and errors of representation (resulting from processes that affect the observation that are not resolved by the forecast model), and possibly non-linearity errors in the case that the shape of the Jacobian

is very sensitive to the atmospheric state. Each of these items individually is not very well known, in particular the degree to which errors are correlated between channels.

Techniques exist that allow the estimation of observation error covariance structures from the assimilation system itself, such as the Methods of Hollingsworth and Lönnberg (1986) or Desroziers et al. (2005). These methods can be used for any sort of data and so could equally well be used to estimate the errors of L2 products as raw radiances. In the Hollingsworth-Lönnberg method, pairs of background departures are used to compute statistics as a function of the separation between the members of each pair. To estimate the observation error, the values of the covariances are extrapolated to zero separation. It is then assumed that the spatially uncorrelated component of the background departures is largely dominated by the observation error. In practice, the choice of extrapolation function to zero separation can be a source of significant uncertainty in the process, and so this step is often neglected, instead taking the covariance and the smallest degree of separation possible to represent the observation error, despite the disadvantages of including background error that is correlated at small length scales in the resultant matrix.

In the Desroziers method, the elements of the error matrix \mathbf{R} are expressed as the expectation value

$$\mathbf{R} = E[\mathbf{d}_a \mathbf{d}_b^T] \quad (7.1)$$

where \mathbf{d}_a and \mathbf{d}_b are the analysis and background departures in the observation space respectively. This relationship can be derived from the quasi-linear estimation theory used as the basis for variational assimilation schemes like 4D-Var. Assuming initial estimates of the weights are reasonable, the Desroziers algorithm produces a refined estimate of the observation error. A detailed description of the practical application of these methods to compute tuned observation errors can be found in Bormann et al. (2010). The operational implementation of error covariance matrices derived using the Desroziers technique has been shown to give positive impact at the Met Office (Weston et al., 2014).

In the case of PC assimilation or reconstructed radiance assimilation, the error structure may be significantly modified by the transformation, and the degree of correlation in the error matrix may be altered, and in the case of reconstructed radiances, significantly increased. Work at ECMWF by Matricardi has recently demonstrated how the neglect of the off-diagonal terms of the PC error covariance matrix can have a negative impact on the skill of the PC based assimilation and forecast system. In the context of reconstructed radiance assimilation, Smith (2015) shows that the use of an incorrect observation error covariance matrix that does not take proper account of all sources of error can have extremely detrimental results. For the assimilation of L2 products, the error structure may be very difficult to estimate accurately, as it will depend on all of the components of the raw radiance error term (or even the PC/reconstructed radiance error term) combined with an a priori error term from the retrieval.

Diagnostic methods for determining error covariances have many assumptions built into them and can only provide an estimate of the observation error terms. Due to these inbuilt assumptions, it is often found that the error term for a given observation type may need to be balanced within the assimilation system so that the weight given to the data is correct within the presence of other observations. Each centre will need to perform its own analysis of errors within the assimilation system, because of differences in the forward model and other model characteristics. Understanding the uncertainty on the predicted error covariance matrix, and methods to handle the effects of limited sampling should be prioritised. Consideration should be given to situation dependence of the observation error matrix (e.g. a different matrix could be applied

over different surface types, or in different regions of the globe) to maximise data usage without jeopardising forecast quality.

Application of the diagnostic methods outlined above is limited because of the breaking of inbuilt assumptions. This severely limits their use, and the resultant covariance matrices often have undesired properties that are hard to compensate. New physically-based methods are being investigated at ECMWF, but further research into ways of developing error covariance matrices should be prioritised, as understanding of the error properties of observations is a critical limiting factor in extracting full benefit from IASI-NG observations.

7.5 Bias correction

It is a feature of most data assimilation techniques that there is an underlying assumption of zero bias between model and observations. Sources of bias between the observation and model should preferentially be removed at source. Such sources of bias may relate to the forward modelling process, for example lack of treatment of carbon dioxide profile variability, or from errors in the radiative transfer model itself or underlying spectroscopy. There may also be persistent features in the forecast model (a model climatology), common examples include stratospheric temperature and surface temperature. They may be an intrinsic feature of the measurement, depending on instrument characteristics. Some sources of bias are easier to eliminate or correct for at source than others, but bias correction remains a requirement. In fact, bias may be a limiting factor in the ability to extract information from a very low noise instrument.

Few data assimilation centres try to remove model bias from the model itself. Thus, to a certain extent, model biases may effectively be assigned to the observation for removal via the bias correction process. In these circumstances, it is commonplace to assimilate some observations without bias correction to help anchor the model to a less biased state: examples of this include GNSSRO observations, and the high-peaking AMSU-14.

It has been suggested that IASI may be a relatively unbiased source of information in certain circumstances, for example for upper tropospheric humidity, and a few channels could be used as an anchor. Further investigation should be made into the plausibility of using IASI-NG as an anchoring observation. For this to be a realistic proposition, it is vital that further research is carried out into sources of bias in the radiative transfer modelling process, and that spectroscopic parameters are further refined.

At the present time, most centres use Variational Bias Correction (VarBC; Dee, 2005) to remove biases from radiance data. This is an adaptive scheme that estimates the bias using a multi-linear regression: the bias predictor coefficients form part of the control vector within the assimilation system. The bias predictors generally include air-mass terms and treatment of scan-dependent biases. The predictors should ideally be optimised to remove observation and forward model operator bias, but not model bias.

Some centres still use a fixed set of coefficients following the scheme of Harris and Kelly (2001). The bias predictors are usually similar to those included in operational VarBC schemes. It is anticipated that by the time of launch of EPS-SG, most NWP centres that currently assimilate IASI will be using VarBC.

The use of VarBC has also been demonstrated to be effective for the bias correction of PC score data from IASI. Matricardi and McNally (2014) show that after an initial training phase of typically two to three weeks, the adaptively computed bias corrections for PC scores perform extremely well, becoming very stable in time and removing almost all systematic differences between the observations and the analysis. Corrections computed for a small number of PC

scores that have the strongest sensitivity to the surface and to the stratosphere are slower to stabilize and tend to drift slightly over time. To a large extent, this mimics the behavior often seen in the corrections computed for window and stratospheric channel radiances, suggesting that same processes that cause drifts in radiance biases (time varying model error and feedback with quality control) are likely to be responsible.

Further research is required into the bias correction of retrieved products (L2 data), which may have complex bias characteristics. Initial experiments with assimilation of L2 temperature and humidity retrievals at ECMWF required a very different approach from the bias correction of radiance data, with different corrections being applied in small geographical regions.

Other methods of bias correction, such as techniques based on neural networks, are possible but are not currently in common use.

Further consideration may be required to assess the effect of using bias coefficients derived from one model configuration in another configuration (e.g. from a global, large-scale 4D-Var system applied to a convective-scale 3D-Var system). Quite apart from differing model biases related to different physics and parameterisations, convective scale models generally do not reach as high into the atmosphere as global models so depending on the source of information above model top the biases may be very different. This is an area of active research for centres that do not have a global model. Research in this area should be prioritised.

7.6 Background errors

Data assimilation techniques rely on a term representing the error in the forecast into which the observations are to be incorporated to produce the analysis. The weight given to the observations in the assimilation system is a function of the both the observation error and the background error. Like the observation error term, the background error matrix can only be estimated, and is held in parameterised form. As such it can never represent the true error. Understanding the properties of the background error terms used in forecasting models can help to predict the likely impact of IASI-NG on the assimilation system at different vertical and horizontal scales: the background error term acts as a filter on the information from the observations.

When adding variables to the control vector, the B matrix should be modified accordingly. When there are cross-correlations between the errors of the new variables and the errors of the existing variables, they should be described as far as possible. These error terms are very specific to the system under consideration, and further discussion on their treatment will be presented in the sections on the relevant application in chapter 8.

Chapter 8

Applications of IASI-NG data and products

8.1 Numerical Weather Prediction

Numerical Weather Prediction centres are principal customers for IASI-NG data. Following the heritage of IASI, IASI-NG is predicted to be a critical component of the global observing system in the coming decades. The introduction of IASI into NWP systems in 2007 gave as great an impact as has been seen on the introduction of any new satellite instrument (Hilton et al., 2009a; 2009c).

Adjoint-based techniques such as the forecast sensitivity to observations (FSO) have shown that in terms of overall contribution to the NWP analysis, IASI has the most impact of any observation in the Met Office forecast (Joo et al., 2013), with similar levels of impact demonstrated at other centres such as Meteo-France.

8.1.1 Main Current Areas of Research

The main priorities for research into the use of IASI-NG in NWP can be tackled with IASI data. These include:

Observation error covariances The observation error term in NWP is highly non-diagonal, and poorly known. Diagnostic methods rely on assumptions that are not valid, and more research into improving error covariance modelling is urgently required, especially if transformed data with non-diagonal noise are to be assimilated.

Assimilation in high-resolution models Use of IASI data in high-resolution models is increasing, but research into ways of mapping increments back onto the model grid should be prioritised.

Cloudy assimilation Use of cloud affected observations remains limited, and this is an area that should be prioritised, with particular focus on using the data in high-resolution models.

Retrieved profiles For assimilation of retrievals following the Migliorini method, as well as observation errors it will be necessary to think about how the data should be bias corrected.

8.1.2 Expected performance of IASI-NG in NWP

The increased spectral resolution had not been expected to give significantly more impact for NWP applications, because the information on temperature and humidity comes from differential sensitivity of individual channel weighting functions in the CO₂ and H₂O absorption bands: IASI already has many channels in these spectral regions and the challenge is to present the data in such a way that information from as many channels as possible can be accessed. Nevertheless, the improved noise performance is expected to yield some benefit for NWP.

Simulated data for IASI and IASI-NG were constructed for 5 242 448 profiles on 60 levels taken from the ECMWF model and considered as the true state (J. Andrey-Andres, pers. comm.). Two series of temperature and humidity vertical profiles retrievals were carried out over 6486 selected profiles using these data. The IASI retrievals use the channel selection currently operational at Météo-France. For IASI-NG, channels with the same centre frequencies have been selected,

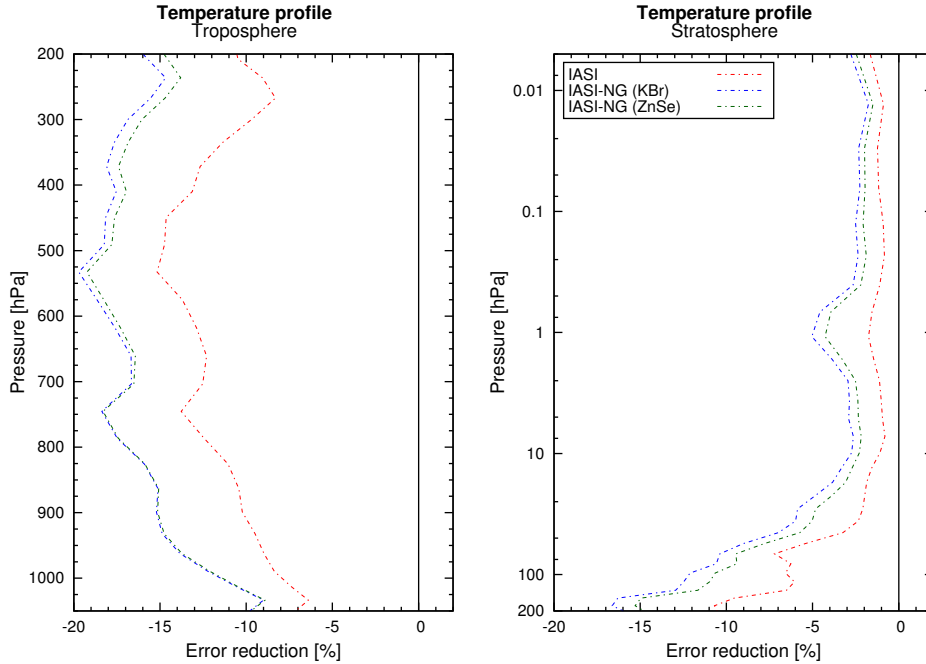


Figure 8.1: Performance of 1D-Var temperature retrievals over a range of profiles for simulated IASI and IASI-NG data. IASI-NG is simulated with two alternative noise profiles. The left figure shows the lower atmosphere and the right shows the full column. Calculated with the NWPSAF 1D-Var package

and observations simulated with IASI-NG spectral resolution and two alternative noise profiles, corresponding to projected noise performance of the two possible prism materials, ZnSe and KBr, as at December 2014. The assumed background errors are those provided with the NWPSAF 1D-Var, originally calculated from the Met Office assimilation system on 54 vertical levels. The first set of inversions were run only considering a diagonal noise for the observations. A full matrix containing all sources of error was diagnosed a posteriori through the Desroziers technique (Desroziers et al., 2005).

Figures 8.1 and 8.2 show the performance of 1D-Var retrievals from the second run of inversions. Regardless of the choice of prism material, assuming the noise profiles are realistic, for the temperature profile and much of the water vapour profile, IASI-NG shows large benefit over IASI. When considering the two IASI-NG profiles, better error reductions are observed for KBr material from 700 hPa to the top of the atmosphere. Below this height there is no difference between KBr and ZnSe. In the case of water vapour profiles, IASI-NG presents again a better performance than IASI at all levels, but no difference is appreciated between the two IASI-NG prism materials.

Figure 8.3, however, shows a similar analysis using a Met Office background error covariance matrix and a 70 level profile set from the Met Office Global model (4348 profiles). In this study, the observations assimilated in all cases were at IASI spectral resolution, for the channels used in the Met Office operational 1D-Var pre-processor. Three different instrument noise profiles were used to simulate the observations (again, no forward model error was added): IASI, and the two IASI-NG profiles for different prism materials. Again, IASI-NG demonstrates improvements in retrieval performance over IASI, but in this case those improvements are much smaller than shown in figures 8.1 and 8.2. Comparison of these two sets of results therefore suggests that the improved spectral resolution of IASI-NG will indeed have important benefits for performance in an NWP system.

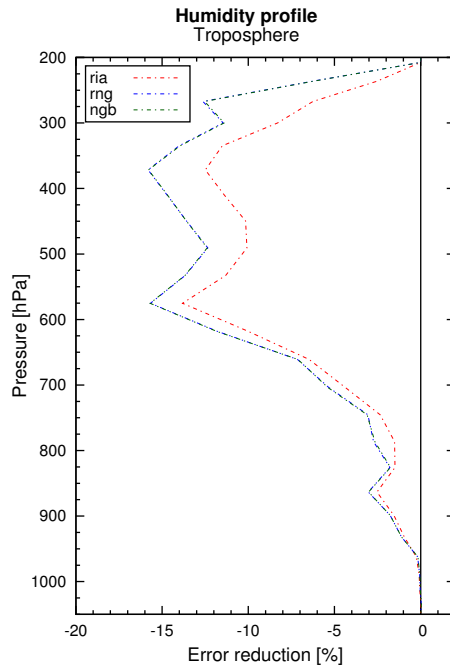


Figure 8.2: Performance of 1D-Var humidity retrievals over a range of profiles for simulated IASI and IASI-NG data. IASI-NG is simulated with two alternative noise profiles. Calculated with the NWPSAF 1D-Var package

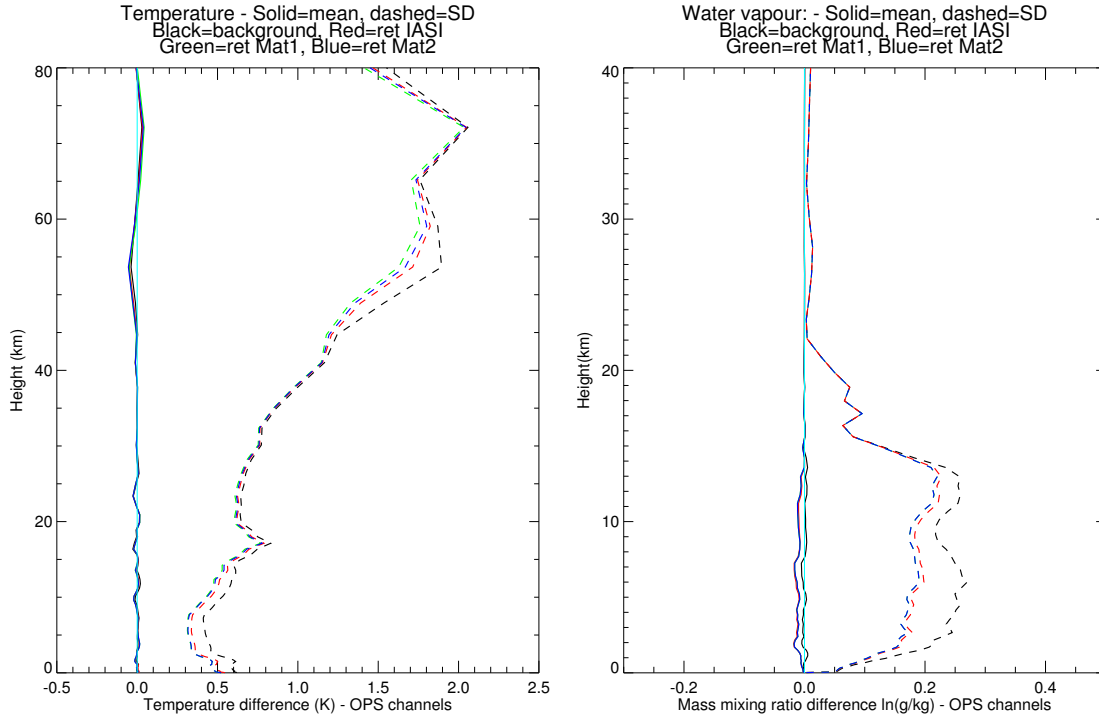


Figure 8.3: Performance of 1D-Var retrievals over a range of profiles for simulated IASI data with IASI (red) and two different IASI-NG (blue, green) noise profiles. Temperature retrievals are shown in (a) and water vapour in (b). Calculated with the NWPSAF 1D-Var using a Met Office B-matrix.

Current operational assimilation systems are restricted in their use of the spectrum because of the computational cost of forward modelling; thus they use a sparse selection of around 200 channels chosen to give the most information content possible in as few channels as possible (Collard, 2007). For IASI-NG, the development of techniques to present the data to the assimilation system in a way that compresses the full spectrum into a manageable number of quantities becomes critical.

One aspect peculiar to NWP as an application is in the treatment of clouds: depending on the characteristics of the data assimilation system and the assimilating model, clouds can be considered either a contaminant, or an intrinsic part of the information available in the observation. Thus, the treatment of cloud will be considered in some detail in section 8.1.5.

The current challenging areas of research in the assimilation of IASI for NWP purposes are:

- an appropriate description of the R matrix or any other development which would assist extraction of information from the water vapour band and thus contribute to more accurate humidity analyses.
- surface parameter retrievals that are currently operational at only a few centres are key parameters to increase the information content of assimilation over continental surfaces.
- analysis of cloud characteristics during the assimilation. Advances in these key areas would also benefit the use of IASI-NG data.

8.1.3 Contamination by unmodelled species.

It remains a possibility that, in the time frame of IASI-NG, NWP forecasting centres will have major trace gases, cloud information, aerosol content and surface properties as active variables in the assimilation system, along with temperature and water vapour. The special case of cloud is expanded upon in section 8.1.5. It is, however, likely that at least some of these will effectively be contaminant species/components within the assimilation system. Methods of treating unmodelled species should be identified, such as screening based on simple detection techniques, to modifying observation error terms when contamination is likely. Additional a priori may be required (e.g. surface emissivity).

8.1.4 The assimilation system

Most forecasting centres currently assimilating IASI data use a 3D- or 4D-Var assimilation system. These are by no means the only options. The Extended Kalman Filter is another option, and there are various Ensemble-based formulations (e.g. 4D-ensemble-Var) that are either in operational use or being actively investigated at the present time. Even in 4D-Var systems, ensemble-based methods are commonly used to provide flow-dependence to the background error term. In ensemble assimilation systems, more research should be conducted into observation selection and quality control, and into the effects of localisation functions on the assimilation of hyperspectral observations.

Another subject of current investigation is the use of long time-window 4D-Var, which may have implications for the way data are assimilated (e.g. over a long enough time window there may be multiple over-passes of IASI-NG allowing the use of the data to generate dynamical information similar to the generation of AVHRR polar winds).

The control vector

The control vector is the vector gathering all the variables which can be modified during the minimization process. It generally is a subset of the background vector and, in the NWP context,

includes at least profiles of temperature and humidity. Depending on the system, some variables may be added to the control vector, such as surface parameters, cloud profile variables (ice and liquid water content) or simple cloud parameters (such as cloud top pressure and cloud amount), and atmospheric constituents (e.g. ozone, methane). The purpose of adding some variables to the control vector is either to be used as sink variable to ease the minimization process or to retrieve new quantities. In the particular case of cloud parameters as sink variables, such as a single cloud fraction and effective emissivity, the goal is to avoid any large non-linearity during the minimization rather than to derive a physically meaningful quantity as these parameters will not be used in the subsequent forecast anyway. It is, however, important to consider whether the use of sink variables will alias genuine information away from items that do form part of the control vector.

The formulation of the control vector may have an impact on the forward model operator, and the ease with which information from the observation can be passed back to the model. For example, a total water control variable consisting of water vapour, liquid and ice combined will probably require a technique to split these components out of the control variable prior to radiative transfer modelling. It is important to consider the implications of such a process.

Background errors

The form of the background error is different for different centres, for example it will depend upon the form of the linear model used in the assimilation system. It is a part of the NWP assimilation system that the scientists responsible for ingest of IASI-NG data will typically have little control over. The form of the matrix will be affected by pragmatic decisions to control the stability of the assimilation process. For example, it is common for cross-correlations between atmospheric variables such as temperature and humidity to be assumed to be zero.

The increasing use of ensemble models allows for flow dependency to be incorporated into the background error term. This should enable better use of the observations via better representation of discrete structures (1D-Var studies have shown that it is very difficult to move a feature that is at the wrong height where a static \mathbf{B} matrix is assumed). However, it should be borne in mind that at the present time, the static component of the \mathbf{B} matrix is given more weight in the construction of \mathbf{B} in order to stabilize the solution. An alternative to flow-dependency in some applications might be the use of a different matrix depending on the conditions (for example, different background errors might be assumed in precipitating areas).

Additional a priori information not included in the control vector

There may be additional information required for RT modelling that is not included in the assimilation system control vector. Examples include surface emissivity and minor atmospheric constituents. The additional information may be available as a passive model variable, or from external sources such as atlases and L2 products, or estimated via parameterisations or regression schemes. In some cases it may be neglected in the forward model and treated instead as an observation error or bias.

8.1.5 Clouds

As described above, clouds are a special consideration for NWP because in some assimilation systems they will be considered a contaminant, but in others an intrinsic part of the information to be extracted from the observation. The ability to extract temperature and humidity information from cloudy scenes depends upon the extent to which cloud variables are accurately modelled by the NWP system and forward operator. The ability to extract cloud information from cloudy

scenes additionally depends on the control vector of the data assimilation system and the way in which the background errors are formulated. Feeding information on the cloud state back to the model is particularly difficult. For example, if the observation is cloudy, but the model column is far from saturation, it can be difficult to initiate cloud formation in the model column. So-called “all-sky” assimilation of IASI data is currently under investigation at ECMWF. Recent work by (Martinet et al., 2013a) investigates the possibility of extracting information on hydrometeors from IASI data with which to initialise forecasts of clouds.

These issues are likely to be exacerbated in limited area model configurations, where each observation will cover an area that contains many model grid points: feeding the information back to each grid-point in a sensible way requires extensive research. Furthermore, the purpose of high-resolution limited area models is to provide more detailed information on variables such as cloud and precipitation, so it is important that this step is done well.

8.1.5.1 Cloudy PC scores

Research into the assimilation of PC scores is currently restricted to clear sky cases. This is an important limitation to the use of the PC system in an operational environment. Matricardi and McNally (2014a) have suggested that it is reasonable to conclude that the steps that have been taken to handle clouds in infrared radiances can indeed be reproduced in PC space. However, to date little progress has been made in implementing the options suggested by Matricardi and McNally (2014a). This is due to the fact that dealing with clouds in PC space is technically demanding within the context of a global assimilation scheme, requiring the recalculation and storage of eigenvector projections and retaining a facility to identify clouds in radiance space before the PC analysis. While these technical demands are not insurmountable in the longer term, they have been considered beyond the demands of the research projects allocated to the study of PC assimilation in NWP. Nonetheless, the results of impact radiance assimilation trials with different cloud treatments demonstrate the importance of handling cloud affected scenes (particularly in the extra-tropical mid-latitudes) and could arguably preclude an operational implementation of PC assimilation until a solution is found. A pragmatic hybrid approach is conceivable where PC scores are assimilated in completely clear sky and, if cloud is detected, the assimilation system could be reverted to radiance assimilation. While this is far from elegant it is technically feasible.

8.1.6 Additional considerations

In the case of clouds and some other atmospheric constituents, the ability of IASI to influence the model via assimilation is dependent on what is available in the background state. In this respect the assimilation community is reliant on advances in the (forecast) model, whose main priorities do not often include furthering satellite data assimilation. Adding variables to the state vector may be of very low priority; this could eventually prevent IASI-NG users from being able to use these variables in the forward model, or to assimilate the corresponding quantities from the observation. Furthermore, if the assimilation technique makes use of a simplified model for physics, the description of additional processes may be needed (e.g. moist processes), which may equally have low priority.

In terms of assimilation of cloud-affected variables, the use of coincident imager data is to be encouraged. The development of a cloud simulator model should be prioritised, to investigate the effects of cloud on radiances and possibly influence in the future the way cloud is represented in the models. The use of ensemble data assimilation methods should be investigated, in terms of new possibilities for modelling cloud properties and variability within the assimilation system.

8.2 Detecting climate change and variability

8.2.1 Context

Climate variability comes from both internal variability and answer to external perturbations, either natural or anthropogenic. Being able to disentangle these various causes and to quantify their respective contributions to the resulting global variability requires: 1. long-term monitoring of various atmospheric variables; 2. products accurate enough to detect signature of climate events and climate change; 3. simultaneous analysis of multiple variables. The main variables are greenhouse gases, aerosols, clouds, precipitation and reactive species involved in tropospheric ozone creation, pollution events (NO_2 , NH_3 , CO , SO_2 , VOCs) and destruction of stratospheric ozone (Ozone Depleting Substances, ODS). Monitoring these variables is thus required to evaluate how the atmosphere responds to potential mitigation policies (e.g. international policy on ODS regulation). As well as having a direct impact on humans (chemical or particle pollution), on ecosystems or on environment (stratospheric ozone), atmospheric composition modulates the global Earth radiative budget and thus directly influences climate. Over the last decade, several programs and initiatives have been installed at European and international levels to assure long-term monitoring of the atmosphere. In particular, GCOS (Global Climate Observing System), in support to the UNFCCC (Global Climate Observing System), has established a list of 50 Essential Climate Variables (ECVs) that require long-term monitoring to quantify the evolution of the atmosphere and climate. An ECV is a geophysical variable that is associated with climate variation and change as well as the impact of climate change onto Earth. GCOS has defined a set of ECVs for three spheres, atmospheric, terrestrial and oceanic (GCOS-82; http://www.wmo.int/pages/prog/gcos/Publications/gcos-82_2AR.pdf). Thirteen of them are directly relevant to Atmosphere and IASI-NG: temperature, water vapour, clouds, aerosols, ozone, greenhouse gases, etc. In this framework, ESA has launched the Climate Change Initiative through the reprocessing of data since the beginning and the delivery of consistent climate data records for 13 ECVs, among which 4 fall in the category ‘Atmosphere’: Clouds, Aerosols, Ozone and Greenhouse gases (GHG). Other ECVs, such as humidity and temperature, are archived by Eumetsat. The Climate research groups and the modeling community are just beginning to confront models with the products, and in the next phase will test the products both for detection and attribution. In the US, OBS4MIPS was set-up to use EOS data (Terra, Aqua, Aura) for the CMIP5 exercise. It should be noted that most of the ECVs are also relevant quantities for atmospheric composition and NWP.

The European Programme Copernicus, in conjunction with ESA Sentinel and EUMETSAT EPS/EPS-SG programs, will cover most of the needs for atmospheric ECVs by establishing a European capacity for long-term observation of the Earth. Maintaining and developing networks of in situ observations and research infrastructures (e.g. ICOS, IAGOS, NDACC, TCCON, AERONET) is the must-have complement to these observations and will have to be insured in the future.

The study of climate also requires improving our understanding of underlying mechanisms. Natural and extreme events (volcanic eruptions, dust storms, severe drought) as well as signatures of human activities (GHG emissions including biomass burnings, pollutants, CFCs and tropospheric ozone) are now detected to some extent by current operating satellite systems. However, the question of their impact on Earth’s climate system remains open and has to be addressed through conjugated efforts of remote sensing and climate modeling communities.

8.2.2 Establishing long time-series

To characterise climate and climate change, data need to be accurate and homogeneous over long time scales. The signals important for the detection of climate change can easily be lost in the noise of a changing observing system. This enforces the need for continuity in an observing system, where observations can be tied to an invariant reference. The term Fundamental Climate Data Record (FCDR) denotes a well-characterised, long-term data record, usually involving a series of instruments, with potentially changing measurement approaches, but with overlaps and calibrations sufficient to allow the generation of products that are accurate and stable, in both space and time, to support climate applications. FCDRs are typically calibrated radiances, backscatter of active instruments, or radio occultation bending angles. FCDRs also include the ancillary data used to calibrate them. In this regard, the GSICS initiative (see chapter 9) is crucial in the creation of FCDRs based on the monitoring and harmonization of data quality from operational weather and environmental satellites. Inter-calibration techniques provide a practical means of correcting biases between sensors and bridging any potential data gaps between non-contiguous sensors in a critical time-series and the intercalibration reference serves as a transfer standard.

The required precision for detecting a climate trend (e.g. 0.1 vs. 0.5 K) that then needs to be translated into the specification of a mission presented to industry is not straightforward. It is directly linked to trend of the targeted ECVs (e.g. 0.6 K per decade trend for surface temperature).

Using satellite observations to establish long time series of ECVs, such as L1c or L2 climatologies or reanalysis, from which climate change signatures can be detected, specifically requires the following four issues to be addressed:

1. lack of homogeneity and continuity between various generations of instruments. In that sense, the proper characterisation of the differences between the 3 successive IASI-NG instruments, as well as between at least Metop-C IASI and Metop-SG-A IASI-NG will be crucial to the establishment of homogenous ECVs throughout the whole Metop/Metop-SG series.
2. difficulty in acquiring knowledge of absolute calibration. Given the lack of a well-defined way of monitoring absolute calibration of IASI-NG, comparison with well-characterized instruments will have to be performed throughout the lifetime of each IASI-NG. One such instrument is the Climate Absolute Radiance and Refractivity Observatory (CLARREO), which seeks to establish high absolute accuracy benchmark climate observations of spectrally resolved thermal IR and reflected solar radiation (B. and Wielicki, 2013).
3. detecting potential instrumental drifts. Two approaches need to be used simultaneously. Firstly, comparing observed IASI radiances with radiances observed from other sounders, either on the same platform (such as HIRS4 and IASI) or on distinct platforms (such as AIRS and IASI), allows wide ranges of brightness temperatures to be compared. Secondly, comparing IASI observed radiances to simulated radiances calculated with a frozen version of a forward radiative transfer model and well described atmospheric situations (radiosondes or reanalysis), allows screening of each channel of each instrument individually. The combination of the two approaches helps to identify which instrument deviates from the other(s).
4. good understanding of the instrument, of the derived products and of their associated uncertainties. This specifically requires proper description and archiving of every algorithm used to monitor the instrument and to derive every level of products.

Most of these issues will be addressed by Calibration/Validation activities.

8.2.3 Long-term monitoring of essential climate variables

Interactions between the atmosphere and the surface, either land, sea or ice, are one of the main drivers of atmospheric composition and circulation. Knowledge of today's surface sources and sinks of the gases involved in the water cycle, biogeochemical cycles and those of aerosols, as well as their spatial distribution and temporal variability is one of the essential ingredients for predicting their atmospheric loads, either for pollution or for further inferring the induced radiative forcing of climate change. Being directly influenced by local (e.g. boundary layer dynamics) and global (e.g. initialization of the convection) processes, the atmosphere is the natural observation point of surface variability and evolution. However, the atmosphere cannot be considered without involving the land and ocean surfaces, since their study strongly relies on the coupling between atmospheric transport models and atmospheric measurements.

Table 6.3 gives the summary of the expected precisions, vertical resolutions and new capabilities offered by IASI-NG compared to IASI. In addition, potential synergies with other instruments on Metop-SG and other platforms may allow further developments; for example for temperature with MWS and RO, for ozone with future limb sounding missions; for aerosol with 3MI and MetImage; and for methane with UVNS/Sentinel-5.

8.2.3.1 Temperature profiles

Upper air temperatures are a key dataset for detection and attribution of tropospheric and stratospheric climate change, measured both by radiosondes and satellite instruments. Temperatures measured by high-quality radiosondes are an important reference against which satellite-based measurements can be calibrated. Upper air temperatures are important for separating the various possible causes of global change, and are vital for the validation of climate models. Infrared (HIRS) and microwave sounders (MSU and AMSU) have been providing atmospheric profiles for almost 30 years. IASI and IASI-NG contribute to the sustained effort of deriving a long-term record by providing information on temperature with global coverage, good horizontal resolution and acceptable accuracy. Performance in cloudy areas is poor, but coupling IR measurements with microwave measurements such as AMSU onboard Metop or MWS onboard Metop-SG provide substantial improvements.

Post-launch validation of retrievals of temperature and water vapour profiles derived from IASI has confirmed an accuracy of less than 1 K for temperature between 800 hPa and the tropopause and better than 10% for relative humidity in the 800–300 hPa altitude range (Pougatchev et al., 2009; Kwon et al., 2012). However, as for any existing thermal infrared sounder, IASI still suffers from a limited sensitivity to the lower part of the troposphere near the surface, and to the tropopause region. Accordingly, the estimated accuracy reaches 2–3 K at the surface and 2 K at the tropopause for temperature. Improvement in the vertical resolution, especially near the surface, is thus a clear priority and one of the main objectives of the IASI-NG mission.

In addition, the improved coverage of the UTLS region will enable a better characterization and monitoring of the tropopause height. Comparison with tropopause height derived from radio-occultation will be mandatory to evaluate accurately the capability of IASI-NG to inform on this variable. For higher altitude, several channels will sound the stratosphere at altitudes not covered by IASI (Crevoisier et al., 2014). However, validation of retrieved stratospheric temperature is not straightforward. Radio-occultation observations might help.

It is worth noting that, beyond the impact on operational meteorology and upper air temperature climatologies, any improvement in the characterization of the thermodynamic profiles will positively impact the retrievals of other atmospheric variables which usually require a good knowledge of the thermodynamic state of the atmosphere.

8.2.3.2 Water vapour profiles

The observations for water vapour profiles are a core requirement for weather forecasting, climate monitoring and are largely dealt with in the framework of CGMS (Coordination Group for Meteorological Satellites).

The continuation of the IASI instrument series through the MetOp-SG program (IASI-NG) will allow for collation of a climate time series of tropospheric temperature and WV profiles spanning over 35 years. This data record will be invaluable for climate studies, and as such should be created in such a way that it meets (or is close to as possible) the performance requirements outlined in Ohring et al. (2005) for water vapour climate records of :

- stability of IASI-Reference of 0.26 % per decade
- accuracy of 5 %.

In addition, the provision of auxiliary information such as a detailed uncertainty estimate, averaging kernels and characterisation of surface parameters (surface skin temperature/emissivity) are also key for understanding the performance and quality of the observations in the IASI time series.

A wide range of sensors is available to measure column water vapour: microwave imagers (SSM/I) and traditional imagers like AVHRR or MERIS on LEO platforms, and GOES and SEVIRI on GEO platforms. Vertical profiles are provided by microwave sounders like SSM/T2, AMSU-B, HIRS/4 and MHS, by hyperspectral infrared sounders like IASI and AIRS, or by radio-occultation observations provided by GRAS on Metop or ROSA on a variety of missions. Currently, the water vapour records used in climate analysis predominantly come from the Special Sensor Microwave Imager (SSM/I), the NASA Water Vapor Project (NVAP), reanalysis (e.g. ECMWF ERA Interim) and in situ measurements. While these records are not necessarily independent from one another, they report different trends and have different climate sensitivities.

The challenges for the coming years are to improve vertical resolution of observations and temporal sampling, to overcome cloud problems and to improve the ability to process sounding data over land. In those regards, the combined use of IASI-NG and MWS will be a priority to reach the performances needed for both NWP and climate. Performing both clear sky (IR) and all-sky (IR+MW) retrievals will also provide insight into sampling biases. A result from the GEWEX Water Vapor Assessment (GVAP) already points to this issue when independent TCWV records from HIRS (IR) and SSM/I (MW) were compared. An EOF analysis performed on 20 years of data from both data sets showed the primary EOF mode of HIRS, which accounts for 18% of the variability to be correlated with precipitation while the primary EOF mode for SSM/I (8% variability) is correlated with ENSO. This difference in climate sensitivity is further demonstrated when a FFT power spectrum analysis is performed on the data sets. Where under-sampling exists, the period for the maximum frequency can be equal to the time series length. Understanding the impact of sampling would be central to any climate time series derived from IASI + IASI-NG.

The 3-dimensional field of humidity is a key variable for global and regional climate models. Polar satellites provide information on tropospheric humidity with global coverage, good horizontal resolution and acceptable accuracy, but with poor vertical resolution. IASI still suffers from a limited sensitivity to the lower part of the troposphere near the surface, and to the tropopause region. Accordingly, the estimated accuracy is worse than 10% near the surface for H₂O where it is the most abundant. Improving the retrievals near the surface is thus a clear priority and one of the main objectives of the IASI-NG mission. In addition, a few IASI-NG channels, located

at the center of its ν_2 absorption band should be specifically sensitive to stratospheric water vapour.

An inclusive monitoring exercise within the retrieval framework would provide a valuable reference for benchmarking performance. To this purpose it is important to use characterised, high (vertical) resolution in situ measurements which also include estimates of uncertainty. Using the GRUAN upper atmosphere network as the key reference, with the possible inclusion of other networks (e.g. SHADOZ) would provide a comprehensive/representative set of reference atmospheric states to validate and train algorithms.

It is worth noting that any improvement in the characterization of atmospheric humidity by IASI-NG will require improving water vapour spectroscopic parameters and the description of its continuum in radiative transfer models, as discussed in chapter 5. Studies of IASI-NG spectra in the window regions, together with the associated humidity and temperature profiles, could contribute to understanding of continuum absorption, although care will have to be taken to separate the continuum signal from other contributions in the window regions.

8.2.3.3 Ozone

Ozone is the most important minor constituent of the atmosphere, because it provides a unique shield to UV radiation from the sun. Ozone, together with species that cause ozone depletion and the chlorofluocarbons that are sources of some of these species, has been monitored with several ground-based and space-borne observations. In the last 20 years chlorofluocarbons have decreased in the troposphere and recently a decrease is also observed in the stratosphere. At the same time the replacing species (hydrochlorofluocarbons and hydrofluocarbons) have increased, but are less of a problem. The ozone hole in the Antarctic, after a continuous increase, no longer grows and in the last few years an onset of recovery is detectable despite the large variability in polar ozone. This recovery is occurring later than anticipated on the basis of the reduced emissions and the cause of the delay is probably to be ascribed to the cooling of the stratosphere caused by the increased greenhouse effect.

Specific objectives for IASI-NG will consist of:

1. contributing to monitoring the formation of the Antarctic ozone hole and its subsequent recovery;
2. monitoring the decrease of ozone in the Arctic in the cold winter period followed by the expected reduction of ozone due to transport (especially through the UTLS) and dispersion of processed air at mid-latitudes;
3. providing some information about the interannual variability of ozone hole;
4. providing specific correlations between temperature/Polar Stratospheric Clouds/Ozone.

8.2.3.4 UTLS

The intrusion of stratospheric ozone into stratosphere is clearly detected with IASI (e.g. Boynard et al., 2009). However, evaluation of the exchanged amounts has not yet been done. Considering characterization of the Upper Troposphere and Lower Stratosphere (UTLS), it is clear that limb sounders like MIPAS or MLS have allowed the start of a global climatology of the composition of the atmosphere in the UTLS. However, their resolution in space and time was revealed to be insufficient to resolve processes of major importance in the UTLS. IASI can provide some useful information that can help with these sampling issues. Thus, ozone concentration is correctly estimated with IASI (Barret et al., 2011). Also, recent results (Barré et al., 2012, e.g.) show the benefit of assimilation limb and nadir sounding to study the region around the thermal tropopause. Several studies have been performed during the phase A of PREMIER, which in

the end was not selected for Earth Explorer 7, to establish the state of the art and precise questions still to be solved. In such a context, IASI-NG could contribute to the establishment of a 3D composition in the UTLS and to estimate the flux of momentum transported by gravity waves.

IASI and IASI-NG do not have the extensive potential of other instruments dedicated to ozone and other reactive species. But their high horizontal resolution, combined with its capability to provide high vertical resolution temperature and WV profiles and to resolve the ozone column in at least 3/5 partial columns (tropospheric, lower and upper stratospheric), makes it very interesting to perform specific case studies on important atmospheric issues. Feasibility studies are needed to examine how this can be implemented, mainly as an off-line research activity, since full documentation of these specific cases will often combine the information provided by other sensors or platforms into sophisticated high resolution (both spatial and temporal) chemical models. Such studies could address:

1. the quantification of stratospheric ozone transport to the troposphere through extended and intense tropopause foldings (cut-off lows) and the subsequent evolution of ozone in the lower atmosphere;
2. heterogeneous chemistry models of ozone depletion that are being tested and improved, but these chemistry studies will benefit from the synergy between the temperature information (critical for polar stratospheric cloud (PSC) formation), cloud/aerosol information (possibly type, size, optical depth, etc.) and ozone information all provided by IASI in the same geometry over a large scene viewed at high horizontal resolution along the track.

8.2.3.5 Clouds

Clouds cover about 70% of the Earth's surface and play a dominant role in the energy and water cycle of our planet. They play a double role in the energy budget of the planet: they reflect incoming solar radiation, which tends to decrease energy absorption, and they absorb energy emitted by the Earth, which tends to increase the greenhouse effect. Better understanding of the role of clouds in the climate system, including cloud feedbacks and indirect effects of aerosols on clouds are two objectives that require an accurate description of clouds and water distribution in the atmosphere. Several cloud physical and microphysical properties are now obtained from various instruments. The synergy of the active and passive instruments of the A-Train mission (Calipso, POLDER/PARASOL, MODIS, AIRS, CloudSat) has particularly enabled the evaluation of cloud / aerosol property retrievals as well as the characterisation of cloud profiles in relation to their radiative properties (height, emissivity, optical depth). Since it has been recently shown that mesoscale systems with similar radiative properties also have a similar vertical structure (Tselioudis et al., 2013), these findings can be directly transposed to clouds determined from IASI and IASI-NG. This mission has also set the ground for the preparation of EarthCare. Climatologies compiled from different satellite datasets can exhibit systematic biases. The Global Energy and Water cycle Experiment (GEWEX) Cloud Assessment, initiated in 2005 by the GEWEX Radiation Panel and finalized in 2012, has provided the first coordinated intercomparison of publically available, global cloud products (gridded, monthly statistics) retrieved from measurements of multi-spectral imagers, IR sounders, and lidar (Stubenrauch et al., 2013).

The high spectral resolution and the improved signal to noise ratio of IASI-NG will allow more detailed studies of some of the physical aspects of the climate system that are yet poorly understood. In particular, it should prove possible to test some of the assumptions behind current theories of the absorption and scattering of IR radiation by cirrus ice crystals (Vidot et al., 2015) and by water vapour in the window regions. The presence of cirrus cloud has a marked

impact on the Earth's radiation budget. However, because of the complexity of crystal shapes and sizes, no single theoretical/modelling approach has been found to be successful over the whole electromagnetic spectrum.

A necessary condition for formation of cirrus and persistent aircraft contrails is cold and humid air, supersaturated with respect to ice. A changing climate affects occurrence and location of ice supersaturation in the upper troposphere and might also lead to an increase of dust storms. The latter plays a role in modifying the properties of cirrus outflows of tropical convective systems. Even if the vertical extent of 'ice supersaturated' layers is often smaller than the vertical resolution of the retrieved water vapour profiles, it has been shown that advanced calibration methods considering relative humidity distributions of thin cirrus (Lamquin et al., 2012) allow the estimation of ice supersaturation occurrence in these atmospheric layers. The improved spectral resolution of IASI-NG leads to a better vertical resolution of retrieved water vapour and therefore to smaller uncertainties in the identification of the condition for cirrus formation.

8.2.3.6 Aerosols

Global warming induced by GHG is modulated by aerosol effects, which remain the dominant uncertainty in radiative forcing, partly because aerosols show a very high spatio-temporal variability. Aerosols are an important variable component in climate and global change studies. They present a broad continuous absorption which covers all the spectral range. Numerous complementary products are now retrieved from various instruments. Observations from MODIS provide high spatial resolution aerosols visible optical depths over sea and land vegetated areas as well as their effective radius. A finer description, aiming specifically at making the distinction between fine and coarse modes will be useful (e.g., profile of optical thickness, parameters to know the type (dust/pollution), etc.). Observations from CALIOP provide accurate aerosol altitudes, but lidar measurements have a low revisit frequency and no operational lidars will be flown in a near future. The very high spectral resolution characterizing AIRS, IASI and to an even greater extent, IASI-NG allows retrieving infrared optical depth of desert dusts (which constitute the largest load in aerosol) together with their mean altitude and size. Aerosol properties are often derived from measurements in the near IR and visible part of the spectrum and then extrapolated to the mid and thermal IR region. For climate change studies it is nonetheless important to understand how well this extrapolation works. IASI-NG IR channels will thus provide a global data set to study, understand and refine aerosol models. Proper combination will be needed between measurements from space sensors operating in the IR and in the visible as well as from the ground with lidars (including depolarisation measurements) to improve aerosol models for all types and sizes and provide a unified picture of their optical properties (absorption, emission, diffusion, etc.) from the IR to the visible-UV.

Even with incomplete knowledge of aerosol properties, IASI-NG will be an extremely useful tool, because of its wide swath and imaging capabilities, to follow in space and time large aerosol episodes and plumes (volcanic eruptions, fires of natural or man-made origin, dust storms, etc.) which, contrary to the background aerosol (with generally moderate optical depth in the IR), will strongly affect, when they occur, the radiances measured by the instrument. The CCI aerosol product comparison also suggested that there may be benefit from combining IASI-NG measurements with multiangle polarimeter products. The 3MI to fly on EPS-SG together with IASI-NG has been designed for operational characterization of aerosols. Hence, studies aiming at combining both instruments will have to be performed.

8.2.3.7 Greenhouse gases: CO₂, CH₄, N₂O

Trace gases other than ozone may be divided into three categories: 1. greenhouse gases affecting climate change, mostly carbon dioxide (CO₂), methane (CH₄) and nitrous oxide (N₂O); 2. chemically aggressive gases affecting the environment (including the biosphere); 3. gases and radicals affecting the ozone cycle, thereby affecting both climate and environment. The presence of trace gases in the atmosphere can have a significant effect on global change as well as potentially harmful local effects through increased levels of pollution (see section 8.3). Since the beginning of the industrial era, the chemical composition of the troposphere has been changing at an unprecedented rate.

In order to predict atmospheric concentration levels, and in turn radiative forcing of climate change by greenhouse gases (GHG), knowledge of today's carbon sources and sinks, their spatial distribution and their variability in time is required. Densely sampling the atmosphere in time and space, satellite measurements of the distribution of global atmospheric GHG concentration could in principle provide a way to improve our knowledge of both natural and anthropogenic surface fluxes. The required precision is nonetheless very high since the trends as well as the diurnal, synoptic, seasonal and interannual variations are two orders of magnitude lower than the background levels.

First estimates of sources and sinks of CO₂ and CH₄ have been obtained from SCIAMACHY, GOSAT and IASI observations (Cressot et al., 2014). Dedicated missions are planned for the near future, either passive (CNES MicroCarb, ESA/Sentinel 5 also flying onboard Metop-SG) or active (CNES/DLR Merlin). They will deliver full columns of GHGs. However, only thermal infrared sounders (IASI, IASI-NG and CrIS), which are mostly sensitive to the mid-troposphere, will provide measurements over several decades as part of EPS/EP-SG and JPSS programs. Moreover, IR sounders allow columns to be retrieved during both day and night, over land and over sea. This is of particular importance for monitoring the evolution of CH₄ at high latitudes, in the context of thawing sub-arctic permafrost, as well as for studying the diurnal cycle of GHG in connection with related variables such as fire (Chédin et al., 2005; Thonat et al., 2015).

The capability of retrieving GHG (especially CO₂) columns from an infrared sounder with a good enough precision for carbon cycle studies relies on the ability to decorrelate the gas signatures from temperature signatures in the observed radiances. In that sense, simultaneous use of IASI-NG observations and MWS observations will be a strong asset of Metop-SG, provided that the observations of both instruments are synchronized. Thanks to the reduced noise in the the ν_3 CO₂ absorption band centered at 2349.2 cm⁻¹ (4.3 μ m), two pieces of information will be available for CO₂ along the vertical, both with improved retrieval errors compared to IASI (Crevoisier et al., 2014). The investigation of the use of the weakest laser band centered at 1064 cm⁻¹ (9.4 μ m, which offer sensitivity to the lower troposphere, will have to be investigated.

Also of great interest, will be the availability of both IASI-NG and UVNS/Sentinel 5 onboard Metop-SG. Coupling the sensitivity of IASI-NG to mid-tropospheric CH₄ and the sensitivity of UVNS to the total column of CH₄ should enable the retrieval of independent pieces of information on the vertical. New retrieval techniques for combining observations in both IR and SWIR will have to be developed to reach this goal. Finally, nitrous oxide (N₂O) is the third most important well-mixed greenhouse gas emitted by human activities in addition to natural biological processes, after CO₂ and CH₄. Only space-based observations can provide the spatial coverage and density of measurements that are needed for global flux inversion of N₂O. They would in particular allow quantifying the link between food production and N₂O concentrations in order to monitor and possibly mitigate the impact of this fundamental sector in human activities on climate. Although some of the spectral bands covered by IASI are sensitive to changes in tropospheric N₂O, a satisfying retrieval of N₂O columns remains to be performed. The increased

spectral resolution and lower radiometric noise of IASI-NG might present the opportunity to retrieve a large portion of the tropospheric column of N₂O. This would represent a very noticeable improvement compared to the current hole in space-based monitoring of N₂O. The following questions need to be explored successively: 1. what is the quality of N₂O partial column retrievals that can be obtained from IASI-NG measurements with significant weight in the troposphere? 2. What is the quality of N₂O surface fluxes that can be inferred from them?

8.2.3.8 Surface

Computing the surface component of Earth radiative budget relies on the knowledge of 3 variables: sea surface temperature (SST), land surface temperature (LST) and land surface emissivity (LSE).

Sea surface temperature (SST) is the water temperature close to the ocean's surface. IASI SSTs, produced from version 5.0 of the IASI Product Processing Facility (PPF), have been validated against drifting buoy SSTs and compared to AVHRR SSTs contained with the EUMETSAT Ocean and Sea-Ice Satellite Application Facility (OSI-SAF) matchup dataset (O'Carroll et al., 2012). The IASI SSTs were found to be of good quality with a slight cool bias compared to drifting buoys (bias -0.32 K, σ 0.32 K) and AVHRR SSTs (bias -0.35 K, σ 0.30 K). The highest quality IASI SSTs had a bias compared to drifting buoys of -0.16 K (σ 0.33 K). Similarly, IASI-NG derived SST will have to be evaluated against other instruments (e.g. AATSR) to characterize its capacity to detect SST trend.

Land surface emissivity (LSE) is defined as the ratio of the energy emitted by the land surface to that emitted by a blackbody at the same temperature and wavelength. As emissivity depends on wavelength, it is referred to as spectral emissivity; it also depends on the viewing angle. LSE substantially varies with vegetation, soil moisture, composition, and roughness (Hulley and Hook, 2010; Salisbury and D'Aria, 1992)), with typical values between 0.65 and 1.0 in the thermal infrared (TIR) range. Lower values are observed over arid deserts, mainly constituted of quartz, in the two Reststrahlen bands at around 4 and 8.5 μm , whereas an LSE close to 1 characterizes dense vegetation, water and ice-covered surfaces. Continental surface emissivity and surface temperature in the thermal infrared window are key parameters for improving a wide range of studies such as the radiation budget (e.g. Zhou et al., 2003), earth-atmosphere interaction (atmospheric temperature and moisture profiles retrieval), and weather, as well as environment monitoring, for example, land cover change (French et al., 2008) and geological studies (e.g. Jiménez et al., 2010). Therefore, from both observational and modeling points of view, an accurate knowledge of surface emissivity and its spectral, spatial, and temporal variations, especially in the atmospheric thermal infrared window, is necessary.

For example, using a constant or an inaccurate emissivity value results in large errors in the surface energy budget estimations. A 10 % error (e.g., from 0.9 to 1.0) on the emissivity approximately corresponds to a 10 % error in the energy emitted from the surface (a portion of which may be compensated by the reflected incoming radiation) (Ogawa et al., 2003; Prabhakara and Dalu, 1976). Analyses of the sensitivity of simulated energy balance to changes in soil emissivity (Zhou et al., 2003) revealed that, on average, over northern Africa and the Arabian Peninsula a decrease in the surface emissivity in the atmospheric window by 0.1 would increase the ground and surface air temperatures by about 1.18 K and 0.88 K, respectively, and decrease surface net and upward longwave radiation fluxes by about 6.6 W m^{-2} and 8.1 W m^{-2} , respectively. A constant emissivity is still often used for land surfaces in energy balance studies and general circulation models (GCMs), because of the limited information on the spectral and spatial distributions and the time variations of the land surface emissivity (Ogawa et al., 2003). Furthermore, it has also been shown that properly accounting for surface emissivity in the solution

of the radiative transfer inverse equation substantially improves the retrieval of meteorological profiles (temperature, moisture) and clouds (Li et al., 2007; Plokhenko and Menzel, 2000). This is particularly the case in arid and semiarid regions where variations in emissivity are large both on spectral and spatial scales. Seemann et al. (2008) show that by using a better assumption of the LSE than a constant value of 0.95, the bias in the retrieval of total precipitable water is improved from 2.1 ± 4.3 to 0.2 ± 2.5 mm relative to ground-based microwave measurements at the Southern Great Plains Atmospheric Radiation Measurement Program (SGP ARM) site. Finally, over continental surfaces, knowledge of the infrared emissivity spectrum allows the correction of observed brightness temperatures for surface emissivity effects, enabling an accurate determination of semitransparent clouds and aerosol properties.

Several LSE databases are currently available, obtained from various instruments and methods at different spectral, spatial, and temporal resolutions. Some LSEs are directly derived from the sensor data: for example, the operational MODIS LSE (MOD11) products are retrieved using a physical algorithm, which takes two observations (night- and daytime) and assumes LSE is invariable while the land surface temperature (LST) may vary (Wan and Li, 1997; Wan, 2008). The final product is only retrieved at six wavelengths (3.75 μm , 3.96 μm , 4.05 μm , 8.55 μm , 11.03 μm and 12.02 μm at a spatial resolution of 0.058°. The Advanced Spaceborne Thermal Emission and Reflection Radiometer (ASTER) on board the Terra satellite is used to derive emissivity from the temperature emissivity separation (TES) algorithm (Gillespie et al., 1998; Hulley et al., 2008). LST and LSE are produced for five TIR bands between 8 and 12 mm at 100 m spatial resolution over North America. The AIRS operational LSE products are retrieved using a multivariate linear regression method followed by a simultaneous physical algorithm (Susskind and Blaisdell, 2008). The monthly LSE database is available for four wavelengths with a spatial resolution of 18 km. On the other hand, the University of Wisconsin Baseline Fit (UW-BF) emissivity database combines moderate spectral resolution MODIS data (MOD11) and high-resolution laboratory spectra from the University of California, Santa Barbara (USCB), and ASTER spectral libraries (Seemann et al., 2008). These latter spectra are used to determine 10 hinge points chosen to capture as much of the shape of the emissivity spectrum as possible. The MODIS emissivities are then used to estimate the emissivity at the 10 hinge points. This approach is able to approximately reproduce the most important features of the emissivity spectrum, more particularly the quartz signatures of the Reststrahlen bands, but cannot capture high spectral resolution fluctuations in the spectrum.

Zhou et al. (2011) derive high-resolution surface emissivity with an algorithm utilizing a combined fast radiative transfer model (RTM) accounting for both atmospheric absorption and cloud absorption/scattering. The retrieval technique separates surface emissivity from skin temperature by representing the emissivity spectrum with eigenvectors derived from a laboratory measured emissivity database (Salisbury and D’Aria, 1992). The Infrared Atmospheric Sounding Interferometer Multispectral Method (IASI-MSM), originally developed by Péquignot et al. (2008) and first applied to high spectral resolution observations from AIRS and then to IASI (Capelle et al., 2012) derives surface infrared emissivity from 3.7 to 14 μm at 0.05-mm spectral resolution together with surface temperature by inverting analytically the radiative transfer equation. IASI-NG will provide the opportunity to improve the spectral resolution of emissivity spectrum. The reduction of the radiometric noise by a factor of 2 (4) compared to IASI will decrease the error by a factor of 1.4 (1.6) at 12 μm and by a factor of 1.3 (1.7) at 4 μm (Crevoisier et al., 2014). Moreover, the availability of METIMAGE observation might provide the opportunity to characterize the variation of the emissivity within one IASI-NG field of view. From a climate point of view, measurements of spectral emissivity from IASI-NG could provide the possibility to study land/ocean processes. Coupling them with the IASI boundary layer humidity and temperature measurements would certainly enhance the interest of surface measurements in the fields

of soil/vegetation interaction, hydrological cycle and ocean productivity studies. The horizontal resolution of IASI-NG will not compete with the spatial resolution of the best multi-spectral imagers (MODIS, etc.) but the much higher spectral resolution and spectral coverage of IASI-NG will enable a better characterization of some processes. In particular, the link between emissivity variability and vegetation cover might give valuable insight in the capability of detected and attributing trend and interannual variability to land-use change.

8.2.3.9 Earth Radiation budget

The Earth-Atmosphere system stays in radiative equilibrium by absorbing incoming solar radiation in the shortwave and emitting radiation in the longwave. Outgoing Longwave Radiation (OLR) is the global longwave radiation outgoing from the Earth-Atmosphere system, integrated over all angles. It is an essential component of Earth radiative equilibrium that allows the system to regulate itself and its temperature by releasing its excess of energy. An accurate estimate of OLR is thus particularly important to study the variability of Earth climate.

Since the 70's, space observation has enabled measuring Earth radiative budget and studying its evolution together with other atmospheric and surface variables. However, large uncertainties are still associated with the role of clouds, water vapour and trace gases in the vertical distribution of atmospheric radiative heating and cooling, as well as in the corresponding climate feedbacks. A better understanding requires improving our knowledge of the links existing between the thermodynamic state of the atmosphere and the vertical repartition of the sources and sinks of Earth radiant energy. The distribution of sources and sinks varies with spectral region. Its monitoring makes sense only over long time periods.

IASI-NG will provide top of atmosphere (TOA) spectral radiances. For clear sky pixels, with minimal RT modelling (assuming near isotropy of the radiation field), the TOA spectral radiances can be converted to TOA upward flux and spectrally integrated over the IASI-NG spectral domain ($645\text{--}2760\text{ cm}^{-1}$). This part of the spectrum covers the thermal IR where a large proportion of the longwave (LW) flux is radiated to space. However, the two wings of the LW spectrum are incompletely covered: 1. The far IR region ($10\text{--}500\text{ cm}^{-1}$) and the "dirty window region" ($500\text{--}600\text{ cm}^{-1}$) where the contribution of the pure rotation band of water vapour is dominant; 2. The end of the thermal IR above 2760 cm^{-1} where some of the atmospheric back scattered solar flux will be mixed with surface/atmospheric emission during the day. It is expected that clear sky RTMs could provide high enough accuracy to calculate the missing contribution (knowing either the IASI-NG radiances over its measured range, or the vertical temperature and humidity profiles measured by IASI-NG and also the other trace species as far as they contribute) to correct the IASI-NG measured TOA flux and to derive the total outgoing long-wave radiation (OLR) flux at the pixel level. Climatologies are then available following methods of resampling/averaging developed for previous earth radiation budget (ERB) sensors (ERBE, ScaRab, CERES), the operational algorithms of which could be tailored to the IASI-NG specificities.

A possible alternative to overall spectrally integrated OLR fluxes is to consider separately the contribution of different radiative species. IASI-NG spectral radiances in selected channels could be used as a proxy to deduce, through an appropriate RTM, the contribution of a given species to the overall radiative forcing.

IASI-NG could provide LW radiative cooling/heating rate profiles through radiative transfer codes, using the IASI-NG measured vertical distribution of temperature and water vapour and temperature together with minor constituents for which IASI-NG will also provide height resolved information. As for the TOA radiative forcing, one could consider to retrieve these altitude

dependent cooling/heating rates, from pre-calculated regressions, directly from the measured radiances in appropriate channels. Various averaging strategies should be designed to produce LW radiative cooling/heating products that could be used either to validate the corresponding radiation modules used by the NWP models themselves or in other applications (chemistry transport models (CTMs) for chemistry studies) which need to combine the LW flux discussed here with the solar short-wave (SW) flux to be calculated by appropriate radiation modules and/or measured by other instruments. Specific studies on the potential to couple the production of such data with some of the computational tasks needed to perform IASI-NG retrievals should be considered. But the approach suggested here (satellite-to-model) may be too indirect or complicated to implement and a better strategy to fully exploit the potential of IASI, could be to validate the TOA spectra calculated from the models directly against IASI-NG spectra (model-to-satellite approach). This will hopefully be possible with the improvement of computational speed and capabilities combined with the approach of variational assimilation of composite products. Clearly more research studies are needed in this field.

8.2.3.10 Synergistic use of IASI-NG

Synergy between variables

The simultaneous observations (i.e. at the same time and the same place) of several atmospheric variables and/or of several characteristics of the same variables can improve the analysis of the data themselves, as well as their interpretation. A recent example has been given by the A-Train which has proven the usefulness of having missions dedicated to the study of the same variable or to related variables. For instance, the joint use of CERES, MODIS, CALIOP and CloudSat has lead not only to an unprecedented precision on the surface radiative fluxes, but also to the vertical characterization of the atmospheric heating rate, which is a new product particularly useful for developing atmospheric models and for the study of the coupling between atmospheric circulation and physical processes. The results obtained from the A-Train (afternoon orbit) could be reinforced by the development of a M-Train (morning orbit) around EPS-SG/Sentinel 5.

A major challenge in our ability to forecast climate change is to better understand the link between clouds, atmospheric circulation, precipitations and radiative budget. In terms of processes, main objectives concern the simultaneous characterization of convection, mixing between boundary layer and free troposphere and water vapour distribution above the tropopause. Major questions in the future will include: coupling between clouds and aerosols; clouds, atmospheric circulation and precipitation; temperature and water vapour in the lower troposphere and the UTLS region; GHG and vegetation. A better understanding of the contribution of atmospheric variables to Earth Radiation Budget is also a major need for improving the ability of climate models to properly simulate its evolution in a changing climate, including vertical cooling rate.

Synergy between instruments

From a methodological point of view, there is a need to further explore the synergistic use between various instruments, either from current missions (A-Train) or planned missions (Sentinel, EPS-SG, EathCare), by coupling active (radars, and lidars) and passive (visible, near and short-wave infrared, thermal infrared, multi-angles) techniques. For instance, coupling measurements of GHGs in the short-wave infrared, sensitive to the full atmospheric column, and in the thermal infrared, sensitive to the mid-troposphere, can help isolating the GHG evolution near the ground where emissions happen. Another example comes from the characterization of aerosols: combination of observations in the visible and in the TIR can help distinguishing fine

and coarse modes of aerosols.

8.3 Air Quality Events and Environmental Monitoring

By events we understand natural or human-induced processes that are not predictable within a timescale of typically a month. Extreme events would be a subset of this class, characterizing the events that are rare as or rarer (in frequency or intensity) than the 10th or 90th percentile of the observed probability density function at a particular place and time. Note that

- While most events are local and episodic by definition, they can have implications on larger scale (regional to hemispheric) because of atmospheric transport.
- Events can have an impact on NWP. In turn, accurate meteorological parameters may be needed for the monitoring of events (e.g. temperature inversion in the PBL etc).
- Many of the events prioritized in this section have direct impacts on atmospheric composition and sometimes indirect impacts on climate; they are therefore tightly related to several topics addressed in other sections.
- The events discussed in this section are based on the heritage from IASI and do not constitute an exhaustive list. It is likely that the monitoring of other types of events will emerge if additional geophysical parameters (or changes in these, such as e.g. changes in surface properties) would be retrieved with sufficient accuracy.
- Monitoring events with IASI-NG may not be possible with compressed L1 data (PCAs or others).

It would be possible to monitor various types of events with IASI-NG, at fairly high spatial resolution and revisit time, considering that an entire suite of improved atmospheric and surface variables may be retrieved simultaneously from the radiance associated to each IFOV. For some events there is no demonstration, while for others there is substantial background information from heritage infrared hyperspectral sounders (IASI but also AIRS, TES). The events discussed below include:

- Volcanic eruptions
- Wildfires
- Sand storms
- Surface pollution episodes
- Industrial accidents

The anticipated contribution of IASI-NG to the detection and monitoring of events largely builds on the successes gained from the IASI mission that were unexpected at that time of the IASI science plan. With IASI, important breakthroughs have in particular been made on the monitoring of volcanic eruptions, from the early detection to the monitoring of emitted plumes in space and time (using SO₂ or ash observations), not forgetting the determination of the total emitted mass (the so-called source term). Additional but more emerging applications with IASI include the measurements of plumes from wildfires, the monitoring of sand storms or of large bad air quality episodes. Most of these applications are made possible with IASI owing to its excellent sampling (global monitoring with relatively high spatial resolution) and instrumental performances. With IASI-NG radiometric and spectral characteristics will be improved over IASI, while the sampling will be similar, hence strengthening the possible applications for event detection.

Programmatic context

Events such as industrial accidents that release pollution, or volcanic eruptions can constitute a threat to local populations and their monitoring and forecasting is as such a key objective of the EU Copernicus program. We anticipate that IASI-NG will make a key contribution to the Atmospheric Monitoring service (currently in a pre-operational phase in MACC-II), in particular with regard to volcanic eruptions and air quality forecasting, but possibly also to other core services (Land, Marine, Climate Change and Emergency Services). The monitoring of such events with IASI-NG would benefit other EU programs and initiatives such as the European Forest Fire Information System (EFFIS).

8.3.1 Volcanic eruptions

Volcanoes emit large quantities of gases and aerosols in the atmosphere during an eruptive phase. In addition to the danger created by lava flows, the emitted gas/ash plume may have important consequences on nearby populations and local ecosystems due to large concentrations of CO₂, acidifying gases and ash. If the eruption is powerful, the eruptive products (gases and ash) may be directly injected into the free troposphere up to the upper troposphere or – in rarer cases – the low stratosphere. This constitutes a threat to aviation for ash-rich clouds, which can persist for several days, transported along the plume’s track, until deposition and dispersion brings the ash concentrations to safe level. The current accepted ash concentration limits are defined for three zones: a low contamination zone (between 0.2 and $2 \times 10^{-3} \text{ g m}^{-3}$), a medium contamination zone (greater than $2 \times 10^{-3} \text{ g m}^{-3}$, but less than $4 \times 10^{-3} \text{ g m}^{-3}$) and a high contamination zone (equal to or greater than $4 \times 10^{-3} \text{ g m}^{-3}$). Flight into a high contamination zone is prohibited while flights into areas with a predicted ash concentration greater than $2 \times 10^{-3} \text{ g m}^{-3}$ may be undertaken at operators’ discretion. After the very ash-rich Eyjafjallajökull eruption in 2010, the operational Near Real Time (NRT) data-streams from satellites were shown to contain quantitative information about height or concentration of hazardous species; however, exploration of the potential of such satellite-derived products only began in earnest after the event. Recommendations were made to strengthen EO capabilities for monitoring the activity of volcanoes around the world, in order to provide useful and timely data, to be used in combination with trajectory models, to provide information to the Volcanic Ash Advisory Centers (VAACs) and other organisations. The Eyjafjallajökull eruption crisis showed that the main uncertainties were on the characterization of the eruption source term, needed for model initialisation, and the determination of the ash cloud height, depth, and concentration.

IASI was shown shortly after launch to provide robust detection of volcanic plumes based on the SO₂ signal strength. The detection is mainly from the ν_3 band, where the combination of strong and weak lines allows the retrieval of SO₂ columns over a large dynamic range of concentrations between 0.5 and 5000 DU. The signals from the weaker ν_1 band, less affected by water and the associated opacity in the low atmospheric layers, as well as the $\nu_1 + \nu_3$ combination band, have also been used but have been demonstrated in fewer cases. Based on the SO₂ measurements, the spatial extent of the plume can be characterized and tracked in space and time (at each overpass), making IASI a useful component of existing operational alert systems for volcanic eruptions, alone or in synergy with other instruments on polar orbits. The ESA-funded SACS system is one such alert service (<http://sacs.aeronomie.be/>). The accurate measurements of the SO₂ columns by IASI, combined with the global coverage, allow us to determine the total emitted mass (the source term) for each eruption in kilotons and to follow its decay in time (see figure 8.4). The source term is one of the key input parameters for trajectory models, but is also crucial for better constraint of the entire atmospheric sulphur budget. Since its launch, all major eruptions have been monitored by IASI.

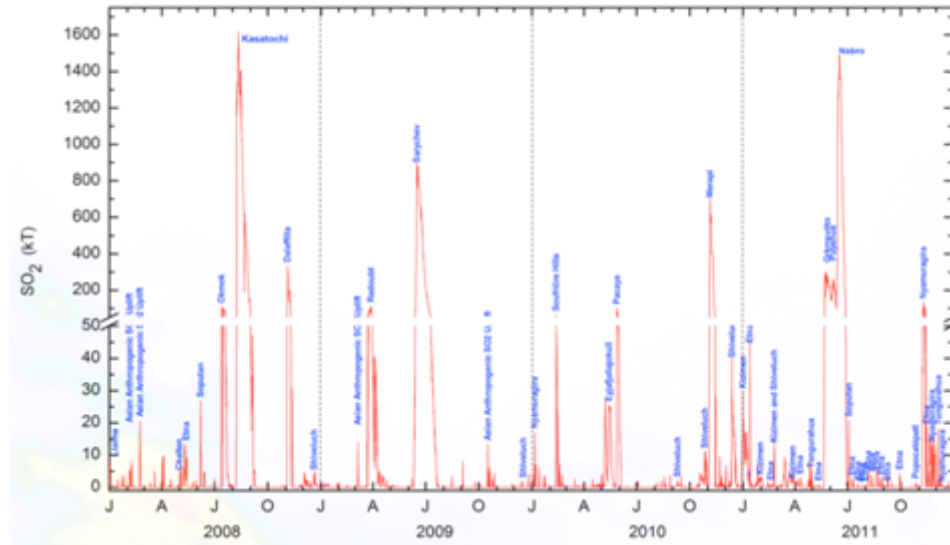


Figure 8.4: 4-year time series (2008-2011) of SO₂ total masses retrieved from IASI-A. From L. Clarisse.

An additional parameter that is needed to make good use of IASI measurements as input to trajectory models is the plume altitude. Recent studies have demonstrated that this parameter could be retrieved from IASI measurements in the SO₂ ν_3 band with a theoretical uncertainty of around 2 km in the 5–18 km range. The information comes mainly from changes in spectral signatures at various altitudes that are created by interference between SO₂ and H₂O lines.

While SO₂ is often a useful proxy for the volcanic plume, ash is much more crucial for aerial safety. SO₂ and ash are sometimes not emitted together or if they are both emitted they may not be released at the same altitude, resulting in different trajectories and dispersion pathways. The Eyjafjallajökull, Grímsvötn and Puyehue eruptions are all typical examples for which the operational systems based on SO₂ alone did not work well. In recent years there has been significant progress in the monitoring of ash plumes using IASI and other IR sounders. It was shown in particular that the infrared extinction features of volcanic aerosols could be differentiated well from other types of aerosols under most situations, using the numerous spectral channels of IASI. An ash detection alert was implemented in the near-real-time SACS system in April 2013 (the climatology from 2007 was also made available), showing no false alerts and good detection sensitivity, even for SO₂-poor eruptions (figure 8.5). From the IASI spectra, column abundance can then be retrieved, along with particle size, albeit with larger errors. The target requirement of $2 \times 10^{-3} \text{ g m}^{-3}$ that defines the limit between low and medium contaminated zones for aerial safety seems to be reached with IASI in most situations. Note that H₂SO₄ particle abundance can also be retrieved, for up to several days/weeks after the last SO₂ signal is seen.

The first validations of the SO₂ column and plume altitude, as well as ash columns, were conducted in the framework of the ESA-SACS/SMASH projects in 2013, during which several algorithms were also inter-compared. While the assessment was not always easy due to the low SO₂ amounts targeted, it was found that IASI was in general able to provide accurate information on SO₂ loadings and altitude, provided that there is sufficient absolute signal. Also the retrieval of AOD, which was analysed especially for the Eyjafjallajökull eruption is very promising for future applications (figure 8.6).

The contribution of high-spectral resolution infrared sounders to the global surveillance of volcanic eruptions has been amply demonstrated with AIRS and IASI. Following the Eyjafjallajökull eruptions in 2010, there have been substantial developments for retrieving quantities

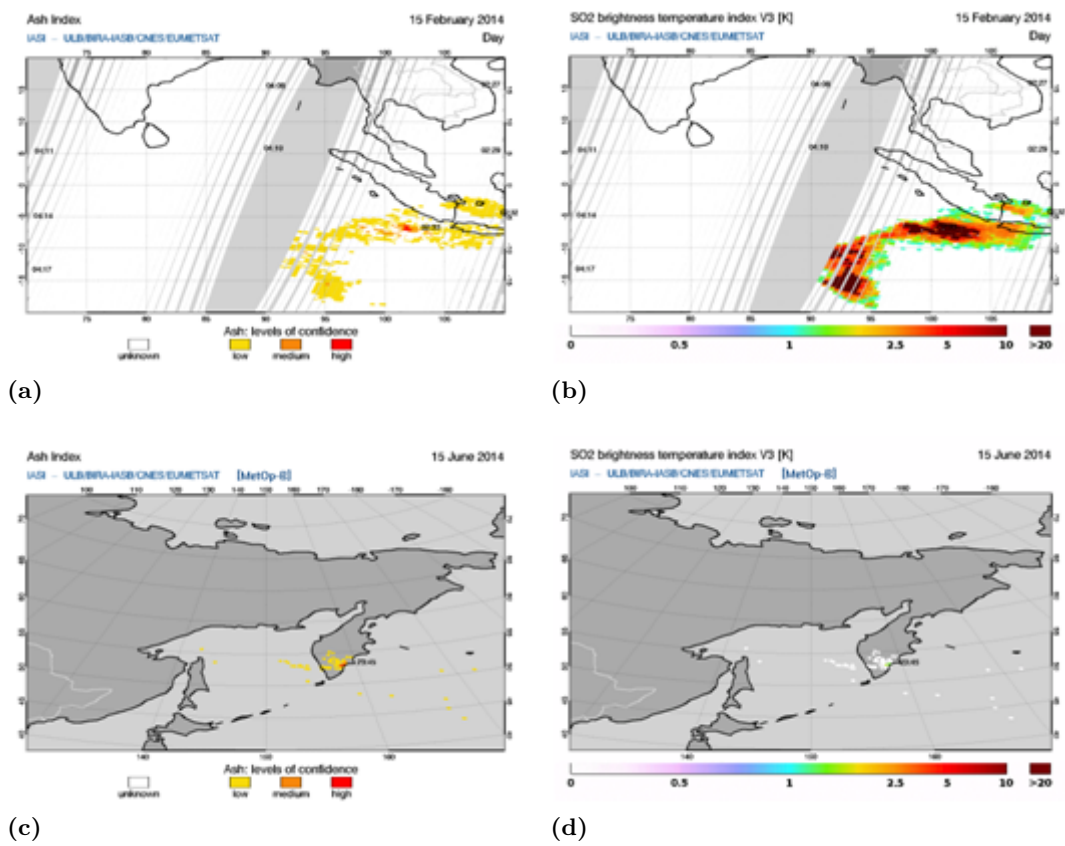


Figure 8.5: IASI-B ash (no unit) and SO₂ (K) detection from (top) the Kelut eruption on 15 February 2014 and (bottom) the Zhupanovsky eruption on 15 June 2014. Source: <http://sacs.aeronomie.be>

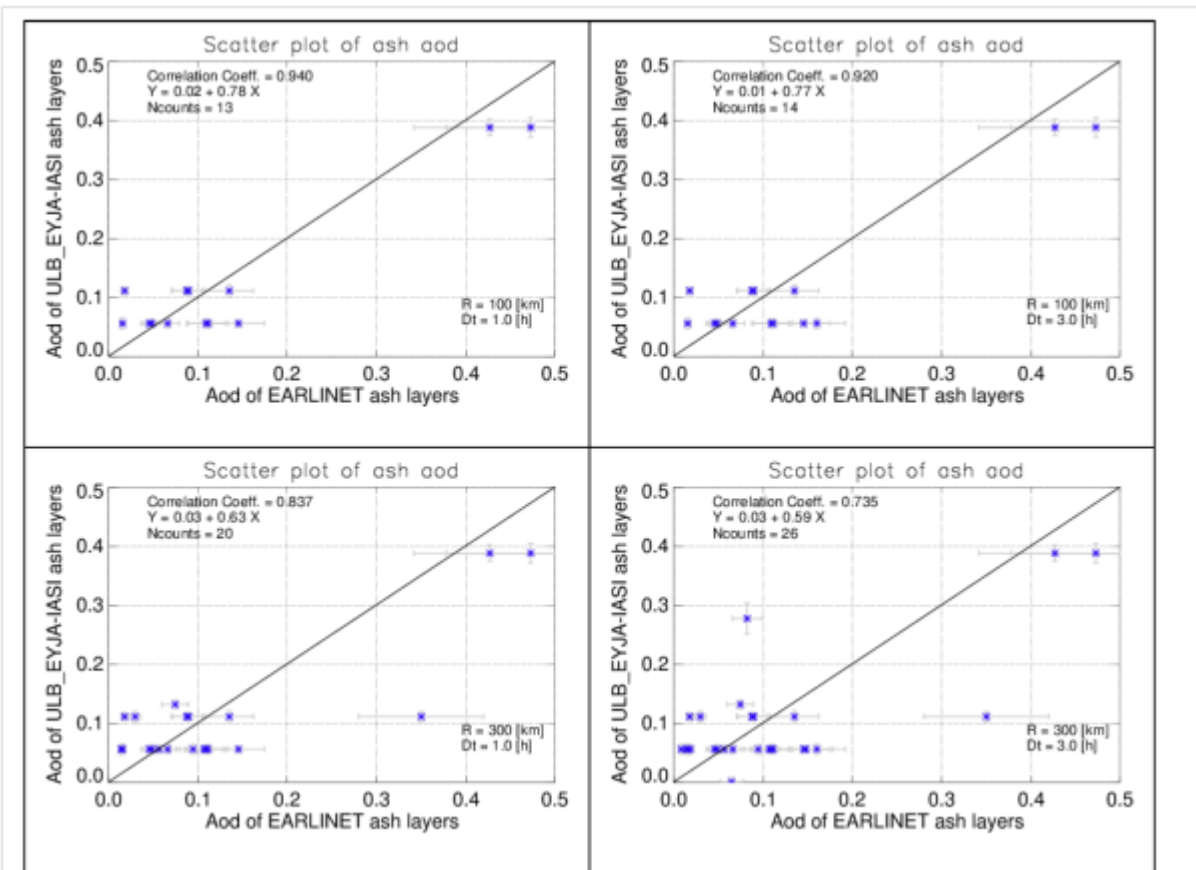


Figure 8.6: Comparison between AOD retrieved from IASI after the Eyja eruption, and those from EARLINET stations. The retrievals are based on an algorithm developed at ULB but similar results with the Oxford algorithm have been obtained.

that are of relevance for improving the alert systems currently in place. These include the early detection of SO₂ or ash clouds, the monitoring of plume dispersion (spatial extent, horizontal/vertical transport) and plume altitude, and total emitted mass. The two quantities are crucial for initialising trajectory models.

With IASI-NG we expect continuation of the monitoring system in terms of spatial and temporal sampling. For operational applications the notification of a volcanic event with IASI-NG would be needed 1–2 hours after the measurement is made. Besides pursuing the current monitoring capabilities, we expect to retrieve each useful parameter with better accuracy with IASI-NG:

- The better radiometric noise will allow the lowering of the detection threshold for SO₂ and most importantly for ash. It is therefore anticipated that the spatial extent of the plumes will be captured better and that the limit between low, medium and high contamination zones will be better defined. This will be crucial for providing robust and timely information to the VAACs and other organisations in charge of aerial safety. For similar reasons, the detection and quantification of H₂SO₄ droplets will be improved.
- The better spectral resolution will increase the vertical sensitivity and the sensitivity to lower-altitude plumes both for ash and SO₂. It is expected that the uncertainty in the determination of the plume altitude (based on SO₂ and H₂O) will be better than 1000 m provided that temperature and humidity and temperature are retrieved with similar accuracy. The measurements of plumes below 5 km will likely be improved.
- The combination of improved spectral resolution and noise could allow better use to be made of the weaker SO₂ bands (ν_1 and $\nu_1 + \nu_3$ combination band) in case of very large eruptions or plumes emitted in the boundary layer. In addition, the measurement of other volcanic gases (H₂S; possibly halogen species) will be favoured.

Besides the operational application, IASI-NG will allow us to continue the record of global emissions of SO₂ and ash from volcanoes started with IASI. Along with more precise measurements of H₂SO₄, this will make it possible assess the role of volcanoes on the global atmospheric composition and on climate.

8.3.2 Wildfires

Fires are an important component of the Earth's system. They can be natural (e.g. ignited by lightning) or human induced (for e.g. agricultural practices, changes in land use). In recent years, and because of the changing climate, the anthropogenic perturbation to the fire system has increased. Fire events have immediate impact on local population but, when very large, also affect air quality rapidly and severely on regional scales, through the emission of smoke or gaseous air pollutants. On longer and larger scales, fires play a central role in global atmospheric composition and climate (see section 8.2). Fire events are currently monitored using mostly broadband imagers, such as MODIS, AVHRR or SEVIRI, which provide rapid information on active fires (thermal anomalies) and radiative power, and indirect information on burned areas. These quantities are central to many environmental studies, especially as they serve as input to emission inventories. Several near-real time services are available, such as the FIRMS (Fire Information for Resource Management System) based on MODIS hotspots or the FIR Global Fire Monitoring system in MACC-II that provides near-real-time emission estimates using measurements from SEVIRI and MODIS. Large uncertainties in the emission remain, however, which are related to the use of standard emission factors for trace gases and a series of hypothesis on vegetation and combustion types. The potential of UV and IR hyperspectral sounders to monitor fire emission products, mainly trace gases (CO, NO₂, VOCs) has been demonstrated in the past decade, but never applied in a near-real time perspective. Similar to what is achieved with volcanoes, the potential of using such measurements for monitoring large

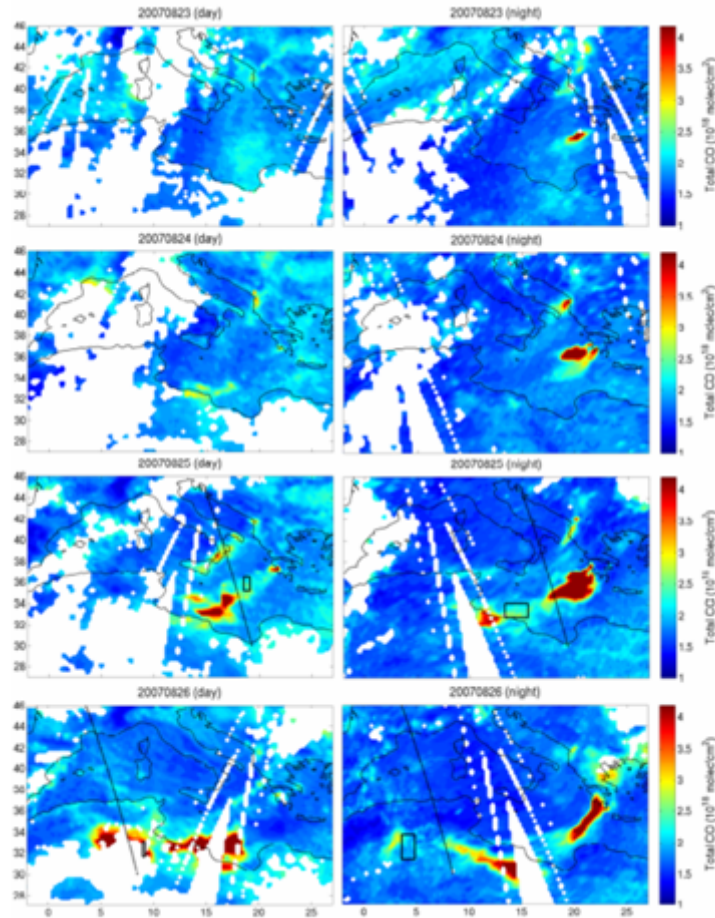


Figure 8.7: CO plume (total CO columns in molecules/cm²) from the fires in Greece, for morning and evening overpasses of IASI-A between 23 and 26 August 2007. From S. Turquety.

fire events (emitted species, extent and dispersion of the fire plumes) exists and could provide strong added value to the current EO concepts.

IASI has several key features for monitoring fire events globally. Due to the wide large spectral range in the thermal infrared and fairly high spectral resolution, it is able to measure various gaseous species commonly emitted by vegetation fires, such as CO but also NH₃ and a series of VOCs, as well as, but with limited sensitivity, fire smoke. With CO, fire plumes can be monitored from the source to further downwind (shown in figure 8.7 for the 2009 Greece fires) and critical information on the emissions can be obtained using top-down estimates. Preliminary studies have shown that the simultaneous measurements of several trace gases with different lifetimes allow investigating reactivity in the plume and partitioning global concentration measurements of several reactive species from all processes into specific concentration distributions from fire emissions.

Considering the emerging applications on fire monitoring with IASI, there could be as well significant contribution of IASI-NG to the near-real-time monitoring of fires. As for volcanoes described in the previous sub-section, the improved instrumental performances of IASI-NG will indeed allow probing the fire plumes with better sensitivity to various reactive species, better vertical resolution and increased sensitivity to the boundary layer. The lower noise of IASI-NG in the atmospheric window should in particular improve the monitoring of smoke aerosols. An

attractive application would be to complement the NRT systems in development, which provide bottom up estimates of gaseous emissions (e.g. FIR in MACC-II) with concentrations (or ideally inferred emissions) from IASI-NG.

8.3.3 Sandstorms

Dust storms or sandstorms (sandstorms refer more specifically to large desert particles), develop under high wind conditions. They are common in desert regions of the Middle East and Africa, but are also frequent in Central Asia. They can occur as well on a smaller scale over any region that has a high volume of loose dirt or sand. The heavier particles travel a relatively short distance compared to the smaller ones (dust), which can travel thousands of miles. Sandstorms from the Sahara Desert often travel right across the Atlantic Ocean, but can in some cases also travel Northward across the Mediterranean Sea to reach central and Western Europe. Dust storms happen rather unexpectedly and are difficult to predict. Locally and regionally they have an impact on visibility, affecting aircraft and road transportation, on air quality. They can damage crop plants.

Large sand plumes are routinely observed from IASI in the outflow of desert regions. While there have been significant advances in the measurements of the plume properties (plume altitude, aerosol size and optical depth), this has mainly been achieved in the perspective of climate applications. Fewer reports exist on the use of IASI for detection and monitoring of sandstorms/dust storms on a near-real-time basis, also large events are frequently seen, such as the transport of Asian dust or sand from the Sahara (see figure 8.8).

There will be the potential with IASI-NG to contribute to the NRT monitoring of sandstorms or dust storms. The improved noise of IASI-NG over IASI will allow better sensitivity. It is also likely that the instrumental performances will allow more accurate determination of the plume's altitude, which would be important for potential applications.

8.3.4 Extreme urban air pollution

Bad air quality episodes develop under different conditions, most frequently in densely populated areas. They are becoming the central health issue in several cities and regions. Photochemical smogs due to emissions of short lived NO_x and VOCs are associated to enhanced O₃ concentrations in the boundary layer and occur in the hot summer months, while chemical smogs are usually related to large concentrations of particles in ambient air along with other gaseous pollutants, and occur generally in cold winter months with stagnant weather. Other pollution events, such as too large PM concentrations after manure spreading in the fields, happen in other periods, sometimes in regions relatively far from the emission source. Some of the episodes can last for only a few hours and can be characterized by a strong diurnal cycle (e.g. O₃ photochemical smog), while other can persist for several days. The type and the acceptable levels of pollutants regulated for air quality vary between countries. For the EU, they have been revised by the directive 2008/50/EC of the European Parliament and of the Council of 21 May 2008 on ambient air quality and cleaner air for Europe, which entered into force on 11 June 2008. Two expert studies by ESA (CAPACITY and follow-on CAMELOT) have examined for several species and parameters the accuracy required in order for satellite sounders to contribute to air quality monitoring.

Satellites measurements have started to be assimilated in chemistry-transport models to support air quality forecast. This is the case for example in MACC-II (see also section 7.2). However, pollution events are still difficult to predict accurately with regard to the level of pollutants, and the exact place and time where exceedance would occur.

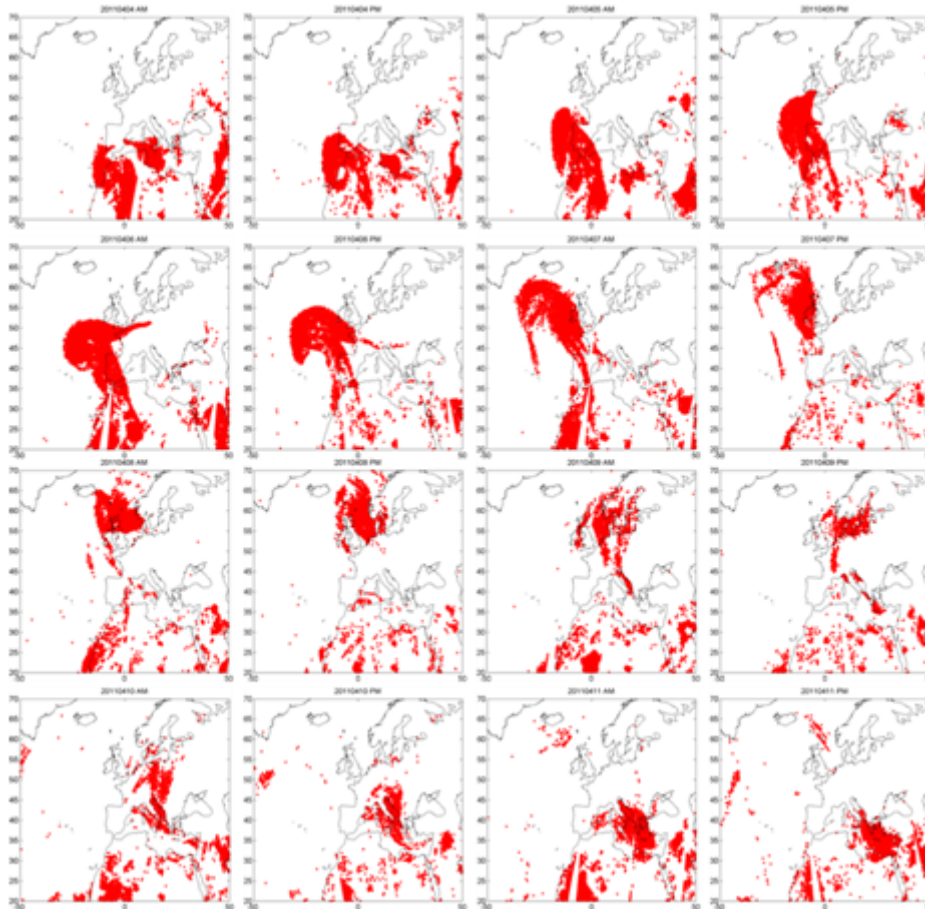


Figure 8.8: Saharan sand storm transported over Europe. For top to bottom and left to right: measurements from IASI-A from 04/04 to 11/04/2011, for each morning and evening overpass. Figure by L. Clarisse.

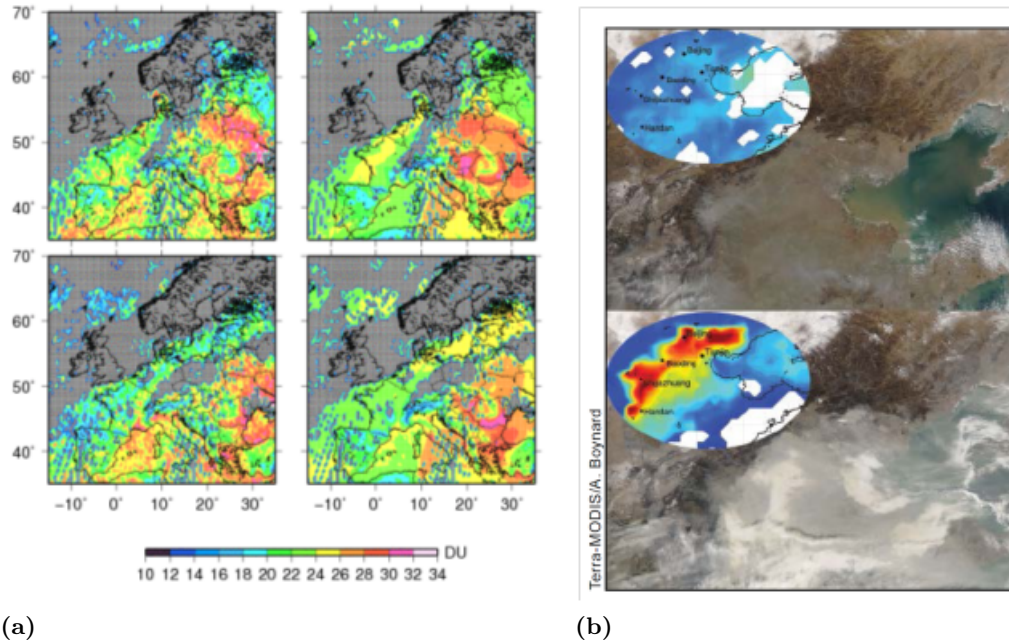


Figure 8.9: (a) IASI measurements of the 0–6 km O₃ column during a heatwave in Europe, on July 27 and 28 2007, compared to CHIMERE model simulations (second column); From Eremenko et al. 2008. (b) IASI measurements of CO before (top) and during (bottom) a large pollution episode in China. The CO concentration field, with enhanced values highlighted from yellow to red color, is superposed on a visible image from MODIS. From Boynard et al. (2014).

IASI measures several trace gases that are of direct relevance for air quality but it has sensitivity to the planetary boundary layer that is currently limiting its use for direct air quality surveillance systems. The following findings with IASI suggest, however, a potential important role for this aspect, especially in combination with models:

- The assimilation of the IASI-derived CO columns have shown positive impact in the MACC system for forecasting concentration CO distributions. The CO measurements have helped modelling extreme events, such as those following the large fires in Russia.
- Large-scale O₃ photochemical pollution episodes can be detected by IASI retrievals of the lower O₃ tropospheric column (figure 8.9(a)). This is possible in particular as such events occur when temperatures are high and the boundary layer is thick, favorising the sensitivity of IASI to the BL. The sensitivity to the lowest layers remains small.
- In case of temperature inversion, pollutants build up in the planetary layer and IASI has much better sensitivity at near-surface levels. Extreme smogs can be detected (figure 8.9(b)), with measurements in particular of CO, SO₂, NH₃ and to lesser extent ammonium sulphate particles.

With IASI-NG the measurements at near-surface level will be better for all pollutants, in terms of sensitivity and accuracy. The vertical sensitivity will be improved, allowing separating frequently processes that occur two different parts of the troposphere. It is anticipated that IASI-NG will be a key element of the EU Atmospheric Monitoring service for air quality forecast by offering measurements of several primary pollutants simultaneously, including, but not limited to, CO, SO₂ and NH₃, which are regulated for air quality by themselves and which are involved in the formation of secondary PM and O₃. The measurements of tropospheric ozone with better sensitivity with IASI-NG will be a major breakthrough.

8.3.5 Industrial/nuclear accidents

With IASI there has been no demonstration that industrial chemical or nuclear accidents could be monitored. In particular, IASI has not detected the nuclear plume after the Fukushima accident. Large-scale industrial complexes are, however, detected based on their emission of CO or NH₃.

Owing to the large series of pollutants that IASI-NG will be sensitive to, the lower noise levels as compared to IASI and better sensitivity to surface concentrations, it is likely that IASI-NG will detect significant industrial accidents if they were to occur.

8.4 Process Studies

As well as forecasting applications, where the emphasis is on using the data to constrain models, air quality applications where data are used to detect and quantify the presence of pollutants and chemical species, and climate monitoring applications where observations are used to detect and measure trends and variability in the atmosphere, IASI-NG observations could be used to perform investigations into physical processes that occur in the atmosphere or Earth surface. The use of IASI data to enhance understanding of such physical processes is an immature area of science, partly because identification of fields where the observations may be of use depends upon having a stable and well-understood product, whether that product is L2 retrievals or the radiances themselves, and then a large body of work performing careful investigations into the spatial and temporal patterns of the product before anomalies are spotted that may lead to enhanced understanding of the processes that affect the measurements.

On the timescale of the launch of IASI-NG, products from IASI will have matured to the level where such investigations will begin to become more commonplace. This chapter lists a few areas where we may expect to see progress in the use of IASI/IASI-NG data to aid understanding of physical processes in the atmosphere and at the surface.

8.4.1 Atmospheric Processes

Atmospheric Processes involve interactions of the atmosphere, biosphere, cryosphere, hydrosphere, and lithosphere and are the result of complex Earth-Sun interactions and include weather and climate. Atmospheric Processes are the driving force behind global energy patterns. Earth's atmosphere contains 78.08 % nitrogen, 20.95 % oxygen, a variable amount (averaging 1.2%) of water vapour, 0.93 % argon, 0.039 % carbon dioxide, and traces of hydrogen, helium, other noble gases, and volatile pollutants, some having greenhouse property effects (e.g., methane). Some of these pollutants are the result of anthropogenic processes. Oxygen is used by most organisms for respiration. Carbon dioxide is used by vascular plants, algae, and cyanobacteria for photosynthesis.

Atmospheric Processes include energy transfer between the Earth's surface and the atmosphere in a variety of ways, including radiation, conduction, and convection; boundary layer processes in the lower atmosphere, where the atmosphere 'feels' the influence of Earth's surface; cloud and aerosol interactions with radiation.

Possible areas where IASI-NG data may contribute to increasing understanding of atmospheric processes are

- Stratospheric physics: IASI performance is very stable in time, and we expect the same of IASI-NG. With many channels sensitive to radiation in the stratosphere, IASI-NG has the potential to provide data that will improve understanding of the stratosphere.

- Polar dynamics.

8.4.2 Processes at the land surface-atmosphere interface

8.4.2.1 Soil moisture daily cycle and its impact over surface emissivity

In the absence of precipitation, the three main mechanisms by which water may be added to the uppermost soil surface are fog deposition, dew formation and water vapour adsorption. Dew is primarily a physical phenomenon, which affects the energy balance at the soil-plant-atmosphere interface. On bare soil, nocturnal dew usually evaporates the following morning, creating a diurnal cycle of water content in the uppermost soil layer. This cycle involves exchange of latent-heat flux between the soil and the atmosphere, thereby affecting the energy balance at the soil surface.

Water vapor adsorption occurs when the surface temperature is higher than the dew-point temperature and the relative humidity of the soil's pores is lower than the relative humidity of the air. Water vapor adsorption is the main exchange mechanism in semiarid and arid regions in presence of rich quartz sand.

The mechanism of water vapour exchange at the interface surface-atmosphere can give rise to a diurnal cycle of soil moisture which, in turn, can produce daily variations in surface emissivity. This is a phenomenon which is normally not taken into account in surface parameters retrieval algorithms which normally consider that emissivity can change on very large time scale in comparison to the very short time scale variations expected for surface temperature.

Diurnal variations in desert sand emissivity during the dry season have been brought to the public's attention recently by Li et al. (2012) who performed an analysis with SEVIRI (Spinning Enhanced Visible and Infrared Imager) observations from the European geostationary platform Meteosat (Meteorological Satellite). A recent analysis performed by some of the authors of this science plan with SEVIRI data (Masiello et al., 2013) confirms this effect and also shows that the time-variation of emissivity closely follows the daily cycle for temperature.

There are a series of basic studies, which can help to explain the phenomenon of diurnal emissivity variations during non-raining days in the dry season and in environmental conditions that do not favor the occurrence of dew formation on a bare sand dune. Agam and Berliner (2004; 2006) brought evidence of the mechanism of direct water vapour adsorption on land surface, whereas Mira et al. (2007a,b) showed that the thermal infrared emissivity of rich-quartz sand strongly depends on soil moisture content.

More recently Moncet et al. (2011) analyzed IASI spectra recorded over a Sahara desert area during the dry season (July 2010). Both descending (daytime) and ascending (nighttime) orbits were considered and the surface emissivity spectrum was retrieved simultaneously with skin temperature and atmospheric parameters. Space co-located day and night IASI observations were used to assess diurnal emissivity variations. The results shown in Moncet et al. (2011) lead one to conclude that the common belief that the desert sand emissivity is stable during the year is not correct and that diurnal variations have to be properly taken into account for a correct retrieval of surface and atmospheric parameters. In this respect, the findings shown in Moncet et al. (2011) specifically point out the importance of using physically-based algorithms to retrieve surface temperature and emissivity. Split-window type algorithms, which are commonly used to retrieve surface parameters from satellite imaging radiometer instruments, such as MODIS and SEVIRI do not take these diurnal emissivity variations into account, which could result in large surface and lower troposphere temperature errors. As an example, ISCCP-MODIS LST differences for July 2003 monthly mean at the time of day MODIS measurements, limited to

clear conditions, show a large misfit mostly evident in arid desert areas where surface emissivity is expected to have larger variations, because of quartz restshralen absorption at 8.6 μm .

With IASI-NG it will possible to consolidate research studies about the physical retrieval of surface and atmosphere parameters already undertaken with IASI. In fact, IASI-NG is expected to play a major role to get insight into understanding the time scale variations of emissivity over desert regions, and, hence, to assess the quality of the satellite remote sensing of surface temperature, which is a parameters of paramount importance for climate.

8.4.3 Identifying climate processes and trends coupling observations and models

In parallel to the continuation of long-term monitoring of the atmosphere, the improvement of our ability to describe the global behaviour of Earth atmosphere, including the underlying processes, its evolution, and its variability, will be a major objective in atmospheric sciences for the next years. This will go through the use, in a more and more coupled way, of satellite data, surface network and model simulations, in order to study processes at various spatio-temporal scales. In that sense, owing to its large spatial coverage, as well as the number of ECVs achievable, IASI-NG will offer invaluable observations for predictions on seasonal to decadal time scales. In particular, it will provide observations for: 1. evaluating models, for example, with regard to how well they replicate extreme events including their temporal variability; 2. improving the understanding of the relevant physical processes; 3. supporting the development of robust statistical methods for assessing extremes and their uncertainties.

Understanding climate processes at different temporal and spatial scales is of great importance for the development of models that can predict climate change at different scales, ranging from seasonal and decadal to centennial. However, the processes that contribute to climate variability and change are not fully understood and are currently the subject of further research. From the work done by the IPCC, it has become clear that many requirements originating from climate modelling need to be considered by the satellite remote sensing community. Therefore, the Climate Modelling User Group (CMUG) of ESA's Climate Change Initiative (CCI) formulated generic requirements directly related to climate modelling that are particularly relevant for the IASI/IASI-NG series. These are:

- Model initialisation and definition of boundary conditions. Prognostic quantities in numerical prediction models for climate need to be initialised at the beginning of a simulation and boundary conditions need to be formulated for non-prognostic quantities. Depending on the prediction scale (seasonal, decadal or longer) different priorities for certain Earth System quantities derived from satellite data and their needed accuracy emerge. Those requirements need to be systematically collected and analysed to make the development of CDRs successful for this application.
- Model development and validation. Satellite observations can be an important part of model development in particular testing the ability of a model to simulate the climatology, annual cycle or specific processes. In models, processes are most often represented in form of parameterisations to allow for computational efficiency. Satellite observations can help to improve the understanding of processes by providing process relevant observations and to validate model parameterisation for instance by analysing diurnal and seasonal cycles or comparing statistical relationships between variables in both the model and the observational domains.
- Data assimilation for climate models. It is envisaged that data assimilation techniques, now mostly used with weather forecast models to improve forecast skill, will also be used to initialise climate models used for seasonal and decadal forecasts. Such forecasts have

imminent importance for climate services. The advantage of using satellite data lies in the homogeneous global coverage. To be assimilated, the observations must represent a prognostic variable of the forecast model. Specific requirements for related satellite products in terms of accuracy, etc. will emerge over the next years and the envisaged architecture needs to be able to respond to such type of requirements.

In order to successfully address these goals, a set of variables and their spatio-temporal resolution suited to perform proper comparisons between IASI-NG and model outputs need to be defined in partnership with climate modelers. Questions that need to be addressed cover: the definition of each variable in the satellite world and the model world; the characterization of spatio-temporal variability in a model grid-cell/time-step; and the representativeness of observed vs. modelled variables. IASI-NG simulators will have to be designed with inputs from general circulation models, chemistry transport models on a global scale, as well as regional models (e.g. for air quality and climate feedbacks). Model-satellite comparisons are mostly conducted with L2 products (e.g. clouds, aerosols, gases). However, approaches based on L1 data themselves are starting to be developed and might provide powerful tools to evaluate models in the near future by exploiting the spectral information of millions of spectra recorded every month by IASI-NG. The use of statistical approaches (such as radiance probability distribution functions) should be encouraged to extract climate variability and trends from the radiances themselves. A comparison between statistical quantities derived either from measurements or from reanalysis or climate models could give access to powerful diagnostics for evaluating models behaviour.

Other areas where it is possible that IASI-NG will contribute include:

- Snow properties
- Ocean-Atmosphere interactions
- CO₂ cycle and biogenic activity of the ocean
- Understanding radiation budgets, including cloud and aerosol radiative forcing
- Non-LTE effects

At the present time it is difficult to anticipate exactly what contributions the data will make, but it will be interesting to watch these areas of research evolve in the coming decades.

8.5 Assessing the impact of IASI-NG

Consideration should be given to the ways of assessing the impact of IASI-NG, both scientifically and in terms of societal benefit.

8.5.1 Assessment of impact in NWP

NWP centres each tend to have their own ways of assessing impact of observations within the system. For example, forecast skill relative to persistence verified against radiosonde observations may be used to evaluate the impact of the addition or denial of a data type. Some centres combine several skill measures into an overall index, where other centres favour the use of particular measures such as anomaly correlation scores. In the case of convection-resolving models, different measures of skill are often used, such as Brier skill scores to measure detection of precipitation events.

Measures such as Forecast Sensitivity to Observations (FSO) may also be used to assess impact on a total energy norm. These measures are useful to examine the impact of individual channels on the assimilation system, but are less direct than the impact on large-scale thermodynamics or small scale weather.

It remains the case that it is difficult to compare impact between different centres because of the proliferation of methods, the different test periods chosen, the different number of cycles performed in a typical assimilation trial etc.

It can also be difficult to assess the impact of satellite data on the types of measure usually employed to measure impact in convective-scale models. Thought should be given to methods of proving the worth of IASI-NG data in these situations.

Chapter 9

Calibration and Validation

The EUMETSAT and CNES Calibration and Validation plans describe the activities planned by EUMETSAT and CNES in the weeks and months after launch to verify the performance of the instrument in space and of the processing software. The operational activities planned by CNES and EUMETSAT include dedicated work during the commissioning phase of the instrument and Level 2 products, and subsequently routine monitoring of instrument performance and reprocessing activities to improve the historical record of data.

Validation will be an important part of IASI-NG success. Validation exercises are needed during the full life cycle of the mission including short-term, long-term and campaign-based validation activities. The purpose of this chapter is to support the IASI-NG project in its endeavour to assess the data quality by comparing the products to data from other sensors which are regarded as a reference. This chapter proposes ways that users may contribute to Cal/Val activities: the involvement of the user community in Cal/Val activities ensures a diversification of techniques and a division of labour that can only enhance understanding of the instrument, leading to better exploitation.

As far as possible, common datasets should be used to assess the performance of the Level 2 products, in addition to any dedicated studies at each centre. The corresponding datasets should be provided on a sufficiently detailed vertical grid, so that fine vertical scale structures can be evaluated (moving towards one hundred levels). Such datasets should be publicly available, to aid contribution from scientists to campaigns (for example, the very successful JAIVEx campaign could provide a model on which future campaigns could be based).

The other important aim is to set out the areas in which currently available observations and methods are insufficient to validate data and products, so that research can be prioritised in these areas. Central to this is the identification of existing and planned instruments, networks, programs, and satellite missions that will be in place when IASI-NG is flying and which are potentially suited to be included in the validation organization. Observational gaps can then be identified, which can be addressed through updating of existing sensors or by starting the development of new instruments or concepts prior to the launch. It is critical that the identification of opportunities to fill these gaps is made as early as possible, in order to find appropriate funding and to plan for technology development.

For Level 1 validation, the aims are to ensure that the instrument is very well characterised with respect to the requirements for the individual budgets that make up the random noise, pseudo-random noise and measurement bias, and to ensure that instrument performance is within the overall budget laid out in the End User Requirements Document.

Measurement bias can be hard to estimate. It is possible to calculate a relative bias with respect to other instruments via double difference techniques (see, for example, the results of Larrabee Strow reported in Hilton et al., 2009a). However, any comparison against model data or direct measurements require the use of radiative transfer code and underlying spectroscopic databases. It is critical that research in these areas, in particular in the development of line-by-line models and spectroscopic parameters is not only carried on, but enhanced, to reduce the biases inherent

in forward modelling radiance data and thus enable proper understanding of the characteristics of the measurements. This is critical for climate applications, but biases are also a limiting factor of exploitation of radiance data in NWP.

Attention should be paid to the outcome of the GAIA-CLIM project (<http://www.nersc.no/project/horizon-2020-gaia-clim>), of which the aim is to establish sound methods for the characterisation of satellite-based Earth Observation data by surface-based and sub-orbital measurement platforms, including model data.

The central questions for IASI-NG Level 2 validation are:

- How representative are the satellite retrieved geophysical variables for the actual atmospheric state?
- What are the systematic and random errors, relative to the User Requirements?
- How well are the temporal variations of each variable captured, from daily fluctuations to annual trends?
- How well are spatial structures captured, from local to global features?

It is important to realize that the answers to these questions depend considerably on the atmospheric situation (e.g. clouds and fronts or clear-sky, variable surface properties), knowledge of auxiliary parameters (e.g. spectroscopy) as well as the knowledge of instrumental characteristics, viewing geometries and instrument noise. With respect to the scientific mission goals, IASI-NG data need to be validated in various key regions around the globe.

Prerequisite are comparisons to temporally and spatially coincident measurements performed by independent instrumentation from various platforms (i.e. ground-based, aircraft, ship, balloon) from a variety of locations around the globe with traceable uncertainty; they are considered to be of high priority. Continental scale projects such as European Copernicus, in connection with modelling and interpretation activities, can help to cope with representativeness errors of both the IASI-NG observations themselves, and the measurements taken from validating instruments. To infer data quality over the mission lifetime, both long-term and campaign mode validation activities are needed. In principle, the full suite of existing, high accuracy and reliable techniques used for every geophysical variable measurement on an operational basis shall be considered, including flask samples, in situ, and remote sensors.

Ground-based infrastructures that consist of various stations that are distributed over the globe are essential to tie the retrieved products to international standards. Aircrafts and balloons, equipped with in situ sensors to infer vertical profiles are of utmost interest for IASI-NG validation, as they provide the most accurate data calibrated against the WMO Standards, thus promising the highest level of confidence. Furthermore, aircraft are quite flexible providing temporally and spatially coincident measurements almost anywhere on the globe (e.g. in data sparse regions without any information or far away from ground-based measurements). Finally, the cross-comparison with other satellite missions measuring geophysical variables at the time when IASI-NG is flying is also of interest.

9.1 User contributions to calibration and validation activities

It is expected that users will perform their own assessments of data quality, both for L1 and L2 data. These activities can greatly assist with instrument characterisation and enhance understanding and development of L2 products, as has been demonstrated on many occasions with existing satellite instruments. The presentations from previous IASI conferences attest to the wide range of activities carried out by users, many of which are pertinent to Cal/Val.

For example, the monitoring of radiance departures from NWP models is a way to establish data quality in all meteorological conditions cheaply and quickly. Dedicated campaigns can be used to compare the measurements from IASI-NG to those of other similar instruments, and to validate Level 2 products. Cal/Val activities may also be planned to fit within existing activities such as field measurement campaigns, which will serve science goals along side instrument characterisation.

9.2 An airborne demonstrator for IASI-NG

The development of an airborne hyperspectral infrared sounder based on the IASI-NG design would be an extraordinary asset, not only for the development phase of the instrument, but also to have an operational means to (i) participate in calibration campaigns / validation (during the flight acceptance phase and beyond); and (ii) provide the scientific community with an operational tool to meet different scientific objectives. The availability of an airborne hyperspectral infrared sounder deployable during operational or scientific measurement campaigns would meet several scientific objectives, among which we can mention:

1. Validation of spectroscopy and radiative transfer: the comparison of spectra measured by the instrument (well calibrated spectrally and radiometrically) and spectra simulated by radiative transfer models using thermodynamic data (temperature, water vapor), gas, microphysical parameters) measured by auxiliary instruments (radiosondes, dropsondes, particle counters) would make it possible to overcome the uncertainties associated with the knowledge of the atmosphere and better detect the inaccuracies associated with radiative transfer modeling and underlying spectroscopy data (line-by-line parameters, absorption cross-section, H₂O continuum, ...). This objective is essential in order to best prepare the direct and inverse radiative transfer models with the increased spectral and radiometric performances of IASI-NG.
2. Study of the sub-pixel heterogeneity: the question of the heterogeneity of atmospheric and surface variables (temperature, humidity, emissivity, aerosols, clouds, etc.) within an IASI/IASI-NG field of view is a critical question for interpreting the observations. The high spatial resolution delivered by the airborne sounder (e.g. 200 m for a flight altitude of 12 km), combined with the good knowledge of the atmosphere provided by auxiliary measures, would make it possible to study this question in detail.
3. Characterization of continental surfaces: The high spatial resolution of the airborne sounder associated with the coverage of the spectral bands conventionally used for the emissivity and surface temperature estimation would better characterize the continental surfaces and connect radiative properties of the surface and type of soil overflow, particularly in relation to the vegetation.
4. Characterization of the atmospheric composition: the airborne sounder would provide information on the gas columns along the trajectory. These measures will thus make a significant contribution to multi-instrumented campaigns aimed at better understanding the content of atmospheric constituents (CO₂, CH₄, CO, O₃, aerosols, etc.) of regions overflow.
5. Instrumental coupling: Various instrumental combinations are possible on board research aircraft to improve the estimation of geophysical variables and to study the contribution of different instruments. For example, it would be possible to study the combination of passive measurements made by the airborne sounder and active measurements performed by cloud / aerosol lidars (RaLi, Cimel) or gas (CHARM-F Merlin demonstrator). The simultaneous use of IASI-NG demonstrator and OSIRIS, demonstrator of 3MI, will prepare the joint use of 3MI and IASI-NG that will fly together on Metop-SG-A.

9.3 Synergistic Cal/Val activities

Although dedicated activities that focus on one part of the required validation (e.g. comparison of IASI-NG measurements against airborne interferometer measurements at the same location; validation of chemical constituent L2 products against insitu measurements; intercomparison of measurements from different satellites via SNO-type studies) are anticipated, it is proposed that Cal/Val activities are carried out in a synergistic way wherever possible, to maximise the scientific outcomes from available funding and manpower. Such examples include:

- Validation campaigns that incorporate other instruments (EPS-SG instruments such as 3MI; MicroCarb; Merlin; ...)
- Validation campaigns that incorporate validation of other IR sounder data (e.g. MTG-IRS; IASI; CrIS).
- Validation campaigns that incorporate as many different instrumental measurements as possible.
- Cross-cutting campaigns (e.g. that include “science” goals with Cal/Val)

The latter are considered to be particularly valuable as they increase possible sources of funding and enhance scientific understanding at the same time as performing validation of the IASI-NG data and products.

There have been several examples of such campaigns that incorporate IASI data. Campaigns that can be considered a particular success include the JAIVEx and ConcordIASI campaigns. For these campaigns, science goals included understanding of specific atmospheric and surface conditions; furthermore data were made public either during or after the campaign and users encouraged to use these data for further scientific study. An example of a study made by the ISSWG members using the JAIVEx data was presented by Hilton et al. (2009b).

9.3.1 Some examples of post-2022 campaigns already planned

9.3.1.1 The MAGIC initiative - multi-instrument campaigns with ground-based and airborne measurements

One of the main limitations of the validation of space missions and more generally atmospheric exchanges along the atmospheric column concerns the current lack of knowledge of the vertical distribution of geophysical variables, in particular in the upper troposphere and the stratosphere.

The MAGIC campaigns (Monitoring of Atmospheric Composition and Greenhouse Gases through Multi-Instruments Campaigns) aim at (i) providing a multi-team, multi-mission space and multi-instrument framework to best prepare validation activities for space missions; (ii) improve our knowledge of the atmospheric, and especially vertical, distribution of thermodynamics variables and gases.

Led by Laboratoire de Météorologie Dynamique (LMD/CNRS), the MAGIC initiative gathers 7 laboratories and receives funding from CNES and CNRS with contributions from ESA. The MAGIC campaigns have 3 scientific objectives:

- The understanding of vertical gas exchanges, in relation to atmospheric transport and gas flows on the surface and in the atmosphere.
- The validation of total or partial gas columns measured from space (the Level 2 products). The main question is then how to compare columns measured from the space, columns measured from the ground, and vertical profiles of concentration measured between 0 and 11 km (plane) or between 0 and 30 km (balloons).

- The estimation of level 2 products themselves, with underlying questions of spectroscopy and a priori knowledge of the state of the atmosphere for inversions of radiances measured in columns of gas (passing from Level 1 to Level 2).

The MAGIC campaigns have 3 programmatic objectives:

- To allow the scientific community to test and evaluate the merits of various instrumentations (on the ground, airborne under balloons or on board aircraft) that can be used to meet the objectives mentioned above. A particular effort will concern the study of the vertical distribution of greenhouse gases and the link between atmospheric profiles of gases and columns, total or partial, measured from the ground and the space.
- To develop validation work on IASI-NG, Merlin and MicroCarb space missions by evaluating the instruments and the strategy to be put in place. The definition of the validation activities of these 3 missions (which each allow the measurement of total or partial columns of greenhouse gases) must be carried out in a spirit of coordination, in order to optimize budget, instrumental effort and scientific objectives. More specifically, these MAGIC campaigns are also intended to provide a framework for deploying demonstrators of future space missions, in particular Merlin and IASI-NG.
- To install French research infrastructures (SAFIRE airborne fleet, balloons) and instruments made and / or operated in the laboratories within various international initiatives: for example, the CoMet campaign organized by the DLR; the European project RINGO; the future validation campaign of Sentinel 5P from ESA, NASA OCO-3, etc.

The MAGIC campaigns rely on SAFIRE Falcon20 measurements of gas concentrations, temperature, humidity, wind, particles and greenhouse gases (CO_2 , CH_4 , N_2O) between 0–11 km altitude. The Falcon20 flies under the satellite track, and can make profiles between these altitudes and specific locations, such as ICOS/TCCON sites. They are complemented by balloon-borne instruments making 0–30 km profiles with AirCore atmospheric samplers, Amulse light laser-diode spectrometers, as well as measurements of total columns with portable Fourier transform spectrometers from the ground (EM27sun and CHRIS).

9.3.1.2 The Stratéole 2 campaign

Stratéole 2 is an international scientific project (France, USA) supported by CNES and NSF (with a contribution of ESA) and led by Laboratoire de Météorologie Dynamique (LMD, France). It is aimed at providing observations of the equatorial upper troposphere and lower stratosphere (UTLS), i.e. between 16 and 20 km of altitude, to better understand dynamical and transport processes in this region. The uniqueness of the project comes from the use of stratospheric balloons developed by CNES (called superpressure balloons), which are able to fly for several months at targeted altitudes. During the flight campaigns, each balloon will be carried by the winds and circumnavigate the Earth a few times. It is currently planned to perform two large campaigns with $\tilde{20}$ balloons each, respectively in late 2020 and late 2023. The two campaigns are meant to sample the opposite phases of an oscillation of the equatorial stratospheric winds, called the quasi-biennial oscillation, as its period is nearly 2 years.

Stratéole 2 inherits from the experience gained by CNES and scientific laboratories during previous long-duration balloon projects: Vorcore 2005 (Antarctica, 27 flights), AMMA 2006 (Tropical Africa and Atlantic, 7 flights), Pre-Concordiasi 2010 (equator, 3 flights) and Concordiasi 2010 (Antarctica, 19 flights). Balloons that will fly in the framework of Stratéole 2 will carry various combinations of instruments in order to address the project scientific objectives. These instruments are:

- flight-level meteorology: pressure (8 Pa accuracy), temperature (0.2 K accuracy), horizontal

- winds (0.1 m/s accuracy)
- fibre optic continuous temperature profiles from the balloon down to 2 km below the balloon (FLOATS instrument, nighttime accuracy: 0.2 K, vertical resolution: 1 m)
- upgoing radiative fluxes
- water vapour (5 % accuracy), and aerosols, both at the balloon flight level and through sounding down to 2 km below the balloon
- ozone
- carbon dioxide (5 % accuracy)
- cirrus clouds, with a balloon-borne lidar

Stratéole 2 flight-level measurements of temperature, water vapour and carbon dioxide observations may be used to contribute to the cal/val of IASI-NG. In addition, the current Stratéole 2 instrumentation includes continuous temperature profiles (day and night) down to 2 km below the gondola (FLOATS instrument), as well as nighttime profiles of temperature and water vapour down to 2 km below the gondola (RACHUTS instrument). There will be 3 flights of the FLOATS instruments and 3 other flights with the RACHUTS instruments during the 2023 campaign. Additional flights may be envisioned if e.g. EUMETSAT considers these measurements as a valuable asset to the IASI and IASI-NG cal/val and is ready to contribute to the additional cost. It may finally be noted that initial plans of Strateole 2 included 6 NCAR Driftsonde instruments in each of the 2020 and 2023 campaigns. Each of these instruments can release 50 dropsondes on demand during the long-duration balloon flights, yielding a total of 300 vertical profiles of pressure/temperature/winds from the balloon flight level down to the surface per campaign (as was done during the Concordiasi programme). This instrument is currently no longer part of Stratéole 2, since its scientific return/cost ratio has been assessed too risky by the American scientific community, who would have had to submit the associated funding proposals to NSF. However, there is still space for the Driftsonde instrument (especially during the 2023 campaign) if a significant funding contribution additional to that of NSF is found.

9.3.1.3 CNES annual balloon campaign

Every year, CNES balloon division organizes a campaign from a dedicated site. These campaigns combine Large Stratospheric Balloons (Ballons stratosphériques ouverts - BSO) as well as meteorological balloons (Ballons légers dilatables – BLD). BSOs can carry up to 1 t of payload, while BLD are typically limited to 3 kg. Currently, balloons can be launched from 3 stations: Timmins (Ontario, Canada), Kiruna (Sweden) and Alice Springs (Australia). By 2022, CNES will be able to offer flights in the equatorial region from northern Brazil (around 10° S). The provision for the entire range of balloons will allow the implementation of flights under BSO dedicated payloads or grouped on the same platform, or flights of nano-instruments (BLD), or BPS. In addition, the load carrying heavy instruments such as telescopes can be performed under large BSO and benefit from the latest developments in CNES fine pointing system

Intensive Cal/Val activities could thus be organized during given annual CNES campaigns in order to benefit from the scientific payloads as well as the human teams already deployed on the field. In addition, CNES plans to expand its balloon offer by proposing transatlantic flights between Kiruna (Sweden) and northern Canada in summer 2021, ie between 5 and 7 days of flight in the daytime between 35–40 km altitude. These long-duration flights will offer the possibility of atmospheric measurements over a range of 5000–6000 km. Instruments that could be flown during such flights include the lidar Be Cool (LATMOS), as well as in situ instruments such as picosDLA (GSMA-DT INSU), Amulse (GSMA) or SPECIES (LPC2E). Various types of radar such as cloud radars or for the study of ocean currents could be considered. These long-duration flights will also allow space mission demonstrators (IASI-NG with Hyperspectral Infrared Sounder, 3MI

with OSIRIS, etc.) to be flown in observational conditions close to measurements made from space. Thanks to their position at high latitudes, these flights will also improve co-location with measurements made from space and will therefore benefit Cal/Val activities.

As concerns temperature and humidity profiles, routine acquisition and dissemination of radio-sonde measurements are organised worldwide which shall be used for validation and routine monitoring. However this is mostly done at synoptic times (00, 06, 12 and 18) and the tendency in many operational launch sites has been to reduce the number of launches to a maximum of two per day. As a consequence, because of EPS and EPS-SG overpass times, the differences in time and space can add significant collocation uncertainties in the overall departures (IASI-NG L2 vs reference) budget. Applying tight match-up criteria has usually the effect of depleting the sample size significantly and of limiting collocations to a few places where regular sonde launches are incidentally favourably synchronised with Metop-SG overpasses. Reducing collocation uncertainties to allow a more direct assessment of the satellite products uncertainties can be obtained with dedicated campaigns. In that case, sondes are released from ground or dropped from aircrafts and balloon-platforms around satellite overpass times, as organised for Metop-A and Metop-B (e.g. Lindenberg/Sodankyla, Jaivex, Salstice, ConcordIasi) or with dedicated sonde launches at ARM sites and airborne campaigns in US for Suomi-NPP/CrIS. Because of the heavy logistics and costs associated, they are usually limited in terms of spatial and temporal coverage.

9.3.2 Validation using NWP model data

9.3.2.1 Level 1

NWP users are in a particularly good position to contribute to L1 Cal/Val activities. Each centre will always perform its own careful analysis of data quality before accepting new observations into the data assimilation system, and for centres with global NWP models, a full range of meteorological conditions can be captured within a few orbits. This is a particular advantage compared with cal/val against radiosondes or other field stations, where specific campaigns must be planned to coincide with satellite overpasses and only a small range of atmospheric conditions can be sampled. Furthermore, NWP analyses provide a framework for consistent assessment of observational datasets, because they ingest many sources of observational data and combine them into a single optimal estimate of the atmospheric state.

Intercomparison studies involving multiple NWP centres allow for an estimation of the degree of error inherent in any comparison of this kind; atmospheric models differ in their internal physical and dynamical equations, spatial resolution and initialisation with observations and as such have different levels of error and biases. Different RT models will also be employed in the forward calculation. However, for a state-of-the-art NWP model, errors in tropospheric temperature are typically of the order of 0.1K, so the models provide an excellent source of validation for the main CO₂ sounding band (and also for L2 temperature profiles). Such activities were carried out for IASI-A; one example intercomparison study was presented in Hilton et al. (2007). One notable example of the specific benefit of incorporating validation by NWP centres into Cal/Val plans is SSMI/S (the Special Sensor Microwave Imager/Sounder on recent DMSP satellites), for which NWP was a critical component in deciphering reflector emission among other issues (Bell et al., 2008; Kunkee et al., 2008). Providing dedicated users with early access to data (i.e. during the commissioning phase) will not only enable such activities to take place, but has the added benefit of allowing users to test their own assimilation software with real data and will thus ensure that the data can be used in operational applications as quickly as possible.

It should be noted that by the time of launch of the first EPS-SG satellite, it is not expected

that many operational NWP centres will incorporate variable trace gases into their NWP models and validation will thus be limited to portions of the spectrum that are not affected by such species. This is not expected to be an important issue for validation of an interferometric instrument.

Convective-scale NWP models should also be considered as a major source of information for validation of spectral information; although limited to small parts of the globe and thus not providing the full range of atmospheric conditions of a global model, the grid size is expected to be only a few hundred metres by the time of launch of EPS-SG. Thus, the variability of atmospheric conditions within the footprint of IASI-NG can be accounted for in validation studies. This is expected to be particularly useful for validation of the water vapour band (horizontal variability of water vapour fields is typically much greater than can be accounted for by global NWP models), and for inhomogeneous scenes.

9.3.3 Validation of Level 2 Products

As mentioned above in section 9.3.2.1, state-of-the-art global NWP models also offer an excellent validation source for L2 products, particularly temperature profiles. Humidity profiles are harder to verify with global NWP models because the horizontal scales of variability for humidity are much finer, and typically smaller than the model resolution. However, as for L1 validation, convective-scale NWP models should allow a better source of validation for L2 humidity profiles: with a grid size expected to be a few hundred metres by that time, variability within the field of view can be accounted for.

Global NWP allows verification across a wide range of atmospheric conditions in a very short space of time. The main limitations of global NWP models as a source of validation for L2 products are in the resolution of the models and in the lack of incorporation of chemical and air quality parameters. Although we might expect that by 2020 many such models will incorporate variable ozone, some aerosol parameters and perhaps CO₂, many chemical species will not be available. However, models such as the Copernicus Atmospheric Monitoring Service at ECMWF can provide an excellent source of global data for validation of many chemical species.

9.4 The challenge

There is a strong heritage from IASI and other IR sounders: several activities can be directly applied to IASI-NG:

- For Level 1: the expertise of monitoring and intercomparison activities performed at CNES/EUMETSAT and some labs, especially in the framework of GSICS, is directly relevant to IASI-NG.
- For Level 2: There are more than 25 atmospheric species retrieved or detected with IASI, in addition to thermodynamic variables, clouds, aerosols, surface characteristics.

However, important challenges remain.

- For well-known products, there is a need for automation of validation and monitoring tools against reference measurements.
- For some research products, there is still a need to define proper validation methods and data sets. The goal here is to be able to validate the full vertical extent of the products. Even for a column product, knowledge of the full profile is needed for validation. Some information may come from atmospheric models, but the description of the stratosphere remains a challenge for many species (e.g. CH₄).

- There are some new products required for IASI-NG that are without algorithm and validation heritage, at least from IASI
- Requirements for IASI-NG are tighter than for IASI and it is questionable whether existing methods and instrumentation are capable of validating the IASI-NG products to the required quality.

The EUMETSAT and CNES Cal/Val plans outline the user requirements for the resolution and accuracy of each individual product and the known sources of validation data.

The validation of the IASI-NG products specified in the EURD will involve as much as possible fiducial reference measurements (FRM). However, depending on the geophysical parameter, there may not exist reference data with sufficient temporal and spatial coverage to allow useful match-ups and statistically representative results.

As concerns temperature and humidity profiles, routine acquisition and dissemination of radio-sonde measurements are organised worldwide which shall be used for validation and routine monitoring. However this is mostly done at synoptic times (00, 06, 12 and 18) and the tendency in many operational launch sites has been to reduce the number of launches to a maximum of two per day. As a consequence, because of EPS and EPS-SG overpass times, the differences in time and space can add significant collocation uncertainties in the overall departures (IASI-NG L2 vs reference) budget. Applying tight match-up criteria has usually the effect of depleting the sample size significantly and of limiting collocations to a few places where regular sonde launches are incidentally favourably synchronised with Metop-SG overpasses. Reducing collocation uncertainties to allow a more direct assessment of the satellite products uncertainties can be obtained with dedicated campaigns. In that case, sondes are released from ground or dropped from aircrafts and balloon-platforms around satellite overpass times, as organised for Metop-A and Metop-B (e.g. Lindenberg/Sodankyla, Jaivex, Salstice, ConcordIasi) or with dedicated sonde launches at ARM sites and airborne campaigns in US for Suomi-NPP/CrIS. Because of the heavy logistics and costs associated, they are usually limited in terms of spatial and temporal coverage.

Along the same lines, FRM may be of limited representativeness, being for instance in situ or ground-based point measurements compared to the IASI-NG footprint size of 12 (Nadir) to 40 (swath edge) km. The evaluation of the collocation or representativeness errors and their contribution in the overall satellite - reference data difference budget is still subject to developments and could follow the Immler et al. (2010), which could be considered here too. The assessment of IASI-NG products uncertainties will therefore have to be completed by comparisons to other satellite products and to numerical models, taking into account the products properties and intrinsic uncertainties.

There are many gaps identified, for which a source of data or new method is required. These include:

- How can the accuracy of temperature retrievals to the requirement of 0.8 K in the lower to mid-troposphere be proved?
- Can the accuracy of specific humidity to the requirement of 5 % be demonstrated within a footprint of 12–40 km? What new instrumentation can be used to help characterise the heterogeneity of the field of view (network of laser heterodyne radiometers?, ...) ?
- What sources of data are available to validate the total column water vapour product?
- Validation methods and data (both direct and indirect) are required for land and ice surface emissivity.
- More data are required to validate cloud detection and fractional coverage. Cloud property validation is a particular problem and very few validations have been performed with IASI.

The challenge is that any validation of pixel products requires a very strict collocation due to the highly variable properties. Common plans for validation with the 3MI instrument would be an asset.

- The data and method to demonstrate cloud liquid water path retrievals to an accuracy of 5% are currently in doubt.
- Suitable flight campaigns and equipment to validate cloud top phase or cloud drop effective radius are rare.
- More work is required to validate dust mean altitude (lidars are the most likely source of validation data).
- More data are required for validation and continuous monitoring of CO profiles, SO₂ columns and nitric acid partial columns, as well as greenhouse gases (CO₂, CH₄, N₂O).

These areas should be prioritised when considering development of new instrumentation and when designing campaigns.

Chapter 10

Priorities for Research

10.1 Data processing

It is important for further research and development that the following information is made available to users by EUMETSAT and CNES:

- A plan for how data and algorithm updates for direct broadcast will be communicated and supplied to users.
- A proposal for updates to Principal Component bases will be communicated and supplied to users, including likely frequency of update.
- Information on algorithms intended to provide land/sea masks and cloud/aerosol detection algorithms.
- A proposed strategy and feasibility study for long-term archiving of key calibration datasets (for example, in view of climate reanalysis requirements).

10.2 Development of radiative transfer capabilities

10.2.1 Spectroscopic data

- A strong emphasis should be put on the continuous support of theoretical and laboratory spectroscopic studies. It is crucial that a compilation of basic line parameters is maintained, as this is fundamental to any use of IASI-NG data.
- An assessment should be made regarding requirements for the introduction of more molecular species, including isotopes, and their required accuracies.
- The IASI-NG community will require access to the latest available spectroscopy and line parameters, and therefore it should be ensured that an up-to-date spectral database is maintained, compatible with RT developments.
- Any requirements regarding the precision of the spectroscopic parameters need to be assessed. For example, in the retrieval of ozone profiles, some inconsistencies have been observed between the IR and the UV/Vis parts of the spectrum, which could be attributed to an inconsistency in the precision of the spectroscopic parameters between the two spectral ranges. Inconsistency problems have also been observed for SO₂.
- Line shapes of water vapour broadening for trace gases need improvement.
- Regarding the database of cross sections, in general, we have access to the absorption coefficients for a set of pressures and temperatures. The experience gained with IASI suggests that we should address the following points:
 - The number of temperature and pressure values available in databases may not be sufficient to ensure that the error made when interpolating to the actual temperature and pressure is smaller than the noise of the instrument.
 - Even where the spectral variation is low, cross section measurements have not been made using the highest spectral resolution (especially in the centre of the absorption band).

- Some measurements have been made with an instrumental noise which was too high, resulting in negative absorption coefficients.

10.2.2 Radiative Transfer Modelling

- Continuous support for line-by-line modelling should be guaranteed. The community would greatly benefit from the development of competing line-by-line codes. There are concerns that line-by-line models are not flexible enough to accommodate the use of line parameters from alternative databases. For instance, LBLRTM uses line mixing coefficients that are not compatible with the GEISA line parameters (only HITRAN line data are compatible).
- Although the semi-empirical MT_CKD model may be adequate for IASI-NG applications, there is still the need for a physically based representation of the water vapour continuum absorption, which should eventually be implemented in state-of-the-art LBL models.
- Further research is needed into the modelling of line mixing processes for CO₂, CH₄, N₂O and, to a lesser extent, water vapour. This is especially true for the 4 μm absorption band of CO₂.
- The increasing uses of IASI-NG for atmospheric chemistry require much work on the spectral parameters for gases which are weak absorbers.
- The effects of pressure and Doppler line broadening should be modelled using a better representation of the line shape than the Voigt profile. Proposed replacements to the Voigt profile will require different broadening coefficients for all the molecules and, consequently, significant updates to LBL models.
- The low noise of IASI-NG in the short wave should allow the exploitation of spectral regions affected by non-LTE effects. Because non-LTE effects can have a large impact on IASI-NG spectra, it is important that they are accurately represented in LBL codes. In parallel, efficient representations of non-LTE effects should continue to be developed for implementation in fast RT models.
- The simulation of radiances in the large number of IASI-NG channels will require fast RT models with enhanced computational efficiency. Likewise, the low noise of IASI-NG will require an even more accurate simulation of the radiances. Therefore, more research is needed into the improvement of existing techniques (e.g. PC based) or the development of novel techniques that would allow the fast and accurate simulation of IASI-NG radiances. It is also crucial that radiances and Jacobians calculated by fast RT models are thoroughly validated against LBL model equivalents.

10.2.3 Radiative transfer in scattering atmospheres

- To allow full synergy, there is a need for a consistent treatment of scattering across the spectrum (e.g. in the treatment of non-spherical ice habits). There is a need to continue the development of fast parameterisations of scattering for NWP and in general for any applications where a full scattering scheme would be too time consuming.
- For aerosol scattering computations more research is needed to characterize the regimes where fast approximate methods work better.
- The validation of the scattering approximations used in fast RTM models is an important step towards the operational use of fast RTM in scattering atmospheres. In that respect it is crucial that results from scattering approximations are compared to results obtained from full scattering schemes. Intercomparison/validation exercises should then be carried out similarly to what is done in clear atmospheres. Ideally, this should include both clouds and aerosols using a wide range of situations including multi-layered clouds, different cloud particles (i.e. water and/or ice) and different aerosol types using appropriate vertical

abundance profiles.

- The effects of three-dimensional cloud structures should also be studied. Effects should be smaller at smaller spatial resolutions but can still be significant. Simplified methods like the one used in RTTOV (Matricardi, 2005) have been developed to deal with inhomogeneous cloud fields. However, they can only provide a gross approximation of the inhomogeneity observed by a satellite borne instrument.
- Efforts on the calculation of optical properties should continue, focusing on an efficient and accurate solution of the problem for non-spherical particles.
- The accuracy of the spherical shape assumption for mineral aerosols needs to be quantified, and, if necessary, suitable alternative models will have to be developed.
- There is a need to understand the relation between optical depths in the visible and IR regions of the spectrum.
- The accuracy of scattering computations can be significantly affected by errors and uncertainties in the parameterisation of the optical properties of the scattering particles. Although several methods exist to compute the optical properties of spherical and non-spherical particles, the representation of the optical properties of an ensemble of scattering particles of different sizes and different habits is still an outstanding issue and more research is needed into the characterisation of the size distributions. This is especially true for ice particles for which a variety of different habits has been observed. In addition, the size distribution of small ice particles is still poorly known.
- There is an urgent need for larger public datasets of aerosol refractive indices and their variability. These datasets should also include information on measured size distributions and their natural variability. This is especially important for mineral aerosols but also for secondary aerosols (sulphuric acid, ammonium salts, boundary layer PM). IASI-NG could be exploited to retrieve refractive indices directly. These refractive indices could then be used to validate those measured in laboratories.

10.2.4 Surface modelling

- Further research should be carried out into the representation of the spectral properties of the surface and their use in databases. There is also a need to understand how complex mixtures of inhomogeneous surfaces is represented. The development and maintenance of global atlas products of emissivity should be encouraged. It is also important that atlases keep track with land use changes.
- Emissivity retrievals as IASI-NG level 2 products should be promoted, and users should be encouraged to evaluate the product for their needs, as specified in the ATBD and using IASI as a proxy.
- The effects of geophysical features such as leads, and chemistry (salinity etc.) on the emissivity properties of surfaces in polar regions should be researched.

10.2.5 Datasets for RT development and validation

- The production of profile datasets that include a wide range of gas species should be prioritised, to aid developments in RT capability.
- In addition, there is a requirement for datasets that include state vectors for clouds and aerosols.
- Profile datasets that avoid interpolation onto a coarse grid should be supported for training and validation of RT models.
- Profile datasets need to include estimates of representative climatological variability of the provided species/geophysical parameters.

- There is a continued requirement for validation campaigns to assess uncertainties in RT models.
- Greater understanding of the relative importance of the different sources of uncertainty in RT modelling is required; e.g. how large the uncertainties are in the spectroscopic data and how they impact the radiances.
- in situ measurements of land surface emissivity, including variation with viewing angle, are required to support model development.

10.3 Development of Retrieval Algorithms

- The algorithmic approach for retrieving geophysical parameters should be tailored to the requirements driven by each application, as the choice of method depends upon the circumstances of the retrieval, e.g. type of a priori data, RT modelling, timeliness requirements etc.
- Care should be taken to evaluate carefully the error properties of the retrieval, and to provide these as frequently as necessary (i.e. with each retrieved profile if required), along with other required components such as averaging kernels.
- When evaluating retrieval methods, the retrievals should, where possible, be evaluated against common datasets for a good intercomparison of error characteristics.
- When validating retrievals, there is usually little to no in situ data for the uppermost atmospheric levels. A range of options should be considered for the uppermost levels, because the choice may impact on the diagnosed properties of the retrieval (e.g. averaging kernel shape).
- The dependence of any Level 2 product on a priori and auxiliary information should be well-characterised and documented.
- The potential for aliasing between different signals should be quantified, especially where algorithms use regions of the spectrum where different species' absorption lines are overlapping in frequency.
- Priority should be given to evaluating the effect of undiagnosed clouds and undetected aerosol, and to finding ways of detecting contaminated observations. It was noted at the 2016 IASI conference, that there are very few people working on clouds in the IASI community.
- Approaches to developing an adaptive bias correction for use in retrievals should be developed. VarBC schemes are common in NWP, where many thousands of observations are used simultaneously with global coverage, so it is easier to estimate updated bias parameters than for a series of independent profile retrievals. Work in this area should be prioritised, because neglected biases will be passed through into retrieved products in a complex manner which will hinder their use in assimilation systems.
- More work should be done on the use of realistic observation error terms, including the treatment of errors that are correlated between channels. This should include estimation of radiative transfer errors. Auxiliary information on potential cloud contamination could be used to modify observation errors.
- For temperature and humidity in particular, users are used to having full profile retrievals provided on many pressure levels. In some cases, such products could be misleading if users are not fully advised of the properties of such retrievals (e.g. insensitivities of the observations or null space). Integrated quantity products should be investigated where these may be more appropriate, and users should be fully informed about the utility of any L2 product for their particular application.
- Different ways of assessing the skill of retrievals should be investigated; in particular enhancing assessments of retrieval schemes to use different measures from just the mean and

standard deviation of fit to in situ data should be prioritised.

10.4 Data assimilation and Numerical Weather Prediction

- Thinning algorithms should be improved based on observation properties and sub-pixel information where possible. Improved observation selection for ensemble assimilation systems should be considered.
- Development of forward and inverse operators for interpolation/aggregation (as opposed to RT models) for convective-scale models should be prioritised.
- Further research should be carried out into physically-based error covariance matrices to properly characterise observation errors.
- Characterisation of bias from radiative transfer and spectroscopy should be prioritised, to ascertain whether some channels of IASI-NG would be suitable as anchor channels in a VarBC scheme.
- The effectiveness of current bias correction techniques should be assessed for convective scale and small-domain regional models where data supply is sparse in time and few observations are available in any given cycle. New techniques should be investigated if required.
- More work needs to be done on the best way to include surface parameter information into the assimilation system, particularly where not available in the control vector.
- All-sky or cloudy assimilation schemes should be prioritised for research, especially for convective scale models, including analysis of cloud characteristics. The use of ensemble systems for characterising cloud properties and variability should be investigated.
- A cloud simulator model should be developed to allow investigation of the way in which clouds in a convective scale model affect radiances.

10.5 Climate Applications

- Work should begin as soon as possible to characterize the difference between IASI-NG instruments, and between IASI-NG and IASI and other current generation hyperspectral sounders.
- Provision of information regarding the absolute calibration of the instrument should be planned from the outset.
- Preparatory work before launch should be carried out to ensure that observation monitoring vs other instruments, and against forward-modelled data using a frozen RT model can commence immediately.
- Preparatory work to ensure the provision and archiving of all documentation on data processing, monitoring algorithms and product derivation is available from launch and in perpetuity.
- Support for the provision of well-characterised high-resolution in situ measurements, such as those provided by the GRUAN network, should be maintained.

10.6 Calibration and Validation

- In view of the tighter requirements on Temperature and humidity retrievals relative to IASI (e.g. 5% for humidity), develop systems and methodologies which allow validation of the products at the required level. This includes being able to characterise the representativeness of the reference measurements with respect to, for example, temporal/spatial

- differences and the intra-pixel variability in 12-40km footprints.
- Explore and support new in situ/ground-based reference sources to address the more demanding requirements. For instance:
 - Methane (12 % in the lower troposphere, 30 % in the stratosphere) and CO₂, with new validation techniques like the AirCore atmospheric sampler or the Amulse laser-diode spectrometer flying under meteorological balloons.
 - Land and ice surface emissivity at 1 % requires totally new reference datasets: in situ measurements such as those done for LST, or running dedicated airborne campaigns or through indirect methodologies.
 - Lidar observations for water-vapour and atmospheric constituents are developing and of big potential for satellite products validation.
 - The potential for using small, cheap instruments in a dense ground-based network should be explored as a means to gathering information about scene heterogeneity (one example could be laser heterodyne radiometers or upward-looking lidars).
 - Cloud products are challenging to validate due to high spatial/temporal variability, which makes it difficult to find suitable correlative reference observations. Statistical comparison with cloud climatologies (e.g GEWEX cloud assessment, ESA-CCI datasets for clouds and aerosols) might provide a way of validating some cloud properties to a given extent.
 - Cloud properties are new products required from IASI-NG/MWS. Their validation can be prepared by liaising with the cloud community and fostering development and exploitation of validation techniques.
 - Foster use of measurements with traceable uncertainties from coordinated networks to achieve routine monitoring of the required geophysical parameters.

Appendix A

IASI-NG specification from the EPS-SG end-user requirements document

A.1 Data Acquisition Requirements

IAS-01010

The IAS shall generate simultaneously radiance spectra for the bands given in table A.1

A.2 Quality Criteria

The IAS measurements will be considered of good quality if data acquisition, timeliness, and accuracy requirements are met.

IAS-01020

The IAS products shall be flagged by the EPS-SG ground segment as being of good quality if

- a IAS acquisition requirements are met
- b IAS timeliness requirements are met
- c IAS spectrum level 1 spectral requirements are met
- d IAS spectrum level 1 radiometric requirements are met
- e IAS spectrum level 1 geometric requirements are met

A.3 Spectral Requirements

Unless otherwise stated the requirements in this section apply:

- To all spectral samples
- To all spatial samples in a scan line
- To all scan lines over each EPS-SG satellite specified lifetime.

IAS-01040

The IAS spectral response function difference between any two spatial samples of the same orbit shall be such that

- a The maximum relative shift of the ISRF centroid is less than 10^{-6} within any single orbit.
- b The maximum relative shift of the ISRF centroid, with respect to the nominal position of the centroid, is less than 2×10^{-4} over the lifetime of the mission.

IAS-01050

- a The IAS spectra at level 1C shall have a spectral resolution of 0.25 cm^{-1}

| Spectral Band | Wavenumber Range (cm ⁻¹) | Purpose | Radiometric Resolution NEΔT@280 K | |
|---------------|--------------------------------------|--|-----------------------------------|-------------------------|
| | | | L1c apodised (K) T/O | L1c de-apodised (K) T/O |
| IAS-1 | 645–690 | Temperature profile, C ₂ H ₂ , HCN | 0.225/0.052 | 0.390/0.090 |
| IAS-2 | 690–770 | Temperature profile, C ₂ H ₂ , HCN | 0.130/0.052 | 0.226/0.090 |
| IAS-3 | 770–1000 | Temperature and water-vapour profiles, SST, surfaces and cloud properties PAN, HNO ₃ , NH ₃ C ₂ H ₄ | 0.130/0.037 | 0.226/0.064 |
| IAS-4 | 1000–1070 | O ₃ column, O ₃ profile, CH ₃ OH | 0.195/0.052 | 0.338/0.090 |
| IAS-5 | 1070–1150 | Surface and cloud properties, HCOOH, volcanic SO ₂ | 0.195/0.037 | 0.338/0.064 |
| IAS-6 | 1150–1650 | Water vapour profile, PAN, NH ₃ , ceN ₂ O, CH ₄ , volcanic SO ₂ | 0.130/0.037 | 0.226/0.064 |
| IAS-7 | 1650–2100 | Water-vapour profile | 0.449/0.075 | 0.778/0.130 |
| IAS-8 | 2100–2180 | Temperature profile, CO profile | 0.156/0.052 | 0.271/0.090 |
| IAS-9 | 2180–2250 | Temperature profile | 0.225/0.075 | 0.390/0.130 |
| IAS-10 | 2250–2420 | Temperature profile | 0.225/0.075 | 0.390/0.130 |
| IAS-11 | 2420–2700 | SST, surface and cloud properties | 0.225/0.075 | 0.390/0.130 |
| IAS-12 | 2700–2760 | CH ₄ | 0.225/0.075 | 0.390/0.130 |

Table A.1: Radiometric resolution for each spectral band of the IAS. T: Threshold O: Objective. The ratio between de-apodised L1c noise and apodised L1c noise is 1.7352.

b The IAS spectra at level 1C shall be regularly sampled at 0.125 cm⁻¹

IAS-01080

The knowledge of the spectral response function shall be such that for any spectral sample the associated radiometric accuracy shall not be increased by more than 0.05(Objective), 0.1(Threshold) K at 280 K.

A.4 IAS Level 1 Radiometric Requirements

Unless otherwise stated the requirements in this section apply:

- To all spectral channels
- To all radiance levels between the minimum and maximum radiance
- To all scan lines over each EPS-SG satellite specified lifetime.

IAS-01090

The IAS radiometric sensitivity (1σ) shall be as given in table A.1 with the NEΔT requirement at 280 K between the minimum and maximum signal. At brightness temperatures different from 280 K the radiometric sensitivity shall be multiplied with the radiometric scaling function.

IAS-01100

The dynamic range of the IAS shall cover the top of atmosphere spectral radiances from 180 to 335 K in terms of brightness temperatures.

IAS-01110

For IAS measurements of a spatially uniform scene at 280 K, the bias error shall be <0.5 K for all channels. At brightness temperatures different from 280 K the requirement shall be multiplied by the radiometric scaling function.

IAS-01120

The orbit stability shall be such that variations of radiometric biases in the measured IAS brightness temperature during any single orbit are <0.10 K (Threshold), <0.05 K (Breakthrough) at 280 K. At brightness temperatures different from 280 K the requirement shall be multiplied by the radiometric scaling function.

IAS-01130

The lifetime stability shall be such that variations of the running average over one orbit of radiometric biases in the measured IAS brightness temperature are <0.10 K (Threshold), <0.05 K (Breakthrough) at a brightness temperature of 280 K. At brightness temperatures different from 280 K the requirement shall be multiplied by the radiometric scaling function. For brightness temperatures >300 K at wavenumbers >2300 cm^{-1} , the Threshold value shall be <0.15 K.

IAS-01140

Calibration differences (biases) between IAS brightness temperatures of different spectral samples/channels of the same spatial sample shall be <0.1 K for a scene temperature of 280 K. At brightness temperatures different from 280 K the requirement shall be multiplied by the radiometric scaling function.

IAS-01150

Calibration differences (biases) between IAS brightness temperatures of different spatial samples of the same spectral sample shall be <0.1 K for a 280 K brightness temperature. At brightness temperatures different from 280 K the requirement shall be multiplied by the radiometric scaling function.

A.5 IAS Level 1 Geometric Requirements

Unless otherwise stated the requirements in this section apply:

- To all spectral samples
- To all spatial samples in any scan line
- To all scan lines over each EPS-SG satellite specified lifetime.

IAS-01160

The IAS shall scan perpendicular to the satellite velocity and cover a field of view of 98° symmetrical within $\pm 4^\circ$ about the geodetic nadir direction.

IAS-01170

The IAS shall not expose spatial gaps due to calibration of the instrument.

IAS-01180

An amount of >95 % of the integrated energy of the respective IAS point spread function shall be contained within an on-ground spatial sample with an area described by an effective diameter $D < 5$ km (Objective), < 8 km (Breakthrough), < 12 km (Threshold), where D describes an area (circular or non-circular) of size $\pi D^2/4$ at nadir. For off-nadir samples the requirement shall be extrapolated with distance scaled after projection on the earth and assuming constant angular sampling.

IAS-01190

During the observation dwell time, the IAS line of sight stability shall be better than ± 0.15 mrad (1 standard deviation).

IAS-01200

The IAS geolocation shall be known to better than 5 km (Threshold), 1 km (Breakthrough), 500 m (Objective).

IAS-01210

The IAS pointing knowledge shall be better than 4.363 mrad (Threshold), 1.745 mrad (Breakthrough).

IAS-01220

- a Within a scan all the IAS spatial samples shall be known with an accuracy better than 0.1 mrad (Objective) / 0.3 mrad (Threshold), and their positions relative to a regular grid shall be within 1 mrad (Objective) / 3 mrad (Threshold). The on-ground spatial sampling distance at geodetic nadir shall be < 10 km (Objective), < 15 km (Breakthrough), and < 50 km (Threshold). For off-nadir spatial samples the requirement shall be extrapolated with distance scaled after projection on the earth and assuming constant angular sampling.
- b The absolute pointing accuracy of the IAS shall be better than 6 mrad.

IAS-01230

- a The IAS shall be synchronised with the VII optical imager for cloud detection within the IAS PSFs. As a minimum requirement the imager shall have spectral channels at 0.670 μm , 0.865 μm , 1.64 μm , 3.75 μm , 10.8 μm and 12.02 μm . The band characteristics for these channels shall be those defined for the corresponding VII channels 12, 17, 24, 26, 37 and 39.
- b The temporal synchronisation of IAS and VII shall be performed within < 16 s
- c The spatial co-registration of IAS and VII shall allow for an assignment of VII spatial sample centres to any IAS PSF coordinates with accuracy < 500 m (Breakthrough), < 1 km (Threshold) at nadir. For off-nadir spatial samples the requirement shall be extrapolated with distance scaled after projection on the earth and assuming constant SSA.

IAS-01240

Within $0.8D$, the IAS point spread function non-uniformity (peak-to-peak ripples) shall be less than $\pm 10\%$.

IAS-01250

The IAS point spread function of each spatial sample shall be characterised out to a distance $2D$ from the barycentre of the IAS PSF.

Appendix B

Current Members of the ISSWG

As at January 2019

Co-chairs

Cyril Crevoisier (LMD)
Fiona Smith (Met Office)

Secretaries

Thomas August (EUMETSAT)
Adrien Deschamps (CNES)

Members

Raymond Armante (LMD)
Claude Camy-Peyret (IPSL)
Cathy Clerbaux (LATMOS/CNRS and ULB)
Pierre-François Coheur (ULB)
Andrew Collard (NESDIS)
Antonia Gambacorta (NOAA)
Reime Eresmaa (ECMWF)
Vincent Guidard (Météo-France)
Robert Knuteson (University of Wisconsin, Madison)
Zsofia Kocsis (OMSZ; Hungarian Meteorological Service)
Marco Matricardi (ECMWF)
Carmine Serio (University of Basilicata)
Jerôme Vidot (Météo-France)

Additional contributions from:

Dave Tobin (University of Wisconsin, Madison)
Hank Revercomb (University of Wisconsin, Madison)

Appendix C

Other contributing authors

Past members of ISSWG

David Edwards (UCAR)
Nicole Jacquinet-Husson (LMD)
Tony McNally (ECMWF)
Larrabee Strow (University of Maryland, Baltimore)
Jonathan Taylor (Met Office)

Further contributors

Nigel Atkinson (Met Office)
Lieven Clarisse (ULB)
Richard Engelen (ECMWF)
Chris Merchant (University of Reading)
John Remedios (University of Leicester)

References

- Agam, N. and P. R. Berliner (2004). ‘Diurnal water content changes in the bare soil of a coastal desert’. In: *J. Hydrometeorol.* Vol. 5, pp. 922–933. DOI: 10.1175/1525-7541(2004)005<0922:DWCCIT>2.0.CO;2.
- Agam, N. and P. R. Berliner (2006). ‘Dew formation and water vapor adsorption in semi-arid environments: A review’. In: *J. Arid Environ.* Vol. 65, pp. 572–590. DOI: 10.1016/j.jaridenv.2005.09.004.
- Amato, U., D. D. Canditiis and C. Serio (1998). ‘Effect of apodization on the retrieval of geophysical parameters from Fourier-Transform Spectrometers’. In: *Appl. Opt.* Vol. 37, pp. 6537–6543.
- Amato, U., G. Masiello, C. Serio and M. Viggiano (2002). ‘The σ -IASI code for the calculation of infrared atmospheric radiance and its derivatives’. In: *Environmental Modelling and Software* vol. 17, pp. 652–667.
- Andersson, E., M. Fisher, R. Munro and A. McNally (2000). ‘Diagnosis of background errors for radiances and other observable quantities in a variational data assimilation scheme, and the explanation of a case of poor convergence’. In: *Q. J. R. Meteorol. Soc.* Vol. 126, pp. 1455–1472.
- Antonelli, P., H. Revercomb, S. L.A., W. Smith, R. Knuteson, D. Tobin, R. Garcia, H. Howell, H.-L. Huang and F. Best (2004). ‘A principal component noise filter for high spectral resolution infrared measurements’. In: *J. Geophys. Res.* Vol. 109. DOI: 1029/2003JD004862.
- Atkinson, N. (2013a). ‘Technical lossless / near lossless data compression’. In: *ECMWF/EUMETSAT NWP-SAF Workshop on efficient representation of hyperspectral infrared satellite observations, 5-7 Nov 2013*. <http://www.eumetsat.int>.
- Atkinson, N. (2013b). *Data compression for MTG-IRS*. Tech. rep. 13. Met Office, Exeter.
- Atkinson, N., F. Hilton, S. Illingworth, J. Eyre and T. Hultberg (2010). ‘Potential for the use of reconstructed IASI radiances in the detection of atmospheric trace gases’. In: *Atmos. Meas. Tech.* Vol. 3, pp. 991–1003. DOI: 10.5194/amt-3-991-2010.
- B. and others Wielicki (2013). ‘Achieving climate change accuracy in orbit’. In: *Bull. Amer. Meteor. Soc.* Vol. 94, pp. 1519–1539. DOI: 10.1175/BAMS-D-12-00149.1.
- Baker, I., M. Hastings, L. Hipwood, C. Jones and P. Knowles (1996). ‘Infrared detectors for the year 2000’. In: *III-Vs Review* vol. 9 (2), pp. 50–58. ISSN: 0961-1290.
- Baldrige, A. M., S. J. Hook, C. I. Grove and G. Rivera (2009). ‘The ASTER spectral library version 2.0’. In: *Remote Sensing of Environment* vol. 113.no. 4, pp. 711–715.
- Baran, A. J. (2012). ‘From the single-scattering properties of ice crystals to climate prediction: A way forward’. In: *Atmos. Res.* Vol. 112, pp. 45–69.
- Baran, A. J., R. Cotton, K. Furtado, S. Havemann, L.-C. Labonnote, F. Marengo, A. Smith and J.-C. Thelen (2014). ‘A self-consistent scattering model for cirrus. II: The high and low frequencies’. In: *Q.J.R. Meteorol. Soc.* Vol. 680, pp. 1039–1057. DOI: 10.1002/qj.2193.
- Baran, A. J., P. Yang and S. Havemann (2001). ‘Calculation of the single-scattering properties of randomly oriented hexagonal ice columns: a comparison of the T-matrix and the finite-difference time-domain methods’. In: *Appl. Opt.* Vol. 40, pp. 4376–4386.
- Baranov, Y. I., W. J. Lafferty, Q. Ma and R. H. Tipping (2008). ‘Water-vapor continuum absorption in the 800–1250 spectral region at temperatures from 311 to 363 K’. In: *J. Quant. Spectros. Radiat. Transf.* Vol. 109, pp. 2291–2302. DOI: 10.1016/j.jqsrt.2008.03.004.
- Barré, J., V.-H. Peuch, Attié, E. A. L. J.-L., L. W. A., B. Josse, M. Claeysman and P. Nédélec (2012). ‘Stratosphere-troposphere ozone exchange from high resolution MLS ozone analyses’. In: *Atmos. Chem. Phys.* Vol. 12, pp. 6129–6144. DOI: 10.5194/acp-12-6129-2012.

- Barret, B., L. Flochmoen, S. E., P. B., M. M. E. and J. Cammas (2011). ‘The detection of post-monsoon tropospheric ozone variability over south Asia using IASI data’. In: *Atmos. Chem. Phys.* Vol. 11, pp. 9533–9548. DOI: 10.5194/acp-11-9533-2011.
- Baum, B. A., P. Yang, A. J. Heymsfield, A. Bansemer, A. Merrelli, C. Schmitt and C. Wang (2014). ‘Ice cloud bulk single-scattering property models with the full phase matrix at wavelengths from 0.2 to 100 μm ’. In: *J. Quant. Spectrosc. Radiat. Transfer*. Special Issue ELS-XIV. DOI: 10.1016/j.jqsrt.2014.02.029.
- Bell, R. (1972). *Introductory Fourier Transform Spectroscopy*. Acad. Press.
- Bell, W., B. Candy, N. Atkinson, F. Hilton, N. Baker, N. Bormann, G. Kelly, M. Kazumori, W. Campbell and S. Swadley (2008). ‘The Assimilation of SSMIS Radiances in Numerical Weather Prediction Models’. In: *Geoscience and Remote Sensing, IEEE Transactions on* vol. 46.no. 4, pp. 884–900. ISSN: 0196-2892. DOI: 10.1109/TGRS.2008.917335.
- Bi, L. and P. Yang (2013). ‘Physical-geometric optics hybrid methods for computing the scattering and absorption properties of ice crystals and dust aerosols’. In: *Light Scattering Reviews* vol. 8, pp. 69–114.
- Bi, L., P. Yang, G. W. Kattawar and R. Kahn (2009). ‘Single-scattering properties of triaxial ellipsoidal particles for a size parameter range from the Rayleigh to geometric-optics regimes’. In: *Applied optics* vol. 48, pp. 114–126.
- Bi, L., P. Yang, G. W. Kattawar and M. I. Mischenko (2013). ‘Efficient implementation of the invariant imbedding T-matrix method and the separation of variables method applied to large nonspherical inhomogeneous particles’. In: *J. Quant. Spectrosc. Ra. Trans.* Vol. 116, pp. 169–183.
- Borbas, E. E., R. O. Knuteson, S. W. Seemann, E. Weisz, L. Moy and H. Huang (2007). ‘A high spectral resolution global land surface infrared emissivity database’. In: *Joint 2007 EU-METSAT Meteorological Satellite Conference and the 15th Satellite Meteorology and Oceanography Conference of the American Meteorological Society*. 24th September 2007. URL: http://www.ssec.wisc.edu/meetings/jointsatmet2007/pdf/borbas_emissivity_data.
- Bormann, N., A. Collard and P. Bauer (2010). ‘Estimates of spatial and interchannel observation-error characteristics for current sounder radiances for numerical weather prediction. II: Methods and application to AIRS and IASI data’. In: *Q. J. R. Meteorol. Soc.* Vol. 136 (649), pp. 1051–1063. DOI: 10.1002/qj.615.
- Boynard, A., C. Clerbaux, P.-F. Coheur, D. Hurtmans, S. Turquety, M. George, J. Hadji-Lazaro, C. Keim and J. Meyer-Arnek (2009). ‘Measurements of total and tropospheric ozone from IASI: comparison with correlative satellite, ground-based and ozonesonde observations’. In: *Atmospheric Chemistry and Physics* vol. 9.no. 16, pp. 6255–6271. DOI: 10.5194/acp-9-6255-2009. URL: <http://www.atmos-chem-phys.net/9/6255/2009/>.
- Boynard, A., C. Clerbaux, L. Clarisse, S. Safieddine, M. Pommier, M. Van Damme, S. Bauduin, C. Oudot, J. Hadji-Lazaro, D. Hurtmans and P.-F. Coheur (2014). ‘First simultaneous space measurements of atmospheric pollutants in the boundary layer from IASI: A case study in the North China Plain’. In: *Geophysical Research Letters* vol. 41.no. 2, pp. 645–651. DOI: 10.1002/2013GL058333.
- Brown, L., D. Chris Benner, V. Malathy Devi, M. Smith and R. Toth (2004). ‘Line mixing in self- and foreign-broadened water vapor at 6 μm ,’ in: *Journal of Molecular Structure* vol. 742, pp. 111–122.
- Capelle, V., A. Chédin, P. E., P. Schluessel, S. Newman and N. Scott (2012). ‘Infrared Continental Surface Emissivity Spectra and Skin Temperature Retrieved from IASI Observations over the Tropics’. In: *J. Appl. Meteor. Climatol.* Vol. 51, pp. 1164–1179. DOI: 10.1175/JAMC-D-11-0145.1.
- Carboni, E., R. Grainger, J. Walker, A. Dudhia and R. Siddans (2012). ‘A new scheme for sulphur dioxide retrieval from IASI measurements: application to the Eyjafjallajökull eruption of April

- and May 2010'. In: *Atmos. Chem. Phys.* Vol. 12.no. 23, pp. 11417–11434. DOI: 10.5194/acp-12-11417-2012.
- Carissimo, A., I. De Feis and C. Serio (2005). 'The physical retrieval methodology for IASI: the σ -IASI code.' In: *Environ. Modelling and Software* vol. 20, pp. 1111–1126. DOI: 10.1016/j.envsoft.2004.07.003.
- Chedin, A., N. Scott, C. Wahiche and P. Moulinier (1985). 'The Improved Initialization Inversion Method - A High-Resolution Physical Method For Temperature Retrievals From Satellites Of The TIROS-N Series'. In: *J. Clim. Appl. Meteorol.* Vol. 24, pp. 128–143. DOI: 10.1175/1520-0450(1985)024<0128:TIIIMA>2.0.CO;2.
- Chédin, A., S. Serrar, N. A. Scott, C. Pierangelo and P. Ciais (2005). 'Impact of tropical biomass burning emissions on the diurnal cycle of upper tropospheric CO₂ retrieved from NOAA 10 satellite observations'. In: *Journal of Geophysical Research: Atmospheres* vol. 110.no. D11. D11309. DOI: 10.1029/2004JD005540.
- Chen, Y., Y. Han, P. van Delst and F. Weng (2013). 'Assessment of Shortwave Infrared Sea Surface Reflection and Nonlocal Thermodynamic Equilibrium Effects in Community Radiative Transfer Model Using IASI Data.' In: *J. Atmos. Oceanic Technol.* In press. DOI: doi:10.1175/JTECH-D-12-00267.1.
- Chevallier, F., J.-J. Morcrette, F. Chéruy and N. A. Scott (2000). 'Use of a neural-network-based long-wave radiative-transfer scheme in the ECMWF atmospheric model'. In: *Q.J.R. Meteorol. Soc.* Vol. 126, pp. 761–776.
- Chou, M., K. Lee, S. Tsay and Q. Fu (1999). 'Parameterization for cloud longwave scattering for use in atmospheric models'. In: *J. Climate* vol. 12.no. 1, pp. 159–169. DOI: 10.1175/1520-0442-12.1.159.
- Clarisse, L., P.-F. Coheur, F. Prata, J. Hadji-Lazaro, D. Hurtmans and C. Clerbaux (2013). 'A unified approach to infrared aerosol remote sensing and type specification'. In: *Atmos. Chem. Phys.* Vol. 13.no. 4, pp. 2195–2221. DOI: 10.5194/acp-13-2195-2013.
- Clarisse, L., D. Hurtmans, A. J. Prata, F. Karagulian, C. Clerbaux, M. D. Mazière and P.-F. Coheur (2010). 'Retrieving radius, concentration, optical depth, and mass of different types of aerosols from high-resolution infrared nadir spectra'. In: *Appl. Opt.* Vol. 49.no. 19, pp. 3713–3722. DOI: 10.1364/AO.49.003713.
- Clarmann, T. von, U. Grabowski and M. Kiefer (2001). 'On the role of non-random errors in inverse problems in radiative transfer and other applications'. In: *J. Quant. Spectrosc. Radiat. Transfer* vol. 71.no. 1, pp. 39–46. ISSN: 0022-4073. DOI: 10.1016/S0022-4073(01)00010-3.
- Clerbaux, C., A. Boynard, L. Clarisse, M. George, J. Hadji-Lazaro, H. Herbin, D. Hurtmans, M. Pommier, A. Razavi, S. Turquety, C. Wespes and P.-F. Coheur (2009). 'Monitoring of atmospheric composition using the thermal infrared IASI/MetOp sounder'. In: *Atmos. Chem. Phys.* Vol. 9, pp. 6041–6054. DOI: 10.5194/acp-9-6041-2009.
- Clerbaux, C., J. Hadji-Lazaro, S. Payan, C. Camy-Peyret and G. Megie (1999). 'Retrieval of CO columns from IMG/ADEOS spectra'. In: *IEEE Trans. Geoscience and Remote Sensing* vol. 37 (3), pp. 1657–1661. DOI: 10.1109/36.763283.
- Clough, S. A., M. J. Iacono and J.-l. Moncet (1992). 'Line-by-line calculation of atmospheric fluxes and cooling rates: Application to water vapor'. In: *J. Geophys. Res.* Vol. 97.no. 15, pp. 761–785.
- Clough, S. A., F. X. Kneizys and R. W. Davies (1989). 'Line shape and the water vapor continuum.' In: *Atmos. Res.* Vol. 23, pp. 229–241. DOI: 10.1016/0169-8095(89)90020-3.
- Clough, S. A., M. W. Shephard, E. Mlawer, J. S. Delamere, M. Iacono, K. Cady-Pereira, S. Boukabara and P. D. Brown (2005). 'Atmospheric radiative transfer modeling: a summary of the AER codes'. In: *J. Quant. Spectrosc. Radiat. Transf.* Vol. 91, pp. 233–244. DOI: 10.1016/j.jqsrt.2004.05.058.

- Collard, A. (2007). ‘Selection of IASI channels for use in numerical weather prediction’. In: *Q. J. R. Meteorol. Soc.* Vol. 133, pp. 1977–1991.
- Collard, A. and A. McNally (2009). ‘The assimilation of Infrared Atmospheric Sounding Interferometer radiances at ECMWF’. In: *Q. J. R. Meteorol. Soc.* Vol. 135, pp. 1044–1058.
- Collard, A., A. McNally, F. Hilton, S. Healy and N. Atkinson (2010). ‘The use of principal component analysis for the assimilation of high-resolution infrared sounder observations for numerical weather prediction’. In: *Q. J. R. Meteorol. Soc.* Vol. 136, pp. 2038–2050. DOI: 10.1002/qj.701.
- Colton, D. and R. Kress (1991). *Inverse Acoustic and Electromagnetic Scattering Theory*. Applied Mathematical Sciences 93. Springer Verlag, Berlin.
- Coudert, L. H., G. Wagner, M. Birk, Y. I. Baranov, W. J. Lafferty and J.-M. Flaud (2008). ‘The H₂¹⁶O molecule: Line position and line intensity analyses up to the second triad’. In: *J. Mol. Spectrosc.* Vol. 251, pp. 339–357. DOI: 10.1016/j.jms.2008.03.021.
- Courtier, P. (1997). ‘Variational methods’. In: *J. Meteorol. Soc. Jpn* vol. 75.no. 211218.
- Cressot, C., F. Chevallier, P. Bousquet, C. Crevoisier, E. J. Dlugokencky, A. Fortems-Cheiney, C. Frankenberg, R. Parker, I. Pison, R. A. Scheepmaker, S. A. Montzka, P. B. Krummel, L. P. Steele and R. L. Langenfelds (2014). ‘On the consistency between global and regional methane emissions inferred from SCIAMACHY, TANSO-FTS, IASI and surface measurements,’ in: *Atmos. Chem. Phys.* Vol. 14, pp. 577–592. DOI: 10.5194/acp-14-577-2014.
- Crevoisier, C., C. Clerbaux, V. Guidard, T. Phulpin, R. Armante, B. Barret, C. Camy-Peyret, J.-P. Chaboureaud, P.-F. Coheur, L. Crépeau, G. Dufour, L. Labonnote, L. Lavanant, J. Hadji-Lazaro, H. Herbin, N. Jacquinet-Husson, S. Payan, E. Péquignot, C. Pierangelo, P. Sellitto and C. Stubenrauch (2014). ‘Towards IASI-New Generation (IASI-NG): impact of improved spectral resolution and radiometric noise on the retrieval of thermodynamic, chemistry and climate variables’. In: *Atmos. Meas. Tech.* Vol. 7, pp. 4367–4385. DOI: 10.5194/amt-7-4367-2014.
- Crevoisier, C., D. Nobileau, R. Armante, L. Crepeau, T. Machida, Y. Sawa, H. Matsueda, T. Schuck, T. Thonat, J. Pernin, N. A. Scott and A. Chedin (2013). ‘The 2007–2011 evolution of tropical methane in the mid-troposphere as seen from space by MetOp-A/IASI’. In: *Atmospheric Chemistry And Physics* vol. 13.no. 8, pp. 4279–4289. DOI: 10.5194/acp-13-4279-2013.
- Daley, R. (1991). *Atmospheric Data Analysis*. Cambridge University Press, Cambridge, UK.
- Dee, D. P., S. M. Uppala, A. J. Simmons, P. Berrisford, P. Poli, S. Kobayashi, U. Andrae, M. A. Balmaseda, G. Balsamo, P. Bauer, P. Bechtold, A. C. M. Beljaars, L. van de Berg, J. Bidlot, N. Bormann, C. Delsol, R. Dragani, M. Fuentes, A. J. Geer, L. Haimberger, S. B. Healy, H. Hersbach, E. V. Hólm, L. Isaksen, P. Kollberg, M. Köhler, M. Matricardi, A. P. McNally, B. M. Monge-Sanz, J.-J. Morcrette, B.-K. Park, C. Peubey, P. de Rosnay, C. Tavolato, J.-N. Thépaut and F. Vitart (2011). ‘The ERA-Interim reanalysis: configuration and performance of the data assimilation system’. In: *Q.J.R. Meteorol. Soc.* Vol. 137, pp. 553–597. DOI: 10.1002/qj.828.
- Dee, D. (2005). ‘Bias and data assimilation’. In: *Q. J. R. Meteorol. Soc.* Vol. 131, pp. 3323–3342. DOI: 10.1256/qj.05.137.
- Deeter, M. N. and K. F. Evans (1998). ‘A hybrid eddington-single scattering radiative transfer model for computing radiances from thermally emitting atmospheres’. In: *Journal of Quantitative Spectroscopy and Radiative Transfer* vol. 60.no. 4, pp. 635–648. ISSN: 0022-4073. DOI: 10.1016/S0022-4073(97)00245-8.
- Delamere, J. S., S. A. Clough, V. H. Payne, E. J. Mlawer, D. D. Turner and R. R. Gamache (2010). ‘A far-infrared radiative closure study in the Arctic: application to water vapor’. In: *J. Geophys. Res. Atmos.* Vol. 115.no. D17106. DOI: 10.1029/2009JD012968.

- DeSouza-Machado, S. G., L. L. Strow, B. Imbiriba, K. K. McCann, R. M. Hoff, S. E. Hannon, J. V. Martins, D. Tanré, J. L. Deuzé, F. Ducos and O. Torres (2010). ‘Infrared retrievals of dust using AIRS: Comparisons of optical depths and heights derived for a North African dust storm to other collocated EOS A-Train and surface observations’. In: *J. Geophys. Res.* Vol. 115, p. D15201. DOI: 10.1029/2009JD012842.
- DeSouza-Machado, S., L. Strow and S. Hannon (1998). ‘kcompressed atmospheric radiative transfer algorithm (kCARTA)’. In: *Satellite Remote Sensing Of Clouds And The Atmosphere II*. Ed. by J. Haigh. Vol. 3220. Proceedings Of The Society Of Photo-Optical Instrumentation Engineers (SPIE). Conference on Satellite Remote Sensing of Clouds and the Atmosphere II, London, England, Sep 23-25, 1997, pp. 156–162. ISBN: 0-8194-2652-0.
- DeSouza-Machado, S., L. Strow, S. Hannon and H. Motteler (2006). ‘Infrared dust spectral signatures from AIRS’. In: *Geophys. Res. Lett.* Vol. 33.no. 3, p. L03801. DOI: 10.1029/2005GL024364.
- Desroziers, G., L. Berre, B. Chapnik and P. Poli (2005). ‘Diagnosis of observation, background and analysis error statistics in observation space’. In: *Q. J. R. Meteorol. Soc.* Vol. 131, pp. 3385–3396.
- Doppler, L., C. Carbajal-Henken, J. Pelon, F. Ravetta and J. Fischer (2014). ‘Extension of radiative transfer code MOMO, matrix-operator model to the thermal infrared - Clear air validation by comparison to RTTOV and application to CALIPSO-IIR’. In: *J. Quant. Spectroscopy and Radiative Transfer* vol. 144, pp. 49–67. DOI: 10.1016/j.jqsrt.2014.03.028.
- Dudhia, A. (1997). *RFM v3 software user’s manual, Tech. Rep. ESA Doc. PO-MA-OXF-GS-0003*. Tech. rep. Dep. of Atmos., Oceanic, and Planet. Phys., Univ. of Oxford, Oxford, UK.
- Dudhia, A., V. Jay and C. Rodgers (2002). ‘Microwindow selection for high-spectral-resolution sounders’. In: *Appl. Optics*. Vol. 41, pp. 3665–3673. DOI: 10.1364/AO.41.003665.
- Dufour, G., M. Eremenko, A. Griesfeller, B. Barret, E. LeFlochmoën, C. Clerbaux, J. Hadji-Lazaro, P.-F. Coheur and D. Hurtmans (2012). ‘Validation of three different scientific ozone products retrieved from IASI spectra using ozonesondes’. In: *Atmospheric Measurement Techniques* vol. 5.no. 3, pp. 611–630. DOI: 10.5194/amt-5-611-2012. URL: <http://www.atmos-meas-tech.net/5/611/2012/>.
- Edwards, D. (1992). *GENLN2: A General Line-by-line Atmospheric Transmittance and Radiance Model. Version 3.0 Description and Users Guide. NCAR Technical Note NCAR/TN-367+STR*. Tech. rep. NCAR. DOI: 10.5065/D6W37T86.
- Eresmaa, R., A. Benedetti and A. McNally (2012). *Diverse profile database of aerosol and trace gas concentrations from the Monitoring Atmospheric Composition and Climate short-range forecasts, NWPSAF-EC-TR-015*. Tech. rep. NWPSAF. URL: https://nwpsaf.eu/deliverables/rtm/nwpsaf-ec-tr-015_macc_profile_dataset.pdf.
- Eresmaa, R., N. Bormann and T. McNally (2014). ‘Implications of observation error correlation on the assimilation of interferometric radiances’. In: *Proceedings of 19th International TOVS Study Conference, Jeju Island, South Korea, 26th March - 1st April 2014*. URL: http://cimss.ssec.wisc.edu/itwg/itsc/itsc19/program/papers/7_04_eresmaa.pdf.
- Eresmaa, R. and A. McNally (2014). *Diverse profile datasets from the ECMWF 137-level short-range forecasts, NWPSAF-EC-TR-017*. Tech. rep. NWPSAF. URL: <https://nwpsaf.eu/reports/nwpsaf-ec-tr-017.pdf>.
- Erismann, J. W., A. Bleeker, J. Galloway and M. Sutton (2007). ‘Reduced nitrogen in ecology and the environment’. In: *Environ. Pollut.* Vol. 150. DOI: 10.1016/j.envpol.2007.06.033.
- Evans, K. and G. Stephens (1991). ‘A new polarized atmospheric radiative transfer model’. In: *Journal of Quantitative Spectroscopy and Radiative Transfer* vol. 46.no. 5, pp. 413–423. ISSN: 0022-4073. DOI: 10.1016/0022-4073(91)90043-P.

- Eyre, J. R. and F. I. Hilton (2013). ‘Sensitivity of analysis error covariance to the mis-specification of background error covariance’. In: *Q. J. R. Meteorol. Soc.* Vol. 139 (671), pp. 524–533. DOI: 10.1002/qj.1979.
- F., C. (2001). *Sampled Database of 60 Levels Atmospheric Profiles from the ECMWF Analysis*. Tech. rep. 4. ECMWF, Reading.
- Fioletov, V. E., C. A. McLinden, N. Krotkov, K. Yang, D. G. Loyola, P. Valks, N. Theys, M. Van Roozendael, C. R. Nowlan, K. Chance, X. Liu, C. Lee and R. V. Martin (2013). ‘Application of OMI, SCIAMACHY, and GOME-2 satellite SO₂ retrievals for detection of large emission sources’. In: *Journal of Geophysical Research: Atmospheres* vol. 118.no. 19, pp. 11, 399–11, 418. ISSN: 2169-8996. DOI: 10.1002/jgrd.50826.
- Fowler, D., M. Coyle, U. Skiba, M. A. Sutton, J. N. Cape, S. Reis, L. J. Sheppard, A. Jenkins, B. Grizzetti, J. N. Galloway, P. Vitousek, A. Leach, A. F. Bouwman, K. Butterbach-Bahl, F. Dentener, D. Stevenson, M. Amann and M. Voss (2013). In: *Philos. Trans. R. Soc. London, Ser. B*. DOI: 10.1098/rstb.2013.0164.
- French, A., T. Schmugge, J. Ritchie, A. Hsu, F. Jacob and K. Ogawa (2008). ‘Detecting land cover change at the Jornada Experimental Range, New Mexico, with ASTER emissivities’. In: *Remote Sens. Environ.* Vol. 112, pp. 1730–1748.
- Gamache, R. R. (2014). ‘CO₂ and H₂O updated line shapes’. Unpublished results.
- Gamache, R. and A.L.Laraia (2009). ‘N₂-, O₂-, and air-broadened half-widths, their temperature dependence, and line shifts for the rotation band of H₂¹⁶O’. In: *J. Molec. Spectrosc.* Vol. 257, pp. 116–127.
- Gamache, R. and J. Lamouroux (2013). ‘Predicting accurate line shape parameters for CO₂ transitions’. In: *J. Quant. Spectrosc. Radiat. Transf* vol. 130, pp. 158–171.
- Gillespie, A., S. Rokugawa, T. Matsunaga, J. S. Cothorn, S. Hook and A. B. Kahle (1998). ‘A temperature and emissivity separation algorithm for Advanced Spaceborne Thermal Emission and Reflection Radiometer (ASTER) images’. In: *IEEE Transactions on Geoscience and Remote Sensing* vol. 36.no. 4, pp. 1113–1126.
- Grieco, G., G. Masiello, M. Matricardi and C. Serio (2013). ‘Partially scanned interferogram methodology applied to IASI for the retrieval of CO, CO₂, CH₄ and N₂O’. In: *Opt. Express* vol. 21, pp. 24753–24769. URL: <http://www.opticsinfobase.org/oe/abstract.cfm?URI=oe-21-21-24753>.
- Grieco, G., G. Masiello and C. Serio (2010). ‘Interferometric vs Spectral IASI Radiances: Effective Data-Reduction Approaches for the satellite Sounding of Atmospheric Thermodynamical Parameters’. In: *Remote Sensing* vol. 2, pp. 2323–2346. DOI: 10.3390/rs2102323.
- Grieco, G., G. Masiello and C. Serio (2015). ‘Operational Monitoring of Trace Gases over the Mediterranean Sea’. In: *Advances in Meteorology* no. 318608. DOI: 10.1155/2015/318608.
- Grieco, G., G. Masiello, C. Serio, R. L. Jones and M. I. Mead (2011). ‘Infrared Atmospheric Sounding Interferometer correlation interferometry for the retrieval of atmospheric gases: the case of H₂O and CO₂’. In: *Appl. Opt.* Vol. 50, pp. 4516–4528.
- Grisvard, P. (1992). *Singularities in boundary value problems*. Vol. 22. Research Notes in Applied Mathematics. New York: Springer.
- Groth, S. P., A. J. Baran, T. Betcke, S. Havemann and W. Smigaj (2015). ‘The boundary element method for light scattering by ice crystals and its implementation in BEM++’. In: *J. Quantitative Spectrosc. Rad. Transfer*.
- Han, Y., P. van Delst, Q. Liu, F. Weng, B. Yan, R. Treadon and J. Derber (2006). *Community Radiative Transfer Model (CRTM)—Version 1, NOAA NESDIS*. Tech. rep. Tech Report 122. Natl. Oceanic and Atmos. Admin, Silver Spring, Maryland, p. 22.
- Hanssen, L. M. and S. Kaplan (1999). ‘Infrared diffuse reflectance instrumentation and standards at NIST’. In: *Analytica Chimica Acta* vol. 133, pp. 289–302.

- Harris, B. A. and G. Kelly (2001). ‘A satellite radiance-bias correction scheme for data assimilation’. In: *Q. J. R. Meteorol. Soc.* Vol. 127, pp. 1453–1468.
- Harrison, J. and P. Bernath (Aug. 2012). ‘Spectroscopic measurements of organic molecules for ACE-FTS’. In: *Proceedings of the 11th ASA conference, Reims*.
- Harrison, J. (2015). ‘New and improved infrared absorption cross sections for dichlorodifluoromethane (CFC-12)’. In: *Atmospheric Measurement Techniques* vol. 8, pp. 3197–3207. DOI: 10.5194/amt-8-3197-2015.
- Havemann, S. (2006). ‘The development of a fast radiative transfer model based on an empirical orthogonal functions (EOF) technique’. In: *SPIE series on Multispectral, Hyperspectral, and Ultraspectral Remote Sensing Technology, Techniques, and Applications*. Ed. by W. L. Smith, A. M. Larar, T. Aoki and R. Rattan. Vol. 6405, pp. 348–358.
- Havemann, S. and A. J. Baran (2001). ‘Extension of T-matrix to scattering of electromagnetic plane waves by non-axisymmetric dielectric particles: application to hexagonal ice cylinders’. In: *J Quant Spectrosc Radiat Transfer* vol. 70, pp. 139–158.
- Havemann, S., J. Thelen, J. Taylor and R. Harlow (2014). ‘The Havemann-Taylor Fast Radiative Transfer Code (HT-FRTC): a multipurpose code based on Principal Components’. In: *in preparation for submission to JQSRT*.
- Hess, M., P. Koepke and I. Schult (1998). ‘Optical Properties of Aerosols and Clouds: The Software Package OPAC’. In: *Bull. Amer. Meteor. Soc.* Vol. 79, pp. 831–844. DOI: 10.1175/1520-0477(1998)079<0831:OPOAAC>2.0.CO;2.
- Hilton, F., P. Antonelli, X. Calbet, T. Hultberg, L. Lavanant, X. Liu, G. Masiello, S. Newman, J. Taylor, C. Serio and D. Zhou (2009b). ‘An investigation into the performance of retrievals of temperature and humidity from IASI’. In: *Proceedings of the Eumetsat Meteorological Satellite Conference, Bath, UK, 21-25 September 2009*.
- Hilton, F., R. Armante, T. August, C. Barnet, A. Bouchard, C. Camy-Peyret, V. Capelle, L. Clarisse, C. Clerbaux, P. F. Coheur, A. Collard, C. Crevoisier, G. Dufour, D. Edwards, F. Faijan, N. Fourrie, A. Gambacorta, M. Goldberg, V. Guidard, D. Hurtmans, S. Illingworth, N. Jacquinet-Husson, T. Kerzenmacher, D. Klaes, L. Lavanant, G. Masiello, M. Matricardi, A. McNally, S. Newman, E. Pavelin, S. Payan, E. Péquignot, S. Peyridieu, T. Phulpin, J. Remedios, P. Schlusser, C. Serio, L. Strow, C. Stubenrauch, J. Taylor, D. Tobin, W. Wolf and D. Zhou (2012a). ‘Hyperspectral Earth Observation from IASI: Five Years of Accomplishments’. In: *B. Am. Meteorol. Soc.* Vol. 93, pp. 347–370. DOI: doi : 10.1175/BAMS-D-11-00027.1.
- Hilton, F., N. C. Atkinson, S. J. English and J. R. Eyre (2009a). ‘Assimilation of IASI at the Met Office and assessment of its impact through observing system experiments’. In: *Q. J. R. Meteorol. Soc.* Vol. 135 (639), pp. 495–505. DOI: 10.1002/qj.379.
- Hilton, F., A. Collard, L. Fiedler and L. Lavanant (2007). ‘Comparison of IASI radiances with NWP models from four operational centres’. In: *Presented at the 1st International IASI Conference, Anglet, France, 13–16 November, 2007*. URL: <http://smsc.cnes.fr/IASI/PDF/conf1/Hilton-poster.pdf>.
- Hilton, F., A. Collard, V. Guidard, R. Randriamampianina and M. Schwaerz (2009c). ‘Assimilation of IASI radiances at European NWP Centres’. In: *ECMWF/EUMETSAT NWP-SAF Workshop on Assimilation of IASI in NWP, 6–8 May 2009*. http://old.ecmwf.int/publications/library/ecpublications/_pdf/workshop/2009/IASI/.
- Hilton, F., A. D. Collard and S. M. Newman (2012b). ‘Identification of NWP humidity biases using high-peaking water vapour channels from IASI’. In: *Atmos. Sci. Lett.* Vol. 13, pp. 73–78. DOI: 10.1002/asl.366.
- Hipwood, L., C. Maxey, N. Shorrocks and R. Wilson (2012). ‘MOVPE-Growth of HgCdTe for Infrared Focal Plane’. In: *Arrays. Proc OPTRO-12 066*.

- Hodnebrog, Ø., M. Etminan, G. M. J. S. Fuglestedt, G. Myhre, C. J. Nielsen, K. P. Shine and T. J. Wallington (2013). ‘Global warming potentials and radiative efficiencies of halocarbons and related compounds. A comprehensive Review’. In: *Reviews of Geophysics* vol. 51, pp. 300–378.
- Hollingsworth, A. and P. Lönnberg (1986). ‘The statistical structure of short-range forecast errors as determined from radiosonde data. Part I: The wind field’. In: *Tellus* vol. 38A, pp. 111–136.
- Hornik, K., M. Stinchcombe and H. White (1989). ‘Multilayer feedforward networks are universal approximators’. In: *Neural Networks* vol. 2, pp. 359–366.
- Huang, H.-L., W. Smith and H. Woolf (1992). ‘Vertical resolution and accuracy of atmospheric infrared sounding spectrometers’. In: *J. Appl. Meteorol.* Vol. 31, pp. 265–274.
- Hulley, G. C. and S. J. Hook (2010). ‘Investigating the effects of soil moisture on thermal infrared land surface temperature and emissivity using satellite retrievals and laboratory measurements’. In: *Remote Sens. Environ.* Vol. 114, pp. 1480–1493.
- Hulley, G. C., S. J. Hook and A. M. Baldridge (2008). ‘ASTER Land Surface Emissivity Database of California and Nevada’. In: *Geophys. Res. Lett.* Vol. 35.no. L13401. DOI: 10.1029/2008GL034507.
- Hultberg, T. and T. August (2013). ‘On the equivalence of reconstructed radiances and PC scores’. Unpublished EUMETSAT internal report.
- Hurtmans, D., P.-F. Coheur, C. Wespes, L. Clarisse, O. Scharf, C. Clerbaux, J. Hadji-Lazaro, M. George and S. Turquety (2012). ‘FORLI radiative transfer and retrieval code for IASI’. In: *J. Quant. Spectrosc. Radiat. Transfer* vol. 113, pp. 1391–1408. DOI: 10.1016/j.jqsrt.2012.02.036.
- Illingworth, S. M., J. J. Remedios, H. Boesch, D. P. Moore, H. Sembhi, A. Dudhia and J. C. Walker (2011). ‘ULIRS, an optimal estimation retrieval scheme for carbon monoxide using IASI spectral radiances: sensitivity analysis, error budget and simulations’. In: *Atmospheric Measurement Techniques* vol. 4.no. 2, pp. 269–288. DOI: 10.5194/amt-4-269-2011. URL: <http://www.atmos-meas-tech.net/4/269/2011/>.
- Immler, F. J., J. Dykema, T. Gardiner, D. N. Whiteman, P. W. Thorne and H. V’omel (2010). ‘Reference Quality Upper-Air Measurements: guidance for developing GRUAN data products’. In: *Atmospheric Measurement Techniques*. DOI: 10.5194/amt-3-1217-2010.
- Jacquinet-Husson, N. and others (2011). ‘The 2009 edition of the GEISA spectroscopic database’. In: *J. Quant. Spectrosc. Radiat. Transfer* vol. 112, pp. 2395–2445. DOI: 10.1016/j.jqsrt.2011.06.004.
- Jiménez, C., J. Catherinot, C. Prigent and J. Roger (2010). ‘Relations between geological characteristics and satellite-derived infrared and microwave emissivities over deserts in northern Africa and the Arabian Peninsula’. In: *J. Geophys. Res.* Vol. 115.no. D20311. DOI: 10.1029/2010GL042816.
- Jolliffe, I. (2002). *Principal component analysis*. Springer-Verlag, New York.
- Joo, S., J. Eyre and R. Marriott (2013). ‘The impact of Metop and other satellite data within the Met Office global NWP system using an adjoint-based sensitivity method’. In: *Mon. Wea. Rev.* Vol. 141, pp. 3331–3342. DOI: :10.1175/MWR-D-12-00232.1.
- Jouglet, D., J. Chinaud and X. Lenot (2013). ‘Radiometric inter-comparison of IASI : IASI-A / IASI-B, IASI / AIRS, IASI / CrIS’. In: *3rd International IASI Conference, Hyères, France, 4–8 February, 2013*. URL: http://smc.cnes.fr/IASI/PDF/conf3/02_01-Jouglet_Denis.pdf.
- Kahnert, F. M., J. J. Stamnes and K. Stamnes (2001). ‘Application of the extended boundary condition method to particles with sharp edges: a comparison of two surface integration approaches.’ In: *Appl. Opt.* Vol. 40, pp. 3101–3109.
- Kahnert, M. (2010). ‘Electromagnetic scattering by nonspherical particles: Recent advances’. In: *J. Quant. Spectrosc. Radiat.* Vol. 111, pp. 1788–1790.

- Kahnert, M. (2013). ‘The T-matrix code Tsym for homogeneous dielectric particles with finite symmetries’. In: *J. Quant. Spectrosc. Radiat. Transfer* vol. 123, pp. 62–78.
- Kalnay, E. (2003). *Atmospheric Modelling, Data Assimilation and Predictability*. Cambridge University Press, Cambridge, UK.
- Klüser, L., T. Erbertseder and J. Meyer-Arnek (2013). ‘Observation of volcanic ash from Puyehue-Cordón Caulle with IASI’. In: *Atmospheric Measurement Techniques* vol. 6.no. 1, pp. 35–46. DOI: 10.5194/amt-6-35-2013.
- Klüser, L., D. Martynenko and T. Holzer-Popp (2011). ‘Thermal infrared remote sensing of mineral dust over land and ocean: a spectral SVD based retrieval approach for IASI’. In: *Atmos. Meas. Tech.* Vol. 4.no. 5, pp. 757–773. DOI: 10.5194/amt-4-757-2011.
- Knuteson, R. O., F. A. Best, D. H. DeSlover, B. J. Osborne, H. E. Revercomb and W. L. Smith (2004). ‘Infrared land surface remote sensing using high spectral resolution aircraft observations’. In: *Advances in Space Research* vol. 33.no. 7, pp. 1114–1119.
- Koepke, P., J. Gasteiger and M. Hess (2015). ‘Technical Note: Optical properties of desert aerosol with non-spherical mineral particles: data incorporated to OPAC’. In: *Atmos. Chem. Phys.* Vol. 15, pp. 5947–5956. DOI: 10.5194/acp-15-5947-2015.
- Kunkee, D., S. Swadley, G. Poe, Y. Hong and M. Werner (2008). ‘Special Sensor Microwave Imager Sounder (SSMIS) Radiometric Calibration Anomalies; Part I: Identification and Characterization’. In: *Geoscience and Remote Sensing, IEEE Transactions on* vol. 46.no. 4, pp. 1017–1033. ISSN: 0196-2892. DOI: 10.1109/TGRS.2008.917213.
- Kwon, E.-H., B. J. Sohn, W. L. Smith and J. Li (2012). ‘Validating IASI Temperature and Moisture Sounding Retrievals over East Asia Using Radiosonde Observations’. In: *J. Atmos. Ocean. Tech.* Vol. 29, pp. 1250–1262.
- Kyle, T. (1977). ‘Temperature soundings with partially scanned interferograms’. In: *Appl. Opt.* Vol. 16, pp. 326–332.
- Lafferty, W. J., A. M. Solodov, A. Weber, W. B. Olson and J.-m. Hartman (1996). ‘Infrared collision-induced absorption by N₂ near 4.3 μm for atmospheric applications: measurements and empirical modelling’. In: *Apl. Opt.* Vol. 35, pp. 5911–5917.
- Lamquin, N., C. J. Stubenrauch, S. Cros, H. Smith, K. Gierens and U. Burkhardt (2012). ‘A global climatology of upper-tropospheric ice supersaturation occurrence inferred from the Atmospheric Infrared Sounder calibrated by MOZAIC’. In: *Atmos. Chem. Phys.* Vol. 12, pp. 381–405.
- Lavanant, L., N. Fourrié, A. Gambacorta, G. Grieco, S. Heilliette, F. I. Hilton, M.-J. Kim, A. P. McNally, H. Nishihata, E. G. Pavelin and F. Rabier (2011). ‘Comparison of cloud products within IASI footprints for the assimilation of cloudy radiances’. In: *Q.J.R. Meteorol. Soc.* Vol. 137, pp. 1988–2003. DOI: 10.1002/qj.917.
- Legrand, M., O. Dubovik, T. Lapyonok and Y. Derimian (2014). ‘Accounting for particle non-sphericity in modeling of mineral dust radiative properties in the thermal infrared’. In: *Journal of Quantitative Spectroscopy and Radiative Transfer* vol. 149, pp. 219–240.
- Li, J., J. Li, E. Weisz and D. K. Zhou (2007). ‘Physical retrieval of surface emissivity spectrum from hyperspectral infrared radiances’. In: *Geophys. Res. Lett.* Vol. 34.no. L16812. DOI: doi: 10.1029/2007GL030543.
- Li, Z., J. Li, Y. Li, Y. Zhang, T. J. Schmit, L. Zhou, M.-. D. Goldberg and W. P. Menzel (2012). ‘Determining diurnal variations of land surface emissivity from geostationary satellites’. In: *J. Geophys. Res.* Vol. 117.no. D23302. DOI: 10.1029/2012JD018279.
- Liu, X., W. Smith, D. Zhou and A. Larar (2006). ‘Principal component-based radiative transfer model for hyperspectral sensors: theoretical concept’. In: *Appl. Opt.* Vol. 45, pp. 201–209.
- Luchetta, A., C. Serio and M. Viggiano (2003). ‘Neural Network to Retrieve Atmospheric Parameters from Infrared High Resolution Sensor Spectra’. In: *Proc. IEEE Int. Symposium on Circuits and Systems*. ISBN: 0-7803-7762-1.

- Ma, Q., R. H. Tipping and C. Leforestier (2008). ‘Temperature dependences of mechanisms responsible for the water-vapor continuum absorption. I. Far wings of allowed lines’. In: *J. Chem. Phys.* Vol. 128.no. 124313. DOI: 10.1063/1.2839604.
- Mackowski, D. W. (2002). ‘Discrete dipole moment method for calculation of the T matrix for non-spherical particles’. In: *J. Opt. Soc. Am.* Vol. A19, pp. 881–893.
- Martinet, P., N. Fourri , Y. Bouteloup, E. Bazile and F. Rabier (2013a). ‘Toward the improvement of short-range forecasts by the analysis of cloud variables from IASI radiances’. In: *Atmos. Sci. Lett.* Vol. 15, pp. 342–347. DOI: 10.1002/as12.510.
- Martinet, P., N. Fourri , V. Guidard, F. Rabier, T. Montmerle and P. Brunel (2013b). ‘Towards the use of microphysical variables for the assimilation of cloud-affected infrared radiances’. In: *Q. J. R. Meteorol. Soc.* Vol. 139, pp. 1402–1416. DOI: 10.1002/qj.2046.
- Masiello, G. and C. Serio (2013). ‘Simultaneous physical retrieval of surface emissivity spectrum and atmospheric parameters from infrared atmospheric sounder interferometer spectral radiances’. In: *Appl. Opt.* Vol. 52, pp. 2428–2446. URL: <http://www.opticsinfobase.org/ao/abstract.cfm?URI=ao-52-11-2428>.
- Masiello, G., C. Serio and P. Antonelli (2012). ‘Inversion for atmospheric thermodynamical parameters of IASI data in the principal components space’. In: *Q. J. R. Meteorol. Soc.* Vol. 138, pp. 103–117. DOI: 10.1002/qj.909.
- Masiello, G., C. Serio, I. De Feis, M. Amoroso, S. Venafra, I. Trigo and P. Watts (2013). ‘Kalman filter physical retrieval of surface emissivity and temperature from geostationary infrared radiances’. In: *Atmos. Meas. Tech.* Vol. 6, pp. 3613–3634. DOI: 10.5194/amt-6-3613-2013.
- Masiello, G., C. Serio, S. Venafra, I. DeFeis and E. E. Borbas (2014). ‘Diurnal variation in Sahara desert sand emissivity during the dry season from IASI observations’. In: *J. Geophys. Res. Atmos.* Vol. 119, pp. 1626–1638. DOI: 10.1002/jgrd.50863.
- Massie, S. T. and M. Hervig (2013). ‘HITRAN 2012 refractive indices’. In: *Journal of Quantitative Spectroscopy and Radiative Transfer* vol. 130, pp. 373–380.
- Masuda, K., T. Takashima and Y. Takayama (1988). ‘Emissivity of pure and sea waters for the model sea surface in the infrared window regions’. In: *Remote Sensing Environ.* Vol. 24, pp. 313–329.
- Matricardi, M. (2003). *RTIASI-4, a new version of the ECMWF fast radiative transfer model for the infrared atmospheric sounding interferometer*. Tech. rep. ECMWF Tech Memo 425. URL: <http://www.ecmwf.int/publications/>.
- Matricardi, M. (2005). *The inclusion of aerosols and clouds in RTIASI, the ECMWF fast radiative transfer model for the infrared atmospheric sounding interferometer*. Tech. rep. ECMWF Tech Memo 474. URL: <http://www.ecmwf.int/publications/>.
- Matricardi, M. (2007). *An inter-comparison of line-by-line radiative transfer models*. Tech. rep. ECMWF Tech Memo 525. URL: <http://www.ecmwf.int/publications/>.
- Matricardi, M. (2008). *The generation of RTTOV regression coefficients for IASI and AIRS using a new profile training set and a new line-by-line database*. Tech. rep. ECMWF Tech Memo 564. URL: <http://www.ecmwf.int/publications/>.
- Matricardi, M. (2010). ‘A principal component based version of the RTTOV fast radiative transfer model’. In: *Q. J. R. Meteorological Society* vol. 136, pp. 1823–1835. DOI: 10.1002/qj.680.
- Matricardi, M., F. Chevallier, G. Kelly and J.-N. Thepaut (2004). ‘An improved general fast radiative transfer model for the assimilation of radiance observations’. In: *Q. J. R. Meteorol. Soc.* Vol. 130, pp. 153–173.
- Matricardi, M. and A. P. McNally (2014). ‘The direct assimilation of principal components of IASI spectra in the ECMWF 4D-Var’. In: *Q. J. R. Meteorological Society* vol. 140, pp. 573–582. DOI: 10.1002/qj.2156.

- Matricardi, M. and R. Saunders (1999). ‘Fast radiative transfer model for simulation of infrared atmospheric sounding interferometer radiances’. In: *Applied Optics* vol. 38.no. 27, pp. 5679–5691.
- Mayer, B. and A. Kylling (2005). ‘Technical note: The libRadtran software package for radiative transfer calculations-description and examples of use’. In: *Atmos. Chem. Phys.* Vol. 5.no. 7, pp. 1855–1877. DOI: 10.5194/acp-5-1855-2005.
- McMillin, L., L. Crone, M. Goldberg and T. Kleespies (1995). ‘Atmospheric Transmittance Of An Absorbing Gas. 4. OPTRAN - A Computationally Fast And Accurate Transmittance Model For Absorbing Gases With Fixed And With Variable Mixing Ratios At Variable Viewing Angles’. In: *Appl. Optics* vol. 34.no. 27, pp. 6269–6274.
- McNally, A. P. (2009). ‘The direct assimilation of cloud-affected satellite infrared radiances in the ECMWF 4D-Var’. In: *Q. J. R. Meteorol. Soc.* Vol. 135, pp. 1214–1229. DOI: 10.1002/qj.426.
- McNally, A. P. and P. D. Watts (2003). ‘A cloud detection algorithm for high-spectral-resolution infrared sounders’. In: *Q. J. R. Meteorol. Soc.* Vol. 129, pp. 3411–3423.
- Meng, Z., P. Yang, G. W. Kattawar, L. Bi, K. N. Liou and I. Laszlo (2010). ‘A database for application to radiative transfer calculations’. In: *Journal of Aerosol Science* vol. 41, pp. 501–512.
- Migliorini, S. (2012). ‘On the Equivalence between Radiance and Retrieval Assimilation’. In: *Mon. Wea. Rev.* Vol. 140, pp. 258–265. DOI: 10.1175/MWR-D-10-05047.1.
- Migliorini, S., A. Geer, M. Matricardi and S. English (2014). ‘All-sky assimilation of selected water vapour infrared IASI channels at ECMWF: strategy and initial trials’. In: *Proceedings of 19th International TOVS Study Conference, Jeju Island, South Korea, 26th March - 1st April 2014*. URL: http://cimss.ssec.wisc.edu/itwg/itsc/itsc19/program/papers/9p_07_migliorini.pdf.
- Mira, M., E. Valor, R. Boluda, V. Caselles and C. Coll (2007a). ‘Influence of soil water content on the thermal infrared emissivity of bare soils: Implication for land surface temperature determination’. In: *J. Geophys. Res.* Vol. 112.no. F04003. DOI: 10.1029/2007JF000749.
- Mira, M., E. Valor, R. Boluda, V. Caselles and C. Coll (2007b). ‘Influence of the soil moisture effect on the thermal infrared emissivity’. In: *Tethys* vol. 4, pp. 3–9. DOI: 10.3369/tethys.2007.4.01.
- Moncet, J. L. and S. A. Clough (1997). ‘Accelerated monochromatic radiative transfer for scattering atmospheres: Application of a new model to spectral radiance observations’. In: *Journal of Geophysical Research: Atmospheres* vol. 102.no. D18, pp. 21853–21866. ISSN: 2156-2202. DOI: 10.1029/97JD01551.
- Moncet, J.-L., P. Liang, A. E. Lipton, J. F. Galantowicz and C. Prigent (2011). ‘Discrepancies between MODIS and ISCCP land surface temperature products analyzed with microwave measurements’. In: *J. Geophys. Res.* Vol. 116.no. D21105. DOI: 10.1029/2010JD015432.
- Moncet, J.-L., G. Uymin, A. E. Lipton and H. E. Snell (2008). ‘Infrared Radiance Modeling by Optimal Spectral Sampling’. In: *J. Atmos. Sci.* Vol. 65, pp. 3917–3934. DOI: 10.1175/2008JAS2711.1.
- Nalli, N. R., P. J. Minnett and P. van Delst (2008). ‘Emissivity and reflection model for calculating unpolarized isotropic water surface-leaving radiance in the infrared. I: Theoretical development and calculations.’ In: *Applied optics* vol. 47.no. 21, pp. 3701–3721.
- Newman, S. M., L. Clarisse, D. Hurtmans, F. Marengo, B. Johnson, K. Turnbull, S. Havemann, A. J. Baran, D. O’Sullivan and J. Haywood (2012a). ‘A case study of observations of volcanic ash from the Eyjafjallajökull eruption: 2. Airborne and satellite radiative measurements’. In: *J. Geophys. Res.* Vol. 117, D00U13. DOI: 10.1029/2011JD016780.
- Newman, S. M., P. D. Green, I. V. Ptashnik, T. D. Gardiner, M. D. Coleman, R. A. McPheat and K. M. Smith (2012b). ‘Airborne and satellite remote sensing of the mid-infrared water

- vapour continuum'. In: *Phil. Trans. R. Soc. A* vol. 370, pp. 2611–2636. DOI: 10.1098/rsta.2011.0223.
- Newman, S. M., J. A. Smith, M. D. Glew, S. M. Rogers and J. P. Taylor (2005). 'Temperature and salinity dependence of sea surface emissivity in the thermal infrared'. In: *Quarterly Journal of the Royal Meteorological Society* vol. 131.no. 610, pp. 2539–2557.
- Ngo, N. H., D. Lisak, H. Tran and H. J.-M. (2014). 'An isolated line-shape model to go beyond the Voigt profile in spectroscopic databases and radiative transfer codes'. In: *J. Quant. Spectroscopy and Radiative Transfer* vol. 129, pp. 89–100.
- Niro, F., K. Jucks and J.-M. Hartmann (2005). 'Spectra calculations in central and wing regions of CO₂ IR bands. IV: software and database for the computation of atmospheric spectra'. In: *J. Quant. Spectroscopy and Radiative Transfer* vol. 95 (4), pp. 469–481.
- No, Y., B. Sohn, Y. Kim, S. Joo and W. Bell (2014). 'IASI channel selection for the Unified Model assimilation system'. In: *Proceedings of 19th International TOVS Study Conference, Jeju Island, South Korea, 26th March - 1st April 2014*. URL: http://cimss.ssec.wisc.edu/itwg/itsc/itsc19/program/presentations/28Mar2014/session_7a/7_03_no.pdf.
- Norman, J., M. Divakarla and N. Goel (1995). 'Algorithms for extracting information from remote thermal-IR observations of the Earth's surface.' In: *Remote Sens. Environ.* Vol. 51.no. 1, pp. 157–168. DOI: 10.1016/0034-4257(94)00072-U.
- O'Carroll, A., T. August, P. Le Borgne and A. Marsouin (2012). 'The accuracy of SST retrievals from Metop-A IASI and AVHRR using the EUMETSAT OSI-SAF matchup dataset'. In: *Remote Sensing of Environment* vol. 126, pp. 184–194.
- Ogawa, K., T. Schmugge, F. Jacob and A. French (2003). 'Estimation of land surface window (8–12 μm) emissivity from multispectral thermal infrared remote sensing – A case study in a part of the Sahara Desert'. In: *Geophys. Res. Lett.* Vol. 30, p. 1067. DOI: 10.1029/2002GL016354.
- Ohring, G., B. Wielicki, R. Spencer, B. Emery and R. Datta (2005). 'Satellite Instrument Calibration for Measuring Global Climate Change: Report of a Workshop'. In: *Bulletin of the American Meteorological Society* vol. 86.no. 9, pp. 1303–1313. DOI: 10.1175/BAMS-86-9-1303.
- Okamoto, K. (2013). 'Assimilation of overcast cloudy infrared radiances of the geostationary MTSAT-1R imager'. In: *Q. J. R. Meteorol. Soc.* vol. 139, pp. 715–730. DOI: 10.1002/qj.1994.
- Pavelin, E. G., S. J. English and J. R. Eyre (2008). 'The assimilation of cloud-affected infrared satellite radiances for numerical weather prediction'. In: *Q. J. R. Meteorol. Soc.* Vol. 134 (632), pp. 737–749. DOI: 10.1002/qj.243.
- Paynter, D. J., I. V. Ptashnik, K. P. Shine, K. M. Smith, R. McPheat and R. G. Williams (2009). 'Laboratory measurements of the water vapor continuum in the 1200–8000 cm^{-1} region between 293 K and 351 K'. In: *J. Geophys. Res. Atmos.* Vol. 114.no. D21301. DOI: 10.1029/2008JD011355.
- Péquignot, E., A. Chédin and N. Scott (2008). 'Infrared continental surface emissivity spectra retrieved from AIRS hyperspectral sensor'. In: *J. App. Meteorol. Clim.* Vol. 47, pp. 1619–1633. DOI: 10.1175/2007JAMC1773.1.
- Peyridieu, S., A. Chédin, V. Capelle, C. Tsamalis, C. Pierangelo, R. Armante, C. Crevoisier, L. Crépeau, M. Siméon, F. Ducos and N. A. Scott (2013). 'Characterisation of dust aerosols in the infrared from IASI and comparison with PARASOL, MODIS, MISR, CALIOP, and AERONET observations'. In: *Atmospheric Chemistry and Physics* vol. 13.no. 12, pp. 6065–6082. DOI: 10.5194/acp-13-6065-2013.
- Peyridieu, S., A. Chédin, D. Tanré, V. Capelle, C. Pierangelo, N. Lamquin and R. Armante (2010). 'Saharan dust infrared optical depth and altitude retrieved from AIRS: a focus over North Atlantic - comparison to MODIS and CALIPSO'. In: *Atmos. Chem. Phys.* Vol. 10, pp. 1953–1967. DOI: 10.5194/acp-10-1953-2010.

- Pierangelo, C., M. Mishchenko, Y. Balkanski and A. Chedin (2005). ‘Retrieving the effective radius of Saharan dust coarse mode from AIRS’. In: *Geophys. Res. Lett.* Vol. 32.no. 20, p. L20813. DOI: 10.1029/2005GL023425.
- Plokhenko, Y. and W. P. Menzel (2000). ‘The effects of surface reflection on estimating the vertical temperature-humidity distribution from spectral infrared measurements’. In: *J. Appl. Meteorol.* Vol. 39, pp. 3–14.
- Pougatchev, N., T. August, X. Calbet, T. Hultberg, O. Oduleye, P. Schluessel, B. Stiller, K. St. Germain and G. Bingham (2009). ‘IASI temperature and water vapour retrievals – error assessment and validation’. In: *Atmos. Chem. Phys.* Vol. 9, pp. 6453–6458.
- Prabhakara, C. and G. Dalu (1976). ‘Remote sensing of surface emissivity at 9 μm over the globe’. In: *J. Geophys. Res.* Vol. 81, pp. 3719–3724.
- Ptashnik, I. V., K. P. Shine and A. A. Vigasin (2011). ‘Water vapour self-continuum and water dimers. 1. Analysis of recent work.’ In: *J. Quant. Spectrosc. Radiat. Transf.* Vol. 112, pp. 1286–1303. DOI: 10.1016/j.jqsrt.2011.01.012.
- Rachet, F., M. Margottin-Maclou, A. Henry and A. Valentin (1996). ‘Line mixing effects in the ... bands of Pure Nitrous Oxide’. In: *JOURNAL OF MOLECULAR SPECTROSCOPY* vol. 175, pp. 315–326.
- Rodgers, C. D. (2000). *Inverse Methods for Atmospheric Sounding: Theory and Practice*. World Scientific, Singapore.
- Rodgers, C. D. and B. Connor (2003). ‘Intercomparison of Remote Sounding Instruments’. In: *J. Geophys. Res.* Vol. 108.no. 4116.
- Rodrigues, R., G. Blanquet, J. Walrand, B. Khalil, R. L. Doucen, F. Thibault and J. Hartmann (1998). ‘Line-Mixing Effects in Q Branches of CO_2 ’. In: *J. Molecular Spectroscopy* vol. 186, pp. 256–268. DOI: 10.1006/jmsc.1997.7453.
- Roman, M. O., C. K. Gatebe, C. B. Schaaf, R. Poudyal, Z. Wang and M. D. King (2011). ‘Variability in surface BRDF at different spatial scales (30/,m – 500/,m) over a mixed agricultural landscape as retrieved from airborne and satellite spectral measurements’. In: *Remote Sensing of Environment* vol. 115.no. 9, pp. 2184–2203.
- Rothman et al. (2009). ‘The HITRAN 2008 molecular spectroscopic database’. In: *J. Quant. Spectrosc. Radiat. Transf.* Vol. 110, pp. 533–572. DOI: 10.1016/j.jqsrt.2009.02.013.
- Rothman et al. (2013). ‘The HITRAN2012 molecular spectroscopic database’. In: *J. Quant. Spectrosc. Radiat. Transf.* Vol. 130, pp. 4–50. DOI: 10.1016/j.jqsrt.2013.07.002.
- Rothman, L., A. Goldman, J. Gillis, R. Gamache, H. Pickett, R. Poynter, N. Husson and A. Chedin (1983). ‘AFGL Trace Gas Compilation - 1982 VERSION’. In: *Appl. Optics* vol. 22, pp. 1616–1627.
- Salisbury, J. W. and D. M. D’Aria (1992). ‘Emissivity of terrestrial materials in the 8–14 μm atmospheric window’. In: *Remote Sens. Environ.* Vol. 42, pp. 83–106.
- Salisbury, J. W., A. Wald and D. M. D’Aria (1994). ‘Thermal-infrared remote sensing and Kirchhoff’s law 1. Laboratory measurements.’ In: *J. Geophys. Res.* Vol. 99, pp. 11897–11911.
- Saunders, R., J. Hocking, D. Rundle, P. Rayer, M. Matricardi, A. Geer, C. Lupu, P. Brunel and J. Vidot (2013). *RTTOV-11 Science and Validation Report*. Tech. rep. EUMETSAT NWP-SAF. URL: http://nwpsaf.eu/research/interproj/nwpsaf/rtm/docs_rttov11/rttov11_svr.pdf.
- Schneider, M. and F. Hase (2011). ‘Optimal estimation of tropospheric H_2O and δD with IASI/METOP’. In: *Atmos. Chem. Phys.* Vol. 11, pp. 11207–11220. DOI: 10.5194/acp-11-11207-2011.
- Scott, N. (1974). ‘A direct method of computation of transmission function of an inhomogeneous gaseous medium: description of the method and influence of various factors’. In: *J. Quant. Spectrosc. Radiat. Transfer* vol. 14, pp. 691–707.

- Scott, N. and A. Chedin (1981). ‘A fast line-by-line method for atmospheric absorption computations: The Automatized Atmospheric Absorption Atlas’. In: *J. Appl. Meteor.* Vol. 20, pp. 802–812.
- Seemann, S. W., E. E. Borbas, R. O. Knuteson, G. R. Stephenson and H. L. Huang (2008). ‘Development of a Global Infrared Land Surface Emissivity Database for Application to Clear Sky Sounding Retrievals from Multispectral Satellite Radiance Measurements’. In: *J. Appl. Meteor. Climatol.* Vol. 47, pp. 108–123. DOI: 10.1175/2007JAMC1590.1.
- Siddans, R., D. Knappett, B. Kerridge, B. Latter, A. Waterfall, J. Hurley and J. Walker (2016). *STFC RAL methane retrievals from IASI on board MetOp-A, version 1.0. Centre for Environmental Data Analysis, 18 March 2016*. DOI: 10.5285/B6A84C73-89F3-48EC-AEE3-592FEF634E9B.
- Smith Sr., W. L., D. K. Zhou, A. M. Larar, S. A. Mango, H. B. Howell, R. O. Knuteson, S. Jr and W. L. (2005). ‘The NPOESS Airborne Sounding Testbed Interferometer – Remotely sensed surface and atmospheric conditions during CLAMS’. In: *Journal of the atmospheric sciences* vol. 62.no. 4, pp. 1118–1134.
- Smith, F. I. (2015). ‘Improving the information content of IASI retrievals for numerical weather prediction’. PhD thesis. University of Leicester, Leicester, UK.
- Smith, W. L., R. O. Knuteson, H. E. Revercomb, W. Feltz, N. R. Nalli and H. B. Howell (1996). ‘Observations of the infrared radiative properties of the ocean-implications for the measurement of sea surface temperature via satellite remote sensing’. In: *Bulletin of the American Meteorological Society* vol. 77.no. 1, pp. 41–51.
- Sobrino, J. A., J. C. Jimenez-Munoz, G. Soria, M. Gomez, A. B. Ortiz, M. Romaguera and R. Libonati (2008). ‘Thermal remote sensing in the framework of the SEN2FLEX project: field measurements, airborne data and applications’. In: *International Journal of Remote Sensing* vol. 29.no. 17–18, pp. 4961–4991.
- Spurr, R. (2008). ‘LIDORT and VLIDORT: Linearized pseudo-spherical scalar and vector discrete ordinate radiative transfer models for use in remote sensing retrieval problems’. In: *Light Scattering Reviews*. Ed. by A. Kokhanovsky. Vol. Volume 3. Springer.
- Stamnes, K., S. Tsay, W. Wiscombe and K. Jayaweera (1988). ‘Numerically stable algorithm for discrete-ordinate-method radiative transfer in multiple scattering and emitting layered media’. In: *Appl. Opt.* Vol. 27.no. 12, pp. 2502–2509. DOI: 10.1364/AO.27.002502.
- Stiller, G. P. (2001). *The Karlsruhe Optimized and Precise Radiative Transfer Algorithm (KOPRA)*, FZKA 6487. Tech. rep. Forsch. Karlsruhe, Germany.
- Strow, L. L. and D. Reuter (1988). ‘Effect of line mixing on atmospheric brightness temperatures near $15\mu\text{m}$ ’. In: *Appl. Opt.* Pp. 872–878.
- Strow, L., S. Hannon, S. De Souza-Machado, H. Motteler and D. Tobin (2003). ‘An overview of the AIRS radiative transfer model’. In: *IEEE Trans. Geoscience And Remote Sensing* vol. 41, pp. 303–313. DOI: 10.1109/TGRS.2002.808244.
- Stubenrauch, C. J., W. B. Rossow, S. Kinne, S. Ackerman, G. Cesana, H. Chepfer, L. D. Girolamo, B. Getzewich, A. Guignard, A. Heidinger, B. C. Maddux, W. P. Menzel, P. Minnis, C. Pearl, S. Platnick, C. Poulsen, J. Riedi, S. Sun-Mack, A. Walther, D. Winker, S. Zeng and G. Zhao (2013). ‘Assessment of global cloud datasets from satellites: Project and Database initiated by the GEWEX Radiation Panel’. In: *Bull. Amer. Meteorol. Soc.* Vol. 94, pp. 1031–1049.
- Sun, W., Q. Fu and Z. Chen (1999). ‘Finite-difference time-domain solution of light scattering by dielectric particles with a perfectly matched layer absorbing boundary condition’. In: *Appl. Optics* vol. 38, pp. 3141–3151.
- Susskind, J., C. Barnet and J. Blaisdell (2003). ‘Retrieval of atmospheric and surface parameters from AIRS/AMSU/HSB data in the presence of clouds’. In: *IEEE Trans. Geoscience and Remote Sensing* vol. 41, pp. 390–409. DOI: 10.1109/TGRS.2002.808236.

- Susskind, J. and J. Blaisdell (2008). ‘Improved surface parameter retrievals using AIRS/AMSU data. Algorithms and Technologies for Multispectral, Hyperspectral and Ultraspectral Imagery’. In: *SPIE Proceedings Vol. 6966*. Ed. by S. S. Shen and P. E. Lewis. doi:10.1117/12.774759. International Society for Optical Engineering.
- Susskind, J., J. Blaisdell, L. Iredell and F. Keita (2011). ‘Improved Temperature Sounding and Quality Control Methodology Using AIRS/AMSU Data: The AIRS Science Team Version 5 Retrieval Algorithm’. In: *IEEE Trans. Geoscience and Remote Sensing* vol. 49, pp. 883–907. DOI: 10.1109/TGRS.2010.2070508.
- Sutton, M. A., S. Reis, S. N. Riddick, U. Dragosits, E. Nemitz, M. R. Theobald, Y. S. Tang, C. F. Braban, M. Vieno, A. J. Dore, R. F. Mitchell, S. Wanless, F. Daunt, D. Fowler, T. D. Blackall, C. Milford, C. R. Flechard, B. Loubet, R. Massad, P. Cellier, E. Personne, P. F. Coheur, L. Clarisse, M. V. Damme, Y. Ngadi, C. Clerbaux, C. A. Skjøth, C. Geels, O. Hertel, R. J. W. Kruit, R. W. Pinder, J. O. Bash, J. T. Walker, D. Simpson, L. Horváth, T. H. Misselbrook, A. Bleeker, F. Dentener and W. de Vries (2013). ‘Towards a climate-dependent paradigm of ammonia emission and deposition’. In: *Phil. Trans. R. Soc. London, Series B*. DOI: 10.1098/rstb.2013.0166.
- Talagrand, O. (1997). ‘Assimilation of observations, an introduction’. In: *J. Meteorol. Soc. Jpn* vol. 75.no. 191209.
- Tarantola, A. (1987). *Inverse Problem Theory: Methods for Data Fitting and Model Parameter Estimation*. Elsevier, New York.
- Tashkun, S. A., V. I. Perevalov, J. L. Teffo, A. D. Bykov and N. N. Lavrentieva (2003). ‘CDSD-296, the carbon dioxide spectroscopic databank: version for atmospheric applications’. In: *Proceedings of 14th International Symposium on High Resolution Molecular Spectroscopy, Krasnoyarsk, Russia, 6–11 July 2003*.
- Tashkun, S., V. Perevalov, J. Teffo, L. Rothman and V. Tyuterev (1998). ‘Global fitting of CO₂ vibration-rotation line positions using the effective Hamiltonian approach’. In: *J. Quant. Spectrosc. Radiat. Transfer* vol. 60, pp. 785–801.
- Tennyson, J., P. F. Bernath, A. Campargue et al. (2014). ‘Recommended isolated-line profile for representing high-resolution spectroscopic transitions (IUPAC Technical Report)’. In: *Pure and Applied Chemistry* vol. 86 (12), pp. 1931–1943. DOI: 10.1515/pac-2014-0208.
- Thelen, J.-C., S. Havemann, S. Newman and J. Taylor (2009). ‘Hyperspectral retrieval of land surface emissivities using ARIES’. In: *Q.J.R. Meteorol. Soc.* Vol. 135, pp. 2110–2124.
- Thonat, T., C. Crevoisier, N. A. Scott, A. Chédin, R. Armante and L. Crépeau (2015). ‘Signature of tropical fires in the diurnal cycle of tropospheric CO as seen from Metop-A/IASI’. In: *Atmospheric Chemistry and Physics* vol. 15.no. 22, pp. 13041–13057. DOI: 10.5194/acp-15-13041-2015. URL: <http://www.atmos-chem-phys.net/15/13041/2015/>.
- Tibault, F., V. Menoux, L. D. R., R. L., H. J.-M. and C. Boulet (1997). ‘Infrared collision induced absorption by O₂ near 6.4 microns for atmospheric applications: measurements and empirical modeling.’ In: *Appl. Opt.* Vol. 36, pp. 563–567.
- Tobin, D. C., H. E. Revercomb, R. O. Knuteson, B. M. Lesht, L. L. Strow, S. E. Hannon and T. S. Cress (2006). ‘Atmospheric Radiation Measurement site atmospheric state best estimates for Atmospheric Infrared Sounder temperature and water vapor retrieval validation’. In: *Journal of Geophysical Research: Atmospheres* vol. 111(D9), pp. 1984–2012.
- Tran, H., J.-M. Flaud, T. Gabard, F. Hase, T. Von Clarmann, C. Camy-Peyret, S. Payan and J.-M. Hartmann (2006). ‘Model, Software and database for line-mixing effects in the ν_3 and ν_4 bands of CH₄ and tests using laboratory and planetary measurements. I. N₂ (and air) broadening and the Earth atmosphere’. In: *J. Quant. Spectrosc. Ra. Transf.* Vol. 101, pp. 284–305.

- Tselioudis, G., W. Rossow, Y.-C. Zhang and D. Konsta (2013). ‘Global weather states and their properties from passive and active satellite cloud retrievals’. In: *J. Climate* vol. 26, pp. 7734–7746. DOI: doi:10.1175/JCLI-D-13-00024.
- Turner, D. D. e. a. (2004). ‘The QME AERI LBLRTM: a closure experiment for downwelling high spectral resolution infrared radiance’. In: *J. Atmos. Sci.* Vol. 61, pp. 2657–2675. DOI: 1175/JAS3300.1.
- Vaida, V., J. S. Daniel, H. G. Kjaergaard, L. M. Goss and A. F. Tuck (2001). ‘Atmospheric absorption of near infrared and visible solar radiation by the hydrogen bonded water dimer’. In: *Q. J. R. Meteorol. Soc.* Vol. 127, pp. 1627–1643. DOI: 10.1002/qj.49712757509.
- Van Damme, M., L. Clarisse, C. L. Heald, D. Hurtmans, Y. Ngadi, C. Clerbaux, A. J. Dolman, J. W. Erismann and P. F. Coheur (2014). ‘Global distributions, time series and error characterization of atmospheric ammonia (NH₃) from IASI satellite observations’. In: *Atmospheric Chemistry and Physics* vol. 14.no. 6, pp. 2905–2922. DOI: 10.5194/acp-14-2905-2014.
- Van de Hulst, H. (1981). *Light Scattering by small particles*. Dover Publications, New York.
- Vandenbussche, S., S. Kochenova, A. C. Vandaele, N. Kumps and M. De Mazière (2013). ‘Retrieval of desert dust aerosol vertical profiles from IASI measurements in the TIR atmospheric window’. In: *Atmospheric Measurement Techniques* vol. 6.no. 10, pp. 2577–2591. DOI: 10.5194/amt-6-2577-2013.
- Ventress, L. and A. Dudhia (2013). ‘Improving the selection of IASI channels for use in numerical weather prediction’. In: *Q. J. R. Meteorol. Soc.* Vol. 140, pp. 2111–2118. DOI: :10.1002/qj.2280.
- Vidot, J., A. J. Baran and P. Brunel (2015). ‘A new ice cloud parameterization for infrared radiative transfer simulation of cloudy radiances: Evaluation and optimization with IIR observations and ice cloud profile retrieval products’. In: *J. Geophys. Res. Atmos.* Vol. 120, pp. 6937–6951. DOI: 10.1002/2015JD023462.
- Walker, J. C., A. Dudhia and E. Carboni (2011). ‘An effective method for the detection of trace species demonstrated using the MetOp Infrared Atmospheric Sounding Interferometer’. In: *Atmos. Meas. Tech.* Vol. 4.no. 5, pp. 1567–1580. DOI: 10.5194/amt-4-1567-2011.
- Wan, Z. and Z.-L. Li (1997). ‘A physics-based algorithm for retrieving land-surface emissivity and temperature from EOS/MODIS data’. In: *IEEE Trans. Geosci. Remote Sensing* vol. 35, pp. 980–996.
- Wan, Z. (2008). ‘New refinements and validation of the MODIS Land-Surface Temperature/Emissivity products.’ In: *Remote Sensing of Environment* vol. 112 (1), pp. 59–74.
- Weng, F., Y. Han, P. van Delst, Q. Liu and B. Yan (2005). ‘JCSDA Community radiative transfer model (CRTM)’. In: *Technical Proceedings of Fourteenth International ATOVS Study Conference, Beijing*.
- Weston, P., W. Bell and J. Eyre (2014). ‘Accounting for correlated error in the assimilation of high resolution sounders’. In: *Q. J. R. Meteorol. Soc.* Vol. 140, pp. 2420–2429. DOI: : 10.1002/qj.2306.
- Wikle, C. and L. Berliner (2007). ‘A Bayesian tutorial for data assimilation’. In: *Physica D* vol. 230, pp. 1–26. DOI: 10.1016/j.physd.2006.09.017.
- WMO (2015). *Guide to the Direct Broadcast Network (DBNet) For Near Real-Time Relay of Low Earth Orbit Satellite Data*. URL: http://www.wmo.int/pages/prog/sat/rars_en.php.
- Wu, X. and W. L. Smith (1997). ‘Emissivity of rough sea surface for 8–13 μm : modeling and verification’. In: *Applied Optics* vol. 36.no. 12, pp. 2609–2619.
- Yang, P., Q. Feng, G. Hong, G. W. Kattawar, W. J. Wiscombe, M. I. Mishchenko, O. Dubovik, I. Laszlo and I. N. Sokolik (2007). ‘Modeling of the scattering and radiative properties of nonspherical dust-like aerosols’. In: *J. Aerosol Sci.* Vol. 38, pp. 995–1014.

- Yang, P., K. N. Liou, M. I. Mishchenko and B.-C. Gao (2000). ‘An efficient finite-difference time domain scheme for light scattering by dielectric particles: application to aerosols’. In: *Appl. Opt.* Vol. 39, pp. 3727–3737.
- Yurkin, M. A. and A. G. Hoekstra (2011). ‘The discrete-dipole-approximation code ADDA: capabilities and known limitations’. In: *J. Quant. Spectrosc. Radiat. Transfer* vol. 112, pp. 2234–2247.
- Zhang, Z., P. Yang, G. Kattawarb, H.-l. Huang, T. Greenwald, L. Jun, B. A. Baumd, D. K. Zhoue and Y. Hue (2007). ‘A fast infrared radiative transfer model based on the adding-doubling method for hyperspectral remote-sensing applications’. In: *J. Quant. Spectrosc. Ra. Trans.* Vol. 105, pp. 243–263.
- Zhou, D., A. Larar, X. Liu, W. L. Smith, L. L. Strow, P. Yang, P. Schluessel and X. Calbet (2011). ‘Global Land Surface Emissivity Retrieved From Satellite Ultraspectral IR Measurements’. In: *IEEE Trans. Geoscience and Remote Sensing* vol. 49, pp. 1277–1290. DOI: 10.1109/TGRS.2010.2051036.
- Zhou, L., R. E. Dickinson, Y. Tian, M. Jin, K. Ogawa, H. Yu and T. Schmugge (2003). ‘A sensitivity study of climate and energy balance simulations with use of satellite-derived emissivity data over northern Africa and the Arabian Peninsula’. In: *J. Geophys. Res.* Vol. 108, p. 4795. DOI: 10.1029/2003JD004083..
- Zhou, L., M. Goldberg, C. Barnet, Z. Cheng, F. Sun, W. Wolf, T. King, X. Liu, H. Sun and M. Divakarla (2008). ‘Regression of surface spectral emissivity from hyperspectral instruments’. In: *IEEE Trans. on Geoscience and Remote Sensing* vol. 46, pp. 328–333. DOI: 10.1109/TGRS.2007.912712.
- Zubko, E., Y. Shkuratov, M. Mishchenko and G. Videen (2008). ‘Light scattering in a finite multi-particle system. A fast infrared radiative transfer model based on the adding-doubling method for hyperspectral remote-sensing applications’. In: *J. Quant. Spectrosc. Ra. Trans.* Vol. 109, pp. 2195–2206.